A Biologically Inspired Jumping and Rolling Robot

Armour, Rhodri

Award date:
2010

Awarding institution:
University of Bath

A Biologically Inspired Jumping and Rolling Robot

Rhodri Huw Armour

A thesis submitted for the degree of Doctor of Philosophy

University of Bath

Department of Mechanical Engineering

May 2010

Table of contents

Acknowledgments

This research could not have been conducted without the support of:

Dr Adrian Bowyer for the encouragement, supervision and valuable guidance provided through the latter stages of this work.

Professor Julian Vincent for the broadening of my view of biology and its obvious potential within engineering.

My father, Dr Andrew Armour for the initial motivation and the valuable discussions regarding the progress and clarity of my work.

Dr Keith Paskins for early insights into jumping techniques in biology and subsequent encouragement and competition throughout this research.

The rest of the Knucklerunners (Paul Riggs, Keri Collins, Jen Wladichuk, Sabine Graf, Dr Thomas Hesselberg, Dr Ed Sells, Dr Ken Savage) for the personal support that only such a group of friends can provide.

My family and friends who are always there.

Other staff members within the Centre for Biomimetic and Natural Technologies.

Abstract

Mobile robots for rough terrain are of interest to researchers as their range of possible uses is large, including exploration activities for inhospitable areas on Earth and on other planets and bodies in the solar system, searching in disaster sites for survivors, and performing surveillance for military applications.

Nature generally achieves land movement by walking using legs, but additional modes such as climbing, jumping and rolling are all produced from legs as well. Robotics tends not to use this integrated approach and adds additional mechanisms to achieve additional movements.

The spherical device described within this thesis, called Jollbot, integrated a rolling motion for faster movement over smoother terrain, with a jumping movement for rougher environments. Jollbot was developed over three prototypes. The first achieved pause-and-leap style jumps by slowly storing strain energy within the metal elements of a spherical structure using an internal mechanism to deform the sphere. A jump was produced when this stored energy was rapidly released. The second prototype achieved greater jump heights using a similar structure, and added direction control to each jump by moving its centre of gravity around the polar axis of the sphere. The final prototype successfully combined rolling (at a speed of 0.7 m/s, up 4° slopes, and over 44 mm obstacles) and jumping (0.5 m cleared height), both with direction control, using a 0.6 m spherical spring steel structure. Rolling was achieved by moving the centre of gravity outside of the sphere's contact area with the ground. Jumping was achieved by deflecting the sphere in a similar method to the first and second prototypes, but through a larger percentage deflection.

An evaluation of existing rough terrain robots is made possible through the development of a five-step scoring system that produces a single numerical performance score. The system is used to evaluate the performance of Jollbot.

Chapter 1 Introduction

Mobile robots, by their very name, are required to perform tasks that require movement over some distance. This may be in or through harsh, dangerous and inaccessible places for humans, or for simple repetitive tasks in human environments in an effort to save manpower and mantime. Mobile robots include land based devices, flying unmanned aerial vehicles (UAV's), and autonomous aquatic or underwater vehicles (AUV's). This thesis focuses only on land based mobile robots which, as of 2006, make up ~35% of the 40000 professional service robots in use (but account for ~50% of the projected sales for 2007-2010), and almost 100% of the 3.5 million domestic robots (IFR Statistical Department 2007). Such mobile devices are currently in use in household environments for vacuuming, mowing lawns, and providing entertainment. They are used for providing security around buildings and in factories for transporting parts or goods. Medical applications currently include similar carrying activities. Military applications include bomb disposal, scouting, ferrying of items and as remotely controlled weaponised mounts. Industrial applications include forestry, mining and hazardous site inspection. Many land based mobile robots are used in research environments to develop new sensing techniques, control methods, decision making processes and artificial intelligence.

The scientific definition of the term robot includes only those devices that automatically perform a given task. Such tasks could be repetitive, as carried out by industrial robotic arms. Or the tasks could be diverse, like those performed by many mobile robots, requiring a level of autonomy when making decisions as to the best course of action. The popular definition of robot also includes those devices that perform a task remote to a human operator under wireless or wired (tethered) human control. Within this work, all are considered valid robots. The challenges of autonomy firstly stem from the requirement for energy, then the control processes involved in interpreting the surrounding environment and deciding on the best course of action. The last two tend to be the realm of the computer scientist. The mechanical engineer undertaking this research has therefore focused on a remotely controlled mobility system with the belief that future cooperation with robotics researchers has potential to lead to an autonomous version, though this falls outside the scope of this work.

Rough and rugged terrain is of particular interest to robotics researchers as it presents difficult challenges leading to a wide variety of possible applications for devices that successfully overcome them. Mobile robots that conduct construction site work, military reconnaissance, disaster survivor location, hazardous waste removal, and planetary exploration all require an ability to operate in unstructured and irregular terrain (Davis et al. 1995). Even mobile robots intended to function in the human urban environment will often require the ability to deal with rough terrain, albeit structured and smooth-surfaced, such as stairs. The sensors and manipulators required to perform specific tasks, for example environmental monitoring and sampling or providing oxygen to survivors, are all required in addition to a working robotic mobility platform. The robotic mobility platform upon which this equipment is based must ensure that it does not become stuck or fall over when making its way through varied terrain to its goal.

The majority of existing mobile robots deal with rough terrain with a single type of movement, such as walking, using wheels or tracks, or jumping. The abilities of each movement limit the relative size of the obstacles that can be surmounted, or the speed at which terrain can be travelled through by a given-sized device. A jumping robot for example would make good but steady progress through a rough area, but continuing to rely on jumping when terrain gets smoother means the specialization would make it slow when compared to a similarly-sized wheeled robot. A wheeled robot would itself have the inverse problem of not being able to get through a certain roughness of terrain at all. A handful of devices have combined two movements in one machine by adding mechanisms to achieve a second mode that complements and counteracts the limitations of the primary mode (Lambrecht, Horchler & Quinn 2005; Salton 2009; Stoeter et al. 2002). Natural organisms are almost universally able to perform multiple movements with only one system, and their inspiration influences this research. Achieving the two modes within one system has been attempted by one group of researchers (Hirai, Matsuyama & Nakanishi 2007), and will be described, but their device has limited abilities.

This thesis focuses on the development of a new, inexpensive, remotely controlled, single structure, multimodal jumping and rolling robot that is able to deal with rough and varied terrains. Being multi-modal is likely to mean that that the device is not the best at

jumping or at rolling due to compromises made to achieve both. However it is hoped that its ability over a variety of terrains is improved by using a multimodal movement strategy when compared with each of the single modes alone. This thesis will show via a scoring system that this new device is useful for rough terrain applications.

The original contributions of this work include:

- The development of a generic methodology that was tuned to allow some quantification of performance of a series of robots.
- The proof-of-concept of combining complimentary movement modes within a single structure. Here using a sphere as both the surface for rolling and the energy store for jumping.

Elements of this work have been published in:

- A paper reviewing the state of the art of rolling in robotics (R.H. Armour & J.F.V. Vincent 2006).
- A paper presenting the development of spherical jumping robot (Armour et al. 2007).
- A forthcoming paper presenting the most recent iteration of a spherical multimodal jumping and rolling robot
- A forthcoming paper illustrating a general scoring technique that could be used to evaluate robot performance.

1.1 Scope

Chapter 1 contains an introduction to mobile robotics and how movement in rough terrain is of particular use and interest. It introduces the aim of this work, which is to produce a single structure multimodal jumping and rolling device. Chapter 2 highlights the various topics that need to be considered to develop a mobile robot for use in rough environments. This includes a look at terrain and size considerations, application possibilities for mobile rough terrain robots, the state of the art of such robots and how nature deals with rough terrain. In addition, jumping and rolling are introduced in the background as those are the movements specifically combined to form a single novel

robotic platform here. Chapter 3 introduces a method by which a series of robotic devices can be evaluated depending on a user's intended application. The three following chapters (4, 5, 6) present the core of this research, describing a series of iterative prototypes, each chapter being broken down into design, experimentation, evaluation, and future considerations. Chapter 4 initiates the design of a multimodal jumping and rolling device by producing a prototype with only jumping ability. Chapter 5 presents the second iterative prototype with modifications to achieve jump direction control and an element of rolling. Chapter 6 presents the final iterations where a rolling and jumping ability are successfully combined within a single device. Chapter 7 presents a discussion of what the prototypes have achieved utilising the evaluation method presented in Chapter 3. It further provides suggestions as to how the third prototype could be developed and how this work could be built upon.

Chapter 2 Background

Before undertaking the design of a robotic mobility platform for rough terrain there are a wide range of subjects to consider. These include an understanding of rough terrain and what constitutes rough terrain; what potential applications are available to rough terrain devices and the current state of the art of those devices. Rough terrain isn't just the realm of robotics, so an introduction to nature's solution is also presented followed by a summary of jumping and of rolling within robotics and nature.

2.1 Understanding terrain

The rough terrain in which a mobile robot is expected to operate maybe very complex, and may consist of a combination of two fundamental elements: the material of which the terrain is constructed, and the geometry of its surface. Materials include such substrates as sand, dust, soil, rock, concrete, pebbles, snow, general vegetation, and grasses all occurring at a variety of moisture contents giving slippery, sticky, and compressible variations. Terrain surface geometry includes elements like slopes, steps, gullies, ditches, walls, fences, cliffs and additional obstacles such as immovable objects (tress, boulders, buildings), ones that can be pushed or deflected (shrubs and grasses), or ones that move themselves (animals, vehicles). A rover driver or autonomous robot would need to determine which elements are most important given its situation and goal, and this would require some sort of terrain assessment.

Terrain can be described qualitatively in words which highlight its overriding features, or it can be described quantitatively using numbers to measure its properties.

Qualitative descriptors provide general information to robotic designers and include factors like whether a surface might be sloping or level, whether there are obstacles, whether there are individual steps or a series of them (human-constructed or apparent), whether there are soft and slippery surfaces, or whether the terrain is waterlogged or dusty. A simple photograph or video recording of terrain from a mobile robot's perspective gives a good idea of this qualitative description, at least to a person. Viewing and interpretation by a human operator allows for quick guidance of the best route. This is a difficult solution to replicate within a control computer, but

attempts are being made by, for example, the NASA-Jet Propulsion Laboratory to produce a perceptual “linguistic” assessment system that can be used to quantify the difficulty and risk associated with robot mobility such that it can be used by a guidance system (Seraji 2003).

Quantitative descriptors offer numerical measures to define different regions against specific criteria and have the potential to provide useful information to robot designers and programmers. Substrate strength, hardness, grain size, temperature, wetness, and density can be determined experimentally on location using physical testing tools such as cone penetrometers and shear vanes. These ultimately give measures of a surface’s ability to support traffic (McBride, Longoria & Krotkov 2003). These tests produce useful substrate definitions, but give no information about potential obstacles and the form of the terrain in a robot’s path.

Current techniques to describe terrain mathematically rely on the presence of existing position data from measurements along profile lines, stereoscopic aerial photographs or previous contour data from maps. These techniques are statistical measures of terrain and include frequency spectrum, fractal dimension, curvature, covariance and auto-correlation, and semivariogram (Li, Zhu & Gold 2005). However, as they are computed from only a sample of terrain points, they can therefore give results that don’t adequately define the actual surface (Li, Zhu & Gold 2005) unless high density data is used. Gathering this data is a time consuming process.

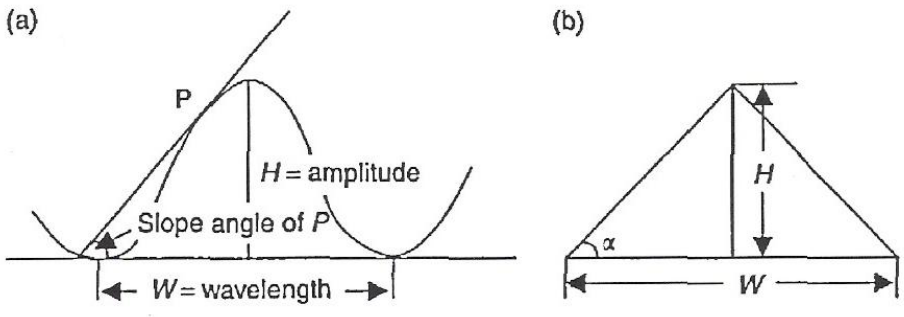

Figure 1 – Terrain roughness vector defined from slope, α, wavelength, W, and relief, H (Li, Zhu & Gold 2005). (a) shows the full relationship and (b) shows a simplified version (see Equation 1)

A more quick and suitable method is to use a terrain roughness vector built from a series of parameters - *relief* and *grain/texture* (Li, Zhu & Gold 2005). *Relief* is the term used to describe the vertical dimension (amplitude) of the topography, while *grain* and *texture* are used to describe the horizontal dimension (wavelength) (Li, Zhu & Gold 2005). These parameters can be connected by 'slope' (gradient) as shown in Figure 1. Therefore, relief, wavelength and slope can be used to define the roughness of a surface. The following mathematical equation (Equation 1) can be used to approximate the relationship of relief, wavelength and slope.

$$\tan\alpha = \frac{H}{W/2} = \frac{2H}{W}$$

Equation 1 – relationship of relief (H), wavelength (W) and slope (α) for a surface (Li, Zhu & Gold 2005)

Where α is the average slope angle, H is the local relief (amplitude) value, and W is the wavelength. If any two values are known, then the third can be calculated, and a series of terrains have previously been classified by slope and relief (Table 1).

Terrain Type	Slope α (°)	Relief H (amplitude) (m)
Plain	<2	<80
Upland	2-6	80-300
Hill	6-25	300-600
Mountain	>25	>600

Table 1 – Terrain classification by slope and relief (Li, Zhu & Gold 2005)

Although adequately describing terrain, this 'terrain roughness vector' requires prior knowledge or information about a terrain. It could be used as a technique to classify terrain once data has been collected by a mobile robot. Terrain data collection can be achieved by using a robot's existing onboard sensors such a gyros, accelerometers, wheel encoders, and drive motor voltage and current readings. The resulting sensor signature could then define a particular type of terrain (Ojeda et al. 2006).

Determining information about a forthcoming terrain is possible using existing sensor technology. The current position and angle of a surface beneath a robot can be determined with level sensors and robot positional data (either externally verified using numerous satellites or fixed base stations, or deduced relatively along the robot's journey). The position of distant points relative to the robot's current position can be determined using range sensors. The density of obstructions can be determined using vision systems.

In an effort to evaluate a series of rough-terrain-capable robots, it would be helpful if a single value could be used to define a particular terrain. For example, it would then be possible to determine if robot X could deal with a terrain Y or only one defined by Y-1. Whether it is possible to define a terrain with a single value is unknown and is a complete study in itself. It is therefore outside of the scope of this research. A discussion of mobile robot evaluation without a single terrain value appears in Chapter 3.

There is little previous research that attempts to describe terrain at a scale useful to mobile robotics. Defence mapping researchers have previously developed something they have named a "Surface Roughness Factor" for a variety of terrains in an attempt to quantify their impact on the speed of military vehicles and troops (Defence Mapping Agency 1994). The values are subjective and "determined by separate groups of experienced vegetation and surface materials analysts" with experience of military vehicle movement. The values range from 0.00 to 1.00 where 0.00 signifies impassable terrain and 1.00 signifies a terrain with no impact on speed. Multiplying the average speed of a vehicle or troops over flat terrain by this factor gives some idea of the anticipated average speed over such terrain. A tabular summary is reproduced below in Table 2.

MAP UNIT CODE (3RD/4TH DIGIT)	SURFACE ROUGNESS DESCRIPTION	ESTIMATED SURFACE ROUGHNESS FACTORS* MEDIUM & LARGE TANKS	LARGE WHEELED VEHICLES	SMALL WHEELED VEHICLES	SMALL TRACKED VEHICLES	FOOT TROOPS
0	No Data	-	-	-	-	-
1	No surface roughness effect	1.00	1.00	1.00	1.00	1.00
2	Area of high landslide potential	0.00	0.00	0.00	0.00	0.00
3	Stony soil with scattered surface rock	0.90	0.90	0.95	0.95	0.95
4	Area of numerous diked fields	0.15	0.00	0.00	0.10	0.10
5	Quarries	0.35	0.10	0.10	0.25	0.25
6	Area of numerous terraced fields	0.25	0.00	0.00	0.10	0.10
7	Extensive surface rock & boulders with scattered thin soil	0.45	0.20	0.20	0.40	0.40
8	Moderately dissected	0.75	0.75	0.65	0.65	0.65
9	Highly dissected	0.25	0.30	0.10	0.20	0.20
10	Area of numerous sinkholes	0.45	0.55	0.50	0.55	0.55
11	Area of hummocky terrain	0.75	0.65	0.65	0.75	0.75
12	Rugged terrain with numerous outcrops	0.10	0.10	0.05	0.05	0.05
13	Salt evaporators with numerous dikes	0.05	0.05	0.00	0.00	0.00
14	Area of numerous walls	0.25	0.05	0.05	0.15	0.15
15	Area of shallow meander scars	0.90	0.80	0.75	0.85	0.85
16	Area of numerous canals/or ditches	0.60	0.40	0.45	0.50	0.50
17	Area of numerous hedgerows	0.40	0.10	0.05	0.15	0.15
18	Area of many small pits and quarries	0.30	0.35	0.40	0.40	0.40
19	Rock outcrops	0.35	0.10	0.10	0.25	0.25
20	Wadis with transverse sand ridges	0.45	0.35	0.40	0.40	0.40
21	Lava plain, rough rocky surface	0.10	0.05	0.00	0.05	0.05
22	Agricultural allotment area, wooden fences, numerous small enclosed areas	0.50	0.30	0.15	0.40	0.40

*Surface roughness factors are indicated with 0.00 having maximum and 1.00 having the least impact on CCM.

Table 2 – Military Surface Roughness Factor (Agency 1994) used as a multiplier for speed over particular terrains. *CCM means Cross-Country Movement

Surface Roughness Factors would be extremely useful when predicting performance of a mobile rover, but the values would be particular to each individual robot (each having a column in Table 2). The values could only be estimated by someone who is very familiar with the abilities of each device over a series of terrains. Because the roughness factors are subjective, there can be no true comparison between estimates unless a standardised series of test environments are available. A series of test environments have been built at the Southwest Research Institute (McBride, Longoria & Krotkov 2003) and used to compare a tracked robot and a walking robot.

The study of engineering surfaces highlights some techniques to evaluate surfaces ultimately through the use of a handful of universal numerical descriptors. The science of surface finishes and texture regards the surfaces of any object as being made up of three different characteristics. Roughness deals with the smallest scale, that of texture. Waviness is a larger characteristic upon which roughness is superimposed and is the variation from an ideal form. Curvature is larger again and closely describes the ideal form (Figure 2).

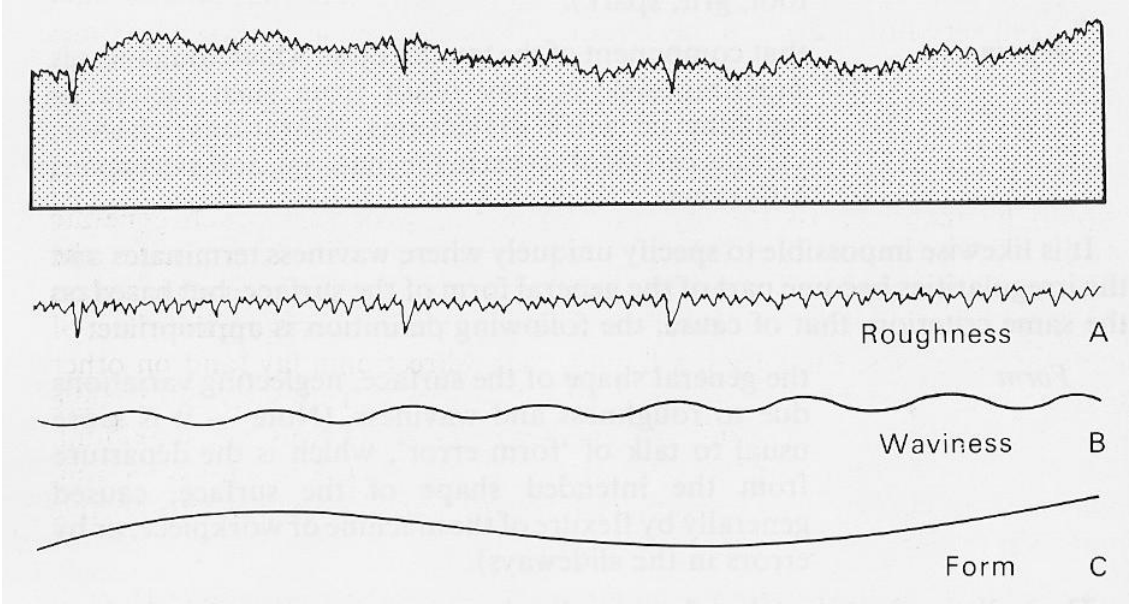

Figure 2 – A surface consisting of roughness (A), waviness (B) and curvature/form (C) (Dagnall 1986)

In the case of terrain, these characteristics are still true, but at a much larger scale. If you take, for example, a rockslide in a mountainous region (Figure 3); the roughness is the surfaces of the individual rocks, the waviness is the combined surface of a series of rocks when viewed from a distance, and the curvature is the slopes of the mountain sides themselves.

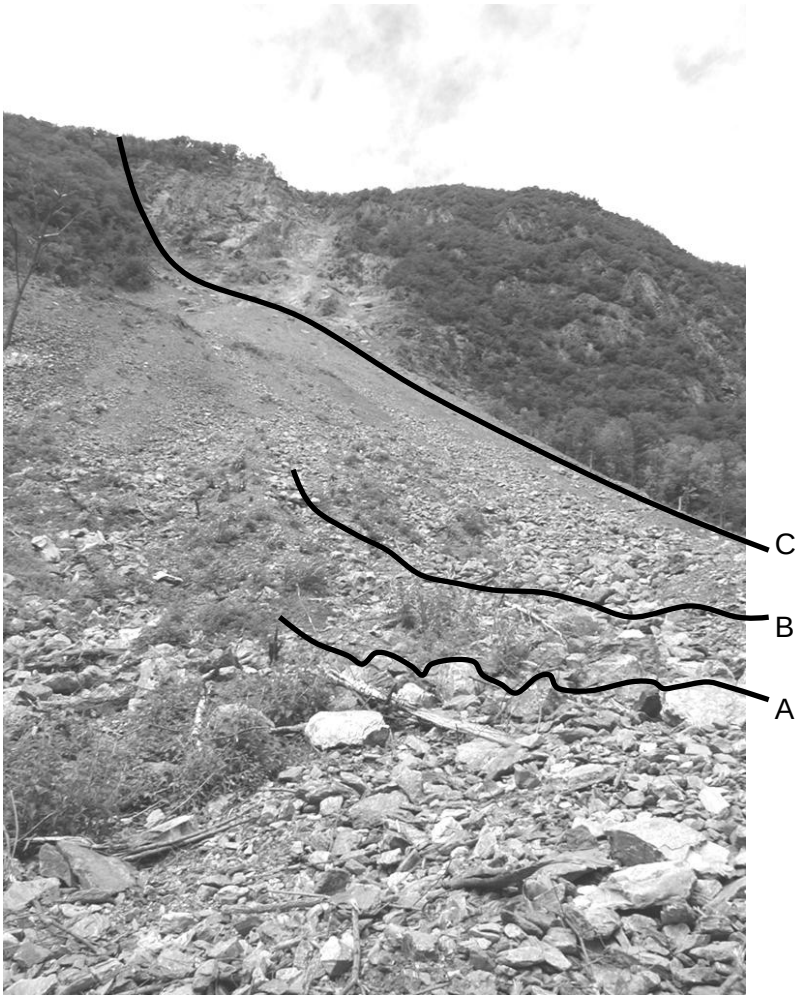

Figure 3 – Large volume rock fall in highgrade metagranites and gneisses. Sechillienne, Romanche Valley, Isere, France. Roughness (A), waviness (B) and curvature/form (C) are highlighted (Giles)

From a conventional surface engineering perspective, roughness is a measure of surface texture and is quantified as the average of measured perpendicular difference of the real surface from its ideal equivalent. For surface quality engineering, large differences (>3.2 μm) indicate a rough surface whereas small ones (<0.4 μm) indicate a smooth surface (Dagnall 1986). Various techniques are available to measure a surface profile with subsequent analysis being used to determine roughness, waviness and curvature. Profiling techniques include contact methods where a suitably sized stylus is drawn across a surface and its movement amplified, and contactless techniques. The Schmaltz Recorder, Contorograph, Tomlinson Surface Recorder,

Profilometer and Talysurf are all variations on the stylus contact method for producing images and data of profiles in manageable sizes and forms (The magnification required to be able to see the surface roughness on a 100 mm length of material might require a paper graph 100 m long without the use of amplified stylus feedback) (Dagnall 1986). Using reflection, a microscope, optical sectioning and a surface texture interferometer are among the non-contact optical solutions (Dagnall 1986). Non-contact electrical techniques include contact resistance and capacitance measures (Dagnall 1986). It is the interpretation of the profiles produced from such techniques that determine roughness (and waviness and curvature).

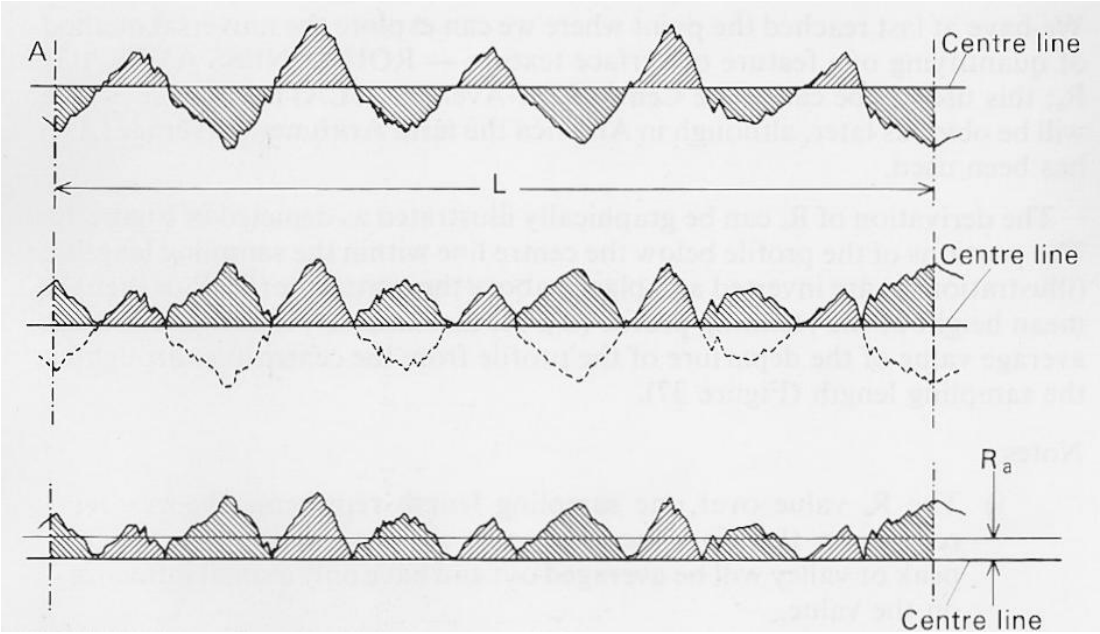

Figure 4 – Determining roughness R_a. Produce datum/centre line over an evaluation length (L) where there is equal area above and below. Add the areas and divide by evaluation length to determine roughness. (Dagnall 1986)

The analysis of the profile requires a datum line to be produced. This is typically a straight line over a suitably small evaluation length positioned where the sums of the areas between it and the peaks above and valleys below are equal. This line, connected to its neighbours, is an approximation of the waviness of a surface. The average roughness can be calculated by adding the areas above and below the line and dividing that by the evaluation length (Figure 4). Curvature is a linear

approximation of the waviness at longer evaluation lengths. Rugosity is another measure of roughness and requires true and apparent surface areas to be determined, but is a word often used interchangeably with roughness, particularly at the scales appropriate to terrain.

From a rough terrain robotics perspective, it is the roughness and waviness that are of primary concern. The use of the physical interaction (friction or displacement) between the feet or wheels of a mobile robot could be used to determine the roughness and waviness of a surface. This assessment can only be conducted after the terrain has been explored and this means a robot would have to venture into a terrain with little knowledge of what is to come. A proposed solution to remotely determine profile could be achieved by the use of some tethered "stylus" which is launched from a robot into unknown terrain, the profile being generated from accelerometers or other devices within it as it is pulled back to the mobile rover. More simple non-contact solutions are desirable and these will have to be carried out either optically using images, or with range-finding sensors. This quickly becomes the realm of image processing and machine vision.

2.2 Size considerations

The physical size of a robot has an important implication for its perception of environmental roughness. For a human, the term 'rough terrain' can be used when forward walking motion is significantly limited by a series of obstacles in the person's path. Typically for the average middle aged person, these obstacles will have to be over 400 mm high to cause a major slowing of forward motion as this is the maximum height that can be simply stepped onto or over (Pheasant 2001). However, for a vehicle or animal much larger than a human, a surface scattered with 400 mm high obstacles could be considered smooth. Similarly, a smooth human-scale surface such as a gravelled track is very rough for an insect like an ant. This relationship between object size and terrain roughness has been termed the "Size-Grain Hypothesis" (SGH). The Size-Grain Hypothesis says that "as terrestrial organisms decrease in size, their environment becomes less planer and more rugose" (rough) (Kaspari & Weiser 1999). This hypothesis is a formalisation of related work (Mandelbrot 1983; Ohmiya 1991;

Morse et al. 1985) and it has been proven with study that smaller ants are better able to explore terrain than larger ones as they are able to venture into gaps within leaf debris (Farji-Brener, Barrantes & Ruggiero 2004). The Size-Grain Hypothesis is likely to be true for small robots, meaning that the requirement to deal with rough terrain increases as their size decreases, and that being small means more terrain is available to explore.

However, care should be taken not to assume that the Size-Grain Hypothesis is always true. Certain environments consist of many planar surfaces which appear rough to a particular sized object, and smooth both to those much larger and much smaller. For example: some areas of a boulder field are just the flat surfaces of individual rocks which at the scale of an ant are smooth.

2.3 Application possibilities

Having a specific application in mind, and its related performance requirements, will offer benefits to the development of a new device or product. It gives the designer a target to aim for. However care must be taken not to disregard early ideas by being too restrictive on eventual requirements. For the purposes of this work, a main application has been selected to guide development (see Section 3.7 p.123), but the challenges of, and applicability to, other potential uses is regularly considered.

There are a wide range of applications that require a mobile robot to move in rough environments, but similarities can be drawn between many of these that reduce the differences to only a handful of tasks. These include earthbound exploration and searching, space exploration, and transportation of payload. These potential applications will be discussed in series, with each commentary building on elements of the last.

2.3.1 Exploration and searching

When exploring or searching, we are looking to discover things of interest. These things might include biological life, special geological structures or features, or just to view something that is not visible from afar. These specific functions require particular

instruments, but all eventualities require accurate movement to specific locations within a terrain.

On earth, many regions have been explored purely by travelling to or through them using human or animal walking. People have created many wonderful vehicles including boats, aircraft and automobiles in an effort to increase the speed of movement and thus the range of exploration, leaving only the most remote, difficult-to-reach and harmful areas to be explored in detail. The entire earth's surfaces has been photographed from the air, but there are areas including volcanoes, the polar regions, cave systems, and dense forests that have yet to be explored from the surface. What links these unexplored areas is the complexity and irregularity of the terrain. Suitably capable robots could be used to explore such remote and inhospitable areas. A mobile robot that is to be used in such environments needs to have a capability and reliability that reflects the terrain and environmental conditions. Here there might be high or low temperatures, wet or humid environments, and all requiring an underlying mobility in rough terrain. Speed of travel is often unimportant when compared with actually reaching an intended destination, but small size would be of benefit, allowing intricate areas to be explored and easier portability to mission departure sites (Farji-Brener, Barrantes & Ruggiero 2004).

These terrestrial unexplored regions of interest are few, but there are regularly occurring natural disaster sites (earthquakes, landslides, hurricane damaged areas) and urban environments that all require searching and movement in rough terrain. If searching for buried survivors, then time and therefore speed is of critical importance, along with minimising size to allow exploration in small pockets of space, and minimising weight to avoid loading unstable structures. Movement in structured, but rough, urban environments is likely to be required by military applications, making both speed and silence important, along with a size and weight that reflects the confines of a building and easy deployability.

The cost involved in using robotic devices to carry out searching and exploration missions has not yet been mentioned. Where human lives are at stake, then cost relates to the price of human life. The allowable cost could therefore be very high. In reality, performance being equal, more low-cost robots could be put into disaster zones

than high cost one, possibly saving more lives. Pure terrestrial exploration tends to be conducted by research institutes; in these cases the cost should be minimised.

2.3.2 Space exploration

Space exploration could be considered as an extension of terrestrial exploration with some very important additional complications. A mobility system able to deal with rough Earth terrain would potentially suit applications on other rocky planets and bodies – the moon, Mars, Jupiter's moon Io, and the moon of Saturn, Titan, are all commonly mentioned for robotic exploration. Requirements with regard to energy efficiency and source, reliability, capability and mass are critical. The expense involved with sending anything of mass and volume into space means that minimising both is very important, so lightweight and deployable or small devices are best.

When compared with terrestrial exploration, space exploration is in its infancy. Telescopes have been pointed to all areas of the sky, and probes have reached outside our solar system. However, only a few people have been outside of our atmosphere and fewer still have stepped on the Moon. There have been a series of robotic vehicles that have ventured as far as Mars (Lindemann et al. 2006; Mishkin et al. 1998) and landings of mobile rovers have been attempted on asteroids (Yoshimitsu, Kubota & Nakatani 2006). The problems of planetary exploration require robotic and remotely-controlled vehicles that are able to deal with all types of terrain. Wheeled vehicles would be very much suited to covering large distances of comparatively smooth terrain, and thus could map the overall features. But robots that can deal with unstructured terrain have the ability to look into complex environments that may contain unique discoveries, and debris and material harbours not seen in smoother regions. For example, Schenker *et al.* (2000) say, "recent imagery of the Martian surface suggest that water resources, if they existed, may be concentrated near cliff edge outflows that will require aggressive mobility strategies to explore in depth."

Gravity is an important consideration in space exploration. When compared with robots that move along in continual contact with the ground, devices that launch themselves into the air (or a vacuum) to overcome particular obstacles would be at an advantage in lower than Earth gravity locations, achieving larger heights and ranges for the same

energy as smaller jumps on Earth. On Mars for example, jumps would be approximately three times as big as on Earth. On the moon the figure would be a factor of six. They would however be at a significant disadvantage in regions with more gravitational force, but no such rocky bodies with gravities larger than Earth exist in our solar system.

There are recent specific applications for robotic rovers on both the Moon and Mars. Significant success has been had with a series of wheeled NASA rovers (Figure 5 and Figure 6) that are/were operational on the surface of Mars (Lindemann et al. 2006). However, their landing site and exploration area are mostly smooth areas away from the potentially more geologically interesting “gullies, overflow channels and hydrothermal regions” which are “rough and sloped with dense rock distributions...and that present severe challenges to the mobility capabilities of current rovers” (Gat 1995)

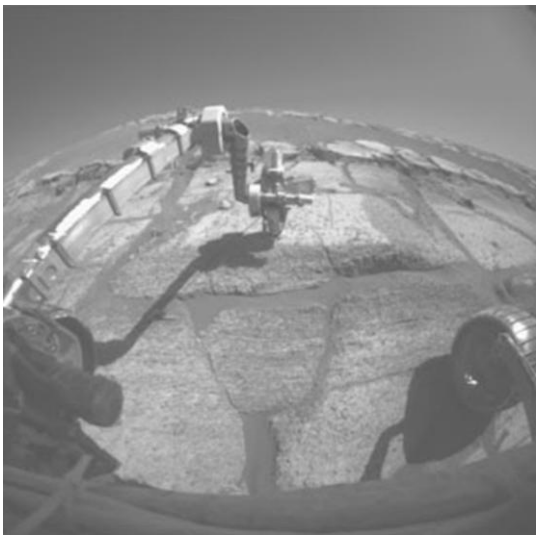

Figure 5 – NASA Mars Exploration Rover “Opportunity” placing its robotic arm onto a rocky outcrop (Tunstel 2007)

Figure 6 – The tracks of NASA Mars Exploration Rover “Spirit” across a region of the Gusev crater on Mars (Tunstel 2007)

Space agencies are resuming interest in the Moon for future manned space missions and as a location for sustainable long-term human presence. NASA suggests that the Moon will provide a useful stepping-stone for manned missions to Mars (Dunbar 2008),

and mobile robots are required to complement manned extra-vehicular activities (Studor 2010). The European Space Agency stated in 1994 (De Lafontaine & Kassing 1996) that a future Moon mission will require “a rover for excursions in the terrain”. The terrain in which this rover is expected to operate is close to the Moon’s South Pole and would allow “a rover to make excursions into the inner part of a permanently shadowed area”. They were very specific with regard to the type of terrain in that area, which has a maximum slope angle of less than 20° and rocks smaller than 0.5 m in diameter. The rover would be expected to travel at up to 1 km/h over a lifetime of 4 lunar days and have a return-home range of 50 km. An autonomous mode should allow for 0.25 km/h speed and localisation accuracy of 500 m. The rover would also be subject to a “thermal environment ranging from -160 °C in the shadow to +140 °C on the sunlit side”. Its operation must “account for the absence of any atmosphere and for the extreme adhesive properties of lunar dust”. “It must operate without the presence of the sun for up to 18 days in a ‘hibernation mode’ and have a mass less than 150 kg” whilst being able to deal with the particularly harsh <70 μm dust environment and the impacts from micrometeorites travelling at up to 1000 km/h (Schenker et al. 2000).

The Martian environment consists of topographic relief much greater than on Earth with highlands mainly in the southern hemisphere and lowlands in the northern (Schenker et al. 2000). Previous landing sites of Mars missions show that rocks cover 8-16 percent of the surface and range in size from pebbles to >1 m in diameter with soil similar to dense clay and silt-infused terrestrial soil covering 80-90 percent of landing sites (Schenker et al. 2000). Temperatures range from -143 °C to +27 °C, but this varies with chosen area of interest. Dust storms regularly occur with wind speeds up to 30 m/s.

The terrestrial testing of a device designed for interplanetary exploration is not easy. The requirement for low gravity environments means expensive experiments may need to be conducted in parabolic flight aircraft and drop chambers, and combined with work in vacuum and temperature simulating environments such as the one at the Space Power Facility at NASA Glenn Research Center’s Plumb Brook site (Schenker et al. 2000). In addition, adequately simulating Martian terrain for example, requires the use of sub-micron dust, which can be toxic to humans if inhaled (Gat 1995).

As an additional note, it may appear that space agencies tend to be quite reserved with the technologies that they finally launch, with great expense, into space. Only technologies that have had many years of proven performance on Earth are considered, due to reliability requirements. Their performance might only be adequate when compared with cutting-edge devices at the time of launch, but this may be due to the lengthy development and build-up time of space missions and the requirement to "fix" designs early on. The forthcoming European Space Agency ExoMars rover for launch in 2018 already has its mobility system fully selected and undergoing testing (Ellery et al. 2005). NASA evaluate designs on a Technology Readiness Level (Schenker et al. 2000) determining what can be launched and what is yet to be satisfactorily proven. So it remains that unproven and cutting-edge devices are generally terrestrial only. There are some possibilities to improve the perceived reliability of state-of-the-art devices by adopting a biologically inspired "sacrificial/redundant" mission strategy. This is where numerous inexpensive small and similar devices are sent in place of a single larger one allowing individuals to fail without jeopardising the overall mission outcome.

2.3.3 Transportation of equipment

The final application for a rough terrain device involves the movement of some payload over irregular rugged surfaces. This payload might be munitions, medical supplies, parts, aid or scientific equipment. A mobile robot that is unable to carry any payload is almost useless. Its internal control sensors may provide some information about its close surroundings or a map of previous obstacles and features along its route and that is all. So to perform a more useful task it is important that it is able to take, or to collect, some additional mass along on its journey. A large rover might be able to carry a significant additional payload with little or no impact on its performance. Tiny devices could have trouble with even small loads, so physical size is again an important consideration.

To improve the versatility of any new rough terrain robotic mobility system all of the above applications should be considered, resulting in a device that could provide a

solution to many applications. The definition of this wide-ranging application follows in Section 3.2, p.123.

2.4 Existing rough terrain robots

There are a wide variety of existing rovers intended to operate in rough environments. The completeness of each solution also varies hugely from paper-based design and predicted performance only, through proof-of-concept prototypes, to fully developed, tested and purchasable solutions. Solutions can be broadly broken down by type of movement and a summary of the techniques, challenges and drawbacks of each is discussed below. A fully quantitative (and qualitative) assessment and scoring method for a variety of rough terrain robotic devices follows in Chapter 3, p.115.

2.4.1 Wheeled

Most numerous among the land-based mobile robots are those running on wheels, and using rotary motion in general. Engineering and industrialisation has its very foundation in rotary motion, and many surface vehicles rely on the rotation of wheels. According to Dawkins (1996), wheels rely on a prior invention or specific environment – that of a road, rail or other hard-packed smooth surface. Animals are far more adept at crossing irregular terrain using only their legs as they provide a versatility that wheels cannot. A horse for example views a wheeled carriage as something that slows it down – not speeds it up. Animals' journey requirements are for hunting and escape, foraging or protecting a home, and if a "road" would help their cause then it would also help the cause of predators, or competing animals. Dawkins believes that if animals had intended to 'invent' the wheel then the construction of the road that would need to precede it relies on a sacrifice of effort away from the act of survival and reproduction. "Thus building a road that might help others will be penalised by natural selection" (Dawkins 1996). It is only with the advent of human society and foresight that roads, and in turn the wheel, become useful.

This does not mean that the wheel is useless for covering rough terrain, but that its initial requirement and discovery was meant for predominantly smooth, flat and hard surfaces. The obstacle-climbing ability of a conventional vehicle with four wheels, all of

which are driven and two of which steer and assuming no protruding bodywork, is fundamentally limited to obstacles of up to ½ wheel diameter. Increasing the diameter of the wheels would allow larger obstacles to be overcome at the expense of increasing vehicle size, and subsequently mass and power requirements. A conventional Ackermann steering arrangement requires forward and aft movement if a vehicle is to go around obstacles, as turning in place is not a possibility, and this limits manoeuvrability. Skid-steer of differential steering adds a turn-in-place capability, but this requires a short wheelbase and wide track.

For rough terrain applications an improvement in obstacle surmountability is required and this has been attempted by various researchers. Sandia National Laboratories developed a relatively simple articulating centrally-pivoted four-driven-wheel vehicle in the early 1990s that is capable of climbing obstacles 1.32 times the wheel diameter (Amai et al. 1994) and using differential steering (Figure 7).

Figure 7 – Photograph of Sandia Ratler variants. Ratler 2 being the largest (Amai et al. 1994)

Clever passive bogey arrangements consisting of many suspension-like components have been used in previous rovers [NASA Mars rovers, Sojourner (Figure 8), Spirit (Figure 6 & 10) and Opportunity (Figure 5 & 10), and the Bluebotics Shrimp (Figure 9)] to improve the single obstacle ability to around two wheel diameters (Lindemann et al.

2006; Mishkin et al. 1998; Estier et al. 2000) and allow for the climbing of stair-like structures. This is achieved by using hub-driven wheels that rotate and climb on all sorts of surfaces including vertical ones where the remaining wheels provide a virtual load contributing to the traction of the climbing wheel.

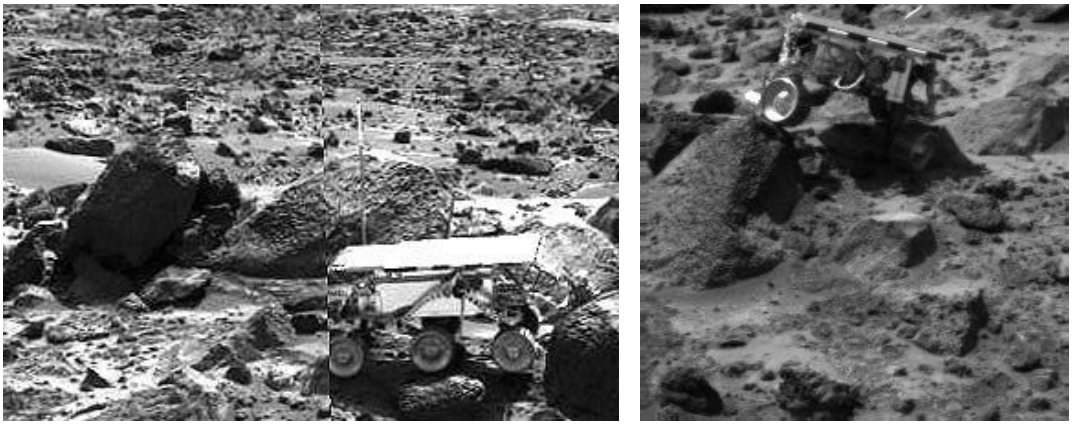

Figure 8 – NASA Sojourner rover climbing obstacles on Mars (black and white images taken from Pathfinder lander) courtesy NASA/JPL-Caltech

The NASA rovers are all six wheeled with the two fore and two rearmost wheels being individually steerable enabling a turn in place movement. The most recent Mars Exploration Rovers (MER) (Figure 10) have been tested at 0.046 m/s on flat compacted ground (Lindemann et al. 2006), but operationally they have achieved an average speed of only 0.0001 m/s (Opportunity) and 0.00004 m/s (Spirit) (NASA-JPL 2010). This figure is however an average speed over a period of almost six years, and takes no account of down time due to being stuck, hibernating, waiting for commands or being extraordinarily careful with movements in challenging situations. The huge difficulties of operating on another planet contributed highly to these robots' restricted rough terrain performance, but one can only consider all three rovers an enormous success given the data they have gathered and experiments they have conducted. In particular Spirit and Opportunity outlived their 90 SOL (Martian day = 24h 39m 35s) mission requirement many times over with the regular wind storms cleaning the dust from their photo-voltaic panels allowing for extended operation. The Spirit rover has recently entered a non-communicative state (as of March 2010), but Opportunity continues to operate and has travelled over 20 km of the Martian surface.

Figure 9 – Bluebotics Shrimp wheeled rover (Bluebotics 2010)

Figure 10 – NASA MER rover during mobility testing before launch courtesy NASA/JPL-Caltech

The Bluebotics Shrimp (Estier et al. 2000) is available for purchase as an inexpensive remotely-controlled robotic mobility system and its small size and impressive two-times wheel diameter obstacle surmountability makes it an interesting device. However, the positioning of additional payloads has an impact on performance and topple-ability and there is certainly no way for it to recover if it falls over. Only its single foremost and single rearmost wheels are steerable, which does allow for turning in place at the cost of dragging the four central wheels.

Although passive bogey arrangements provide improvements with little increase in control complexity, the limited capabilities of wheeled rovers in rough terrain has not gone unnoticed. The NASA Sojourner rover and Mars Exploration Rovers Spirit and Opportunity, although, as mentioned, proving very successful in their six-year-long-journeys, were “designed to negotiate moderately rough terrain under close guidance by human operators” (Gat 1995). This implies that they were never intended to be used in what NASA considers rough environments. They were designed for “mobility over continuous natural surfaces having area rock densities of 5 to 10%, modest inclines (<30% or 16.7 °), and a hard base with modest soft debris or sand pack” (Schenker et al. 2000). Terrains that might cause the wheels to slip, such as gravel and sand were, and still are, considered unsafe for traversal (Seraji 2003) by these wheeled devices

since becoming stuck results in the end of the mission. The Mars Exploration Rover Spirit is currently stuck in a sandy area after breaking through the crusty surface layer and has entered a hibernation mode with no hope of recovery.

What are of significant benefit with wheeled robots are the simplicity of design, the availability of established technologies and predictability of performance. Wheeled rovers can be, and for path planning and artificial intelligence research are often, based on toy remotely controlled vehicles. This has the advantage of a robust and inexpensive mobility system with often only two channel speed and steering control required.

2.4.2 Tracked

Tracked vehicles also rely on rotary motion, but the track around the driven wheels provides more traction, a lower surface contact pressure, and more buoyancy in soft substrates such as sand, snow and deep vegetation. A differential or skid steer system allows for turning in place, albeit with significant churning of the ground and losses of energy (Siegwart et al. 2002). The length and depth of the track and centre of gravity of the vehicle determines the height of obstacle that can be overcome, or the width of trench that can be spanned. Many proposed rescue robots are based on tracked mobility systems (Kang et al. 2005; Sheh 2005b; Suthakorn et al. 2008) as are highly-developed military robots which are widely used in active theatres (iRobot-Corporation 2009a; iRobot-Corporation 2009b; Foster-Miller 2008a; Trentini et al. 2007). Having two pairs of tracks, or additional tracked arms reaching forward or aft, improves rough terrain mobility and enables a level of recovery when the robot topples over onto its side or back. The speed of these tracked devices on comparatively smooth surfaces is far greater than any other type of rough terrain robot with the iRobot Warrior (iRobot-Corporation 2009a) being able to achieve 4 m/s. This is likely to come as a result of the significant development expenditure and the need of high speed for military applications.

Figure 11 – Foster-Miller TALON IV Engineer carrying a 39 lb simulated projectile (Foster-Miller 2008b)

Figure 12 – Foster-Miller SWORDS (TALON chassis) (Rose 2007)

The Foster-Miller TALON (Figure 11) tracked remotely operated vehicle is widely used in military applications and was the first robot to be used to explore the debris of the World Trade Centre disaster in New York. It is a simple twin track design, which limits its ability to self-right after falling over. It is, however, obviously robust. One was “blown off the roof of a Humvee in Iraq while the Humvee was crossing a bridge over a river. TALON flew off the bridge and plunged into the river below. Soldiers later used its operator control unit to drive the robot back out of the river and up onto the bank so they could retrieve it” (Foster-Miller 2008a). The TALON chassis provides a versatile platform for mounting a variety of manipulators and detectors for applications to deal with IEDs (improvised explosive devices), detect mines and X-ray baggage. A SWORDS version has been fitted with weaponry and is the first weaponized robotic platform to be used in military theatre (Figure 12).

The more versatile iRobot Warrior (Figure 13) and smaller Packbot (Figure 14) are also in use for military applications and differ from the TALON in having additional tracked forward arms which can be rotated to lie alongside the main chassis tracks during transport, or forward extending the effective chassis length and providing traction on surfaces above and ahead of the robot. The same arms enable them to recover after falling on their sides.

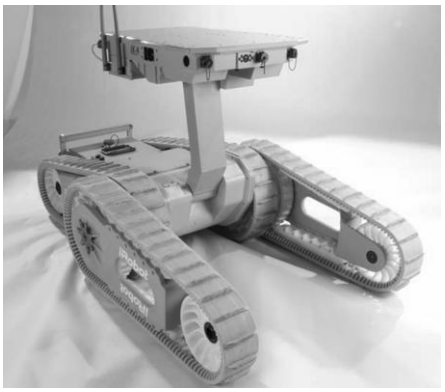

Figure 13 – iRobot Warrior 710 chassis (iRobot-Corporation 2009a)

Figure 14 – iRobot Packbot 510 (iRobot-Corporation 2009b)

The Robomotio Inc. Shape-shifting Tracked Robotic Vehicle (STRV) developed for Defence R&D Canada (Trentini et al. 2007) also uses four tracks, but along with track rotation here each axle-pair can be rotated allowing for some interesting movement modes (Figure 15). This solution is still undergoing development and as yet has not achieved the ruggedness of the Foster-Miller and iRobot offerings.

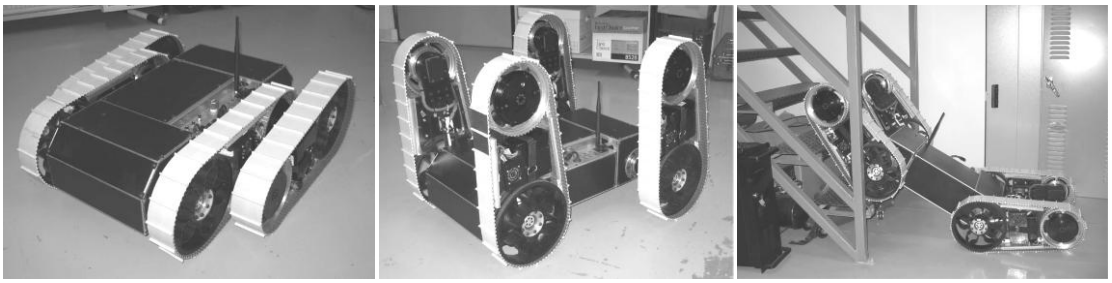

Figure 15 – Robomotio Shape-shifting Tracked Robotic Vehicle (Trentini et al. 2007)

A particularly cheap tracked rover that has successfully competed in the RoboCupRescue challenge, the Redback (Figure 16), is based upon a tracked radio controlled toy – the $100 MGA Tarantula (Figure 17). Similarly to the STRV, the toy has four tracked “flippers” which are controlled in pairs to enable the ground clearance to be changed on demand and stairs to be climbed. Even when modified into a robot with improved versatility, environmental sensors, individual arm control (providing an additional rotational swimming-like arm motion when the tracks are proving ineffective), and vision based mapping capability, a group of 100 such devices are certainly less

expensive than a single off-the-shelf military tracked robot. Its plastic construction means that cost effectiveness comes at the expense of reliability, but having numerous devices to perform a mission allows for failure of individuals.

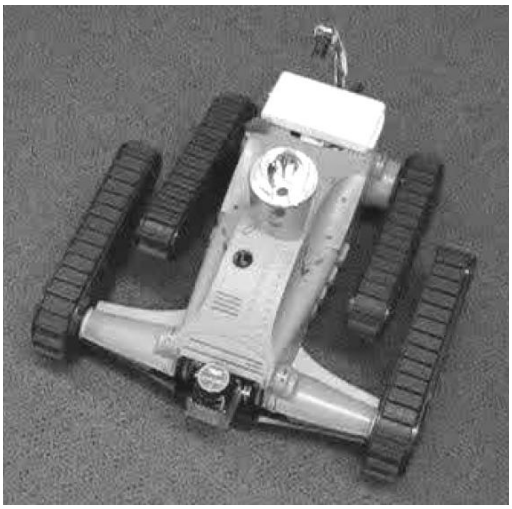

Figure 16 – The Redback robot (Sheh 2005a)

Figure 17 – MGA Tarantula remotely controlled toy (Sheh 2005b)

2.4.3 Walking

Legged robots are a large area of study due to the inspiring results available from the natural world. Insects and spiders, with their numerous legs, are very stable when moving through unstructured terrain, and roboticists have attempted to mimic their motion and performance. However, “few exhibit the speed and robustness seen in even the simplest animals” (Clark et al. 2001). The main reason for this is the way in which numerous legs, each with many degrees of freedom, are moved and controlled.

Lightweight engineering actuators suited to mobile robotic applications are typically rotary in motion, but legs generally require linear muscle-like actuators which can require large power sources, or are slow, expensive, in their infancy, or unreliable (Hollerbach, Hunter & Ballantyne 1992). Research into pneumatic, hydraulic and shape memory alloy actuators is intended to create biological style legs (Klute, Czerniecki & Hannaford 1999; Clark et al. 2001).

With many degrees of freedom per leg, the control of stable multiple legged robots is therefore complex, with each individual foot position being critical and requiring monitoring as the body moves forward over it. Reducing the number of legs does little to reduce complexity, as capable bipedal, and monopedal, robots require dynamic balancing throughout their movement (Wei et al. 2000; Okubo, Nakano & Handa 1996; Raibert 1986; Brown & Zeglin 1998; Paul, Dravid & Iida 2002). Legged animals are very capable in a variety of terrain, and that ability comes from their multitude of sensors, powerful actuators and mechanical advantage joints, large brains, or passive-adaptive systems. Many insects for example, use their entire spiny legs as “feet” and have evolved especially for movement in rough environments (TED Video Conferences 2007). Animals often have compliant members and structures in their legs to account for mistakes without the need for direct control.

A very impressive version of a conventional and complex walking robot is BigDog by Boston Dynamics (Figure 18). The device has been developed as a “mule” for transporting equipment usually carried by soldiers, and should be able to go anywhere a person or animal could walk or run. The device stands as tall as a large dog and is powered by a 15 hp 2-stroke internal combustion engine. Its four hydraulically actuated legs consist of three elements and animal like hip, knee, and ankle joints with compliance and impact dissipation designed in the foot. The balance and posture control is complex and adjustments to attitude and leg position occur at 200 Hz. Its ability in rough and unstructured terrain is remarkable, being able to deal with slipping on icy services, being pushed and bumped by external forces, along with the usual slopes and substrates that soldiers walk across.

Figure 18 – Photograph of BigDog walking up a snow covered slope (Raibert 2008)

There are some noteworthy exceptions to the “walking is expensive and complicated” tenet within robotics. A selection of simple robust open-loop walkers are being developed (Clark et al. 2001; Altendorfer et al. 2001) along with similarly simple pseudo-legged devices using conventional rotary driven “wheels” made of a series of radial leg-like elements (Jeans & Hong 2009; Lambrecht, Horchler & Quinn 2005).

RHex (Altendorfer et al. 2001) is a cockroach-inspired open-loop six compliant-legged walker and uses a series of gaits predominantly via a stable alternating tripod. The legs are simple in construction using a bow shaped form to allow for compliance, and each is controlled by a single rotating actuator at its sprawled hip connection with the body. This results in a relatively simple six degree-of-freedom walking robot with onboard power and performance comparable to tracked devices (McBride, Longoria & Krotkov 2003). RHex is able to surmount obstacles 1.5 times its leg length, and is able to deal with a wide range of terrains (grassy meadows, mud and sand, streams, stairs etc). It is currently being developed as a purchasable solution for military applications by Boston Dynamics, whilst work continues on research versions (Figure 19).

Figure 19 – Research RHex undergoing grain substrate testing in the Mojave Desert. Image courtesy of Kod*lab, University of Pennsylvania.

Mini-Whegs (Morrey et al. 2003) is a walking robot using a chassis and drive train similar to a wheeled vehicle, but with driven wheels made of 3 leg-like elements located at 120° to one another (Quinn et al. 2002). These wheels are named Whegs and "combine the speed and simplicity of wheels with the climbing mobility of legs" (Quinn et al. 2002) successfully surmounting obstacles approaching one Wheg-diameter in height. Mini-Whegs (Figure 20) is a two-axle version of the previous three-axle Wheg device (Quinn et al. 2001) and all four Whegs of Mini-Whegs are driven by a single drive motor operating at a constant speed. Direction control is similar to an automobile, with a steerable front axle (Figure 21) placing each foot of the front Whegs forward and to the left or right of the previous foot. Whegs' mobility over unstructured terrain is good, and its small size (50 mm high) results in the ability to overcome comparatively large, but numerically small obstacles of around 40 mm. The largest obstacles are only surmountable when the Whegs are in phase so the front axle therefore has a passive 60° slackness built in allowing for the feet to align on the obstacle and lift the robot onto

it. More recent variants have additional mechanisms on the body to provide a jumping movement that enables Mini-Whegs to clear obstacles up to 200 mm in height [(Morrey et al. 2003) and Section 2.6.7.5.3, p.87].

Figure 20 – Mini-Whegs 7 (Lambrecht, Horchler & Quinn 2005)

Figure 21 – Mini-Whegs steerable front Wheg (Lambrecht, Horchler & Quinn 2005)

In a similar vein to Whegs is IMPASS from Virginia Tech. An “Intelligent Mobility Platform with Active Spoke System” (Jeans & Hong 2009), IMPASS has similar legged rimless wheels (Figure 22), but here there are six elements and they are fully active with a complex hub mechanisms allowing for variable length. Both active-spoke wheels are driven from a single fixed axle with no differential. A differential is used in a conventional vehicle to ensure that during cornering the inside wheel is able to rotate slower than the outside one tracking a different radius path. The variable “wheel” diameter of IMPASS removes this requirement and therefore the feet are always aligned with one another (Figure 23). The variable leg length allows the centre of mass of the device to be carefully controlled, which is particularly useful when tackling obstacles because the mass can be raised directly to just over the lip of a step. The tail of the body provides tripod stability when walking with “1-1” walking, but more stable

movement is possible with “2-2” closed-loop steps locating two feet of each “wheel” on the substrate (Hong, Jeans & Ping 2009)[1]. The control and complexity of the device make it difficult for it to be inexpensive, relatively slow in movement and at this time tethered to a control and power station.

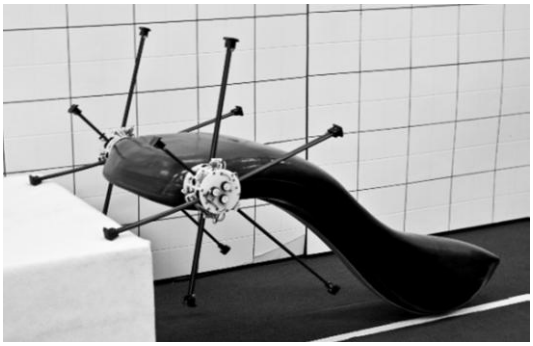

Figure 22 – IMPASS (Jeans & Hong 2009)

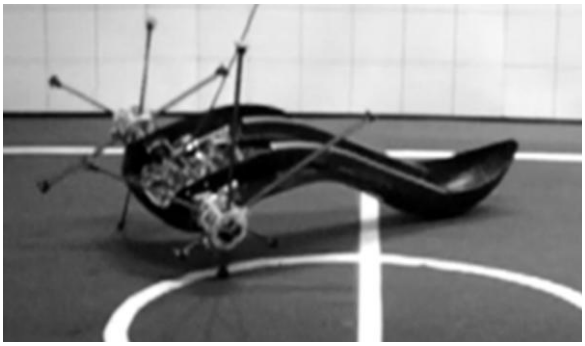

Figure 23 – IMPASS negotiating a turn (Hong, Jeans & Ping 2009)

2.4.4 Serpentine

Snakes and other limbless animals move using an undulating motion through a variety of terrains. There are only a handful of purely snake-like robots where the forward movement is provided by a series of body segments. Their potential unstructured terrain performance is likely to be good, with snake-like robots being able to fit through any opening the head can fit through, allowing exploration in tight enclosed spaces. Their rough terrain mobility has the potential to be remarkable, as fully active serpentine robots would be able to rear-up, lifting their head onto overhanging and unsupported structures. Such abilities will be ultimately related to overall snake length and the mass of each segment of the robot. However, rough terrain performance is generally unreported, and past review studies consider speed upon flat surfaces only (James & et al. 2009). It is likely that the challenge of building and controlling such multi-degree-of-freedom devices is of higher priority to researchers at this time. For

[1] The “1-1” walking gait of IMPASS is achieved when only one “foot” on each “wheel” is in contact with the surface for the majority of the time. A “2-2” walking gait is when two “feet” on each “wheel” are in contact with the surface at any given time. This “2-2” gait is only possible due to the ability to vary spoke length of each “foot”.

example, the GMD-SNAKE2 (Figure 24) (Klaassen & Papp 1999) consists of cylindrical body segments, each being able to control its position relative to the next in three-degrees-of-freedom. There is a ring of driven wheels around each cylinder. No mention of the robot's actual performance is made.

Figure 24 – GMD-SNAKE2 (Klaassen & Papp 1999)

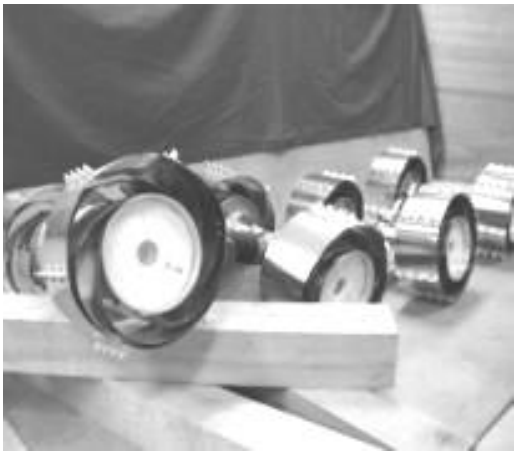

Figure 25 – Genbu robot (Kimura & Hirose 2002)

Other devices such as a train of Millibots (Brown et al. 2002) consist of tracked segments joined by single degree-of-freedom active joints, but again rough terrain performance is not discussed. Another simple tethered device, Genbu (Figure 25), this time with passive universal joints and identical segments consisting of a pair of driven wheels, has achieved an obstacle surmountability of 1.4 times wheel diameter (Kimura & Hirose 2002), but little additional performance information is reported.

A highly-developed serpentine solution, although not intended for movement in rough environments, has resulted in a snake/salamander inspired amphibious robot consisting of similar segments joined by actuated hinges. It allows for undulating crawling and swimming (Crespi et al. 2005). The addition of passive wheels (Figure 26) on each section allows for a wave-like motion on smooth surfaces, and alternative segments with lateral simple rotating legs (Figure 27) provide salamander-like walking on beaches. The terrain-covering performance of the device is not discussed in the literature.

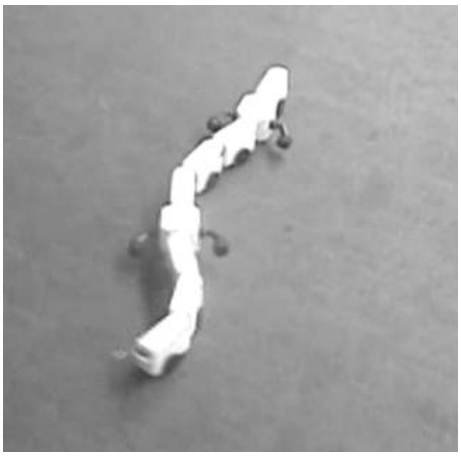

Figure 26 – Video still showing wheels in place on Amphibot during crawling (Video by A.Crespi, courtesy Biologically Inspired Robotics Group, EPFL)

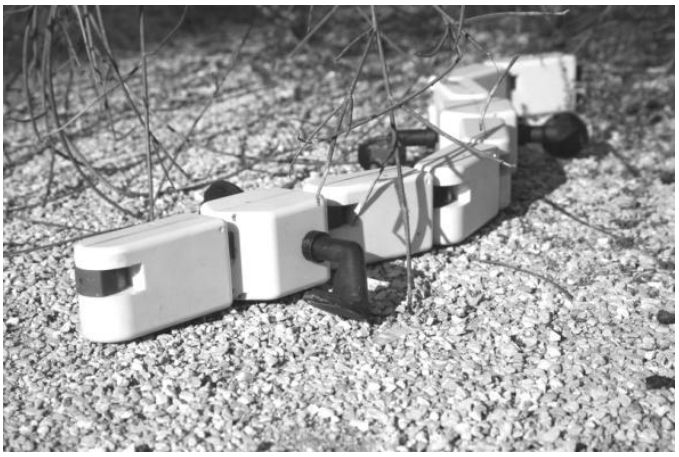

Figure 27 – Photograph of Amphibot with legged segments for salamander like swimming and walking (Photograph by A.Herzog, courtesy Biologically Inspired Robotics Group, EPFL)

The two OmniTread (OT) devices from the University of Michigan (Borenstein & Borrell 2008; Borenstein, Granosik & Hansen 2005; Granosik 2005) in either 4-inch (100 mm) (Figure 28) or 8-inch (200 mm) (Figure 29) diameters do have reported performances resulting, most impressively, in the ability to climb vertical enclosed spaces such as pipes. Each segment of the robot is square in section with a pair of belt tracks on each outer face (8 tracks per segment). Their mobility is remarkable; the robots are able to reach and pass through small holes above the ground in walls, and climb onto table-like overhanging structures. However the remote operation requires three operators due to the large number of degrees of freedom of the multi-axis bellow joints connecting the five or seven similar segments of the devices. Only the 4 inch diameter OT4 carries its own batteries onboard. The OT8 is tethered.

Figure 28 – OmniTread 4 (Borenstein & Borrell 2008)

Figure 29 – OmniTread 8 (Granosik 2005)

An interesting proposal for a serpentine-like robot design is based on a whole skin locomotion (Molfino, Zoppi & Rimassa 2007) achieved by a completely moving outer surface. The attempt here is to produce a robot body of segments where every surface contributes to movement making it impossible to get stuck on edges and protrusions in the environment. As yet nothing more than basic model of a single section has been produced (Figure 30).

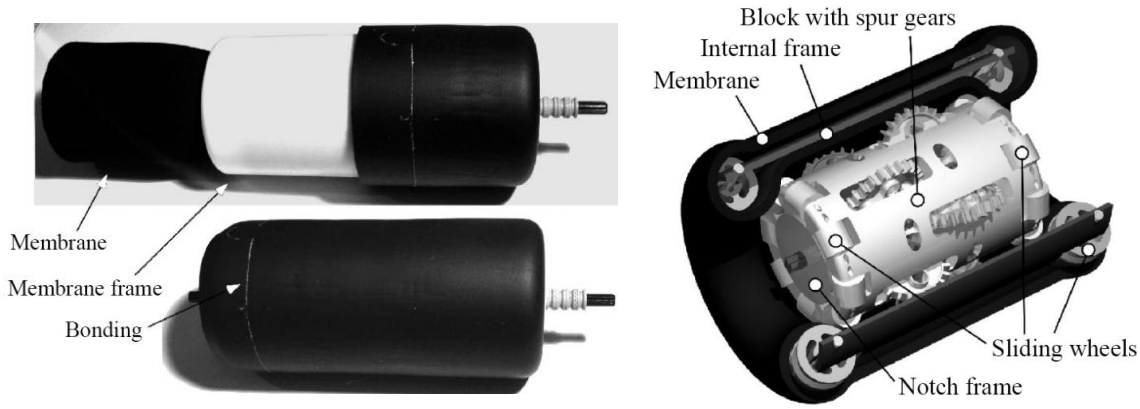

Figure 30 – Sliding membrane locomotion (Molfino, Zoppi & Rimassa 2007)

Related to serpentine robots are entirely self-reconfigurable robots consisting of a series of identical intelligent segments. These allow for multiple arrangements and many modes of movement such as wheel-like rolling, spider-like walking, and caterpillar-like crawling. M-Tran 3 (Figure 31) (Kurokawa et al. 2005) and Polybot (Yim, Duff & Roufas 2000) are a pair of reconfigurable devices that, similar to most

serpentine robots, have the potential to be capable in rough and unstructured environments. However, their control is very complex resulting in expensive solutions with little application-specific testing.

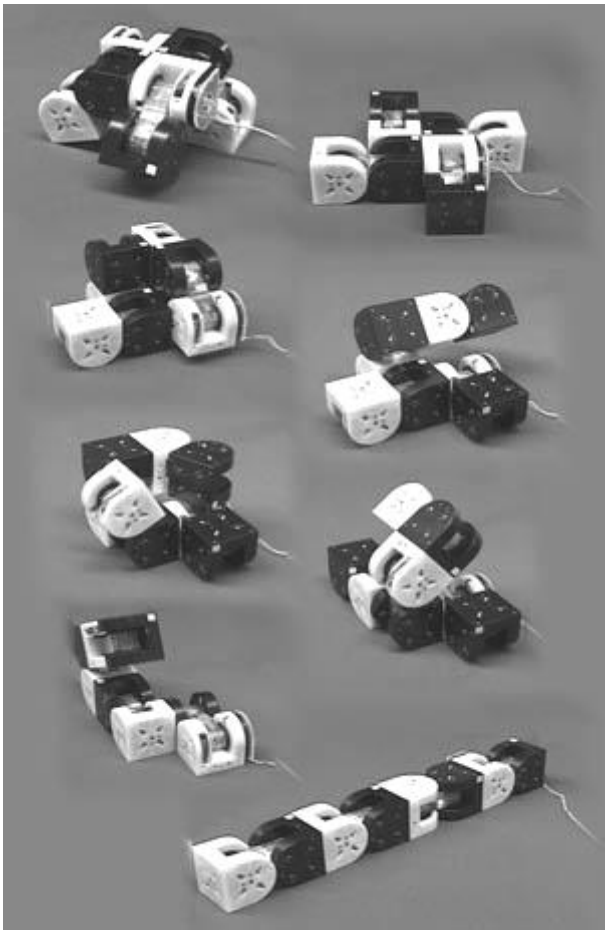

Figure 31 – M-Tran 3 self-reconfigurable robot consisting of 4 elements changing from a four-legged configuration to a snake-like serpentine one. (Kurokawa et al. 2005)

2.4.5 Jumping

Jumping is another movement adopted by a selection of robots for travelling across rough terrains. These will be discussed in Section 2.6.7, p.74.

2.4.6 Hybrid or Multimodal

Combining two different forms of movement together in one device can offer significant advantages if the modes achieve vastly different performances. Most of the rough terrain multimodal robots discovered complement a primary walking or wheeled movement for smoother terrains, with a jumping one for rougher areas. These robots are discussed in Section 2.6.7.5, p.85.

Some non-jumping robots with multimodal movements have been found. The reconfigurable devices mentioned previously (see Section 2.4.4) obviously have the ability to walk, crawl and roll depending on configuration, but here the difference in capability of each technique is small. All will produce similar speeds on smooth surfaces (unless long legs are built from a number of reconfigurable elements) with only crawling and walking being applicable to rough terrain, but again at similar speeds.

2.5 Nature's solutions to movement over rough terrain

The modern engineer is regularly drawn to the natural world for inspiration when considering problems that appear to have been "solved" by nature. This is a technique called biomimetics, biomimicry or bioinspiration, where the study and analysis of organisms ultimately results in an engineered analogue for a similar problem. The tools biology uses to build systems are fundamentally different from those used by engineers (Clark et al. 2001) and the evolutionary process and requirements for growth, reproduction and survival can sometimes mean that the natural "solution" isn't perfect. It is therefore up to the biomimeticist (or an engineer working in conjunction with a biologist) to interpret whether the natural solution is useful for their problem. Organisms often have interrelation between systems, so biomimicry is not simply a case of copying complete organisms or assuming an individual sub-system would work independently, but one of observation, understanding, reasoning and application of the most important extractable elements. For example, the motive system of an animal is inseparably linked to the respiratory and digestive systems for an energy source, so care must be taken when producing copied motive systems.

Movement in rough terrain is something land animals deal with regularly. Terrains include steep cliffs where yaks, mountain goats and snow leopards live, tree tops where monkeys climb, tall grasses where grasshoppers jump, marshland where frogs jump, and decomposing leaf litter where ants explore. Legs are the dominant feature of land animals, and appear to be almost perfectly adapted for each individual's requirement for movement across a surface. Land animals move to find food, escape from predators, pursue prey and find a mate. They do this by walking, running, hopping/bounding, jumping, crawling, climbing, flying and to some extent rolling (see Section 2.7.2). The type of movement depends greatly on the size of the animal and the terrain in which they need to move. In general larger animals fly, run and swim faster (in actual speed rather than body-lengths per second) than smaller ones, and when comparing animals of similar size, flying is faster than running which is in turn faster than swimming (Alexander 1982). The net cost of transport (metabolic energy needed for locomotion per unit mass) illustrates that for running mammals, it is the same for all speeds, but that in general larger animals have lower costs of transport than smaller ones; and that for animals of similar size, swimming is most economical, then flight and finally running (Alexander 1982) with the spread becoming wider at smaller sizes. Ignoring swimming which has the benefit of a reduced mass-related gravitational force, the difference between flight and running is mainly due to the huge speeds possible in flight rather than the power requirement [which is very high for flight (Alexander 1982)].

No information has been found that relates the most successful (numerous) animals of a particular size, to the movements adopted in a particular type of rough terrain, but (as mentioned previously) it has been shown that as size reduces, the terrain becomes comparatively rougher [(Kaspari & Weiser 1999) and Section 2.2]. Thus the movements adopted by the smallest animals are likely to be more applicable to mobile rough terrain rovers than those of larger animals. At decreasing sizes, walking is obviously very popular, but it appears that combining walking with movements such as jumping and flying to clear obstacles and improve terrain surmountability is of significant benefit. Without an in-depth ecological study across a range of terrains and animal sizes it is not possible to confirm this hypothesis.

Walking is predominant in biology, but the control requirements to mimic multi degree-of-freedom legs generally make its robotic application quite complex. Wheeled movements are obviously common in robotics, but as mentioned previously, from a biological perspective circular motion is rare (Garcia-Paris & Deban 1995; Henschel 1990; Ovaska 2002; Caldwell 1979; Brackenbury 1997; Full et al. 1993). Flying is power hungry and the robotic requirement to be on the surface for most application tasks would require regular take-offs, which require even higher power levels, and potentially dangerous landings. Jumping is a technique that allows for some of the obstacle-covering capability of flying, but without the continuous power requirement associated with flying. Its periodic and cyclical motion means that the average power required is lower, but its average speed is also low. Therefore using biology to inspire a movement solution for rough terrain would suggest that jumping has potential for success, particularly when combined with another movement. If compared to biology, whose jumping organisms are relatively popular in rough terrain, the numbers of existing solutions for jumping in robotics is few.

The number of multi-modal robots combining jumping with another movement is fewer still, and only a single tethered device (Hirai, Matsuyama & Nakanishi 2007) has been presented that uses the same structure to deliver both movements as legs do for organisms. Natural organisms achieve multiple modes of movement in a whole variety of ways. For example, considering walking and running as one mode, legs (and arms) are also used to achieve jumping, climbing and swimming in a whole range of animals. This improves versatility for little additional cost in terms of increased mass. Such a solution is non-specialized and gives only adequate performance in each movement. It can be seen that, with specialization toward one movement, a sacrifice in another is often the result. A locust for example is very specialized for jumping with a pair of very large legs. As a result they are awkward walkers.

2.6 Jumping

Jumping is clearly of benefit when producing a robot for use in rough terrain and was used by the robots developed for this thesis. Thus an introductory study of jumping is

presented here. This includes looking at jumping in nature and existing jumping (and jumping multi-modal) robots.

2.6.1 What is jumping?

For an object to jump vertically, a suitably massive sub-component of its structure needs to be extended away from the remaining mass of the object. Through the conservation of the momentum contained within this large moving mass, the object will lift from the substrate when it is fully extended. This is best visualised diagrammatically (Figure 32).

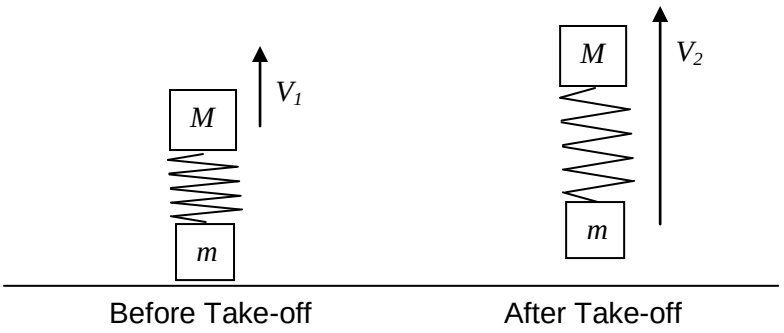

Figure 32 – Jumping in general

Before take-off, the larger mass, M, is accelerated upward by a compressed spring or contracting muscle, reaching a velocity of V_1 just before take-off. At that point the spring is fully extended and the smaller mass, m, begins to move such that a short time after take-off both the masses are travelling at the same velocity V_2. Assuming no losses through spring oscillation and a zero-mass spring, momentum is conserved and the following equation applies instantaneously after take-off.

$$M \times V_1 = (M + m) \times V_2$$

Equation 2 – conservation of momentum

This is true for all jumping, so to maximise the height of a particular jump V_1 and the ratio $M{:}m$ should both be maximised. In reality, significant losses occur since the

masses are not rigidly connected after take-off. This comes from the over extension and oscillations of the spring. These losses can be minimised if $M >> m$.

2.6.2 Projectile motion

When considering useful jumps, the equations of projectile motion are important. These equations take no account of air resistance. (It has previously been shown that air resistance is "completely insignificant" for non-flying animals larger than a Bushbaby (*Galago senegalensis*) - a small primate weighing approximately 0.25kg (Schmidt-Neilsen 1984).)

Maximum range:

$$d = v^2 \times \frac{\sin 2\theta}{g}$$

Equation 3 – maximum jump range

Where d = distance covered, v = launch velocity, θ = launch angle, g = vertical acceleration due to gravity. This assumes that landing is at the same height as take-off; That is the robot is not jumping up or down hill.

Maximum height:

$$h = \frac{(v \sin \theta)^2}{2g}$$

Equation 4 – maximum jump height

Where h = maximum height, v = launch velocity, θ = launch angle, g = vertical acceleration due to gravity.

From Equation 3, it can be seen that a take-off angle of 45° gives the maximum range between take-off and landing sites of the same height, and Equation 4 shows that an angle of 90° will (unsurprisingly) give maximum jump height. The direction of the jumping thrust should be parallel to a line joining the object's centre of gravity and the

centre of the contact patch of its foot to ensure that no unwanted rotational motion is introduced. Ideally therefore, for a long range jump the centre of gravity should be accelerated along a line 45° to the horizontal through the contact patch of a jumping device to maximise the distance covered. A steeper angle should be used for overcoming large obstacles at the expense of horizontal range.

2.6.3 Energy in jumping

The following equations relate different forms of energy, and, since energy is conserved, it is possible to use these equations to determine the performance of jumping prototypes.

Kinetic Energy:

$$K.E. = \frac{mv^2}{2}$$

Equation 5 – kinetic energy

Potential Energy of suspended mass:

$$P.E. = mgh$$

Equation 6 – gravitational potential energy

Where v = velocity, m = mass, g = vertical acceleration due to gravity, h = height.

In any organism or machine, the height and distance of the jump depends on the velocity at take-off. Velocity is dependent on energy produced, E, derived from Equation 5:

$$v = \sqrt{\frac{2E}{m}}$$

Equation 7 – take-off velocity

Jump distance, d, in terms of energy is defined by the following equation from Equation 3:

$$d = \frac{2E \sin 2\theta}{mg}$$

Equation 8 – jump range in terms of energy

Jump height, h, is directly related to energy by the following equation from Equation 6:

$$h = \frac{E}{mg}$$

Equation 9 – jump height in terms of energy

This means that to maximise both distance and height, the energy to mass ratio must be as large as possible. Again this is unsurprising. The physical size, although often linked to mass due to material density, has no effect on the jump unless air resistance is considered.

2.6.4 Landing (or crashing)

The subsequent impact with the ground is also an important consideration. The above energy equations are valid in reverse with the potential energy at peak height being converted into a vertical impact velocity with the ground as shown in Equation 10, assuming no energy is lost due to air resistance and that the ground level is the same as at take-off.

$$v = \sqrt{2gh}$$

Equation 10 – vertical landing velocity

This velocity and resulting kinetic energy (Equation 5), combined with any energy resulting from horizontal movement, must be dissipated by the structure of the landing device. Legs or extremities can be used as shock absorbers to minimise the forces on the important internal organs and components. Larger animals such as toads and frogs

use their legs to decelerate their bodies (Dagg 1977) or knowingly jump into soft substrates such as grasses and ponds (Biewener 2003), but smaller animals often crash land directly onto their bodies (Paskins 2007). However, with reduced impact energies due to smaller mass and the additional effects of air resistance decreasing the impact velocity, they survive. In animals, critical internal organs are also softly suspended by tissues acting as springs and dampers to avoid the transmission of forces directly into them. Jumping up onto something minimises the change in height after the peak of the trajectory thus also reducing impact energy.

Landing also gives the opportunity to recover some energy used in the previous jump. This is something that hopping animals such as kangaroos have perfected (see Section 2.6.6.5.1). Careful positioning of legs or feet before landing and suitable energy absorbing mechanisms allow some of the kinetic energy before impact to be recovered rather than dissipated.

2.6.5 Summary

In summary successful jumping requires that:

- The ratio of body mass to “leg” mass is maximised.
- The line of “foot” contact to centre of gravity (the launch angle) at take-off should be around 45 to 60° to overcome obstacles.
- The overall energy to mass ratio should be large to maximise jump height and range.
- Consideration as to what happens when landing should be taken into account by protecting important components.

2.6.6 Jumping in nature

2.6.6.1 Continuous hopping

Animals that adopt continuous hopping are usually moving over comparatively smooth surfaces, but at high speed using a bounding motion. Kangaroos (*Macropus*) are a

prime example of this jumping mode and can travel quickly over long distances with relative ease (Alexander & Vernon 1975). This comes from their regenerative hopping where around 40% of the kinetic energy of landing is stored in tendons in the legs ready for use in the subsequent jump (Alexander & Vernon 1975). This form of jumping is very much suited to high speed travel over flat terrain, but this leads to high continuous power requirements even with the regenerative hopping.

2.6.6.2 Pause-and-leap jumping

As a prime example of pause-and-leap jumping, grasshoppers appear to jump in semi-random directions when escaping from predators, falling on their sides when landing and getting back to their feet before launching again. This pause-and-leap jump is a much slower method of covering large distances than a hopping approach, but needs far less power input. The jump energy is stored during the pause in a mechanical or chemical system and released as a sudden burst - the leap. Upon landing the process repeats. The lengthy rest period allows time for recharging and for simple direction control to be employed (Bennet-Clark 1975).

It is this pause-and-leap jumping approach that seems to be particularly suited to small inexpensive robots. Jumping robots should be able to clear obstacles larger than themselves with relatively simple construction and direction control. This should enable a jumping exploration robot to be cheaper than a similarly-capable conventional walking robot, allowing many to be used in place of a single robot, and for a semi-sacrificial team mission strategy to be employed.

The details of the specific energy storage systems in a range of jumping animals and other natural explosive movements will be discussed below, but general consideration should first be made of the issues surrounding jumping by organisms.

2.6.6.3 Comparative jumping performance in animals

Much of the work presented here has been adapted from Bennet-Clark (Bennet-Clark 1977) - a key piece of work on jumping animals.

Animals use muscles as their primary source of jump energy. When jumping vertically, and neglecting air resistance, the height attained by any object is dependent on the initial upward velocity v (Equation 11). For a given take-off velocity, the size or weight of an object has no effect on jump height (it does however have an effect in relation to the potential for damage when landing).

$$h = \frac{v^2}{2g}$$

Equation 11 – jump height

Where h is jump height, v is vertical launch velocity, and g is the acceleration due to gravity.

For an animal to jump to 1 m in height, it must achieve a vertical velocity of 4.4 m/s just as it leaves the ground (from which point it will decelerate to its peak height). This is true for all animals and any other device that might jump. For small animals, which accelerate through a distance comparable to their size, this means that the power that needs to be delivered by their muscles is far larger than muscle can attain. Muscle performance is similar across the entire animal kingdom and the proportion of body mass made up by muscle is also comparable, meaning that all animals of all sizes should therefore jump to the same height. This in turn means that for small animals to perform the relatively higher jumps they do, muscle energy must be stored somehow ready for rapid release as a jump.

In any organism or machine, the height and distance of the jump depend on the velocity at take-off (see Equation 3 and Equation 4, p.51). Velocity is dependent on the energy produced (see Equation 7, p.52). Equation 8 and Equation 9 (p.53) mean that to maximise both distance and height, the energy to mass ratio must be as large as possible. Maximising the energy to mass ratio can be achieved by increasing energy or minimising mass.

Increasing the energy requires stronger structures to react against the higher forces involved. But improving strength generally increases the mass. Unless a stronger and lighter structure can be produced, this will not improve the energy to weight ratio.

Reducing the mass of a structure or skeleton often reduces strength, so the force should remain constant below a strength threshold throughout the time of the jump so as not to cause damage. Thus the velocity should rise linearly over this time due to the constant force. The power, or force x velocity, should also rise linearly to a maximum value until take-off. This is summarised in Equation 12 relating power, mass and length to jump height, h, in animals (Bennet-Clark 1977):

$$h = \left(\frac{2sP}{m} \right)^{\frac{2}{3}} \times \frac{1}{2g}$$

Equation 12 – jump height in terms of power and acceleration distance

Where s = acceleration distance and P = peak power output, in addition to the terms specified previously.

In animals, it can be reasonably assumed that s is proportional to the animal's length, and P is proportional to muscle mass which is in turn proportional to total mass. Thus h is proportional to $length^{2/3}$.

Figure 33 is based upon these equations above and is an adaptation of a graph first presented by Bennet-Clark (1977) to illustrate how different animals perform when jumping. The horizontal lines show energy density and the sloping lines are a measure of power per unit weight. The power to weight ratio is of importance when looking at animals, since the limit for direct muscle action is around 100 W/kg (Bennet-Clark 1977). Animals performing substantially above that use more power than their muscles can deliver directly, so they must store muscle energy and release it through a power amplifier in a similar way to a catapult.

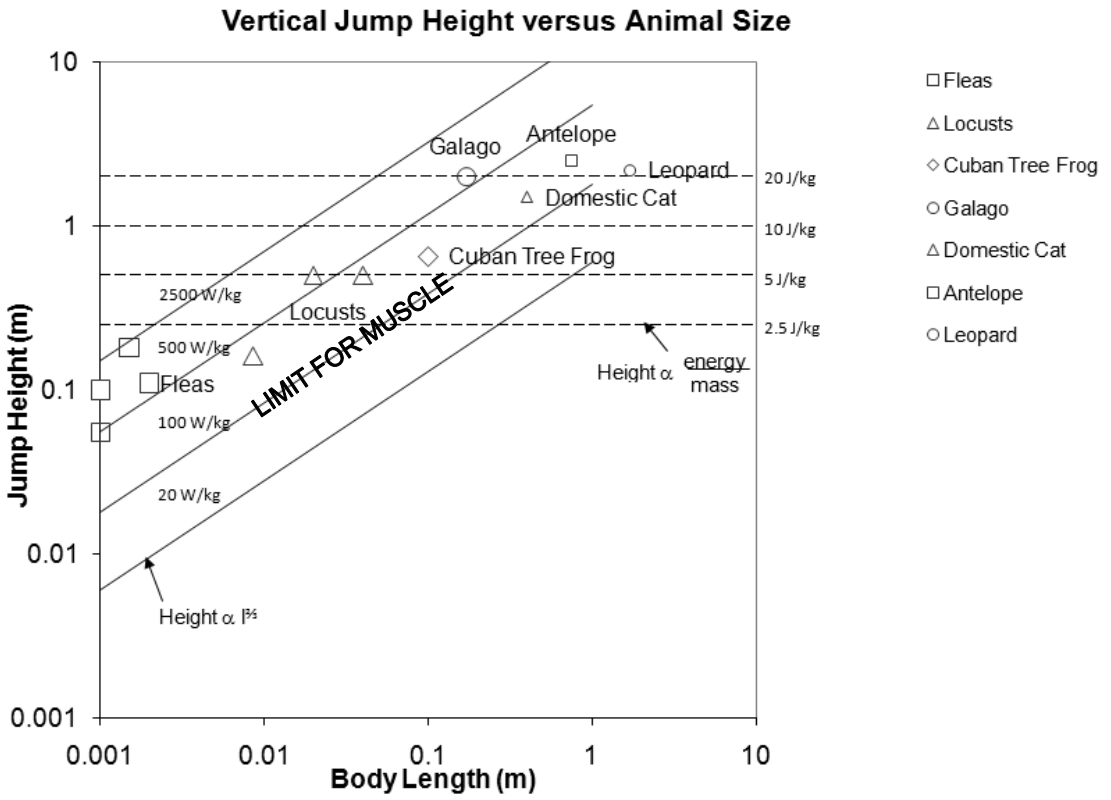

Figure 33 – Jump height against body length for a variety of animals [adapted from (Bennet-Clark 1977)]

Those animals that appear to excel at jumping (e.g. fleas and locusts) do not attain the absolute heights of even the average jumpers many times their size. This means that their energy density (energy per unit mass) is smaller, but to jump at all their power densities must be far larger. This implies that jump impressiveness, where the jump height is many times the height of the animal, is dependent on high power density – and these high powers can only be delivered through energy storage mechanisms.

Nature evolves toward different jumping solutions depending on the requirements of a specific organism – a flea jumps vertically in an attempt to reach a passing host which it may or may not be able to see, whereas a locust tries to achieve range to escape a predator, move on to the next plant, or initiate flight. It is here that care must be taken not to copy a particular organisms jumping mechanism without considering the intended application. For example, fleas are impressive jumpers when looking at the

ratio of jump height to animal height, but actual numerical height is small and they have little jumping range.

2.6.6.4 Energy storage in nature

Large animals have the advantage of being able to use muscle work directly via skeletal mechanisms to generate the forces required for jumping. But as discussed, smaller animals have to use their muscle energy indirectly through an energy store. Just as in engineered mechanical energy storage systems, nature uses the compression, stretching or bending of a specific elastic material in conjunction with predominantly muscle-driven mechanisms to store energy for jumping. This potential energy stored within a material allows for rapid release thereby providing the power required for small animals to jump. This spring-like material often makes up a very small percentage of the body mass of an animal [0.4 % of the weight of a kangaroo and 0.3 % of the weight of a locust, for example (Bennet-Clark 1977)], and yet stores enough energy for a significant jump. Just like Hookean springs (see Section 2.6.8.1.1), as the stored energy is returned to the system, the force falls as the material regains its original shape. When such a material is used in conjunction with a mechanism that provides variable mechanical advantage, the profile of the release force can be tuned in such a way to as to maintain the force during release. This allows the system to approach the ideal condition of a constant jump impulse – i.e. constant force throughout the time for release until take-off.

However, this rapid energy release has the potential to damage the muscles attached to the energy store, so catches are used in many insects (Bennet-Clark & Lucey 1967; Heitler 1974) to ensure that the contractor muscle has time to become slack before release is triggered. It is likely that similar catches are not required in larger animals as the time period for extension is longer than that required for the relaxation of the muscles.

A review of some of the extraordinarily diverse ways in which individual organisms have approached the issue of energy storage for explosive release follows.

2.6.6.5 Jumping animals

2.6.6.5.1 Kangaroo (Macropodidae)

Although considered by many as a regenerative hopping animal, kangaroos do store energy between jumps. They use perhaps the most straightforward way of storing energy: large tendons in the legs of the kangaroo allow around 40 % of the energy required for each hop to come from elastic storage (Alexander & Vernon 1975).

The regenerative aspect of successive jumps has a huge impact on a kangaroo's efficiency of movement. With most animals, the energy required to move at high speeds is greater than that required at low speeds. However for the kangaroo and other hopping animals, the energy required to move at high speeds is the same (or sometimes less) than that required at low speeds (Alexander & Goldspink 1977). This is a result of the increase in distance covered for each hop in conjunction with the storage of jump energy between landing and subsequent take-off.

2.6.6.5.2 Dog (Canis familiaris)

Although very much specialised for running, there is evidence to suggest that the dog stores energy when required to jump far or high. Two of the main muscles (ankle and knee extensor) in the leg behave essentially as passive elastic bodies, probably storing energy in their associated tendons, while the hip extensor operates directly during the jump (Alexander 1974).

2.6.6.5.3 Bushbaby (Galago)

The highest reliably reported jump recorded for a 0.25 kg Bushbaby is 2.25 m (Hall-Craggs 1965). Although the apparent specific power output of such a jump (2350 W/kg) implies the presence of a sophisticated energy storage and release system, studies suggest that the muscle power amplification system simply relies on a combination of sequential movements; "countermovement, catapult, and squat-jumping with compliant tendons" (Aerts 1998). The amplifier appears to be principally located in the main muscle-tendon extensor complex (Aerts 1998) of the upper leg.

2.6.6.5.4 Bullfrog (Rana catesbeiana)

Like many of the jumping animals, bullfrogs are able to jump higher and further than should be possible given their muscle power. Therefore they must use some sort of amplification to perform such jumps. Researchers have proposed that the energy stored within an elastic mechanism (likely to be a tendon) in series with the main jumping muscles in the leg, combined with a variable effective mechanical advantage mechanism within the leg results in a system that is able to deliver the required power (Roberts 2003). Unlike small insects which store all the jump energy delivered by the muscles, the leg muscles in frogs are used directly during the jump, but are uncoupled from the movement through elastic elements that allow the muscle to contract at an optimum power. By varying the effective mechanical advantage, the force output of the system can be controlled, which also provides some level of inertial catch when acting with poor mechanical advantage at the beginning of the release (Roberts 2003).

2.6.6.5.5 Locust (Schistocerca)

Locusts jump to escape from danger, launch themselves for flight, or simply as a more rapid form of locomotion than walking (Heitler 1974). All these indicate that jump range is the important characteristic. Locusts are highly specialised for jumping. Prior to a jump, the insect crouches for a few seconds before rapid extension of its metathoracic tibiae. Locust legs are long when compared with body length and the location of the locust's centre of gravity means that there is little torque generated (indicating lost energy) when jumping (Bennet-Clark 1975). Owing to the locust's size, the power required to achieve the required take-off velocity for their impressive jumps indicates that muscles are not used directly. Thus the locust has evolved a novel catapult and catch mechanism to provide energy storage and subsequent rapid release.

The rapid extension of the metathoracic leg is made possible by structural specialisations at the femoral-tibial joint (knee) shown in Figure 34. These specialisations consist of two elements allowing the force of the large extensor muscle to be held by the much smaller flexor muscle; the first is the differing (and continually changing with joint angle) lever ratio of the two muscles, and the second is a mechanical lock which engages on the flexor tendon when the leg is fully flexed (Heitler

1974). The lever system is based entirely on geometry and the apparent pulley-wheel-like nature of the lump over which the flexor tendon runs. This gives a varying ratio of 260:1 in favour of the flexor muscle, when the leg is fully flexed, to a ratio of 35:1 in favour of the extensor muscle at ~90° extension (Heitler 1974). The locking mechanism relies on the combined engagement of a dome shaped cuticular lump [subsequently referred to as Heitler's lump (Bennet-Clark 1975)] on the tibia that engages with a complementary depression in the femur, and the activation of the flexor muscle and the associated two arms of the flexor tendon fall into grooves either side of the cuticular lump. In this position, the tibia is locked against the femur, and considerable tension can be generated in the extensor muscle and associated tendons without the tibia moving (Heitler 1974), storing energy in elastic elements of the extensor system (Brown 1967). These elastic stores include stretching of the extensor tibia apodeme and the bending of a cuticular semilunar process (Bennet-Clark 1975). The lock is released only by the relaxation of the flexor muscle once most of the work from the extensor muscle has been stored in the elastic elements of the leg. If the Heitler's lump is surgically removed then the range of a locusts jump is much reduced and the "click" sound is no longer evident (Bennet-Clark 1975).

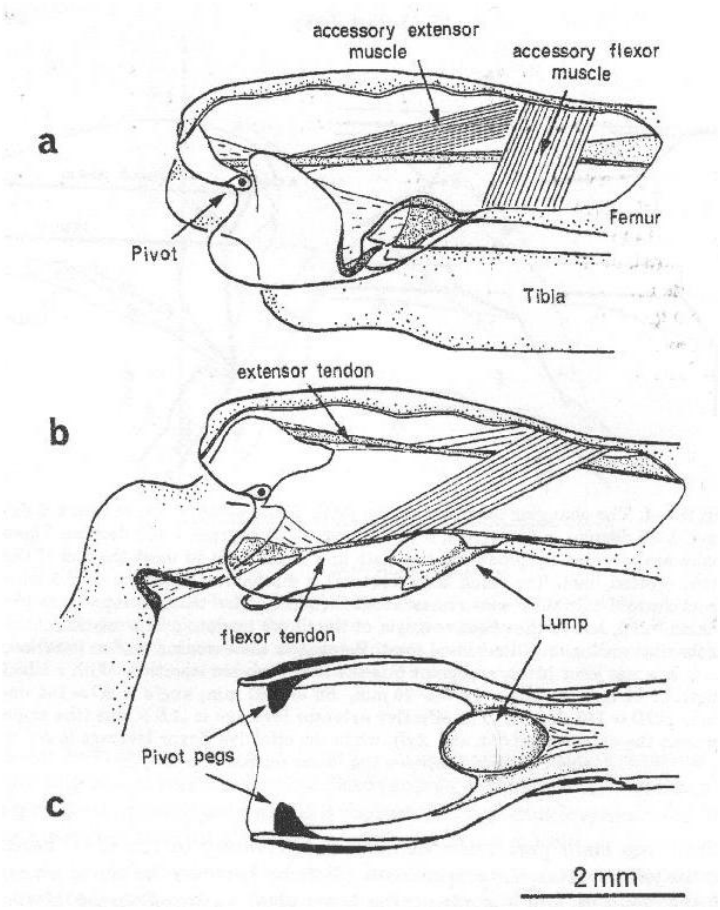

Figure 34 – Locust knee fully flexed with the lock engaged (a) and partly extended with flexor tendon running over Heitler's lump (b) (Heitler 1974)

2.6.6.5.6 Fruit-fly larva (Ceratitis capitata)

A maggot's "walking" movement is generally slow and energetically costly, but the fruit-fly larva can achieve a 200-fold increase in speed by jumping. It is an example of the few jumping soft-bodied organisms (Maitland 1992). The larva achieves a jump by arching itself such that its head is in contact with the tail allowing a pair of mouth hooks to grip the posterior forming a tight loop. Tension is then built up in the helical muscles of the body wall to power the jump and at peak contraction the loop becomes unstable, buckles and flattens toward the ground (Figure 35). Disengagement of the mouth hooks allows the tail to contact with the ground and the body to straighten launching the larva into the air (Figure 36). The cheese skipper (*Piophila casci*) performs ~20 cm high jumps in a similar way (Mote 1914).

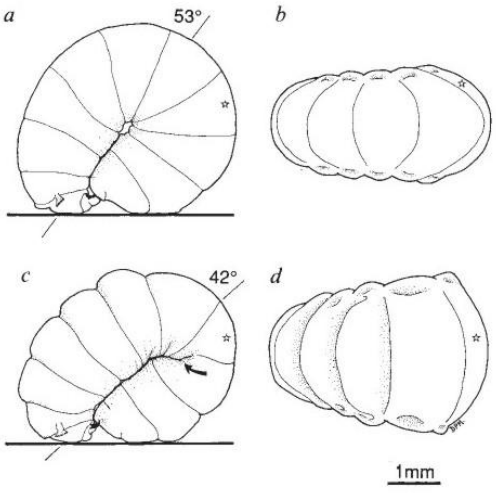

Figure 35 – Fruit-fly larva storing energy in its body through buckling (Maitland 1992)

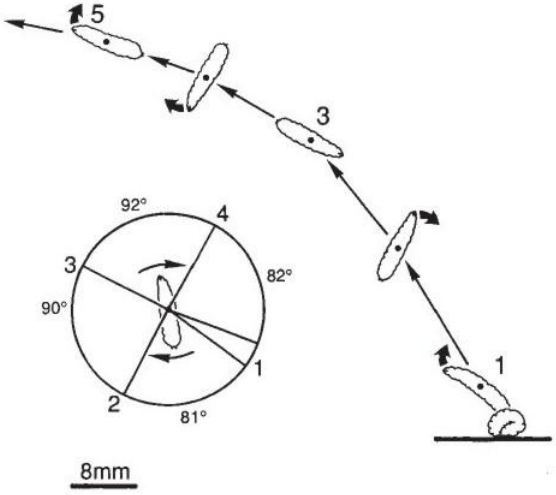

Figure 36 – Jumping trajectory of fruit-fly larva (Maitland 1992)

2.6.6.5.7 Click beetle (Coleoptera elateridae)

The click beetle takes its common English name from the noise it makes when jumping. Unlike other jumping insects, it does not use its legs to provide the energy for take-off, but the interaction between its body segments. The click beetle jumps from a

position on its back by arching its back and then rapidly “jack-knifing” its body (Evans 1972) (Figure 37), using the momentum of its now moving prothorax to launch itself from the substrate. This rapid motion is possible only through a catch mechanism that enables energy to be stored within the series elastic elements associated with a large muscle inside the prothorax, and in the bending or deformation of the cuticle (Evans 1973). The catch is made from a friction hold generated between a step on the peg of the prosternum, and the edge of the mesosternum (Evans 1972). When released, this peg slides down a track in the mesosternum. This catch can remain locked for as short as the time required to generate tension in the jumping muscle (<0.5 s), or for many minutes, indicating that there is likely to be a trigger involved, although its operation has not been discovered (Evans 1972).

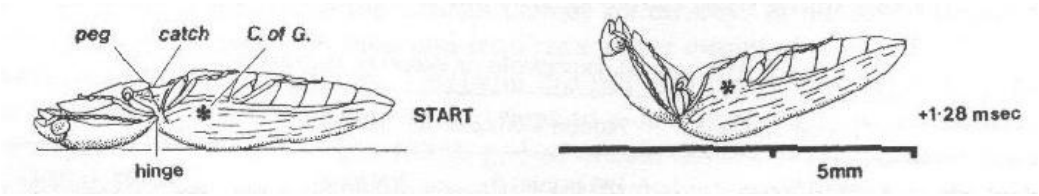

Figure 37 – Click beetle prior to jump (left) with peg locked against edge of mesosternum and 1.28ms later illustrating rising centre of gravity (Bennet-Clark 1976)

2.6.6.5.8 Flea beetle (Blepharida sacra)

The flea beetle jumps much like a flea, for escape or simply locomotion. The jump of the flea beetle relies on the storage of the energy from a pair of tibial extensors within a special scroll like structure called the metafemoral spring located within the hind femur (Ker 1977). The metafemoral spring is made from a natural composite consisting of well-oriented fibres of the polysaccharide α-chitin in conjunction with a protein matrix (Furth 1982). This makes it difficult to replicate or produce artificially. Energy storage occurs in the unrolling of the scroll-shaped spring (Figure 38) which exhibits a non-Hookean softening response (Ker 1977). A catch mechanism is also present which relies on the over-centreing of the femoral-tibial joint. To initiate take-off, the secondary extensor contracts such that the joint becomes under-centred and the tibia begins to rotate through force applied by the metafemoral spring (Ker 1977).

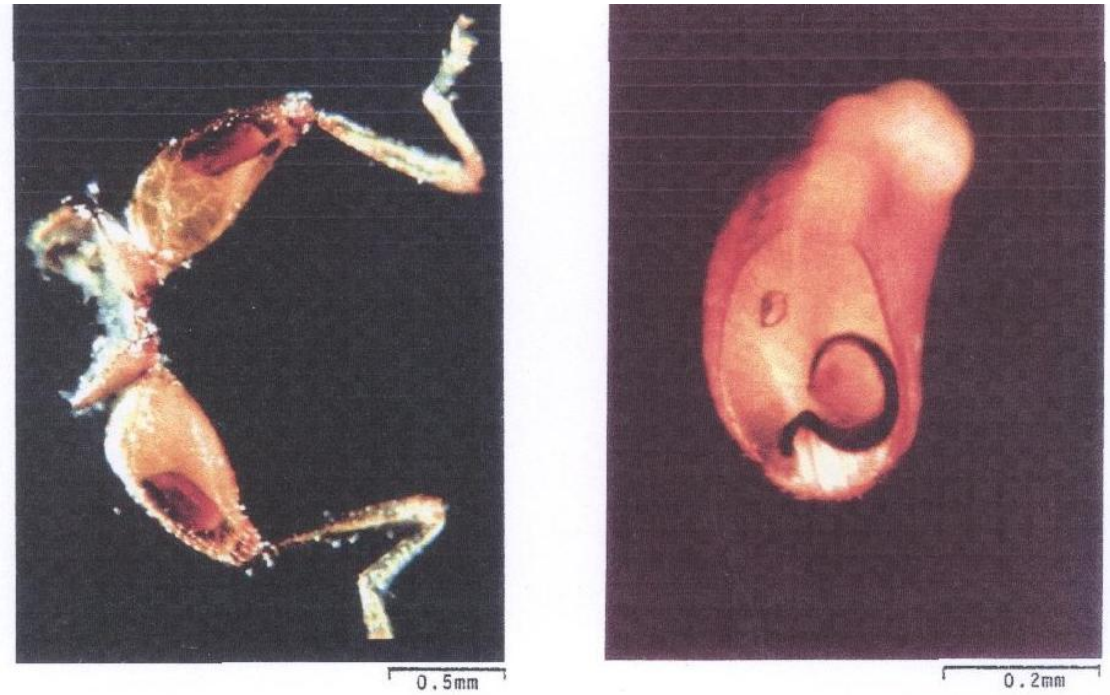

Figure 38 – Flea beetle hind legs with darker scroll spring (left) and detail of scroll form (right) (Ker 1977)

2.6.6.5.9 Springtail (Dicyrtoma ornata)

Springtails are an example of the few jumping organisms with a bi-stable jumping mechanism. There is a springing organ in springtails where energy is slowly stored and rapidly released. A torsion-type spring arrangement relies on special geometry to produce the bi-stable mechanism (Figure 39). Muscles and internal abdominal hydraulic pressure apply force slowly against elastic elements within the springing organ which acts as a valve that regulates the build up of energy before releasing it explosively for jumping (Brackenbury & Hunt 1993).

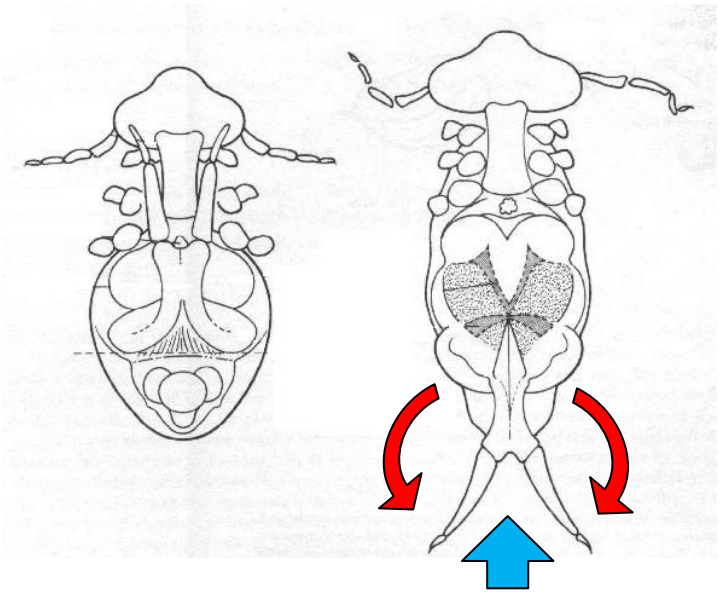

Figure 39 – Springtail jumping organ in bi-stable compressed and released state (Brackenbury & Hunt 1993)

2.6.6.5.10 Trap-jaw ant (Odontomachus bauri)

The fast moving jaw of the trap-jaw ant (Figure 40) is typically used for capturing prey, but it seems that by changing their head orientation, the jaws of these 12 g ants can make them jump into the air. The ants perform two types of action that result in leaving the ground: 1) Bouncer defence – where a simultaneous strike against a predator or prey results in a backward motion of the animal at a take-off angle of about 27° and jump range of 22 cm, and 2) Escape jump – where the ant purposely uses its jaws against the substrate to propel itself high into the air with a take-off angle of about 76°

and a jump height of 8 cm (Patek et al. 2006). In both cases the ant rapidly performs backward somersaults through the air. Energy is stored in the jaws when the ants completely open their mandibles, engage a locking catch within the mandible joint and then use large closer muscles to generate tension in the closer apodeme (Gronenberg 1996). The catch is released using a small trigger muscle.

Figure 40 – Trap-jaw ant (Patek et al. 2006)

2.6.6.5.11 Flea (Spilopsyllus cuniculus)

The Flea is widely regarded by popular science to be the best jumping animal due to its small size as a proportion of the height it can jump. It can jump a vertical distance equivalent to 150-200 times its own height. The flea represents one of nature's few organisms that jump vertically for locomotion rather than escape. Its small size and the height to which it jumps indicates that it must store muscle energy comparatively slowly before jumping. The mechanism providing this energy store (Figure 41) relies on the compression of a pad of rubber-like material called resilin which has an elastic efficiency of 96 % (Jensen & Weis-Fogh 1962). The volume of this pad is adequate to provide the energy required for the flea's jump (Bennet-Clark & Lucey 1967). The compression/shear of this pad (Bennet-Clark & Lucey 1967) is carried out by the contraction of the large dorso-ventral muscle whose tendon attachment at the trochanter results in an over-centre catch arrangement which operates in conjunction

with several cuticular locking devices (Gronenberg 1996). After the dorso-ventral muscle relaxes, the over-centre catch can be released using the small trochanter depressor muscle which changes the angle of attack of the tendon with respect to the joint resulting in rapid release of the stored energy through rotation of the femur (Gronenberg 1996).

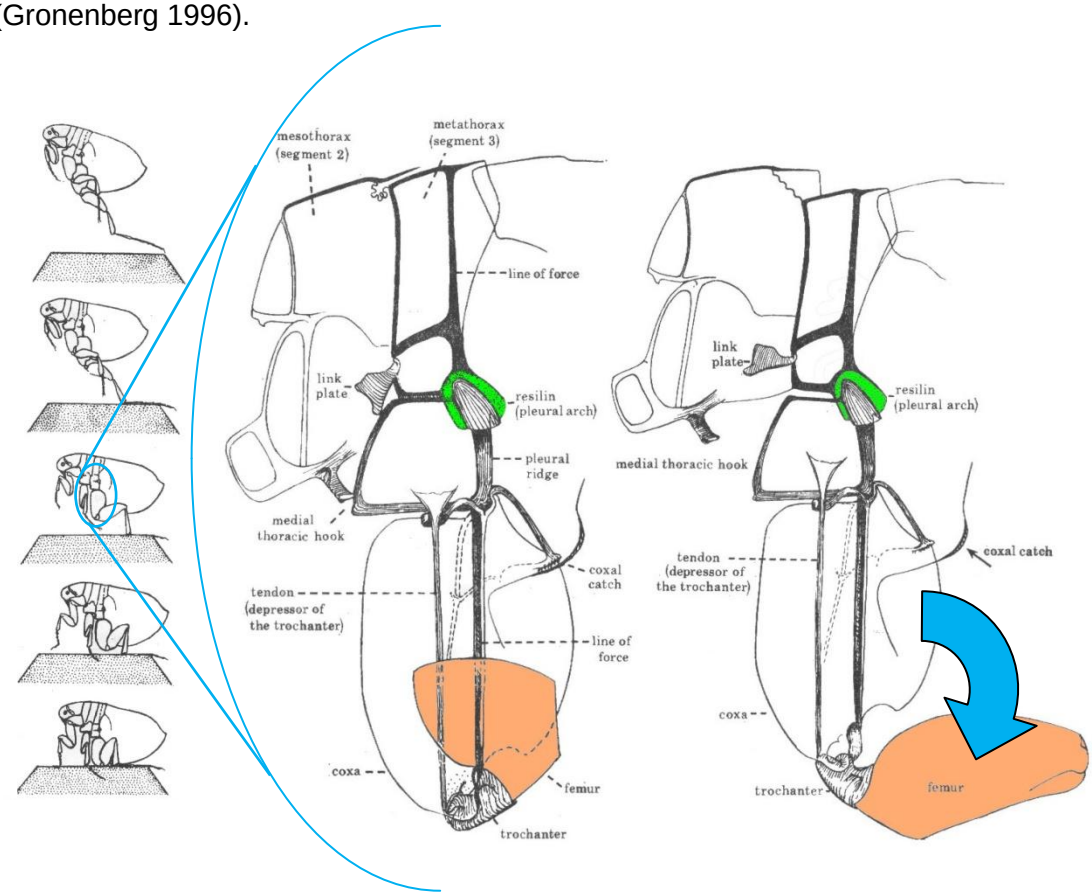

Figure 41 – Left: A flea jumping (Rothschild et al. 1975) Right: The jumping mechanism of the flea relies on the compression and expansion of a resilin pad (highlighted green) and results in the rapid motion of the femur as the pad expands (Rothschild et al. 1975).

2.6.6.5.12 Dromedary Jumping-slug (Hemphillia dromedaries)

Some mention must be made here to a series of slugs, as they have the word "jumping" in their name. This is a misnomer, and a jump by them of any description has never been recorded (Ovaska 2002). The animal performs rapid side to side and curling and uncurling movements, but never achieves a jump. The intention of such movements is to startle predators, so it is much more likely that the predator would

jump in surprise. Jumping slugs will be revisited later (see Section 2.7.2.2.3) as their movements can result in rolling away from predators.

2.6.6.6 Organisms that store mechanical energy for other purposes

Apart from jumping, energy is stored within organisms for other purposes, some of which may give inspiration to novel engineered jumping mechanisms. A selection are presented here for information, but other organisms exist that use elastic mechanisms to deliver rapid movements (Simons 1993; Wassenbergh et al. 2008).

2.6.6.6.1 Fast strike of Mantis shrimp (Odontodactylus scyllarus)

The peacock mantis shrimp (Figure 42) performs an extremely fast strike with its feeding appendage to stun or injure prey with destructive cavitation forces (Patek 2004). The speed of this action requires that energy is stored and rapidly released. Energy is stored in the compression of a hyperbolic-parabaloid (saddle-shaped) spring exoskeletal structure and a latch mechanism within the appendage joints (Patek 2004).

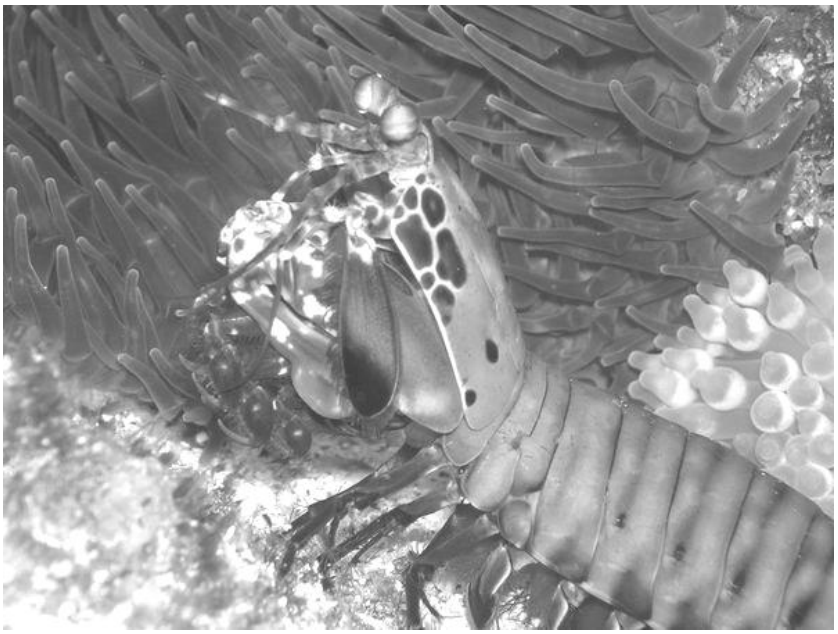

Figure 42 – Mantis shrimp courtesy of Keir Davis

2.6.6.6.2 Pollen dispersion in bunchberry dogwood (Cornus Canadensis)

By explosively releasing stored mechanical energy in the flower stamens of the bunchberry dogwood (Figure 43), its pollen is launched into the air in what is claimed to be the fastest movement by a plant [3.1 m/s for the stamens, and 6.7 m/s for the petals (Edwards et al. 2005)]. This explosive release improves the possibility of pollination both through insect pollination and wind pollination (Edwards et al. 2005). The stamens operate very much like a miniature medieval trebuchets – complete with payload (pollen) and flexible strap allowing the pollen to be launched faster than would be possible with a simple catapult (Edwards et al. 2005).

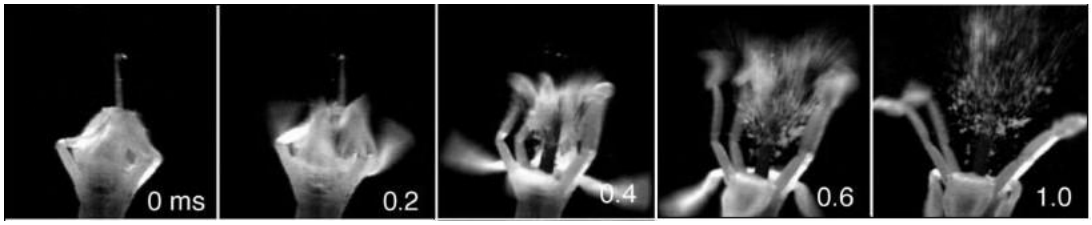

Figure 43 – Bunchberry dogwood flower opening with time in ms marked (Edwards et al. 2005)

2.6.6.6.3 Extension of Chameleon (Chamaeleo melleri) tongue

The tongue of the chameleon rapidly extends at speeds of up to 6 m/s to capture comparatively large prey. To achieve such velocity, a catapult system must be employed. The tongue consists of a rod of cartilage forming its skeleton (Figure 44), the accelerator muscle which provides the power supply, and a series of nested sheaths of collagen beneath the muscle and concentric with the tongue skeleton which form the energy store (Muller & Kranenbarg 2004). The accelerator muscle contracts radially around the tongue skeleton and in so doing elongates. As it elongates, it stretches the helical collagen fibres storing energy within them. This stored energy is recovered only at the tip of the cartilage skeleton, where the taper forces the tongue forward as the collagen regains its resting shape (de Groot & van Leeuwen 2004). There is no requirement for a latch as the release is controlled by the accelerator muscle. This “sliding spring” is compact and easy to control (Muller & Kranenbarg 2004).

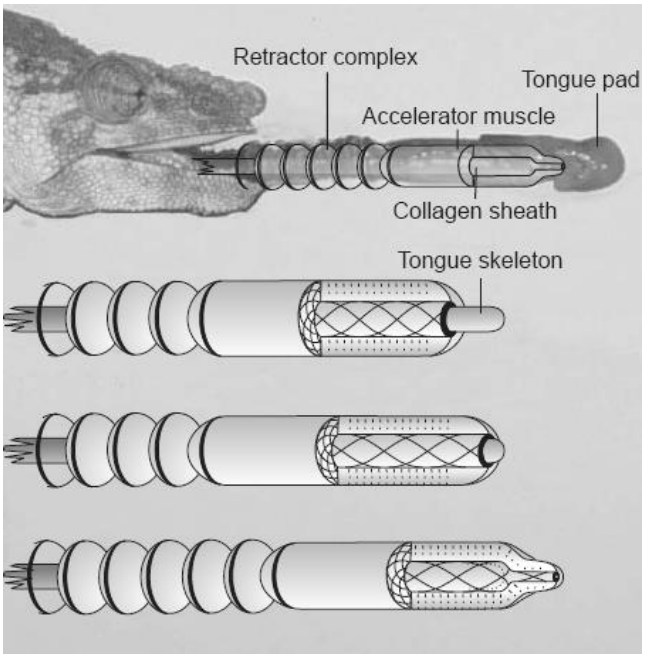

Figure 44 – Chameleon tongue catapult mechanism (Muller & Kranenbarg 2004)

2.6.6.6.4 Closure of Venus flytrap (Dionaea muscipula)

It is well known that the Venus flytrap rapidly closes to trap prey (Figure 45). This rapid movement is initiated by mechanical stimulation of trigger hairs which in turn "actively" changes one of its principle curvatures – the exact process of which remains poorly understood (Forterre et al. 2005). However, this small movement causes the curved bistable leaves of the trap to rapidly move from a stable convex shape to a stable concave shape (Forterre et al. 2005). This ingenious mechanism enables plants to achieve muscle-like movements.

Figure 45 – Venus fly trap open and closed (Forterre et al. 2005)

2.6.6.7 Summary of mechanical energy storage in nature

Table 3 shows a summary of the mechanical energy storage methods in these example organisms.

Organism	Energy storage medium
Kangaroo	Tension in elastic elements in series with muscle
Dog	Tension in elastic elements in series with muscle
Bushbaby	Tension in elastic elements in series with muscle
Bullfrog	Tension in elastic elements in series with muscle and variable mechanical advantage
Locust	Tension in elastic elements, bending of spring elements and variable mechanical advantage
Fruit-fly larva	Tension in elastic elements, bending of spring elements, and buckling of tissue
Click beetle	Tension in elastic elements in series with muscle and bending of spring elements
Flea beetle	Bending of spring elements
Springtail	Bistable mechanism from bending of spring elements
Trap-jaw ant	Unknown
Flea	Compression of elastic elements
Mantis shrimp	Bending of spring elements
Bunchberry dogwood	Bending of spring elements
Chameleon tongue	Compression of elastic elements
Venus flytrap	Bistable structure

Table 3 – Summary of mechanical energy storage methods in nature sorted in decreasing size for jumping animals, followed by non-jumping energy storage (highlighted)

As expected, Table 3 shows that as jumping animal size decreases, then bending and compression of spring-like elements, combined with catch mechanisms, becomes more prevalent. Larger animals are often directly actuated by their muscles (in conjunction with series elastic elements to protect muscle tissue and to provide compliance where required) for jumping.

The key points to take from this section are:

- That the requirement of energy storage mechanisms depends greatly on the actuators available at the scales required. Muscle tissue is of almost uniform performance when compared with the numerous actuators and energy delivery systems available within engineering.
- Storing energy within materials, structures and mechanisms allows low-density energy sources to ultimately produce high-density energy movements. This is considered power amplification.
- Catch and over-centring mechanisms are present in biology to protect muscle tissue from damage due to rapid extension during take-off. Such mechanisms provide time for muscles to relax prior to energy release.
- Maintaining a constant force delivery during take-off reduces the requirement for restraining large, but short duration, peak forces and ensures that velocity rises linearly during take-off. Constant force levels allow for more energy to be delivered for a particular strength of skeletal structure.
- Maximising the distance through which the more massive accelerated part of the body moves before take-off maximises launch velocity, but minimises the required forces. Jumping animals achieve this with long legs.
- Internal organs are protected by compliant elements such that transmitted landing forces (and sometimes take-off forces) are reduced.
- No animal simply has only the ability to jump; even specialised jumping insects have small legs on which they can walk when required. This then implies that although jumping can be the main form of locomotion, another type of movement adds to the flexibility, adaptability and reliability of an organism.

2.6.7 Jumping in robotics

As mentioned previously, jumping is movement adopted by some robots for travelling across rough terrains and over substantially large obstacles. Although very few in number, the suitability of jumping robots for movement in unstructured environments is the major factor contributing to their being researched. Being able to jump clear over an obstacle, or make sequential jumps up an unstructured slope such as a staircase or

rock fall is a great advantage over robots that remain in continuous contact with the surface. Jumping robots fall into two distinct types, those that continually hop or bound, and those that take a periodic approach with lengthy pauses followed by single explosive jumps.

The hopping devices (Brown & Zeglin 1998; Okubo, Nakano & Handa 1996; Paul, Dravid & Iida 2002; Raibert 1986; Wei et al. 2000) move much like a kangaroo would over comparatively smooth surfaces. They have actuation, complexity and control issues more challenging than even conventional walking robots. These challenges include, among other things, active balancing, dynamic stability, and terrain and external input adaptability. This results in expensive devices with, as yet, few results pertaining specifically to rough terrain mobility.

The periodic pause-and-leap jumping robots are much simpler, and most researchers are keen to discuss their rough terrain capability as that is often their primary focus. For these devices, the direction of an individual jump can be selected independently and prior to the jump itself. Jump energy is generally converted from a low energy-density source such as small battery-powered motors, or photovoltaic cells. The jump energy is stored as potential energy in materials and mechanisms within the device ready for rapid release. The techniques previously used to store potential energy include coil springs, bending springs, within fluids/fuels or occasionally in swinging pendulums. A series of robots employing each technique are discussed below. After successful take-off, landing is of critical importance to jumping robots. It is very difficult to control what happens upon impact with the ground, so the ability to survive the landing, recover and ready itself for another jump is important.

Jumping is particularly suited to space exploration activities. Wheeled and legged robot mobility will not be improved by a lower gravity as the obstacle surmountability of wheels or legs does not increase with decreasing gravity. Instead, as gravity becomes lower, robots that jump gain considerable ability to overcome large obstacles (Fiorini, Cosma & Confente 2005). Some rovers have been developed specifically for very small gravities – such as those on asteroids and other astrological bodies (Nakamura, Shimoda & Shoji 2000; Raibert 1986; Shimoda, Kubota & Nakatani 2002; Yoshimitsu et al. 2003). However these devices can only operate in a very small selection of

environments, none of which are earthbound or on other planets or moons of interest. Rovers that jump on Earth can be expected to perform better when located on Mars or the Moon.

2.6.7.1 Coil spring based designs

2.6.7.1.1 NASA JPL / Caltech "Hopper"

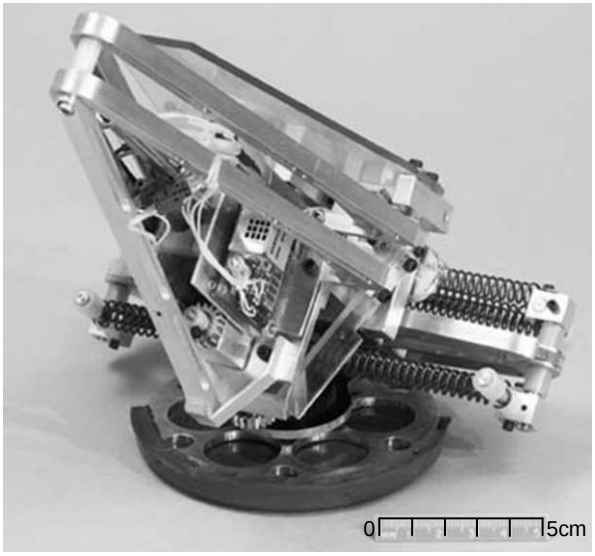

Figure 46 – JPL Hopper (prototype 2) (Fiorini & Burdick 2003). The robot jumps in a selected direction, crash-lands, and then re-rights itself using actuated levers on its bodywork.

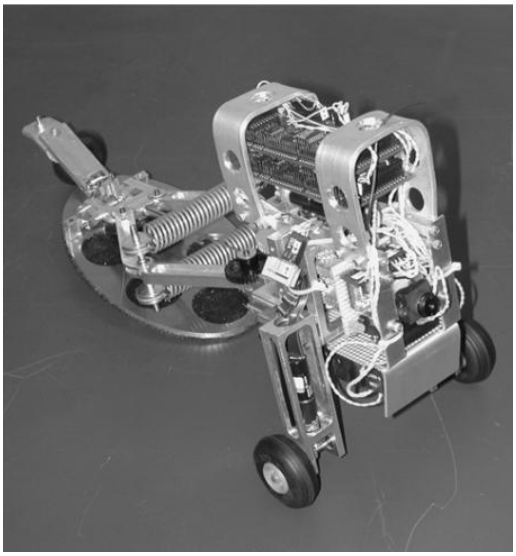

Figure 47 – JPL Hopper (prototype 3) (Fiorini & Burdick 2003). The robot jumps in a direction determined by driving to a take-off point. The small wheels provide fine position control, but are for indoor use only.

Researchers at NASA Jet Propulsion Laboratories (JPL) and Caltech have developed a series of jumping robots called "Hoppers" (Fiorini & Burdick 2003) – the most recent of which are pictured in Figure 46 and Figure 47. Each robot is based around a 6-bar linkage and spring mechanism (Figure 48) and a simple lead screw driven compression system and catch. The energy is stored in the linkage/spring mechanism using a DC motor driving a lead screw that rotates and compresses the head toward the foot of the robot. By driving the motor in the other direction, the jump direction can be controlled.

The jump angle is fixed at 50°. Energy is released by driving the lead screw a little further onto a wedge which separates the catch. The initial prototype could right itself if it fell on its side using levers on its outside.

The most interesting aspect of the jump system is the force-displacement profile of the 6-bar linkage and spring system, since a non-linear spring profile has been produced from a linear coil spring (Figure 49). This gradually-increasing release force rises to a peak before it then reduces ensuring that the acceleration of the device rises for as long as possible until take-off. This is in contrast to a typical linear spring where the force is highest at the start. This is very important for light jumping robots, which may undergo premature lift-off (Hale et al. 2000) where the robot leaves the ground before all of the energy is released.

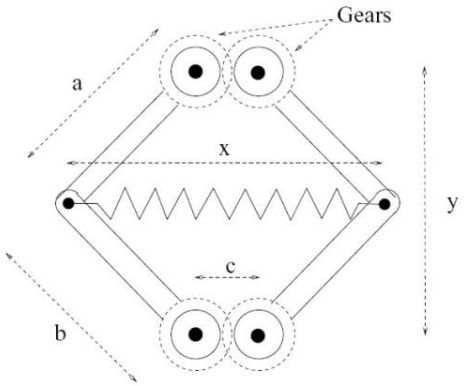

Figure 48 – Schematic diagram of JPL hopper 6-bar geared jumping mechanism (Fiorini & Burdick 2003)

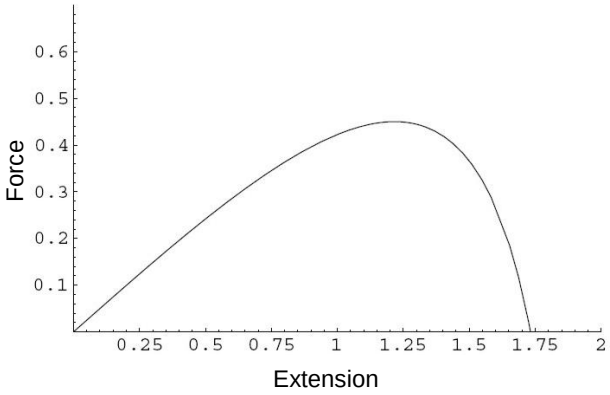

Figure 49 – Force verses extension for JPL hopper 6-bar mechanism (where a=b and with a Hooken spring constant) (Fiorini & Burdick 2003)

The robot is remotely controlled using a pair of radio signals which allow an operator to view images from its onboard camera and to monitor its position and initiate jumps. The power for movement is carried onboard.

The intended application of this device is as a space exploration robot.

The third and most recent prototype (Figure 47) is based upon the same 6-bar linkage and spring mechanism, but adds an adjustable launch angle and fine motion control

using a trio of wheels. Here energy is stored by winding a cable around a capstan. By driving the motor in the other direction, the jump angle can be adjusted from 0° to ~85°. The direction is controlled by powering the small fine motion control wheels such that a suitable orientation is achieved before take-off. The energy is released by freewheeling the capstan around which the cable is wound. This prototype does not have the self-righting feature of the second prototype since the goal was to test the integration of fine and coarse motion. The small wheels don't provide fully multimodal movement (see Section 2.6.7.5), as they are for relatively benign terrains and for functional testing only (Fiorini, Cosma & Confente 2005).

2.6.7.1.2 University of Utah Monopod Jumping Robot

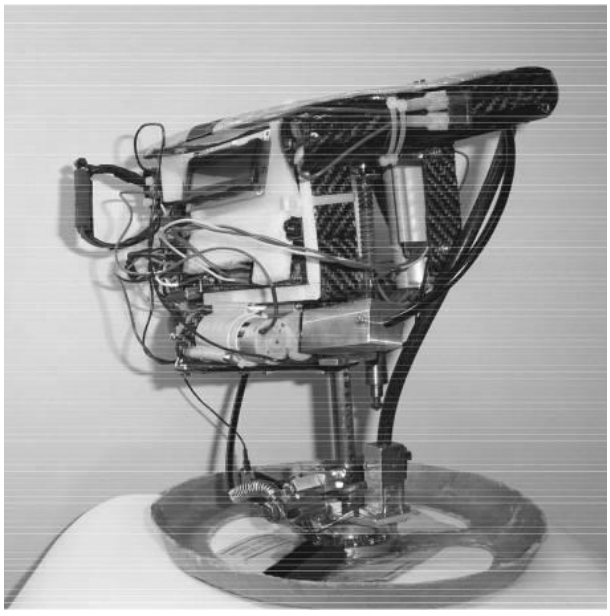

Figure 50 – Monopod Jumping Robot courtesy of James Allison

The robot shown in Figure 50 (Allison 2002) was designed as a student project and an entry into the 2002 Robo-Olympic events of high jump, long jump and obstacle course. This means that the conditions in the operating environment were known in detail, allowing the design to be specifically tailored to that environment.

The design centres on the compression of a coil spring using a piston within a cylinder and subsequent jumping by launching the outer cylinder and associated control

masses and power supply away from the foot. The spring is compressed using a ball screw and a latch mechanism. Direction is controlled by rotating the main body around the foot. All the battery power for the device is onboard along with sensors and a microprocessor so the robot is autonomous and does not require remote control.

2.6.7.1.3 IMT Lucca Institute for Advanced Studies "Grillo"

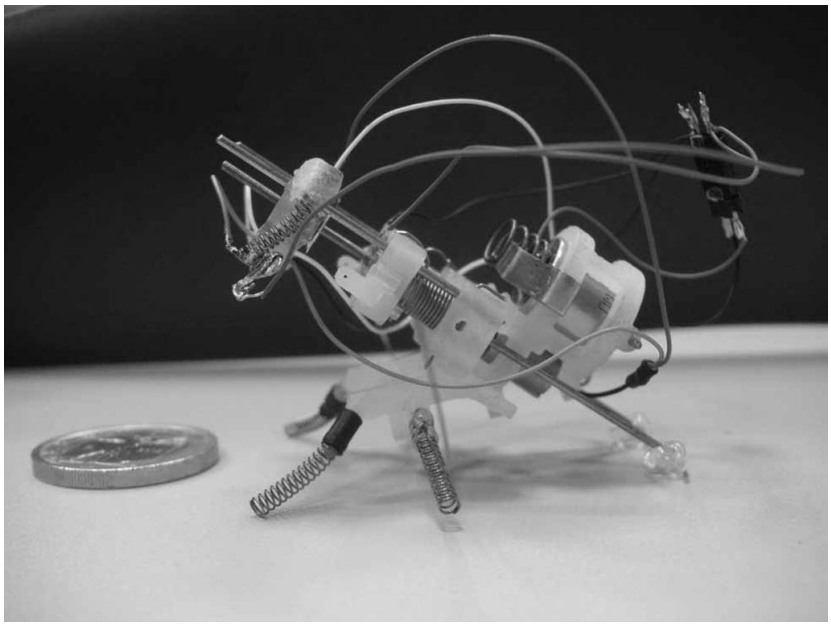

Figure 51 – Grillo prototype courtesy of IMT (Scarfogliero, Stefanini & Dario 2006)

The intention of the Grillo (Figure 51) robot is to make long-jumps in quick succession in a half "pause-and-leap" half "hopping" gait. Thus the charge time between each jump is hoped to be small, possible even taking place during flight as well as subsequently using some regenerative kinetic energy storage on landing. The device is designed to jump at 45° to the horizontal to maximise range.

The initial prototype (Figure 51) uses a small motor to drive a linear cursor attached to the leg mount. This stores energy in the stretching of a pair of coil springs. A small permanent magnet is used as the catch mechanism which releases when the force in the springs exceeds the magnetic attraction (Scarfogliero, Stefanini & Dario 2007). Although jumping successfully, this prototype did not achieve the jump frequency the

researchers were aiming for. Subsequent prototypes will load the springs using a heavily geared cam.

2.6.7.2 Bending spring based designs

2.6.7.2.1 EPFL 7g Jumping Robot

Figure 52 – 7g jumping robot courtesy of EFPL

The 7g Jumping Robot (Figure 52) developed at the Ecole Polytechnique Federale de Lausanne (EFPL) can jump 27 times its own height (Kovač et al. 2008). The team's specified performance benchmark was a 75° launch angle enabling a 10 g device to jump over an obstacle 1 m in height. This resulted in a power requirement far in excess of what could be delivered directly, so energy from a small actuator is stored within a pair of torsion springs at the "hip" of the device. The small DC motor loaded the springs via a cam ensuring constant torque on the motor. A catch mechanism relied on the continued rotation of the cam allowing an instantaneous release of stored energy into the leg. A four-bar linkage leg mechanism is employed as geometric adjustments of it allow simple modification of the take-off angle, acceleration time and the trajectory of the foot (Kovač et al. 2008). In the main, the robot is constructed from high performance engineering plastics and through the use of finite element analysis (FEA) the weight of the robot's aluminium leg was reduced by 23 %. It is understood that further improvements are possible through similar analysis of other components. The

device appears to be remotely controlled using IR. Its configuration means that it cannot control the direction of jumps or re-right and re-orient itself after landing. However, a caged version has been developed to allow for passive self righting and jump direction control at the expense of jump impressiveness (Kovač et al. 2010). It would be difficult for such a small device to carry a significant payload.

2.6.7.3 Fluid powered designs

2.6.7.3.1 Sandia "Hopper"

Figure 53 – Piston and combustion chamber of the Sandia Hopper photographed without its passively self-righting outer part-spherical shell. Image courtesy of Sandia Corporation

The initial application for this DARPA-funded project, was a small and robust robot that could be used by soldiers to infiltrate hostile areas. Since then another DARPA project has taken over and the application has evolved into a mobile anti-tank minefield that is able to fill any breaches created by enemy mine-clearing missions (Altshuler 2002).

Researchers at Sandia have developed a hopping device (Weiss 2001) that utilises the combustion of liquid propane to fire a piston into the ground launching the device (Figure 53) up to 4 m into the air. The device jumps semi-randomly making general progress in the required direction rather than accurate progression from one point to another. The hopper adopts a weighted self righting system and a steering system that takes a bearing from an internal compass before moving an off-centre control mass which tilts the device in the intended direction of the jump.

2.6.7.3.2 Tokyo Institute of Technology "Air hopper"

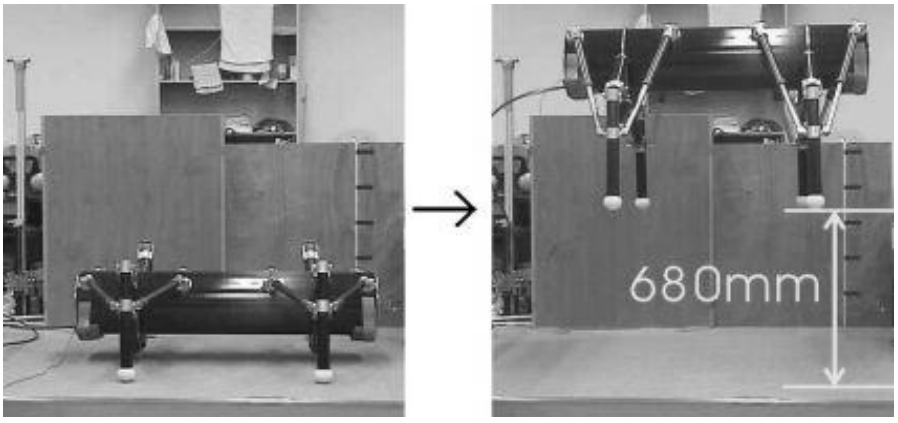

Figure 54 – Air hopper performing a vertical jump. Image courtesy of Tokyo Institute of Technology

This device is designed as a search and rescue robot. The intention is that it could be used after a large earthquake in which there is danger of further collapse of structures and where there is large obstacles over which a typical walking robot would not be able to navigate. By employing a jumping movement strategy it is supposed that the early rescue missions after a disaster could be more successful.

The design of this robot (Kikuchi, Ota & Hirose 2003) is based upon a cylindrical body with 4 legs which are widely spread providing a stable platform (Figure 54). Each leg is made of a four bar linkage driven by a pair of pneumatic cylinders based upon bicycle pumps. The air supply to the cylinders is external and in its current state, the device is unable to walk forward or jump in a direction other than vertically.

2.6.7.3.3 University of Tokyo "Mowgli"

Figure 55 – Mowgli jumping onto a chair (Niiyama, Nagakubo & Kuniyoshi 2007)

Mowgli (Figure 55) is a pneumatically powered bipedal jumping and soft-landing robot using six McKibben artificial muscle actuators (Niiyama, Nagakubo & Kuniyoshi 2007). Each leg is independently controlled and consists of hip, knee and ankle joints. The device jumps very much like a human and the researchers have taken great care to ensure that the robot lands gently. The device is tethered to a pneumatic and electrical power supply.

2.6.7.4 Momentum based designs

2.6.7.4.1 Kagoshima University Pendulum Jumping Machine

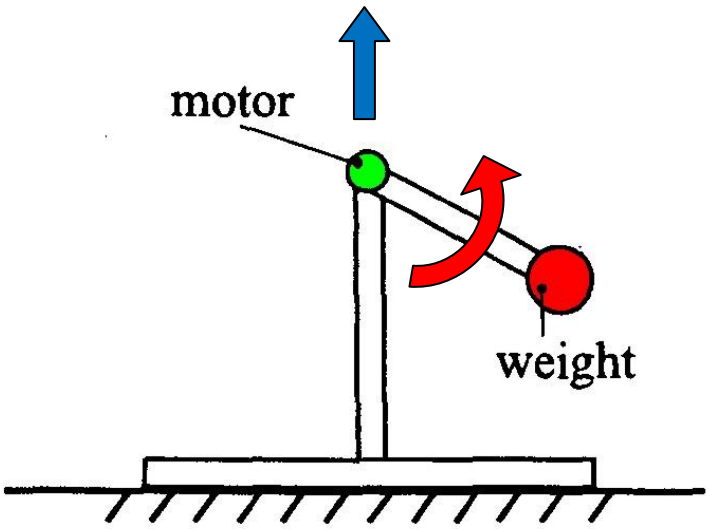

Figure 56 – Two link pendulum driven jumping machine (Hayashi & Tsujio 2001). Rapidly moving the weight forward and upward encourages the whole device to leave the ground.

When a human jumps vertically, as well as bending and extending the legs which provide most of the jumping energy, the arms are also swung upward in a pendulum fashion to improve the jump height. A number of papers suggest that the arm swing improves vertical jumping performance in humans by around 10 % (Vanezis & Lees 2005). The team at Kagoshima university have used this phenomenon to develop a pendulum jumping machine (Hayashi & Tsujio 2001). An illustration of the jumping machine in shown in Figure 56

The machine consists of a body, with a flat foot with a central mast at the top of which is mounted a servo motor, and an arm with a weight at its tip which is driven by the servo motor. By swinging the arm using a rectangle command voltage into the servo, the machine is able to make a small vertical jump. A forward jump has been difficult to reproduce with a single pendulum, but a robot with multiple counter-rotating pendulums

has successfully climbed tiny steps. No provision is made for directional control. The robot is considered to be tethered since the power and jump control for the device are external.

2.6.7.5 Multimodal jumping designs

A series of robots combine jumping with another form of movement to improve usefulness over a variety of terrains. Researchers have generally adopted one of the energy storage techniques above and integrated them with another mode of movement. It is difficult to determine from published research if the multi-modal ability of the devices presented was considered from the outset, or if the second mode was added at a later date after discovering limitations with the primary movement. There is a disadvantage of introducing additional modes of movement. This would be an increase in complexity and weight, and the resultant likely decrease in single-mode performance and reliability, and increase in cost.

2.6.7.5.1 University of Bath "Glumper"

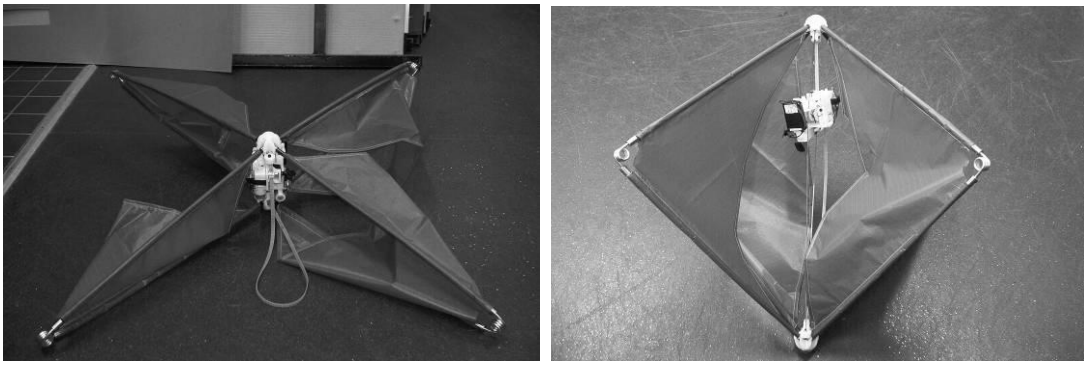

Figure 57 – Glumper in its charged and resting states (Armour et al. 2007)

The name of this device comes from its Jumping and Gliding motion for covering rough terrain (Paskins 2007). Glumper (Figure 57) is Octahedral in form with carbon fibre reinforced plastic tubes along its edges and four torsion springs at its knees. At its main vertices are rapid prototyped pin joints between which run a toothed belt and a compression thread. A pulley within a control box drives along the belt so attaching the weighty control box to the accelerated portion of the device. A second motor in the

control box winds the compression thread around a capstan slowly pulling the vertices of the device toward one another storing energy in the torsion springs. The capstan is automatically released at full compression using a series of levers. Wing-like membranes secured between the leg elements unfold as the device launches. The aim of the wings was to reduce landing impact velocities and improve range through gliding. This gliding movement comes almost as a free by-product of the primary jumping movement as no separate mechanism was required to deploy the wings. However, the performance was not improved as anticipated owing to insufficient gliding control. The device has no direction control.

2.6.7.5.2 University of Minnesota "Scout"

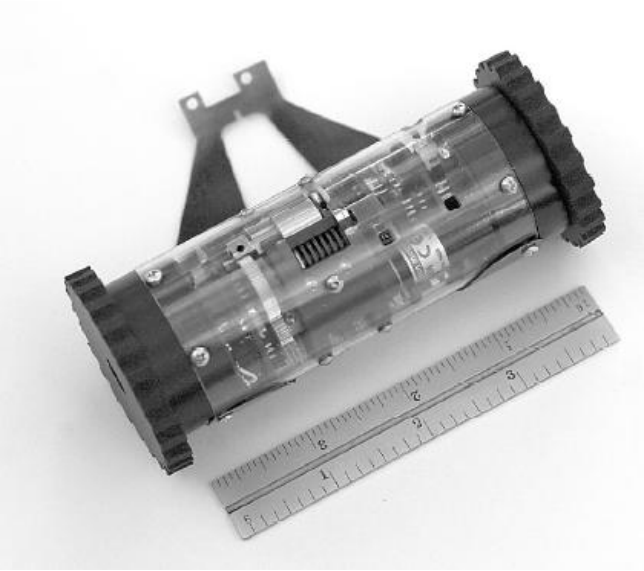

Figure 58 – Scout robot courtesy of University of Minnesota. Rule measure is in inches.

The Scout robot (Figure 58) (Stoeter et al. 2002) was developed as a platform for distributed robotic systems where multiple devices would work in conjunction to achieve a common mission goal. Funding from various US military sources means that the primary application for the Scout is one of observation and scouting in urban military environments. The robots need to be small and move rapidly across smooth surfaces whilst being able to negotiate steps.

The Scout robot uses a pair of wheels for movement on smooth surfaces, but complements that with a flexible leaf spring to enable it to jump onto and over obstacles around six times its height. Sensors include a camera, accelerometers and encoders. Additional specialised tools or sensors can be incorporated for specific tasks or measurements.

2.6.7.5.3 Case Western Reserve University "Jumping Mini Whegs"

Figure 59 – Jumping Mini-Whegs™ version 9J (Morrey et al. 2003)

The Whegs robot was introduced previously in the walking section (2.4.3 p.37) but a version that jumps has also been developed (Lambrecht, Horchler & Quinn 2005). The 9J version of the robot (Figure 59) is powered by two motors. One motor rotates the four Whegs and a second motor is used to provide a jumping movement. The jumping capability was added to improve Whegs' ability to surmount large obstacles. Jumps are achieved by employing a four-bar linkage and coil spring. The spring is stretched using

a motor within the chassis, and released automatically via an over-centre mechanism when the spring is fully extended (Morrey et al. 2003).

2.6.7.5.4 Sandia National Laboratory "Precision Urban Hopper"

Figure 60 – Sandia National Laboratory Precision Urban Hopper (Salton 2009)

The Sandia National Laboratory Precision Urban Hopper (Figure 60), developed as part of a DARPA program, is a small ~0.1 m high four-wheeled skid-steer vehicle that can jump over obstacles "40-60 times its height" using an additional jumping leg mounted on the chassis (Salton 2009). Little detail of the robot's performance or construction is available in the public domain.

2.6.7.5.5 Ritsumeikan University Deformable Jumping Robot

The only multimodal device that, like animals, achieves two movements with a single mechanism is the deformable rolling and jumping robot (Hirai, Matsuyama & Nakanishi 2007) by Ritsumeikan University. Although very much at the prototype stage, and a further development of a wheel-like device (Sugiyama 2006; Sugiyama & Hirai 2004), the 5 g tethered 90 mm diameter sphere-like device has been shown to roll slowly in all directions on smooth surfaces, climb slopes of ~10°, and jump to twice its resting diameter. The device is constructed of three springy metal hoops with twenty-two radial shape memory alloy spokes. Applying a voltage to the spokes causes them to contract moving the centre of gravity of the whole device toward its rim and careful control of the order in which they are contracted allows for a rolling motion (Figure 61). The springy

outer hoop allows the shape memory alloy actuators to store potential energy ready for rapid release as a vertical jump (Figure 62). As yet there is no possibility for direction control of a jump and no range to any jump. This is the only recorded multimodal device that achieves two distinctly different modes of movement with one structure, but it is of limited speed in both modes and requires a tether for control and power supply.

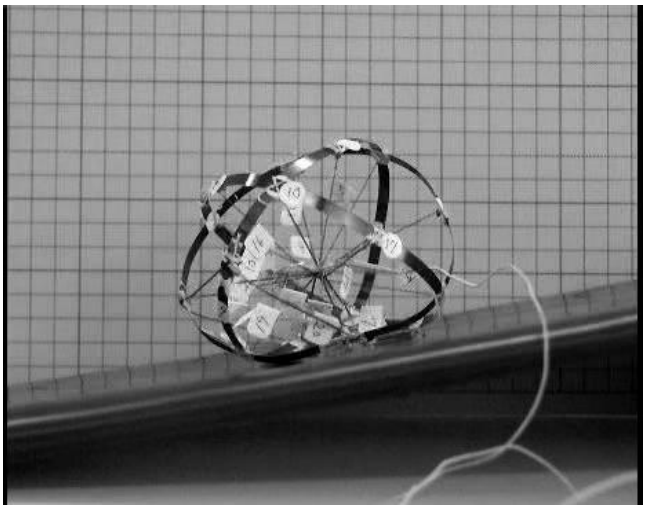

Figure 61 – Spherical soft robot rolling up a slope (Hirai, Matsuyama & Nakanishi 2007)

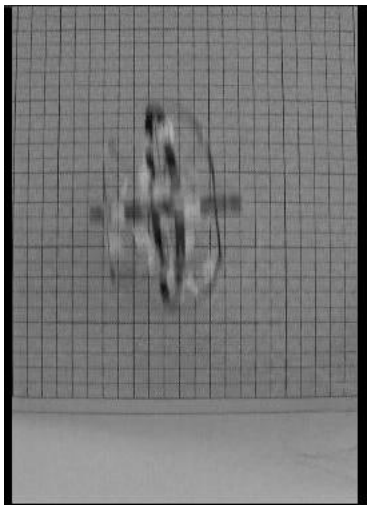

Figure 62 – Spherical soft robot jumping (Hirai, Matsuyama & Nakanishi 2007)

2.6.7.6 Comparative review of jumping robot performance

Most of the jumping and jumping-multimodal robots presented here are included within the performance summary in Section 3.1, p.118. However, the use of the additional jumping performance evaluation technique discussed in Section 2.6.6.3, p.55, gives another more focussed viewpoint, and offers a comparison to nature's jumpers. Figure 63 shows a new version of this graph with the robots added.

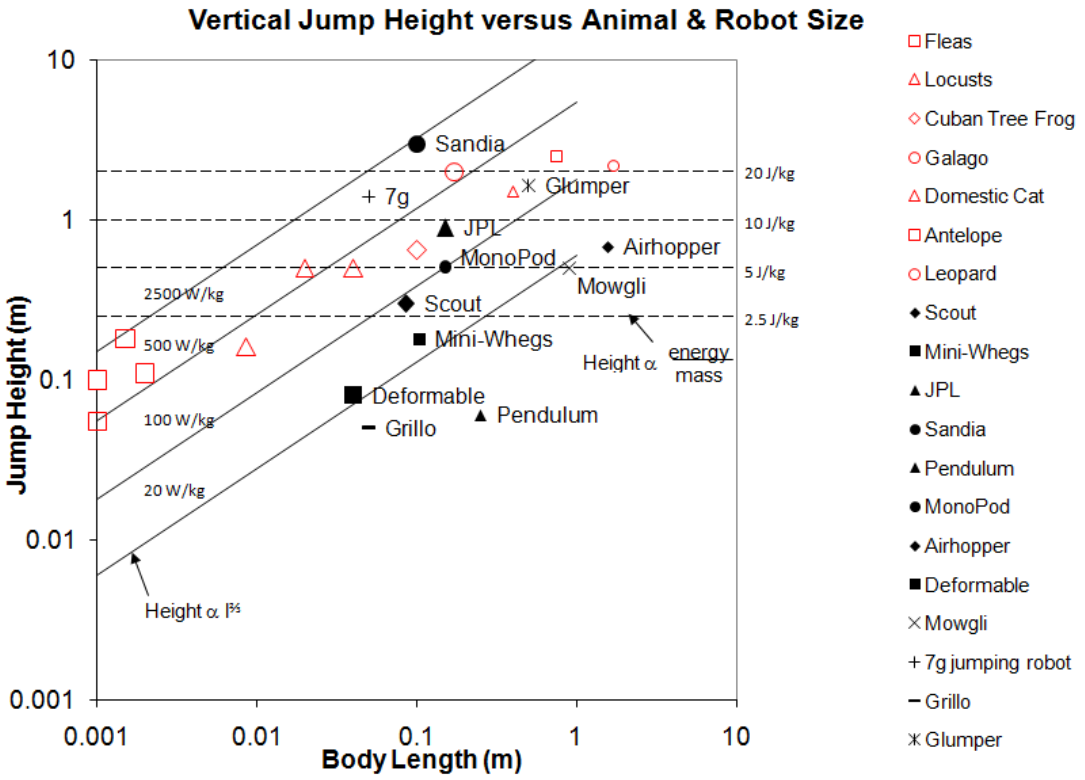

Figure 63 – Height of jump v. length of a selection of animals (outlined markers) and robots (solid markers). The graph also shows required specific energy (J/kg) and specific power (W/kg) to produce a jump assuming that the objects accelerate through their own body length and that there is no air resistance [from (R. Armour & J.F.V. Vincent 2006)].

Plotting the robots on Figure 63 was made using some assumptions that should be specifically mentioned. The recorded jump height in published research is often the cleared height (particularly for small devices), but some researchers focus on the change in height of the centre of gravity of the device between a resting state and the peak of the jump (particularly for large devices where the shape changes significantly). But since it cannot usually be determined which is which from the published sources the height recorded in Figure 63 is simply the jump height presented in the publications. It does appear to be the case that many of the robots accelerate to their take-off velocity through a distance of the order of their own resting 'length' so the lines of constant energy and power density are probably valid. The "body length" of each robot was determined as the 'resting' horizontal dimension of the device. The jumping devices tended to be of similar lengths in all three dimensions – varying up to a few

fold, but not orders of magnitude larger. However, unlike nature, their densities are wide ranging and therefore masses are not so explicitly linked to physical dimensions due to their differing materials and structures (some being entirely hollow for instance). This has important implications when comparing robots along the lines of constant power which are derived from an equation containing mass (Equation 12, p.57).

Those devices optimised for vertical jumping (rather than jump range or those having another form of locomotion) clear the largest heights as would be expected. Figure 63 makes no allowance for those devices that use jumping as a secondary form of locomotion, or complement a primary jumping movement with another type. They should therefore be judged with care as there are likely to be substantial limits to their jumping capability due to the additional masses associated with their other movements.

Nevertheless, some potentially useful comparisons of the robots can be made using Figure 63. The four highest jumping robots, the Sandia hopper, 7g jumper, JPL hopper and Glumper, have both comparatively high energy and power densities when compared with the other devices. The Sandia hopper in particular beats all other robots (and animals) in jump height, and energy and power densities. This can be expected as a result of its exploding hydrocarbon fuel source which has a particularly high energy density.

If one were choosing only jump height as a measure of performance then Glumper performs slightly better than the 7g jumping robot. This equates to a slightly higher energy density. However, if the chosen performance measure were the jump height in multiples of body height then the 7g jumping robot performs considerably better than Glumper as it is much smaller. This appears to equate to a larger power density, but since body length and mass are not so closely related within engineering as they are in biology, the values shown may not reflect the true power to weight ratios of the robots.

In general, to enhance the performance of any of these robots, improvements should be made either to their energy density (when jump height is the most important factor) or to power density (when a combined jump height but small size/weight is important).

An improvement in energy density relies only on an increase in the stored energy levels or a reduction in mass. More stored energy typically equates to more force which would generally result in the requirement for stronger weightier structures. However the use of non-linearity in the force profile of an energy storage mechanism could substantially help here, as is the case with some of the animal systems. Reducing mass relates to detailed material selection and the optimisation of component design using techniques such as finite element analysis. In this regard engineers would seem to have a distinct advantage over nature as they have at their disposal a much wider range of materials with differing properties (such as density and stiffness). However natural machines are built from the cellular level upwards. This allows effects such as continuously-varying elasticity through an organ – something that traditional engineering manufacture would find difficult.

An improvement in power density requires those modifications above in conjunction with a reduction in physical size (and all of the associated complications regarding the reduced distance through which to deliver the stored energy). It would therefore seem most effective to concentrate efforts on the simple reduction in mass of a device to improving jumping performance until limits are reached.

2.6.8 Energy storage in engineering devices

The development of a pause-and-leap jumping device requires some understanding of the available techniques in which different forms of energy can be stored within materials and engineered mechanisms. These include conventional springs, elastomers, non-linear springs, bistable mechanisms, combustible fuels, and compressed gases. In the main these can be divided into energy stored in materials and energy stored in mechanisms.

2.6.8.1 Energy storage in materials

All solid materials behave as a spring when deflected or stretched-over small deflections before yield or fracture. They return to their original form after a force is applied. Producing simple shapes from materials results in simple springs which store potential energy when deformed, returning it as kinetic energy when released.

2.6.8.1.1 Simple Hookean springs

A Hookean spring is linearly elastic such that the strain energy stored in a compressed or stretched spring is equivalent to the area beneath the force-displacement curve. For a typical Hookean spring this stored energy is:

$$strain\ energy\ stored = \frac{kx^2}{2}$$

Equation 13 – energy stored in Hookean spring

Where k is the spring constant and x is the displacement. Assuming a particular force limit is available for deformation, more strain energy can be stored in a softer (smaller k) spring over a greater displacement (x) than can be stored in a stiffer spring over a smaller distance (Figure 64). Thus by maximising the displacement, the stored strain energy can be maximised for a maximum available particular force.

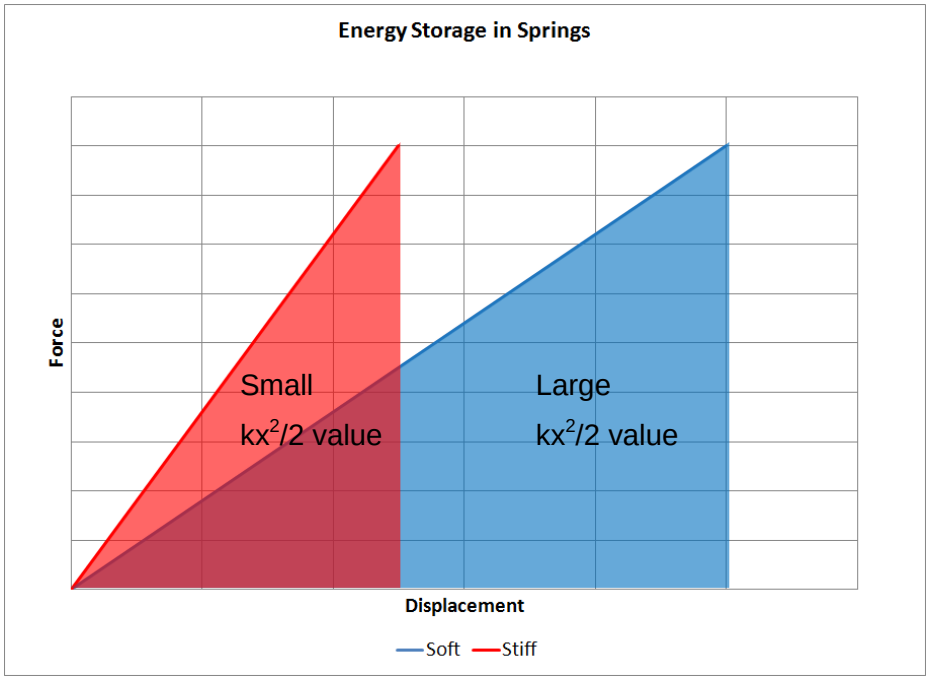

Figure 64 – Energy storage in springs

Similarly, if displacement were the limiting factor (because of the size of the device for example), and large forces were available, then a stiffer spring would be able to store

more energy for a given displacement. However, in the case of many engineered devices, it is the peak force that is of major concern as that has major implications for the design of force-reacting components.

When using Hookean springs for storing jumping energy it is important to note that the force, and therefore acceleration, is highest at release and both reduce as the spring returns to its original shape (Figure 65). As mentioned above, this fact could have important implications for extremely light-weight jumping robots, since it is possible that the initial shock force is sufficient to lift the device from the ground. This premature lift-off means that the remaining stored energy is wasted since it has no surface to push against (Hale et al. 2000).

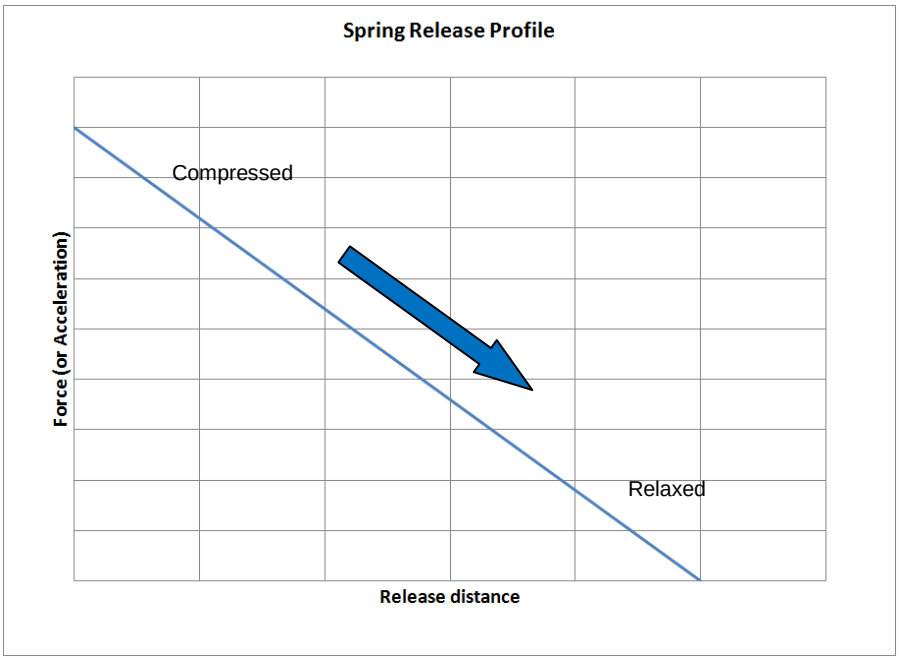

Figure 65 – Force reduction as spring releases

2.6.8.1.2 Spring material

In general the spring stiffness, k, of any material is fixed until a point where yield or catastrophic failure occurs, in turn leading to plastic deformation or material failure respectively. Graphs of Force verses Displacement, and Stress (σ) verses Strain (ε) are often used interchangeably as they have the same shape (Figure 66). This is

because both the stress and strain are obtained by dividing the force and displacement by constant factors.

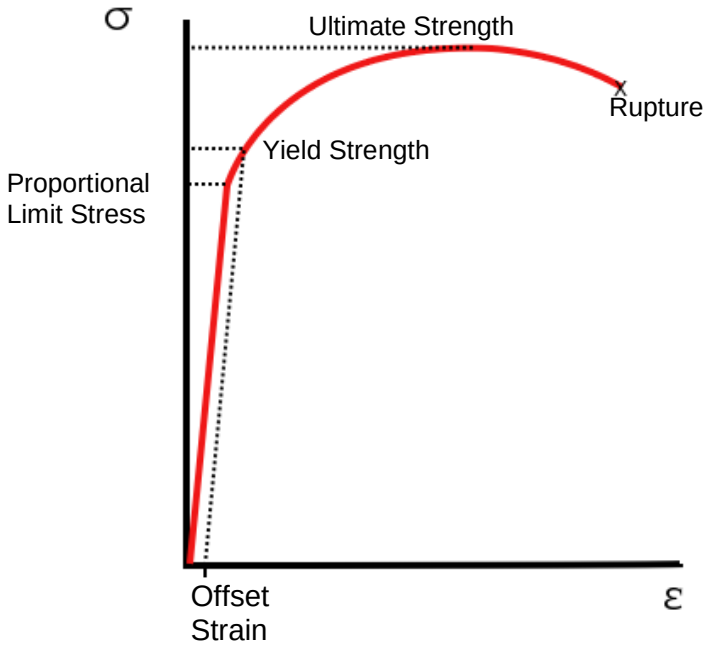

Figure 66 – Typical Stress (σ) – Strain (ε) curve for a metal

When choosing the best material for a spring for a jumping device, consideration should be made of the spring's anticipated function. Does the spring need to store a maximum amount of energy for a given weight? Does it need to store a maximum amount of energy for a given volume? The maximum energy (U) stored per unit volume in a solid piece of material stressed to a stress σ is:

$$U = \frac{\sigma^2}{2E}$$

Equation 14 – energy stored in a material

Where E is the Young's modulus. Equation 14 is only true for stresses below the yield stress σ_f so no matter the shape of the spring the best material for springs of a given volume is those with the highest value of:

$$\frac{\sigma_f^{\,2}}{E}$$

Equation 15 – best material for energy store

If weight is more important than volume then dividing this factor by the density of the material gives the strain energy stored per unit weight. Figure 67 shows the distribution of some materials with their specific modulus (E/ρ) and specific strength (σ/ρ) plotted. Materials with equal values of strain energy stored per unit weight occur on lines with a slope of 2 (highlighted in Figure 67). The materials which store the most strain energy per unit weight are elastomers and engineering ceramics.

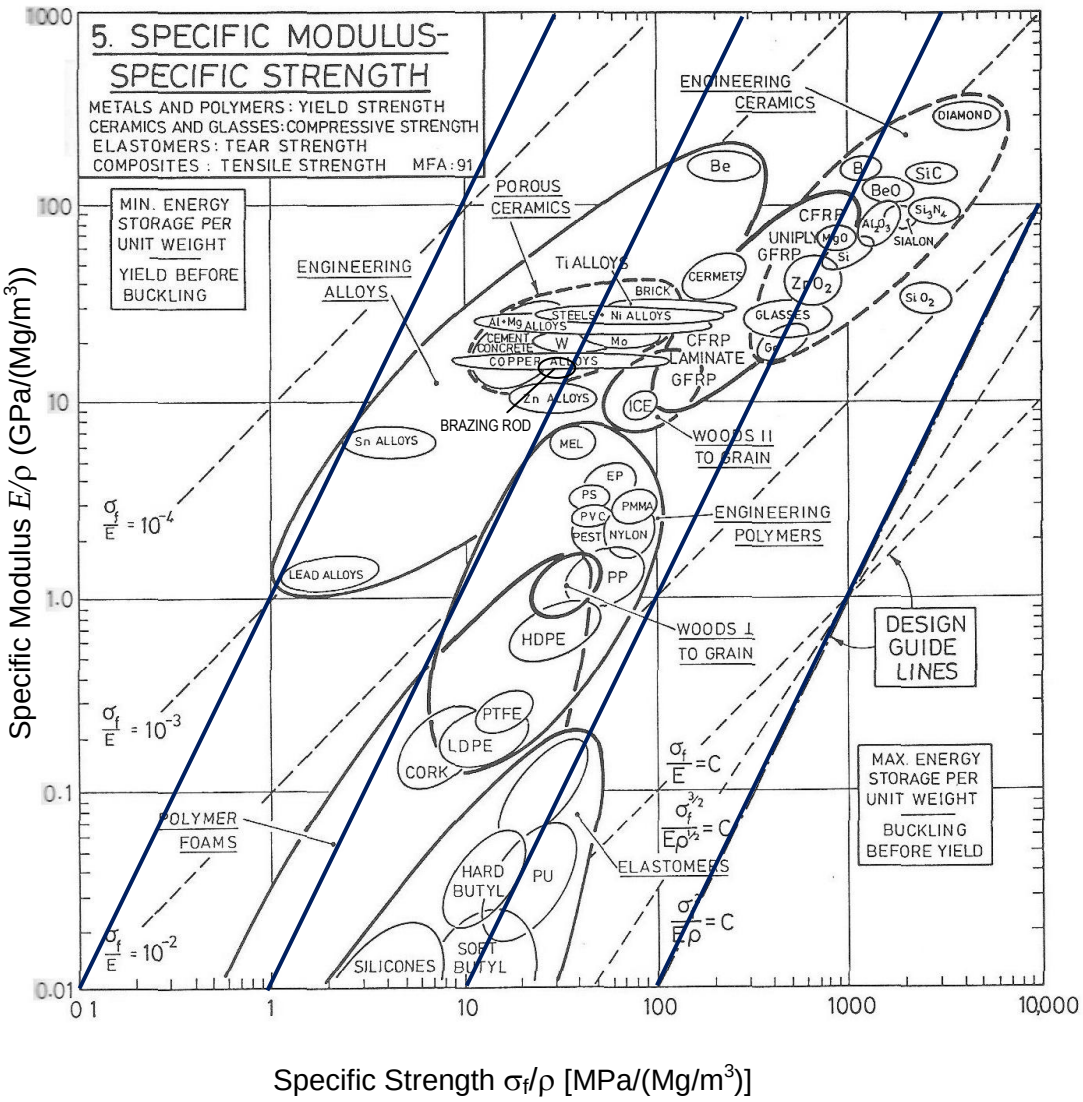

Figure 67 – Graph of specific modulus against specific strength (Ashby 1993). Brazing rod is highlighted (see Section 4.2.2.1, p.178) and heavy diagonal lines indicate materials with equal values of strain energy stored per unit weight.

2.6.8.1.3 A particular note on elastomers

Elastomers typically follow Hooke's law when stretched or released quickly. Elastomers are, however, viscoelastic. This means that they exhibit hysteresis in the stress-strain curve and also undergo stress relaxation and creep. When an elastomer is held under constant strain, there is a change in stress with time due to the relaxation of the polymer chains. Thus, for use in a strain energy storage capacity, elastomers must be

charged and released quickly to maximise the ratio of returned energy to input energy. This may not suit a slow charging “pause-and-leap” jumping device.

The physical properties of elastomers also change with their external environment, so careful consideration should be made when specifying elastomers for use in cold or hot climates, or ones that will be in continual sunlight for example.

These factors have major implications for the use of elastomers in a jumping device and usually preclude their use in slow-charging devices.

2.6.8.1.4 Combustion of fuels

Combustible fuels are already a dense store of potential energy. When burned, this energy is released and turned into useful work, as in an internal combustion engine. Using a similar combustion chamber/piston arrangement produces a useful jumping device, but the fuel source is likely to be limited as it cannot be easily recovered from the environment.

2.6.8.1.5 Compression of gasses

When contained within a chamber, energy can be stored in the compression of gases. By adding non-return valves to the compression mechanism, low levels of force can be repeatedly applied building the pressure within a chamber. Rapidly releasing this pressurised gas could generate useful mechanical motion. The main problem with compressed fluid sources is the requirement for a chamber to contain the increasing loads. Such chambers need to be strong. Compressing a gas can occur either isothermally, where the temperature is kept constant by transferring heat to the surroundings, or adiabatically, where the temperature of the gas changes as it is compressed. Adiabatic compression is more efficient as there is no loss of energy to the surroundings, but it requires perfect thermal insulation unlike an isothermal process. That insulation will, of course, add to the weight and volume of the robot.

2.6.8.2 Energy storage in mechanisms

Using Hookean springs as a basis, mechanisms have been developed which amplify the energy stored. A variety of these mechanisms will be described here.

2.6.8.2.1 Non-linear / Progressive springs

Non linear springs are often used in engineering systems. They are usually made from a series of dissimilar Hookean springs or from different shapes of the same material producing a resultant single spring with nonlinear properties. By their very design, this will always be an increasing stiffness system where the more compliant elements are compressed/extended first before the applied load or displacement exceeds the capability of the less stiff spring. In general non-linear or progressive springs exhibit curved force-displacement curves as shown in Figure 68.

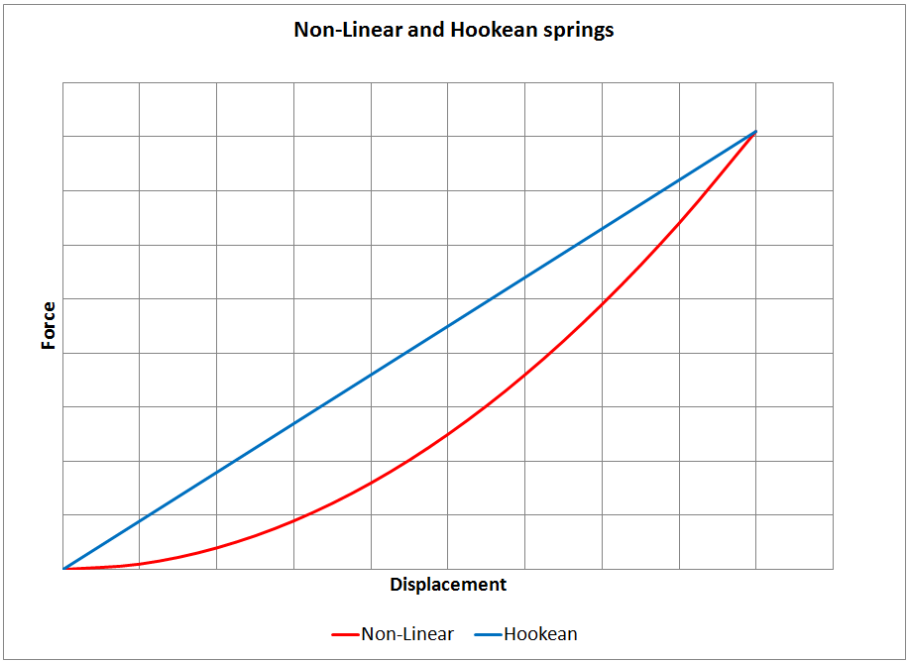

Figure 68 – Non-linear spring

As energy stored is equivalent to the area beneath the curve it can be seen that non-linear springs following this stiffening profile store less energy for a given force and

displacement than a Hookean spring. This makes them less suitable as a strain energy store.

Non-linear springs can be created in many different ways. A coil spring made of tapered wire means that the portion of the spring made with the thinner wire and lower spring constant will compress before the portion made with thicker wire and larger spring constant. Nesting a long light helical spring inside a short heavier spring gives a stepped increase in spring constant. A cone of rubber, when compressed also exhibits an increasing spring constant with displacement.

The energy stored in this type of non-Hookean spring is less than that assumed by the $kx^2/2$ relationship

2.6.8.2.2 The Compound bow

There is an exception to this increasing spring constant non-linear spring – The compound-action bow (Figure 70, Figure 71) which essentially has a widely changing spring constant with displacement. Almost all historical archers' bows can be reasonably approximated by Hooke's law. Bows are available in different 'weights', which is a measure of the spring constant, ranging from those which are easy to draw by a child to ones that are very difficult even for a strong man. However, the compound-action bow, patented by H.Wilbur Allen (1969) provides a completely different draw (displacement) verses force curve (Figure 69).

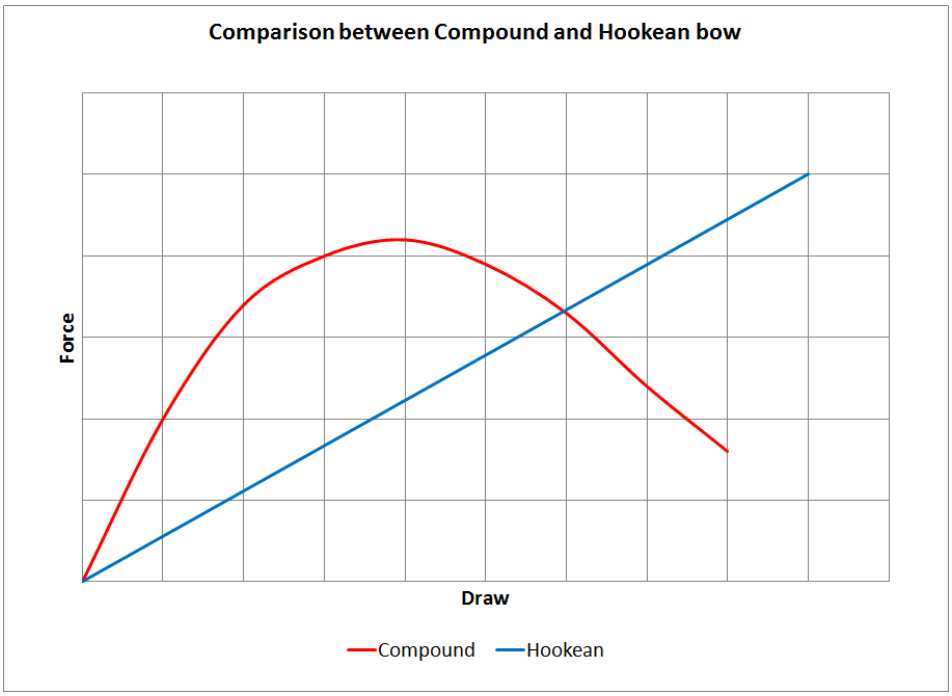

Figure 69 – Typical draw vs. force curves for archery bows

By adding a block and tackle pulley to an existing bow, Allen thought that the mechanical advantage offered by the pulley system would enable a heavier weight bow to be drawn. The first prototypes had very short draw lengths and so could not fire arrows very well. However, after incorporating cam shaped wheels or eccentrics into the pulley systems a more usable draw length was achieved. The introduction of these components also had an enormously beneficial side-effect – that the peak stiffness of the bow occurred at mid-draw and then reduced to a much lighter stiffness at full draw. This allowed an archer to comfortably hold a very heavy bow at full draw which would ultimately launch an arrow with more speed and more accuracy.

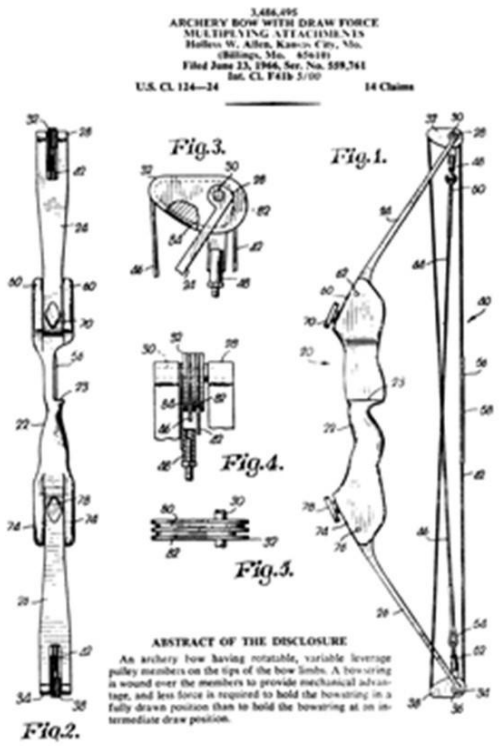

Figure 70 – Image from compound bow patent application (Allen 1969)

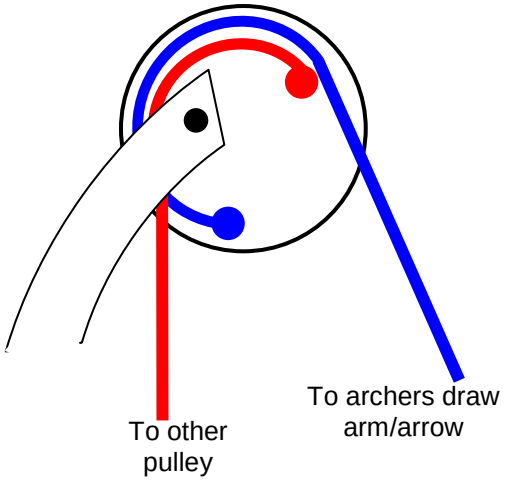

Figure 71 – The principles of a compound bow. As the archer draws the cable back, the pulley is forced to rotate which shortens the other cable pulling the bow arms together

The interesting point of note is that, when released from a compound bow, the arrow initially experiences a gentle force that rapidly increases as it accelerates. This is the opposite of what the arrow experiences when fired from a conventional recurve bow – here it experiences a high force which steadily decreases as the arrow moves forward. This means that the arrow used with a recurve bow has to be stiffer and therefore generally heavier than the arrow used with the equivalent compound bow.

If a similar spring mechanism could be adopted for a jumping device, the maximum amount of energy stored could be greater than that stored in a linear spring without requiring a high-force compression mechanism. This means that the displacement can be very large allowing for more energy storage, since the spring force reduces after a point. This is best illustrated graphically (Figure 72). Bearing in mind that the area

beneath each line is a measure of the energy stored, it is clear that the compound bow in this case stores more energy for a given force and displacement than a Hookean one. Whether the energy returned from the bow is entirely equivalent to the energy input, or whether the bow follows the exact force-displacement profile of loading is unknown.

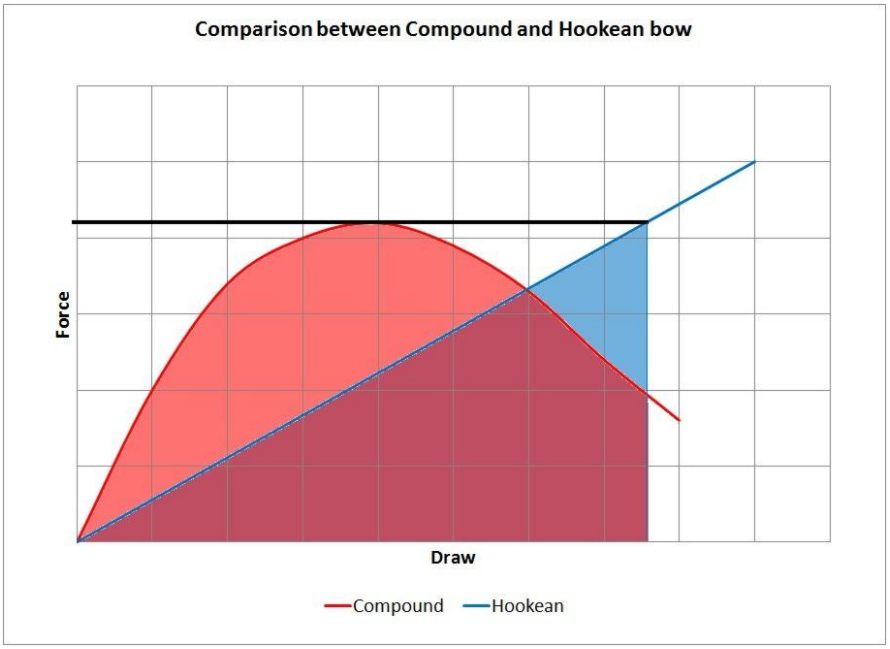

Figure 72 – For a given peak force the energy stored in a Compound bow (red area) is larger than that stored in a Hookean bow (blue area)

2.6.8.2.3 Bistable mechanisms

Bistable materials and mechanisms are interesting since they are stable in two positions, but release energy when moving from one stable form to another. Energy has been successfully stored in a bistable structure consisting of two non-linear metal tape springs. The device (Santer & Pellegrino 2003) which is 10 cm x 10 cm jumps around 12 cm vertically.

2.6.8.2.4 The Negator / Constant force spring

By careful design and construction it is possible to produce a constant force spring – a spring that resists with the same force no matter the displacement. The negator is

made from a flat length of spring steel wrapped spirally around itself. In its relaxed state it resembles a tight roll of metal tape. When unravelling the roll, the uncurling of the metal strip results in a steady force. This property is best illustrated visually (Figure 73). The constant force for any deflection results in the possibility of very large energy storage for a given force limit – a practical energy storage limit obviously comes from the available displacement. A significant limitation in the possible application of a Negator comes from the fact that energy can be stored only by extending the spring – not by compressing it.

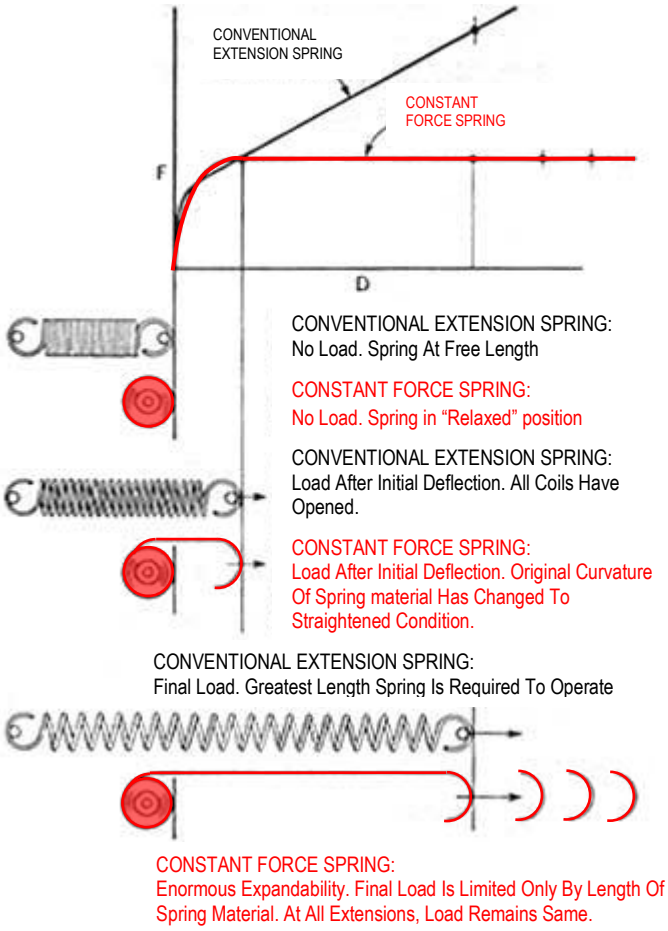

Figure 73 – Constant force spring compared to a Hookean spring courtesy of Stock Drive Products / Sterling Instruments

2.6.8.3 Summary

As in biology, the ideal response of an energy storage system for use in a jumping device would have a constant force for any value of displacement. This maximises the storage of energy, ensures that a "skeleton" need only restrain one unvarying force value, and produces gradual velocity increase during take-off (constant acceleration). A constant returned force for any displacement would allow the energy stored in a mechanism to approach twice that stored in a conventional Hookean spring. Only the Compound Bow and Negator are able to store more energy for a given force limit and displacement than a conventional spring. However, the compound bow has numerous additional elements which would add weight to a jumping device, and the Negator works only in extension and its metal coils tend to be heavy. Combining a conventional Hookean spring with a multiple-bar mechanism could lead to interesting force-displacement profiles.

2.7 Rolling

A rolling movement would improve the speed and energy economy of a jumping device over terrains that are smooth and level, leaving the jumping ability for obstacles and rough areas. Combining a movement suitable for smooth surfaces and one suitable for surmounting obstacles has been researched previously (Stoeter et al. 2002; Salton 2009) with devices that combine two separate systems in one device. Combining a rolling type movement with a jumping one has only been attempted in one prototype concept (Hirai, Matsuyama & Nakanishi 2007) and, although achieved within one structure, it is controlled and powered via a tether rather than remotely. A consideration of existing rolling techniques within robotics and nature follows.

2.7.1 Rolling in robotics

There are many rolling robots in development, but it is early days for all of them with mainly proof of concept studies being undertaken rather than optimisation for maximum performance and potential development into products. These proofs of concept include the design of the mobility system, but also make significant consideration of control system and path planning issues. Few of the prototypes have a specific application in

mind, but their number means there is obviously wide research interest in rolling robots. Suitable applications can be found once the rolling and control issues have been solved, but they will likely involve smooth terrain (Figure 75) or structured urban environments (Figure 74).

Figure 74 – Photograph of Gyrover in action (Brown & Xu 1997). Gyrover is a gyroscopically stabilised rolling wheel.

Figure 75 – Photograph of Groundbot patrolling an open area (Rotundus 2010).

It is important to distinguish between a true rolling robot and simply one with large wheels and a reaction point with the ground. It seems suitable to define a rolling robot as one that rolls on its entire outer surface rather than just external wheels and does not need to react any of its rotating torque against the ground with additional wheels or contact points. Thus such robots will tend to be spherical or cylindrical in form and therefore have a single axle (or no axle at all) and a completely active outer surface – i.e. a surface that is completely involved in the movement (Figure 76).

Figure 76 – Photographs of Rollo Prototype 3 which, unlike rolling devices with a fixed axis, is able to roll on any part of its surface and turn in place. (Halme et al. 1996; Rover-Company 1996)

Although only suited to movement on relatively level and smooth (but sometimes soft) surfaces, a spherical rolling robot has the following advantages over a wheeled robot or walking robot in similar terrains:

- It is possible to enclose the entire robot system inside a shell and thus provide mechanical and perhaps even environmental protection to components and equipment.
- There are no body extremities that can catch on obstacles.
- The entire outer body is driven (or rotating), helping the device to cover uneven or soft surfaces.
- Spherical robots have no ‘side’ to fall over upon from which they cannot recover.
- Spherical robots have a lower ground contact pressure when rolling across compliant surfaces due to their having a larger footprint than a simple narrow wheel or small foot, so they can be used for travelling on soft substrates such as sand, snow, brush or vegetation and for paddling through water. It should, however, be noted the a perfectly rigid sphere moving over a perfectly rigid surface has only point contact with the surface and as such consideration of the hardness of a spherical outer structure should be made depending on expected terrain types.

- Rolling spheres can potentially move in any direction and therefore can turn almost in place when meeting obstacles over which they cannot roll.
- Spherical robots can recover from collisions easily.

The current state-of-the-art in rolling robots all feature a common technique, but have seven different methods for achieving movement (R.H. Armour & J.F.V. Vincent 2006). All are based around the principle of moving the centre of gravity of a wheel or sphere outside the outer shell's contact area with the ground. This causes the wheel or sphere to 'fall' in that direction and thus roll along. This is best displayed diagrammatically as in Figure 77.

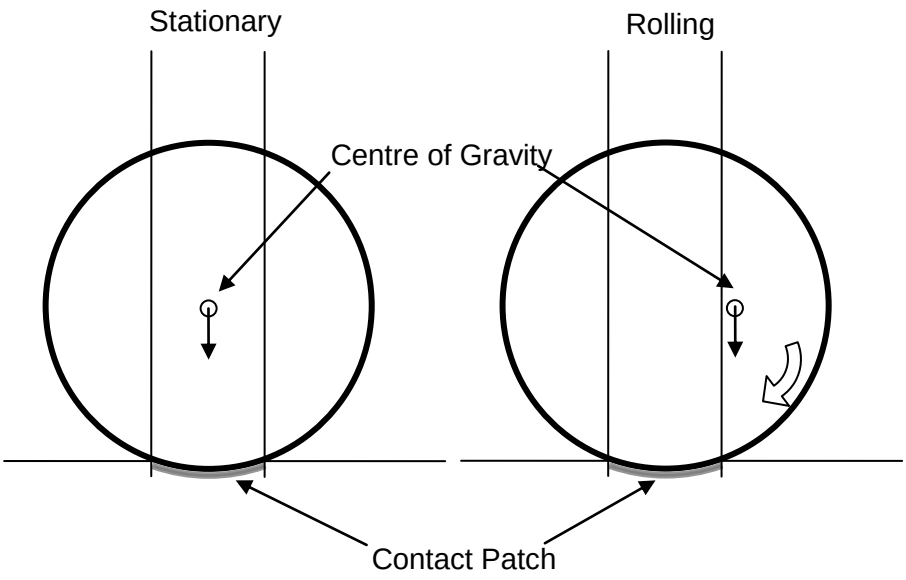

Figure 77 – Rolling achieved by moving centre of gravity outside of contact patch

Moving the centre of gravity results in the generation of a torque around the geometric centre of the sphere or cylinder. The amount of torque generated, and thus the ability to overcome substrate variations and slopes, depends on the ratio of the moving mass of the ballast to the remaining mass of the outer structure. Substantially improved slope and obstacle surmountability has been achieved through the use of gyroscopes to generate additional torque that can be explosively released (Schroll 2010). The rigidity of the outer surface and substrate upon which it is rolling also has an influence, particularly as contact patch area is large with compliant surfaces and substrates.

The suitability of each of the seven principles (R.H. Armour & J.F.V. Vincent 2006) developed for existing devices to achieve this rolling movement depends on proposed application requirements. Some applications require robustness, some require accuracy of movement or the ability to turn in place, and some require the ability to passively, but safely, roll down slopes when required. Armour (2006) has presented a subjective scoring technique for the seven principles, which ultimately resulted in no clear winner. All seven movement principles achieved similar scores with no clearly superior solution suitable for every application. It remains that enabling the centre of gravity to be moved as much as possible in all directions within a sphere, produces the most versatile devices.

2.7.2 Rolling In nature

Nature has not adopted a rolling motion very frequently, and examples are rare. This is not to say there are no rolling organisms, but only a few have been discovered. In nature, rolling appears to be a secondary form of motion to a pre-existing walking or slithering ability. Tumbleweed *(Salsola tragus)* is a possible exception, although a plant that has any movement mode is rare in itself. Within the natural world there appears to be two variants of rolling which are referred to here as ‘passive’ and ‘active’. Passive rolling requires external forces such as wind or gravity to drive the movement. Active rolling is where the organism expends its own energy to achieve rolling and thus controls its rolling such that it is able to move in a specific direction.

2.7.2.1 Passive rolling

Passive rolling organisms include the plant Tumbleweed, and animals such as the Web-toed Salamander *(Hydromantes platycephalus)* and Namib Golden Wheel Spider *(Carparachne aureoflava)*. For the last two, rolling is adopted only as an escape mechanism during attacks from predators as it allows for higher average speeds than walking. The web-toed salamander curls itself into a hoop, with its dorsal side outermost, and rolls down slopes with rocky surfaces far faster than would be possible by simply running down the slope (Garcia-Paris & Deban 1995). The Namib Golden Wheel Spider, after a short run-up, cartwheels down sand dunes (Figure 78) when attacked by its nemesis – the tarantula wasp *(Pompilid)*. It rolls down slopes steeper

than 15° at 1 m/s (~20 rotations per second) for up to 100 m until the slope becomes too shallow or the spider straightens its legs (Henschel 2005). Although not faster than their running speed of 0.9-1.4 m/s, rolling means there is no need to rest after short distances (less than 2 m) when running (Henschel 1990). Passive rolling only requires that an animal adopts a circular or spherical in form and ensures that its centre of gravity remains approximately at the geometric centre of its round shape.

Figure 78 – Namib Wheeling Spider rolling courtesy Michael Fogden / Minden Pictures

Figure 79 – Tumbleweed courtesy of S.E.Blackman

This passive rolling motion is also adopted by the Russian thistle / Tumbleweed. It can cover large areas of flat land distributing seeds over a wide compass making it more likely that one seed will fall in a suitable area for growth. Tumbleweed is unusual in its rolling, since it harnesses the force of the wind to roll over a wide area of smooth and level land. Tumbleweed lives for only one season. Its most recognised form is a rounded skeleton of a normal plant (Figure 79). However, there was a time in its life when it was a bright green rooted plant. During the spring and summer, the plant grows like a normal shrub. But in autumn, after the dry summer, a specialised layer of cells in the plant stem allows the dried plant to break away from its roots and to begin its wind-driven journey. During rolling, the plant disperses up to 250,000 seeds over a wide area.

It is the form of tumbleweed that ensures its ability to roll. The plant is almost spherical in its rolling state and its large surface area generated by the intricate branch structure

harnesses enough wind force to overcome the plant's weight. The wind velocity gradient across a surface (low wind speed near to the substrate surface which increases with altitude) contributes to the rotation and subsequent rolling. Rotation would occur even if the plant never touched the substrate over which it is moving (Vogel 2003). The centre of gravity of the whole plant is not at the centre of the 'sphere', and it is thought that this causes the plant to bounce as it rolls. This encourages seeds to be released, and improves its speed by keeping it airborne, removing the rolling resistance with the ground (Antol et al. 2003).

'Tumbleweeding' is being pursued as a form of low-cost locomotion for a range of exploratory rolling robots being developed by NASA (Antol et al. 2003; Antol et al. 2006; Lorenz, Jones & Wu 2002) and the European Space Agency (Jakubik et al. 2004). One is shown in Figure 80. There is no possibility of choosing which direction these devices might travel as they move only in the direction of the prevailing wind. Since the motive power source is free, it allows such tumbleweed robots to cover large, albeit smooth, areas with very little energy expended on movement. Some gentle direction control might be possible by moving the centre of gravity of the sphere to the left or right as it rolls, but the general direction will remain downwind meaning that such devices are unsuitable for a wide range of typical mobile robot applications. For applications with no time constraint, another possibility would be to anchor a tumbleweeding robot when the wind is blowing the wrong way, and releasing it only when the wind is in the right direction.

Figure 80 – Passively rolling wind-driven NASA Mars Tumbleweed Rover undergoing testing Arroyo Seco park in Pasadena, California (Lorenz, Jones & Wu 2002)

2.7.2.2 Active rolling

Active rolling is most interesting, since robots utilising this sort of movement are able to choose in which direction to travel. After an extensive literature search, only a handful of active rolling organisms have been discovered by the author – the caterpillar of the Mother-of-Pearl moth *(Pleurotya ruralis)*, the stomatopod shrimp *(Nannosquilla decemspinosa),* and the Dromedary Jumping-slug (*Hemphillia dromedaries*).

2.7.2.2.1 Mother-of-Pearl moth (Pleurotya ruralis) caterpillar

The caterpillar of the Mother-of-Pearl moth, when attacked with sufficient aggression, fixes its tail onto a surface and pushes its foremost segments backward quickly with its front legs. Once the head reaches the tail, the caterpillar rolls into a wheel shape (Figure 81) with its back outermost and continues to roll for up to 5 complete revolutions (Brackenbury 1997). Speeds of around 40 cm/s have been measured, which is about 40 times faster than its normal walking speed. This means that the ~25 mm long caterpillar will have moved itself ~125 mm in around 0.3 s; enough to

outrun a predator. This form of retreat obviously surprises a predator and gives the caterpillar valuable time to escape. The series of rolls is all driven by a single impulse so it cannot be considered a continuous rolling motion. However as the rolling is not achieved simply by adopting a rounded form, the Mother-of-Pearl moth caterpillar performs active rolling.

Figure 81 – Photographs of the Mother-of-Pearl moth caterpillar during rolling (Brackenbury 1997)

2.7.2.2.2 Stomatopod shrimp (Nannosquilla decemspinosa)

Nannosquilla decemspinosa is a shrimp that adopts an active rolling motion when washed up onto a beach. It spends most of its time underwater in its burrow where it waits for prey. It swims only a small distance, up to one body length, out of its burrow to collect its food. Because of its elongated body and short laterally projecting legs, the adult cannot walk when out of the water. Its long and low body rests on the substrate and the friction is too large for its legs to drag it along. The legs are not strong enough to lift its body from the surface. When a wave washes it from its burrow, onto the beach and out of the water, it performs up to 2 m of backward somersaults (20 – 40 rotations) returning to the water (Caldwell 1979; Full et al. 1993). The rolls do not occur uninterrupted since the animal ends up lying on its back after each cycle and then expends another pulse of energy. A diagram of the rolling motion is shown in Figure 82. The loops are very flat in the dorsoventral plane which improves rolling stability and, when rolling, tend to lean down-beach and so will passively steer back into the water. The stability of each roll is good since for much of the time the centre of gravity

of the animal is close to the ground such that it does not tend to topple over. There is a definite pause after each somersault which also gives a useful stable resting point.

Figure 82 – Diagram of *Nannosquilla decemspinosa* rolling by performing back-flips moving from right to left (Caldwell 1979)

2.7.2.2.3 Dromedary Jumping-slug (*Hemphillia dromedaries*)

The Dromedary Jumping-slug is perhaps misnamed, as mentioned in Section 2.6.6.5.12. It never actually leaves the ground at any point during its gymnastic side-to-side flapping or rapid coiling and uncoiling of its body. Such motions are performed as an attempt to startle a predator. In addition the rapid movements sometimes break the surface tension between the slug's foot and the substrate and could lead to falling from a surface or tumbling out of harm's way (Ovaska 2002). Although the slug has no control of where it might end up after this thrashing movement, it is considered to perform active, rather than passive, rolling.

2.7.2.3 Summary

As in Robotics, rolling in nature requires some specific attributes. For passive rolling these are simply to adopt a round form and wait for external forces to do their work. For active rolling they require the ability to change where the centre of gravity lies within the round shape, through the moment of body elements.

Chapter 3 An evaluation technique

The development of a new mobility system suited to rough terrains requires some method by which to determine performance. In particular it requires a method with which to compare performance between widely different devices. Standard measures of performance include quantitative values such as mass, size, speed and so on, and, although useful individually, it would be of benefit to combine them in some way into a single numerical score. But unlike standard measures, a single score cannot hope fully and accurately to give a measure of a performance that is suitable for every potential user's needs due to the differing requirements between users. Thus a score must be obtained by considering a specific user's application and the specific required measures associated with that application. This chapter presents a scoring technique that attempts to quantify performance for a mobile robot in a variety of different categories. It results in a method for comparing widely differing devices against specific application requirements, but does not intend to generate unquestionable results.

It is almost impossible to generate a universal scoring system that will adequately suggest the most suitable device for every user's requirement, as each user has a unique application or idea of performance. Attempts have been made to produce universal measures, but these rely on common testing arenas (Jacoff, Weiss & Messina 2003; Sukhatme & Bekey 1996; Sukhatme, Brizius & Bekey 1997; Jacoff, Messina & Evans 2002; McBride, Longoria & Krotkov 2003) where the time taken and energy used to traverse a particular test arena are often determined to be suitable measures. Of these experimental tests, only one attempts to produce a single performance metric. This single score is required as it is the basis for the RoboCupRescue urban search and rescue competition, which uses standardised National Institute of Standards and Technology (NIST) testing arenas. The competition hopes to encourage the development of robots to "negotiate complex and collapsed structures, find simulated victims, determine their condition and locations, and generate human readable maps to enable victim recovery" (Jacoff, Weiss & Messina 2003). The proposed scoring system uses the summation of a series of normalised scores given by independent human judges, divided by the number of operators, and all factored by a weighting depending on arena complexity. Individual scores are achieved in factors

such as map quality, victim location and impacts with the arena. The performance metric calculation is shown in Figure 83. Surprisingly, for a human rescue application where reducing the time to reach a survivor is critical, it appears that there is no score relating to time within the performance metric.

$$\begin{pmatrix} arena \\ weighting \end{pmatrix} \times \left(\frac{\begin{pmatrix} map \\ quality \end{pmatrix} + \begin{pmatrix} victim \\ location \end{pmatrix} + \begin{pmatrix} victim \\ tag \end{pmatrix} + \begin{pmatrix} victim \\ situation \end{pmatrix} + \begin{pmatrix} victim \\ state \end{pmatrix} - \begin{pmatrix} arena \\ bumping \end{pmatrix} - \begin{pmatrix} victim \\ bumping \end{pmatrix}}{(1 + number\ of\ operators)^2} \right)$$

Figure 83 – RobocupRescue competition performance metric (Jacoff, Weiss & Messina 2003)

Another scoring technique is the one developed by Tunstel (Tunstel 2007) for evaluating the performance of the Mars Exploration Rovers using the relative measure of what is commanded by operators in each instruction cycle, and the resultant actions of the rover. “Primitive performance metrics” are computed for each factor, resulting in individual dimensionless performance ratios that can be combined into an aggregate score. This scoring system assumes that each of the required performances is weighted equally, and, once weighting is incorporated, it becomes a very subjective scoring procedure. Tunstel’s method (Tunstel 2007) is another way in which to compare a user’s requirements with the user-perceived performance in a subjective way. Any non-experimental method used to produce a single score will have a subjective element.

The evaluation technique developed as part of this work is also subjective and user centred. The scoring method is straightforward, consisting of five steps:

1. **Complete a table of reported, implied or estimated, quantifiable and qualitative performance measures** in a variety of applicable categories. A certainty percentage can be associated with the final score if a record is made of those values that are estimated or assumed.
2. **Generate a selection of application-specific requirement measures** based upon the available categories in the table produced in Step 1.

3. **Assign weights.** Any scoring system must take into account the relative importance of a particular requirement. Rather than allow for a fixed total number of points for each category, it is better to use the "fixed-sum" method (Ullman 2003) where 100 points are distributed between all the requirements; the most going to those of high importance. Weights of zero mean that a particular category is unimportant.
4. **Normalise category-values.** As the resulting single performance number will be related to the product of the weights and the associated values, it is critical that each value must be normalised to ensure that large specific values don't artificially skew the final score. The performance measures in each category are therefore graded against a user-specific application requirement using the following values:

   -2 if the device very much fails to achieve the requirement
   -1 if the device somewhat fails to achieve the requirement
   0 if the device achieves the requirement
   +1 if the device somewhat exceeds the requirement
   +2 if the device very much exceeds the requirement

   The breakpoints between 0 and +1, and +1 and +2 etc. have to be carefully determined by the user. (Those requirements that are either yes/no, true/false, etc. achieve +1 if they agree and -1 if they disagree.)
5. **Calculate overall score** using a summation of the products of the weights and the normalised category values. The numerical scores returned after step five will have values ranging from approximately -200 to +200. Those devices with a score approximately equal to 0 meet the requirement in general, but large positive scores highlight better performing devices. Negative scores belong to devices not meeting the requirements, but they should not be ignored entirely particularly when building new solutions based upon existing designs.

The workings of the scoring system are described below through the use of a single example for evaluating rough terrain robots. Two more examples will be introduced later, to give an idea of how the scores might change for different applications.

3.1 Step 1 – Produce performance measures table

Step 1 requires that a table of measures of recorded and published performance be produced. For the purposes of this thesis, the table considers a number of unstructured terrain mobile robots (Table 4). The performance categories were selected to more or less match the common requirements for rough terrain applications. However, the table may not contain every possible piece of information for every eventual rough terrain application. The contents for the table were found after extensive searching of the available literature. Where possible, the published data was used before any interpretation, estimation and opinions were used to complete the remaining fields. Videos are often used by research teams to display "performance" in an easy to understand form, so some performance measures had to be estimated directly from the available footage. Due to the lack of information in certain areas, it proved impossible to produce a complete table without making a series of assumptions. These are all given below. The use of assumptions, although subjective, does result in a complete account of a device in a series of common categories. The table of measures (Table 4) are compiled in such a way that true data, estimated data and assumed data are each highlighted separately. A "certainty %" will be introduced later (see Section 3.5) to highlight those devices that have adequate true data from those with many estimated and assumed values.

3.1.1 Assumptions

- In general where no entry exists for a single device within a similar selection of its peers, then the value used is the average of its peers, so as to not skew the data subsequently used to compare motive techniques.
- Slope - It is clear that a jumping robot must have the ability to climb a slope with a series of successive jumps, but the published results for all of the devices listed make no mention of that capability specifically. It can be reasonably deduced that up to certain slope angles, a jumping robot will still jump up the slope, until the steepness results in jumps vertical in orientation. Based on an average take-off angle of around 60° to the horizontal, this would result in the ability to climb a substantial slope. In reality, the tumbling occurring after landing

may result in an overall backward motion for some jumping devices, so an assumed slope capability of 20° appears reasonable.

- Gap - Where gap spanning ability is not reported, an assumed ability of ½ track unit length for tracked vehicles (the main chassis track where there are multiple track lengths), ½ wheel diameter for wheeled rovers, and 1 leg-length for walking rovers is used. Jumping rovers tend to have their jump range reported.
- Step - Similarly for step or obstacle surmountability, assumed values are 1/3 track unit length for tracked vehicles (with a small additional step height added for multiple tracked devices). Wheeled, walking and jumping devices generally have obstacle surmountability size reported.
- Speed – For multimodal devices, the speed value is the maximum speed achieved with either of the modes.
- Payload – Those devices that already have additional sensors that are not used for control, movement or localisation are assumed to be carrying an interchangeable scientific payload of 1 kg. Those devices that only gather observational data using existing control sensors are assumed to be able to carry no additional payload. This may not be a problem for certain non-scientific applications.
- Robustness – Whether a device is robust or not, is determined from whether it will survive a drop of about 1.5 m. Jumping robots often land from such heights, but other rovers' capability is estimated where required.
- Cost – No mention of the actual costs of the devices is made in any of the literature. Neither purchase price, research and development, or material costs are disclosed. Some researchers use words such as "cheap" and "inexpensive", but there is no monetary value associated with that. Given the absence of any monetary values, an estimate of productionised cost has been chosen. This estimate is based on a variety of factors such as complexity, level of development, and proposed application.
- Range – Those rovers that have no reported range, but a finite capacity power supply, are given the average values of similar devices. Those powered using a tether, unless its length is reported, are given a nominally short range of 100 m

due to a maximum tether length. Those powered by photovoltaic cells are given a very long range (substantially above any range required by an application).

- Lifetime – Where rovers use a power tether or photo-voltaic cells to charge onboard batteries, their lifetime is assumed to be something substantially larger than any required application lifetime. Though often unreported for finitely powered devices, there must be a lifetime for all rovers and therefore the average value for similar devices is provided for unreported ones.

		Physical Properties				Motive Performance										Economic Properties	Useability			Energy Issues				
	Robot	Size			Mass	Obstacle height cleared (walking / wheeled)		Obstacle height cleared (jump)		Span cleared (Jump Range / Gap)	Max slope climb	Control Direction	Self-righting?	Speed		Movement accuracy	Modes of movement	Cost	Payload	Robustness	Control	Batteries	Range	Lifetime	Power source	Energy consumption
	red = calculated / estimated blue = assumed / averaged grey = auto calculated	length (m)	height (m)	width (m)	(kg)	(m)	(body lengths)	Cleared Height (m)	(body lengths)	Range / Gaps (m)	(°)	y/n	y/n	(m/s)	(body lengths/s)	(good/ fair/ poor)	1 / 2 / 3	($)	(kg)	survive 1.5m drops (yes/no)	remote / tethered	y / n	(km)	(hrs)		
Jumping	JPL Hopper Generation3	0.15	0.15	0.15	1.3	0.00	0.00	0.9	6.00	1.90	20	yes	no	0.020	0.13	poor	2	5000	0	yes	remote	yes	1.031	12	batteries but with photovoltaic option	125J / jump
	Utah Monopod	0.15	0.3	0.2	2.4	0.00	0.00	0.51	3.40	0.31	20	yes	no	0.080	0.53	poor	1	250	0	no	autonomous	yes	1.031	3	Batteries	25J / jump (spring o/p)
	IMT Grillo	0.05	0.05	0.04	0.015	0.00	0.00	0.05	1.00	0.00	20	no	no	0.080	1.60	poor	1	500	0	no	none	yes	1.031	3	3v 300mAh battery	
	EPFL Miniature Jumper w/cage	0.15	0.18	0.15	0.0143	0.00	0.00	0.62	4.13	0.42	20	yes	yes	0.140	0.93	poor	1	500	0	yes	remote	yes	0.045	0.105	LiPo battery	350mW/jump
	University of Bath Glumper	0.5	0.5	0.5	0.7	0.00	0.00	1.17	2.34	2.00	20	no	yes	0.080	0.16	poor	2	100	0.25	yes	none	yes	0.048	3	100 jumps on battery	
	Sandia Hopper	0.5	0.7	0.5	2.5	0.00	0.00	4	8.00	5.00	20	yes	yes	0.080	0.16	poor	1	500	0	yes	autonomous	no	3	10	combustable fuel	
	EPFL 7g Miniature Jumper	0.05	0.05	0.02	0.007	0.00	0.00	1.5	30.00	1.95	20	no	no	0.080		poor	1	500	0	yes	remote	yes	0.045	0.1	Li-Po battery	
	Tokyo Institute Airhopper	1.56	0.5	1.1	20	0.00	0.00	0.68	0.44	0	20	no	no	0.080		poor	1	1000	0	no	tethered	no	0.1	1000	Pneumatic supply	
	University of Tokyo Mowgli	0.4	0.5	0.4	3	0.00	0.00	0.5	1.25	0.5	20	no	no	0.080		fair	1	1000	0	no	tethered	no	0.1	1000	Pneumatic supply	
	Kagoshima Pendulum Jumper	0.25	0.25	0.1	0.72	0.00	0.00	0.06	0.24	0	20	no	no	0.080		poor	1	500	0	no	tethered	no	0.1	1000	Electric supply	
Walking	Boston Dynamics Big Dog	1.1	1	0.3	109	0.50	0.45	0.8	0.73	1.00	35	yes	yes	2.000	1.82	fair	1	100000	154	yes	remote	no	10	2.5	15Hp IC single 2-stroke engine powered hydraulics	
	Rhex (2001 version)	0.53	0.21	0.52	7	0.30	0.57	0	0.00	0.20	45	yes	yes	0.500	0.94	fair	1	5000	0	yes	remote	yes	2.625	1.5	2 x 12v 2.2Ah	100W average
	Sprawlita	0.16	0.08	0.06	0.275	0.04	0.22	0	0.00	0.00	24	yes	no	0.550	3.44	poor	1	500	0	no	tethered	no	0.1	1000	pneumatic supply	
	ESA Prolero	0.23	0.2	0.22	1.5	0.10	0.43	0	0.00	0.10	20	yes	yes	0.765	3.32	fair	1	5000	1.5	no	tethered	yes	0.1	1000	batteries	3W
	Dante II Carnegie Mellon	3.7	3.7	2.3	770	1.30	0.35	0	0.00	0	80	yes	no	0.008	0.00	poor	1	10000	130	no	tethered	no	0.3	1000	basesation generator (volcano side)	2kW
	IMPASS Virginia Tech	2	1	1	10	0.91	0.46	0	0.00	0.50	30	yes	yes	0.167	0.08	fair	1	5000	0	no	tethered	no	0.1	1000	tethered	
Multi-modal	Jumping Miniwhegs	0.104	0.05	0.076	0.191	0.04	0.41	0.2	1.92	0.10	20	yes	yes	0.900	8.65	poor	2	500	0	yes	remote	yes	13	4	2 x 3V CR2 batteries	
	Minnesota Scout	0.085	0.05	0.11	0.2	0.00	0.00	0.3	3.53	0.25	20	yes	yes	0.310	3.65	fair	2	1000	0	yes	remote	yes	1.302	1.167	battery	
	Ritsumeikan Uni Deformable Sphere	0.09	0.09	0.09	0.05	0.00	0.00	0.18	2.00	0.01	20	no	yes	0.009	0.10	poor	2	500	0	yes	tethered	no	0.1	1000	Electric supply	
Tracked	Tehzeeb	0.97	0.4	0.8	30	0.30	0.31	0	0.00	0.25	40	yes	no	1.435	1.48	good	1	1000	0.25	no	remote	yes	1	0.667	battery	
	Redback	0.5	0.25	0.5	5.5	0.40	0.80	0	0.00	0.15	45	yes	yes	0.170	0.34	fair	1	1000	1.5	no	remote	yes	1	0.333	8x 2.5Ah NiMh	
	ROBHAZ-DT3	0.74	0.47	0.29	39	0.25	0.34	0	0.00	0.19	40	yes	no	2.700	3.65	good	1	1000	0.25	no	remote	yes	1	1	Lithium-polymer rechargeable Battery	
	iRobot Packbot 510 FasTac	0.686	0.406	0.516	25	0.30	0.44	0	0.00	0.34	45	yes	yes	2.578	3.76	good	1	50000	20.9	yes	remote	yes	10	4	battery	
	Foster Millar Talon	0.864	0.427	0.572	60	0.40	0.46	0	0.00	0.43	45	yes	no	2.300	2.66	good	1	50000	45	yes	remote	yes	23.18	2.8	2 x 32v 300W/h Lead acid	
	iRobot Warrior 710	0.89	0.46	0.77	155	0.47	0.53	0	0.00	0.61	45	yes	yes	4.170	4.69	good	1	50000	68	yes	remote	yes	16.59	3.4	12 BB-2590/U batteries	
	RoboMotio Inc. STRV	1.32	0.24	0.65	42.3	0.70	0.53	0	0.00	0.24	45	yes	yes	1.400	1.06	good	1	50000	44.63	yes	remote	yes	16.59	3.4	battery	
Wheeled	Activrobotics P3-AT	0.5	0.36	0.49	9	0.10	0.20	0	0.00	0.11	24	yes	no	0.800	1.60	good	1	10000	14	no	autonomous	yes	17.28	6	12V 252Wh	
	CMU Corky	1	0.97	0.42	18	0.10	0.10	0	0.00	0.33	29.8	yes	no	0.304	0.30	fair	1	1000	0.25	no	remote	yes	4.374	4	2x 12V 8Ah for motors, 2 x 7.2V 1800mAh electrics	
	Bluebotics Shrimp	0.639	0.278	0.428	5.4	0.22	0.34	0	0.00	0.06	40	yes	no	0.350	0.55	good	1	500	3	no	remote	yes	2.52	2	12V NiMh 4200mAh	
	NASA Pathfinder Sojourner Rover	0.65	0.3	0.48	10.5	0.20	0.31	0	0.00	0.07	29.8	yes	no	0.007	0.01	good	1	1000000	0.25	no	remote	yes	1000	1000	.22sqM solar panel of 234 5.5mil GaAs cells, 9 x LiSOCl2 D-cells	10W when driving
	NASA MER Spirit & Opportunity	1.6	1.5	2.3	180	0.25	0.16	0	0.00	0.13	30	yes	no	0.046	0.03	good	1	1000000	0.25	no	remote	yes	1000	1000		
	ESA ExoMars	1	1	1.1	200	0.30	0.30	0	0.00	0.20	25	yes	no	0.020	0.02	good	1	1000000	40	no	remote	yes	1000	1000		
	Sandia Ratler II Rover	1.26	0.52	1	115	0.67	0.53	0	0.00	0.25	30	yes	yes	0.600	0.48	good	1	1000	18	no	autonomous	yes	4.32	2	four 12 V, 26 Ah, lead-acid gel-cell batteries	>500W
Serpen-tine	OT4 Omnitread (UofMichigan)	0.94	0.082	0.082	4	0.42	0.45	0	0.00	0.49	45	yes	yes	0.120	0.13	fair	1	10000	0	no	remote	yes	0.533	1.25	battery	
	OT8 Omnitread (UofMichigan)	1.27	0.186	0.186	13.6	0.46	0.36	0	0.00	0.66	30	yes	yes	0.100	0.08	fair	1	10000	0	no	tethered	no	0.1	1000	tethered 70W drive motor + pneumatic supply	

Table 4 – Rough Terrain Robot Performance Summary. Red cells highlight assumed or averaged entries. Blue shaded cells highlight calculated or estimated entries. Data compiled from (Burdick & Fiorini 2003; Fiorini & Burdick 2003; Allison 2002; Scarfogliero, Stefanini & Dario 2007; Scarfogliero, Stefanini & Dario 2006; Kovač et al. 2010; Paskins 2007; Weiss 2001; Kovač et al. 2008; Kikuchi, Ota & Hirose 2003; Niiyama, Nagakubo & Kuniyoshi 2007; Hayashi & Tsujio 2001; Raibert 2008; Boston Dynamics 2008; Altendorfer et al. 2001; Clark et al. 2001; Martin-Alvarez et al. 1996; Bares 1999; Jeans & Hong 2009; Hong, Jeans & Ping 2009; Lambrecht, Horchler & Quinn 2005; Quinn et al. 2002; Quinn 2006; Stoeter, Burt & Papanikolopoulos 2003; University of Minnesota Centre for Distributed Robotics 2005; Stoeter et al. 2002; Kapsner 1998; Hirai, Matsuyama & Nakanishi 2007; Sugiyama 2006; Suthakorn et al. 2008; Sheh 2005b; Kang et al. 2005; iRobot-Corporation 2009b; Foster-Miller 2008a; iRobot-Corporation 2009a; Trentini et al. 2007; MobileRobots 2008; Burion et al. 2004; Estier et al. 2000; Mishkin et al. 1998; Lindemann et al. 2006; Ellery et al. 2005; Amai et al. 1994; Borenstein, Granosik & Hansen 2005; Borenstein & Borrell 2008; Granosik 2005)

3.2 Step 2 – Define application

Without an idea of application, a user cannot hope to be able to evaluate which solution fits their needs the best. The required performance factors for any robotic mobility system fall broadly into a set of categories including:

- Physical Properties: e.g. size, mass, packability/deployability, easy of transport.
- Economic Properties: e.g. cost, number of operators, availability of spares, ease of maintenance.
- Movement ability: e.g. speed, terrain types, accuracy of movement, stability.
- Usability: e.g. robustness, complexity, level of autonomy, payload capacity, damage from/to surroundings, environmental survivability (temperature, dust, moisture), modes of movement.
- Energy Properties: e.g. power source, range, lifetime, power consumption, efficiency.

Using these categories as a base, and the suggested potential rough terrain applications from Section 2.3 (p.24), three example applications have been defined in terms of the performances required. One of those example applications will be taken through the entire workings of the scoring system as an illustration. The second and third will be shown towards the end of this chapter.

An important consideration throughout the application definition is whether it is the actual value of the performance or a non-dimensional performance value that is applicable. A non-dimensional performance may illustrate impressive robots, but it does not necessarily reflect usefulness. For example, a tiny 50 mm tall robot may be able to get over obstacles 10 times its size (500 mm), but a larger robot 500 mm tall that can clamber over obstacles twice its size (1000 mm), could be considered more able.

3.2.1 Example Application 1 – General rough terrain exploration

The first example application is a general one for rough terrain exploration. Such an application would require the ability to move in fairly rough terrains, be relatively small, portable, inexpensive, and be able to operate remote to the user. The use of the suggested categories above results in the application requirements shown in Table 5. It is clear that not all of the potentially suitable measures are contained within the application definition. This is a result of the limitations of the information provided in the table produced in Step 1. For example, a collapsible or packable robot might mean that it would be very easy to transport to a start position. However, the disassembly/reassembly information for robots is not generally available in the published materials. Packability or collapsibility therefore, remains outside of the useable application requirements.

Physical Properties	Size: up to 0.5 m x 0.5 m x 0.5 m Weight: <10 kg
Motive Performance	Must have direction control Speed: ~1 m/s Cleared obstacle height: 0.5 m Slopes: 30° Gaps: 0.25 m Must not fall over or get stuck
Economic Properties	Inexpensive (under $1000)
Usability	Payload capacity of 250 g Survive 1.5 m drops Remotely controlled (wireless)
Energy Issues	Battery powered with photovoltaic consideration Range of 3-5 km Lifetime of 3-5 hrs

Table 5 – Example application 1: General rough terrain exploration application definition

3.3 Step 3 – Assign weights to categories

For the example application, the assignments of the 100 weights are shown in Table 6.

Category	Weights
Size smaller than $(0.5m)^3$	7
Mass under 10kg	7
Direction control	11
Speed ~1m/s	5
Obstacle height cleared 0.5m	11
Slope capability of 30°	5
Gap cleared 0.25m	6
Un-toppleable (self-righting yes/no)	8
Cost (<$1000)	12
Payload over 0.25kg	5
Robust (yes/no)	7
Control type (remote minimum)	5
Uses batteries (yes/no)	5
Range >2km	3
Lifetime >4hrs	3
Total	**100**

Table 6 – Example application 1: weights assignment

3.4 Step 4 – Grade the performance in each category

Each value needs to be measured relative to an application requirement datum. Category-values are assigned as follows: +1 if the device is a bit better, +2 if it is much better, 0 if it achieves the required performance, -1 if it is a little worse, and -2 if it is a

lot worse. The assignment of category-values is very subjective and user-focussed with linear or non-linear break-points entirely optional. The value assignment for the example exploration application is shown in Table 7.

In the case of this research, an enlarged version of the table produced in Step 1 (Table 4) automatically assigns category-scores depending on the datum values and break-points. Considering the JPL Hopper from Table 4; this robot weighs 1.3 kg. This results in a category-score for Example Application 1 of +1, as the robot falls in the 1-5 kg bracket.

Category	Category score assignment
Size smaller than $(0.5m)^3$	$+2 \leq (0.1m)^3$, $+1 \leq (0.25m)^3$, $0 \leq (0.5m)^3$, $-1 \leq (0.75m)^3$, $-2 > (0.75m)^3$
Mass under 10kg	+2≤1kg, +1≤5kg, 0≤10kg, -1≤20kg, -2≤20kg
Direction control	+1=yes, -1=no
Obstacle height cleared 0.5m	+2≥1m, +1≥0.75m, 0=0.5m, -1≥0.25m, -2<0.25m
Gap cleared 0.25m	+2≥0.6m, +1≥0.4m, 0≥0.25m, -1≥0.15m, -2<0.15m
Slope capability of 30°	+2≥60°, +1≥45°, 0≥30° -1≥15°, -2<15°
Un-toppleable (self-righting yes/no)	+1=yes, -1=no
Speed ~1m/s	+2≥4m/s, +1≥2m/s, 0≥1m/s, -1≥0.5m/s, -2<0.5m/s
Cost (<$1000)	+2≤$100, +1≤$500, 0≤$1000, -1≤$5000, -2>$5000
Payload over 0.25kg	+2≥0.55kg, +1≥0.4kg, 0≥0.25kg, -1≥0.15kg, -2<0.15kg
Robust (yes/no)	+1=yes, -1=no
Control type (remote minimum)	+2=autonomous, +1=remote, -1=tethered, -2=none
Uses batteries (yes/no)	+1=yes, -1=no
Range >2km	+2≥6km, +1≥4km, 0≥2km, -1≥1km, -2<1km
Lifetime >4hrs	+2≥24hrs, +1≥10hrs, 0≥4hrs, -1≥2hrs, -2<2hrs

Table 7 – Example application 1: category-value assignment

3.5 Step 5 – Calculate overall scores

Multiplying the category-scores from Step 4 with the weights defined in Step 3, and adding them together, has the effect of highlighting those devices that perform well in the most important areas, within a single numerical score.

A certainty percentage can also be associated with the achieved scores. This percentage relates to the number of accurately known values in Step 1 (the table of published performances) when compared to the number of categories used to produce the score. For example, if 5 category-values for a particular robot are accurately known, then its certainty percentage is 33.3 % for Example Application 1, which considers a total of 15 categories.

The numerical scores against Example Application 1, for the 35 devices presented in Step 1, are shown in Table 8. Although performance is not necessarily related to movement type, it is useful to use that as an additional value to distinguish the best performing variety. This appears as the fourth column in Table 8.

Robot	Score	Certainty %	Type
Sandia Hopper	55	66.7	Jumping
University of Bath Glumper	47	73.3	Jumping
EPFL Miniature Jumping with cage	38	66.7	Jumping
EPFL 7g Miniature Jumper	35	66.7	Jumping
JPL Hopper Gen3	30	66.7	Jumping
Jumping Miniwhegs	28	80.0	Multimodal
Boston Dynamics Big Dog	22	73.3	Walking
iRobot Warrior 710	20	80.0	Tracked
Minnesota Scout	19	80.0	Multimodal
Utah Monopod	6	60.0	Jumping
iRobot Packbot 510 FasTac	6	80.0	Tracked
Sandia Ratler II Rover	4	80.0	Wheeled
RoboMotio Inc. STRV Defence R&D Canada	3	46.7	Tracked
Ritsumeikan University Deformable Sphere	-3	60.0	Multimodal
Redback	-5	73.3	Tracked
Foster Millar Talon	-7	73.3	Tracked
Rhex (2001 version)	-9	60.0	Walking
Bluebotics Shrimp	-19	73.3	Wheeled
ESA Prolero	-20	60.0	Walking
OT4 Omnitread (UofMichigan)	-20	86.7	Serpentine
IMPASS Virginia Tech	-27	33.3	Walking
Sprawlita	-28	60.0	Walking
Tehzeeb	-35	53.3	Tracked
ROBHAZ-DT3	-40	66.7	Tracked
Activrobotics P3-AT	-41	73.3	Wheeled
CMU Corky	-42	46.7	Wheeled
Dante II Carneige Mellon	-46	73.3	Walking
University of Tokyo Mowgli	-48	53.3	Jumping
OT8 Omnitread (UofMichigan)	-48	73.3	Serpentine
IMT Grillo	-56	40.0	Jumping
ESA ExoMars	-56	66.7	Wheeled
Kagoshima Pendulum Jumper	-62	40.0	Jumping
NASA Pathfinder Sojourner Rover	-62	46.7	Wheeled
NASA MER Spirit and Opportunity	-78	60.0	Wheeled
Tokyo Institute Airhopper	-94	73.3	Jumping

Table 8 – Example application 1: achieved scores displayed in decreasing score order

Table 8 shows that for the example rough terrain exploration application, only thirteen robots achieve scores above zero. The top five devices are all jumping robots, with jumping multimodal devices also scoring reasonably well. Those high-scoring jumping robots tend to be inexpensive and simple, with a combination of reasonable rough terrain capability and small size. This makes them particularly suitable for this general rough terrain exploration application. The highly developed and tracked robots (iRobot Warrior and FasTac, and Robomotio STRV), and a single comparatively large walking device (BigDog) score reasonably well. Only one wheeled robot achieves a positive score. Apart from the less developed jumping robots, wheeled, walking and serpentine robots perform poorly for this rough terrain application. This pattern of scores is somewhat expected given that few walking and wheeled devices have the rough terrain capability required without sacrificing size, and associated issues, in the case of wheeled robots, and complexity, and associated issues, in the case of walking and serpentine robots. What is a little surprising are the poor scores achieved by the hugely successful NASA Mars Exploration Rovers and Sojourner rover. Although they have managed to travel significant distances over a variety of terrains performing scientific experiments along the way, their movement abilities do not suit the example rough terrain exploration application. Their costs are also very high.

Figure 84 gives an illustrative view of the scores on the horizontal axis, in combination with the certainty of those scores, on the vertical axis. The devices that appear on the right side of the chart are suited to the application. Those appearing left of the 0-score line are not suitable. Devices in the upper portion of the chart have a higher certainty than those in the lower portion. Therefore, robots appearing in the upper right corner of the illustration are both suitable for the application and can be confidently said to be so. Those devices that have scores just less than 0, and also have low score-certainties, have the possibility of achieving greater scores if new performance details become available. The inverse is also possible, where such devices could be awarded lower scores depending on the contents of any new performance details. Reading Table 8 in conjunction with the representation of scores in Figure 84, gives a visual guide of performance.

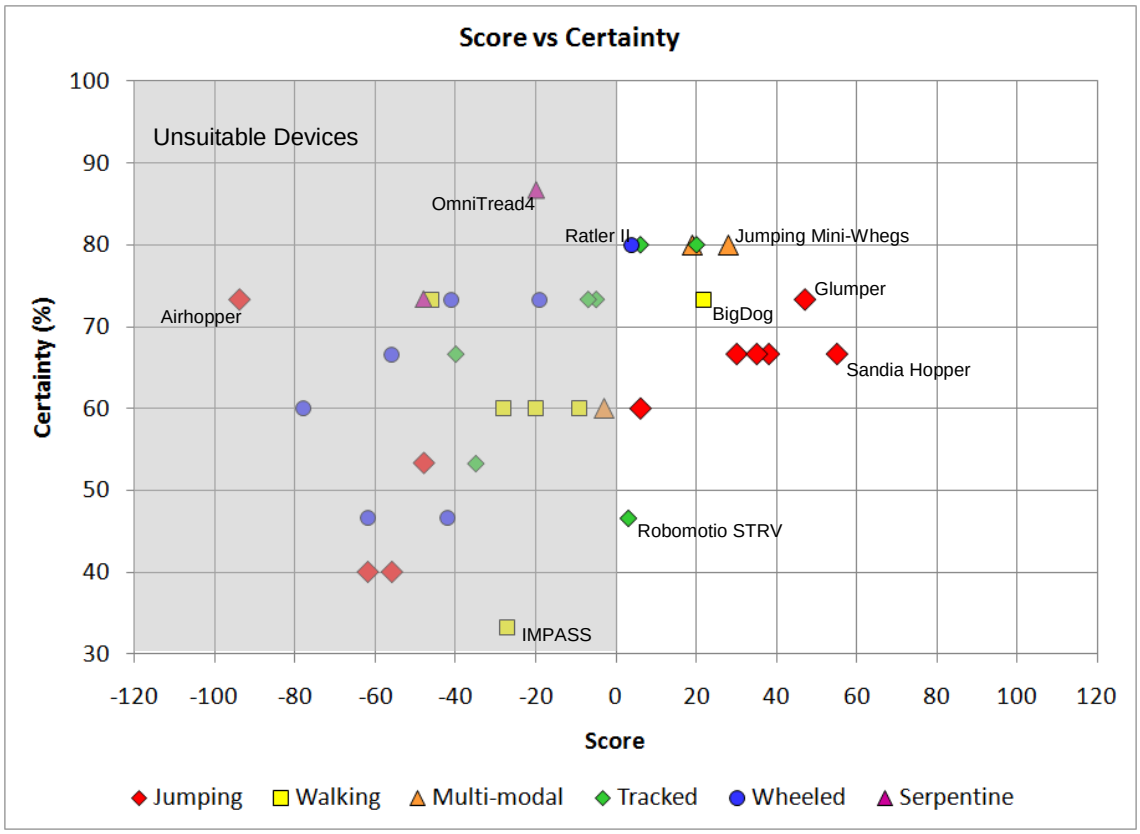

Figure 84 – Example application 1: achieved score and certainty. Some of the robots have been labelled, but the reader is encouraged to use Table 8 in conjunction with this figure.

From Figure 84, it is easy to see that the jumping devices appear to do rather well, as do the multimodal devices and the more developed tracked and walking robots. In particular, the multimodal devices have reasonable certainties so they would be a good choice for this application.

The data used within the scoring system allows for other representations of "performance" to be produced. It is up to the user of the scoring system as to how the scores and existing data are best shown. Here the decision was made to display the two most heavily weighted categories (obstacle cleared height, Figure 85, and cost, Figure 86) and lightly weighted (range, Figure 87, and lifetime, Figure 88) against the scores and certainty using a series of four bubble charts. It is difficult to produce sensible visual representations of performance in categories where there are only two

possibilities, for example in the case whether a device has direction control or not. In each of the figures, the area of each bubble is associated with the certainty of the score for that device. The outline bubbles toward the top of the figures, give a key for the certainty. The size of the bubble does not necessarily mean that the actual accurate score for the device will lie within the bubble's area, but it gives some indication of the true location. Bubbles that span the zero-score line indicate that a device may fall below the minimum requirements of the application, or equally, achieve a small positive score.

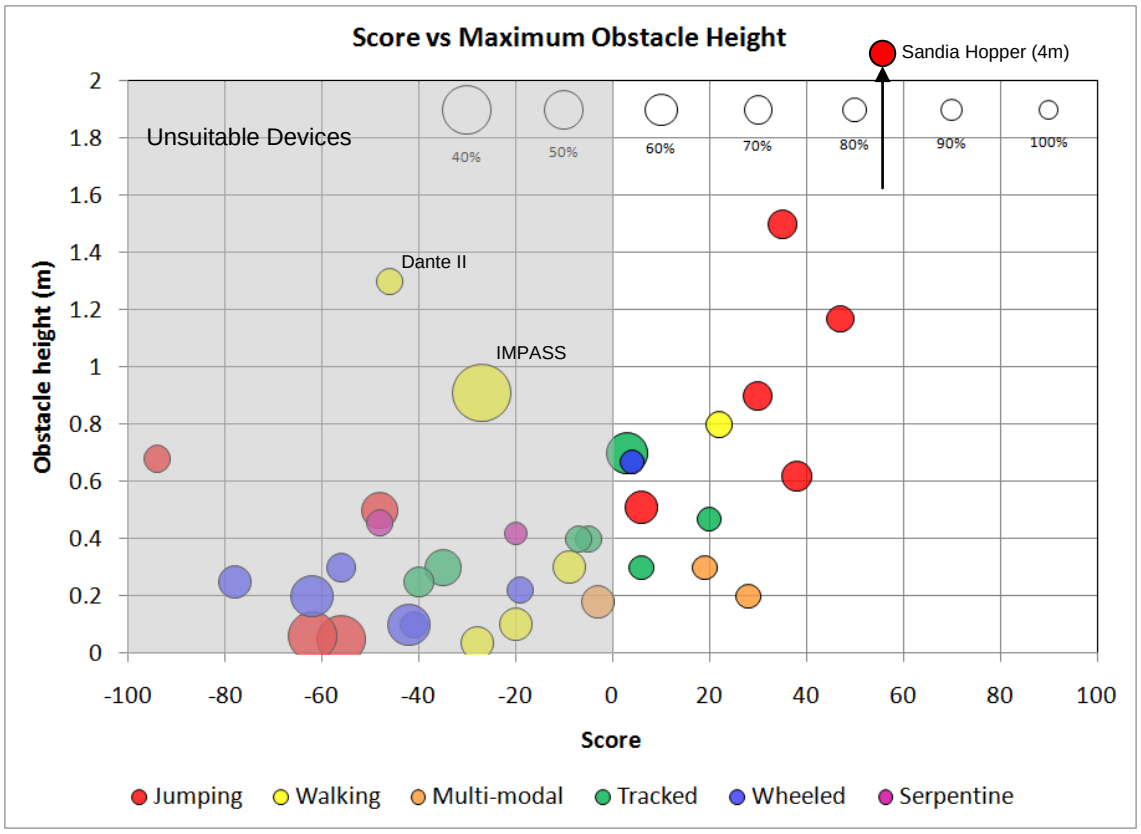

Figure 85 – Example application 1: score verses obstacle height. To spread the datapoints, the device that overcomes the highest obstacle (Sandia Hopper) has been placed outside of the plot area.

Figure 85 shows that in general as the size of the obstacle over which a particular robot can climb increases, its score also increases. This is because the weight associated with obstacle surmountability has a high value of eleven. Therefore it results in a

correlation between score and the size of obstacle that can be overcome. The outlying jumping device (Sandia Hopper) deals with very large obstacles, jumping eight times its own height, and has an obstacle-surmountability far in excess of any other device. The two walking devices, Dante II and IMPASS appear as outliers, as they have a good ability to overcome large obstacles, but actually score poorly. This is due to a variety of additional factors such as tethered power supplies and low speed.

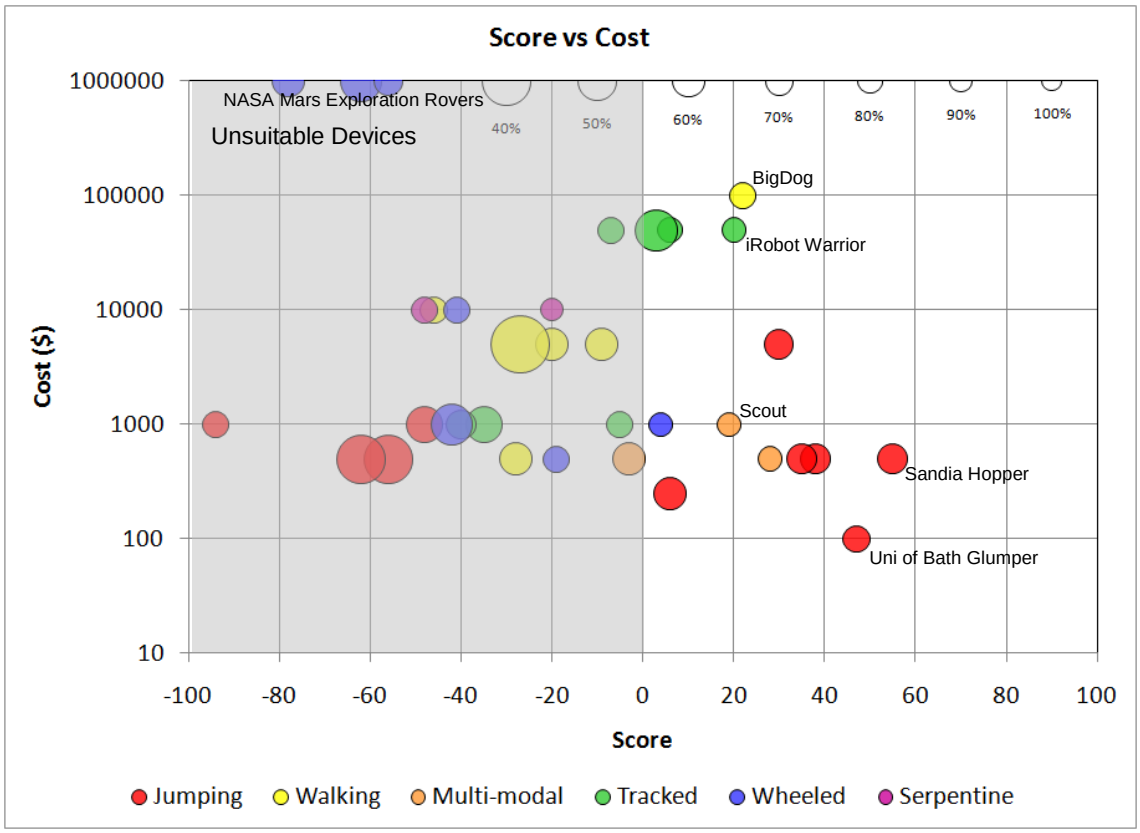

Figure 86 – Example application 1: score verses cost.

In Step 1, cost appeared as an assumed value for almost every device, so care must be taken when reading Figure 86. It should also be noted that the price axis is logarithmic as there is a large range of estimated costs. As cost has a weight of twelve points, it could be expected that cheaper devices will score better. Figure 86 shows that in general this is holds true. The inexpensive jumping robots score well. The inexpensive multimodal devices also achieve positive scores The more expensive tracked and walking devices also score well, even though their costs are high. A cost

reduction of tracked devices would most definitely improve their scores, perhaps enough to surpass jumping robots in their suitability for a rough terrain exploration application.

For additional information a graph of two of the least important categories, range and lifetime, are shown in Figure 87 and Figure 88 respectively.

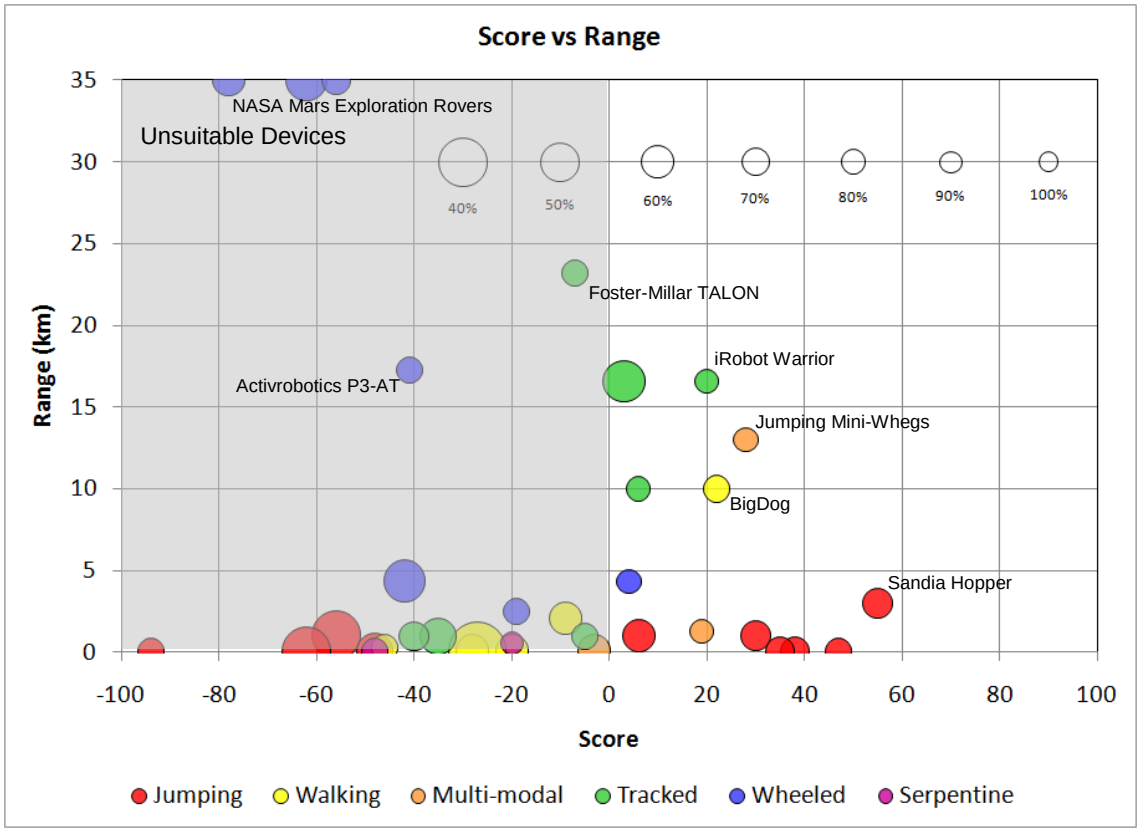

Figure 87 – Example application 1: score verses range. Devices with unlimited range are shown at 35 km.

Figure 87 shows that score and range are not at all correlated. Those wheeled rovers using photovoltaic power supplies, although with unlimited range (here shown as 50 km so as to appear on the graph), do not score so well overall as the jumping devices with short ranges. If the importance (weight) of range were increased, then the tracked rovers appear to be well positioned to improve their scores, and become most suitable for the proposed application.

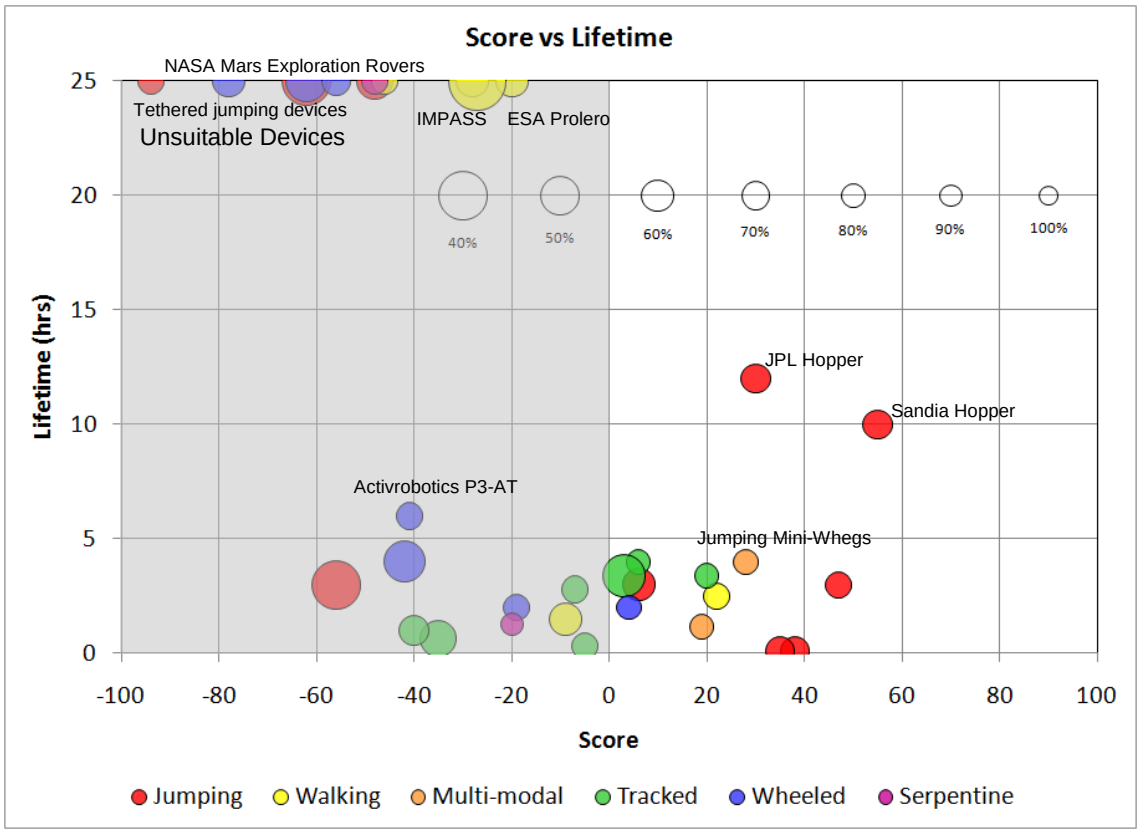

Figure 88 – Example application 1: score verses lifetime. Devices with unlimited lifetime are shown at 25 hrs.

Figure 88 shows that lifetime and score are not closely related. Those devices with long lifetimes, either from tethered power supplies or photovoltaic panels (similarly to above, shown here as 25hrs for clarity), do not necessarily score well. Ignoring those with long life, there does seem to be some correlation between score and lifetime, with jumping devices having reasonable life. Improving lifetime across the board, using better batteries for example, will improve the scores of all the battery powered robots, but the jumping devices would maintain their lead. The battery type is not incorporated into the score, and it could very well be that the batteries used by jumping devices are already much lighter in weight than those more conventional batteries in ground-based rovers.

The first example used throughout the description of the scoring system has produced some interesting results. It suggests that jumping devices appear particularly suited to

a general rough terrain exploration application. A similar application to this example one will be defined at the end of this chapter, and subsequently used to evaluate the novel devices presented in this thesis (Chapter 7, p.295).

3.6 Additional examples

In an effort to prove the suitability of this scoring system for other potential applications, a pair of additional examples has been used.

3.6.1 Example Application 2 – Military application

The second example is to determine the best robots for a military application. Step 1 of the method is the same as the previous example, as the raw data from the robots has not changed. Step 2 involves the definition of a military application. As the same data table is referred to, the application definition cannot use categories unavailable in Table 4. A military application requires things like high speed, robustness, a large payload capacity, a manageable mass and remote control.

Physical Properties	Mass under 50 kg Payload over 8 kg
Motive Performance	Obstacle height cleared 0.2 m Gap cleared 0.25 m Slope capability of 30° Direction Control Speed over 2 m/s
Usability	Robust (yes/no) Control type >remote
Energy Issues	Range >2 km Lifetime >4 hrs

Table 9 – Example application 2: military application definition

Step 3 requires the assignment of weights to the application definition. These are shown in Table 10.

Category	**Weights**
Mass under 50 kg	5
Obstacle height cleared 0.2 m	7
Gap cleared 0.25 m	7
Slope capability of 30°	7
Direction Control	20
Speed over 2 m/s	18
Payload over 8 kg	12
Robust (yes/no)	15
Control type >remote	5
Range >2 km	2
Lifetime >4 hrs	2

Table 10 – Example application 2: weights assignment

Step 4 requires that the normalised category-values are determined. This is achieved using the assignments shown in Table 11.

Category	**Category score assignment**
Mass under 50 kg	+2≤10 kg, +1≤30 kg, 0≤50 kg, -1≤75 kg, -2>75 kg
Obstacle height cleared 0.2 m	+2≥0.4 m, +1≥0.3 m, 0≥0.2 m, -1≥0.1 m, -2<0.1 m
Gap cleared 0.25 m	+2≥0.6 m, +1≥0.4 m, 0≥0.25 m, -1≥0.15 m, -2<0.15 m
Slope capability of 30°	+2≥60°, +1≥45°, 0≥30° -1≥15°, -2<15°
Direction Control	+1=yes, -1=no
Speed over 2 m/s	+2≥10 m/s, +1≥4 m/s, 0≥2 m/s, -1≥1 m/s, -2<1 m/s
Payload over 8 kg	+2≥30 kg, +1≥15 kg, 0≥8 kg, -1≥2 kg, -2<2 kg
Robust (y/n)	+1=yes, -1=no
Control type >remote	+1=remote, +1=autonomous, -1=tethered, -2=none
Range >2 km	+2≥6 km, +1≥4 km, 0≥2 km, -1≥1 km, -2<1 km
Lifetime >4 hrs	+2≥24hrs, +1≥10hrs, 0≥4hrs, -1≥2hrs, -2<2hrs

Table 11 – Example application 2: category-value assignment

Step 5 involves the production of the final scores and certainty, and this is shown in Table 12.

Robot	Score	Certainty %	Type
iRobot Warrior 710	109	81.8	Tracked
Foster Millar Talon	89	72.7	Tracked
Boston Dynamics Big Dog	84	72.7	Walking
iRobot Packbot 510 FasTac	75	81.8	Tracked
RoboMotio Inc. STRV Defence R&D Canada	62	72.7	Tracked
Sandia Hopper	18	63.6	Jumping
JPL Hopper Gen3	11	63.6	Jumping
EPFL Miniature Jumping with cage	-4	72.7	Jumping
Sandia Ratler II Rover	-5	81.8	Wheeled
Rhex (2001 version)	-7	63.6	Walking
Dante II Carneige Mellon	-8	800.0	Walking
ESA ExoMars	-11	63.6	Wheeled
Minnesota Scout	-16	81.8	Multimodal
OT4 Omnitread (UofMichigan)	-20	90.9	Serpentine
Tehzeeb	-26	72.7	Tracked
Jumping Miniwhegs	-27	81.8	Multimodal
ROBHAZ-DT3	-27	63.6	Tracked
OT8 Omnitread (UofMichigan)	-27	72.7	Serpentine
IMPASS Virginia Tech	-29	27.3	Walking
Utah Monopod	-32	54.5	Jumping
EPFL 7g Miniature Jumper	-37	63.6	Jumping
Redback	-39	63.6	Tracked
Activrobotics P3-AT	-42	72.7	Wheeled
Bluebotics Shrimp	-44	72.7	Wheeled
University of Bath Glumper	-50	63.6	Jumping
NASA Pathfinder Sojourner Rover	-58	45.5	Wheeled
CMU Corky	-64	27.3	Wheeled
NASA MER Spirit and Opportunity	-66	54.5	Wheeled
University of Tokyo Mowgli	-76	36.4	Jumping
Sprawlita	-85	63.6	Walking
ESA Prolero	-85	54.5	Walking
Ritsumeikan University Deformable Sphere	-88	54.5	Multimodal
Tokyo Institute Airhopper	-102	54.5	Jumping
Kagoshima Pendulum Jumper	-125	36.4	Jumping
IMT Grillo	-134	36.4	Jumping

Table 12 – Example application 2: achieved scores displayed in decreasing score order

Another way of visualising the results is with a graph of score verses certainty. This is shown in Figure 89.

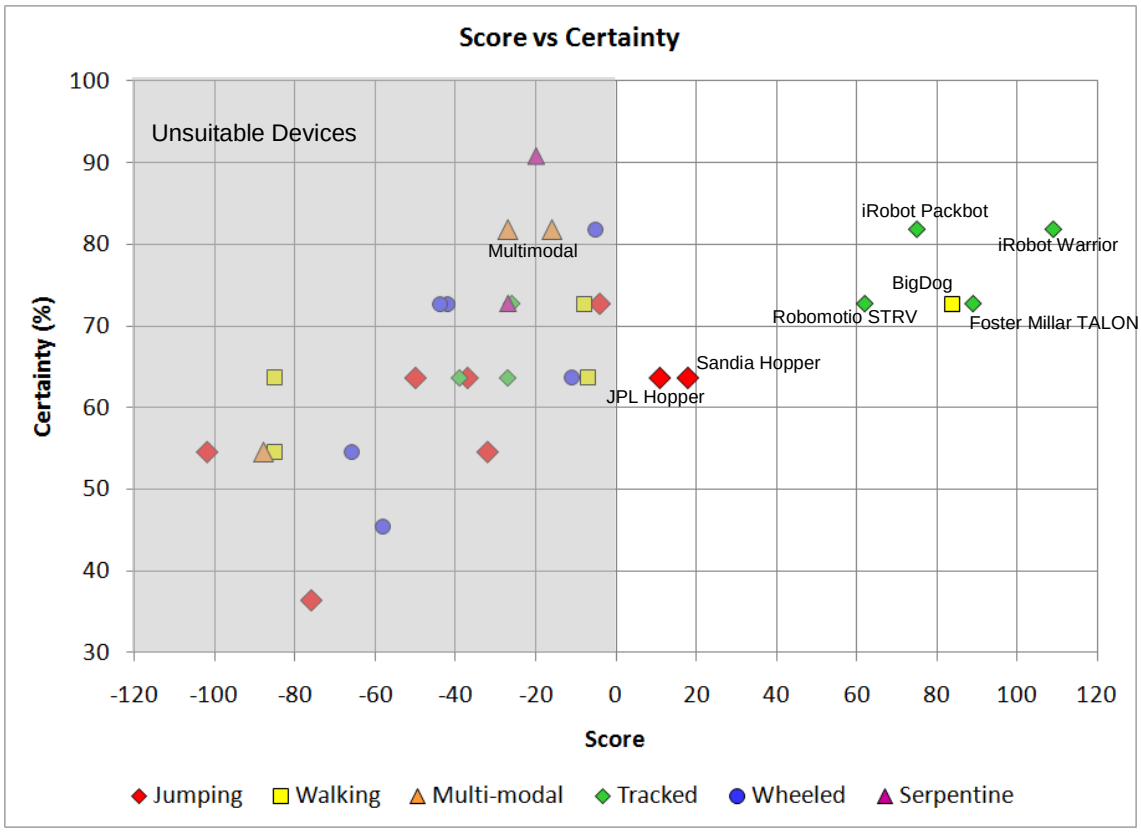

Figure 89 – Example application 2: scores and certainty for example military application. The two lowest scoring devices, both jumpers, the IMT Grillo (-134) and Kagoshima Pendulum Jumper (-125), are not shown.

Table 12 and Figure 89 show that only seven robots meet or exceed the requirements. Five of those seven devices have large certainties of above 70%. Those five devices are the walking Boston Dynamics Big Dog, and the four tracked devices of the iRobot Packbot 510 FasTac, the Foster Millar Talon, the iRobot Warrior 710, and the RoboMotio Inc. STRV. All of these have been designed specifically for military applications where speed, and an ability to carry large loads and deal with moderately rough terrain is required. The remaining positive scoring devices are both jumpers; the Sandia Hopper and JPL Hopper. Both robots get this positive score despite being unable to achieve the heavily-weighted high speed or payload requirements, their main

points advantage coming from being light in weight and being able to overcome large obstructions. Although the JPL hopper is intended for space exploration, the Sandia hopper is backed with DARPA military funding. This particular example goes some way to prove that the proposed scoring system gives valid results.

3.6.2 Example Application 3 – Environmental surveying application

The third example application is one of an environmental/plant/heard monitoring system for large farms, such as those found on the plains of Australia. Here the speed of movement is comparatively unimportant, but devices must be inexpensive, as many would be required in a variety of locations. The ability to deal with very rough terrain isn't critical, as it is likely that most fields will be relatively smooth. Devices should be autonomous and be able to carry a sensor payload of a few hundred grams. Long lifetime is important, although range need not be, if individual devices are approximately located by hand at the outset. This implies a small size and mass, particularly if the robots are to be scattered from a helicopter or light aircraft. The steps of the scoring process are illustrated below.

Like the previous example applications, the raw data of the rough terrain robots has not changed and Table 4 applies for Step 1.

The application definition required for Step 2 is shown in Table 13.

Physical Properties	Size smaller than 0.3 m x 0.3 m x 0.3 m Mass under 10 kg
Motive Performance	Obstacle height cleared 0.1 m Gap cleared 0.1 m Slope capability of 5° Direction control Un-toppleable (self-righting)
Economic Properties	Inexpensive (under $500)
Usability	Payload over 0.25 kg Robust Control type = autonomous
Energy Issues	Must use batteries Lifetime >24 hrs

Table 13 – Example application 3: environmental monitoring application definition

The assignments of the 100 available weights required in Step 3, is shown in Table 14.

Category	**Weights**
Size smaller than 0.3 m x 0.3 m x 0.3 m	5
Mass under 10 kg	5
Obstacle height cleared 0.1 m	3
Gap cleared 0.1 m	3
Slope capability of 5°	3
Direction control	10
Un-toppleable (self-righting yes/no)	10
Cost (<$500)	20
Payload over 0.25 kg	4
Robust (yes/no)	15
Control type autonomous	10
Must use batteries (yes/no)	5
Lifetime >24 hrs	7

Table 14 – Example application 3: weights assignment

The category-value assignments are shown in Table 15.

Category	**Category score assignment**
Size smaller than $(0.3\ m)^3$	$+2 \leq (0.1\ m)^3$, $+1 \leq (0.2\ m)^3$, $0 \leq (0.3\ m)^3$, $-1 \leq (0.5\ m)^3$, $-2 > (1\ m)^3$
Mass under 10 kg	+2≤1 kg, +1≤5 kg, 0≤10 kg, -1≤20 kg, -2≤40 kg
Obstacle height cleared 0.1 m	+2≥0.3 m, +1≥0.2 m, 0=0.1 m, -1≥0.05 m, -2<0.05 m
Gap cleared 0.1 m	+2≥0.3 m, +1≥0.2 m, 0≥0.1 m, -1≥0.05 m, -2<0.05 m
Slope capability of 5°	+2≥20°, +1≥10°, 0≥5° -1≥2.5°, -2<2.5°
Direction Control	+1=yes, -1=no
Un-toppleable (self-righting yes/no)	+1=yes, -1=no
Cost (<$500)	+2≤$10, +1≤100, 0≤$500, -1≤$1000, -2>$1000
Payload over 0.25 kg	+2≥1 kg, +1≥0.5 kg, 0≥0.25 kg, -1≥0.1 kg, -2<0.1 kg
Robust (yes/no)	+1=yes, -1=no
Control type autonomous	+2=autonomous, +1=remote, -1=tethered, -2=none
Must use batteries (yes/no)	+1=yes, -1=no
Lifetime >24 hrs	+2≥96 hrs, +1≥48 hrs, 0≥24 hrs, -1≥12 hrs, -2<6 hrs

Table 15 – Example application 3: category-value assignment

Combining the weights and category-values provides the results for Step 5. The score are shown in Table 16, and a graph of scores and certainty shown in Figure 90.

Robot	Score	Certainty %	Type
EPFL Miniature Jumping with cage	61	76.9	Jumping
Jumping Miniwhegs	57	84.6	Multimodal
Minnesota Scout	43	84.6	Multimodal
Sandia Hopper	41	69.2	Jumping
University of Bath Glumper	29	84.6	Jumping
EPFL 7g Miniature Jumper	26	76.9	Jumping
Ritsumeikan University Deformable Sphere	26	69.2	Multimodal
Utah Monopod	11	69.2	Jumping
JPL Hopper Gen3	3	76.9	Jumping
iRobot Packbot 510 FasTac	2	76.9	Tracked
iRobot Warrior 710	2	76.9	Tracked
Redback	1	76.9	Tracked
RoboMotio Inc. STRV Defence R&D Canada	-1	46.2	Tracked
Sandia Ratler II Rover	-1	84.6	Wheeled
Rhex (2001 version)	-2	76.9	Walking
Bluebotics Shrimp	-5	76.9	Wheeled
ESA Prolero	-7	69.2	Walking
Boston Dynamics Big Dog	-8	84.6	Walking
Sprawlita	-10	76.9	Walking
OT4 Omnitread (UofMichigan)	-14	84.6	Serpentine
Foster Millar Talon	-18	69.2	Tracked
ESA ExoMars	-23	53.8	Wheeled
NASA Pathfinder Sojourner Rover	-30	53.8	Wheeled
Kagoshima Pendulum Jumper	-32	53.8	Jumping
Activrobotics P3-AT	-35	76.9	Wheeled
IMPASS Virginia Tech	-36	38.5	Walking
OT8 Omnitread (UofMichigan)	-36	76.9	Serpentine
CMU Corky	-37	38.5	Wheeled
NASA MER Spirit and Opportunity	-37	61.5	Wheeled
Tehzeeb	-39	61.5	Tracked
ROBHAZ-DT3	-40	69.2	Tracked
University of Tokyo Mowgli	-46	46.2	Jumping
IMT Grillo	-58	46.2	Jumping
Dante II Carneige Mellon	-62	84.6	Walking
Tokyo Institute Airhopper	-73	69.2	Jumping

Table 16 – Example application 3: achieved scores displayed in decreasing score order

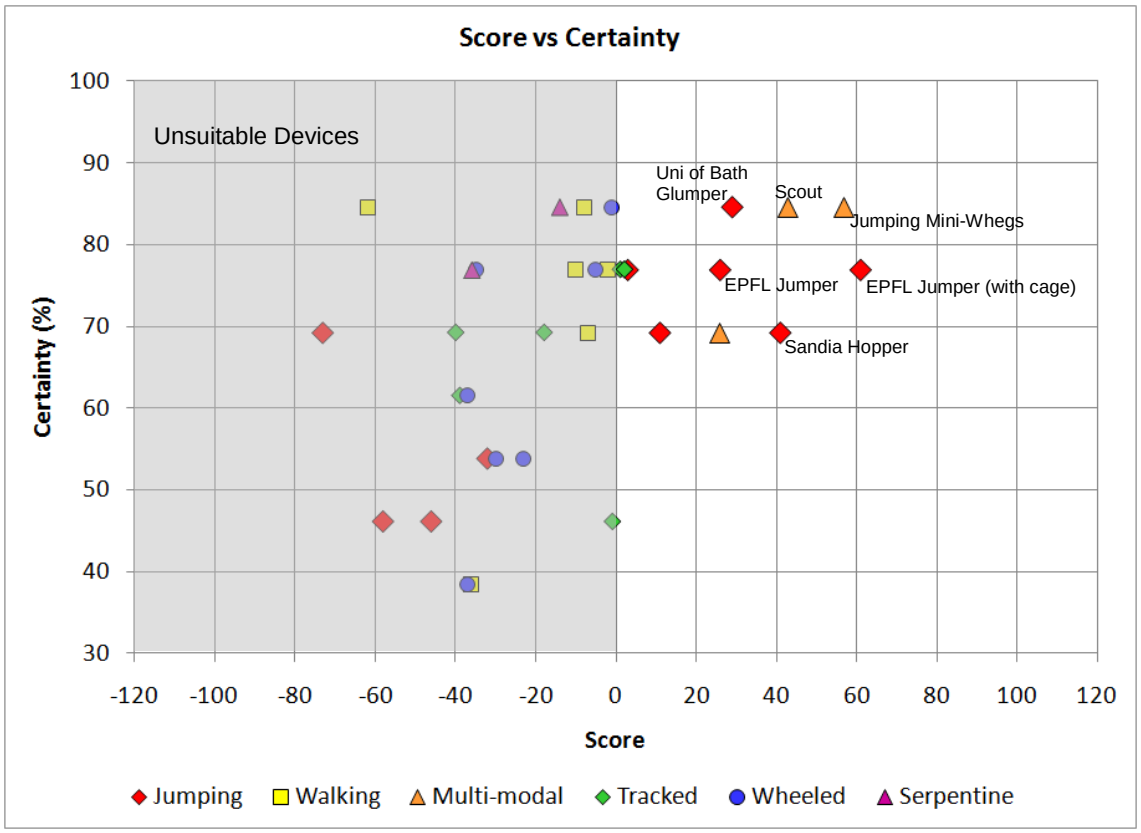

Figure 90 – Example application 3: scores and certainty for example environmental monitoring application

Any robot exceeding a 0 score would be suitable for the application. This includes twelve devices. Most of the devices can achieve the movement capability required, but the importance of cost and robustness has a big impact on suitability. The small jumping and multimodal robots are inexpensive and robust due to the requirements of safe landings. The devices that do not meet the requirements tend to be complex and therefore typically delicate and expensive. As cost is so important, but the scoring relies very much on estimated monetary values, care should be taken when interpreting results. Other applications that have most weighting for estimated values may not suit the scoring system as well as those more closely matched to known and accurate entries.

These three example applications illustrate the workings of the evaluation method and provide some reassurance that, for appropriate rough terrain applications, it provides a reasonable suggestion as to the most suitable devices.

3.7 Evaluation for chosen application

For the purposes of the research presented in this thesis, a general rough terrain application was chosen. Rather than providing a series of hard-and-fast must-haves, this application provided a guide to what is desirable, and expected to be achievable within this research. The application, when used in conjunction with the scoring system, provides a reasonably objective way of evaluating the robotic mobility systems produced. The final scoring, Step 5, will appear at the end of this thesis (Chapter 7), but the remaining steps can be presented here. Step 1 is common to the previous examples, as the raw data has not changed, but results will be added when the properties and performance of the developed devices are known. The selected application for Step 2 is largely based on the first example of rough terrain exploration, but its development and definition has been described fully based on the categories suggested: *physical properties, economic properties, movement ability, usability, and energy properties.*

3.7.1 Physical properties:

- Size – The mobility system must be able to fit through doorways, windows, and into small gaps, whilst simultaneously being portable by a single person. The Size-Grain Hypothesis (see Section 2.2, p.23) implies that smaller devices would have more areas to explore. There are also practical size implications specifically related to the research described in this thesis, due to manufacturability and available workspace. Combining these requirements implies that something under 0.5 m in each dimension would be a maximum size and that smaller sizes, to a point, are better.

- Mass – To be portable by a single person, and to avoid overloading any delicate terrain structures in disaster sites, the device must be < 10 kg.

- Scalability – A mobility system design that scales up and down may be of advantage if a family of varying sizes has differing masses, volumes and capabilities. When used as a team this family has the potential to leave no area unreachable.

- Packability – Being able to be collapsed for storage and transportation would be of advantage particularly for space applications.

3.7.2 Motive performance:

- Direction control – Without the ability to choose the direction in which to travel, a mobility system is of little use.

- Overcoming obstacles – The mobility system should be able to overcome obstacles of the order of 0.5 m in height, as this encompasses urban step heights and reasonably sized obstacles. It is in turn expected that the device should be able to overcome obstacles of the order of its own height or length if working to the limit of possible size.

- Climbing stairs (actual or apparent) – A set of steps between floors needs to be overcome and this is analogous to a slope consisting of rocks or boulders which have varying step heights, but numerous surfaces upon which to rest.

- Spanning gaps – The mobility system should be able to span gaps such as cracks in terrain of around 0.25 m.

- Climbing slopes – The mobility system should be able to climb reasonable comparatively smooth slopes of around 30°.

- Topple-ability – The mobility system must not fall over without being able to re-right itself.

- Speed – The mobility system need not be hugely fast, but it should not be terribly slow. A human walking pace is assumed appropriate, which is around 1 m/s.

- Accuracy of movement – The mobility system needs to maintain a reasonable distance to a chosen course. This should be within 0.5 m.

- Soft terrains – The ability to deal with soft vegetation, sand, gravel, dust, and snow, would be advantageous.

3.7.3 Economic properties:

- Device cost – From a practical standpoint any prototype device produced as a result of this research is dependent on the very limited budget available (<$1000).

- Ease of maintenance – Reducing the labour cost involved with repair and maintenance requires simple designs and easily replaceable components.

- Number of operators – A mobility system that requires many operators can be considered more expensive than one that can be operated by an individual. This implies that the device needs simple operation and control, or for it to be autonomous.

3.7.4 Usability:

- Payload capacity – The device must be able to carry a useful payload. For simple environmental monitoring and mapping this payload can be assumed to be the weight of a modern smartphone which already has satellite positioning (GPS), accelerometers, video and still camera capabilities, microphone, wireless communication (GPRS, 3G, Bluetooth, Wi-Fi) and sufficient computing power for mobility system control. Such a device weighs around 250 g.

- Robustness – The mobility system must be robust enough to survive falls from collapsing rubble piles, and moving or sliding terrains. Continued operation after a fall of 1.5 m down a pile of rubble is assumed suitable.

- Reliability – The mobility system is intended to operate for many kilometres without external intervention so this must be designed in. The use of backup

systems to allow continued operation after single component failure would be of advantage.

- Complexity – Very complex designs are likely to result in a lack of robustness and reliability unless considered carefully.

- Level of autonomy – The more autonomous a robot the easier it is for it to be used. If a series of waypoints can be input into its control system and it can automatically move between them no matter the terrain then that is of great advantage. The scope of this project excludes integration of autonomy with the mobility system.

- Damage to surroundings – Damage of any kind, whether it be noise, “foot” prints, trampling of vegetation, or knocking down of structures is not desirable.

- Environmental survivability – Rough terrain generally occurs in outdoor environments and as a result consideration as to the temperature range, moisture level (including rain), and wind speeds of a mission site is useful. For practical testing purposes it is assumed that an average habitable European climate is satisfactory with temperatures ranging from -10 °C to 30 °C with testing conducted in a variety of mist, dew and rainwater.

- Modes of movement – Multiple modes of movement may lead to increased complexity, but advantages arise due to movement styles applicable to specific terrains. As multimodal movement is of particular interest within this thesis, it is weighted significantly higher than might be normally expected for an exploration application.

3.7.5 Energy issues:

- Power source –The power source for a robotic mobility system could include liquid, gas or solid fuels, or electrical supplies (mains/batteries/capacitors). Compressed air or hydraulic supplies could be available for tethered operation. Space applications almost require a rover to have electrical and/or photovoltaic operation. For the purposes of simplicity for this research, off-the-shelf batteries

are acceptable as battery technology continues to improve enabling more power to be available for a given mass and size.

- Range – A range of a three or four km in a variety of terrains, including rough and complex ones, is assumed appropriate for most applications.

- Lifetime – Combined with the proposed speed, the operational lifetime could be a handful of hours. In reality the availability of a method for refuelling/charging any device is the true limit of lifetime. Having energy autonomy is of great benefit where motive power can be harvested from the environment. A rover with photo-voltaic recharging or operation is limited only by available sunlight, but it should be noted that mountainous regions with few sunlight hours, forests with dense canopies, and the inside of buildings seriously restricts this possibility.

- Energy efficiency – The amount of energy consumed and wasted is of critical importance when a mobility system has to carry all the energy it requires for a particular mission. Wasted energy should be minimised and the use of passive movement encouraged – for instance when moving downhill.

3.7.6 Application performance summary

For ease of use, this list has been presented as a performance summary for a rough terrain exploration robot (Table 17). Some desirable properties described in the categories above have to be ignored due to the limits of available information from Step 1 (Table 4). After Step 2, the chosen application requirement closely resembles the first example.

Physical Properties	Size: up to 0.5 m x 0.5 m x 0.5 m Weight: <10 kg
Motive Performance	Must have direction control Speed: ~1 m/s Cleared obstacle height: 0.5 m Slopes: 30° Gaps: 0.25 m Must not fall over or get stuck
Economic Properties	Inexpensive (<$1000)
Usability	Payload capacity of 250 g Survive 1.5 m drops Remotely controlled (wireless) Multiple modes of movement would be advantageous
Energy Issues	Battery powered with photovoltaic consideration Range of 3-5 km Lifetime of 3-5 hrs

Table 17 – Actual application performance summary (Step 2)

Steps 3 and 4 can be shown in a single table (Table 18) with both weight and category-value assignments.

Category	Weights	Category score assignment
Size smaller than $(0.5m)^3$	4	+2≤$(0.1m)^3$, +1≤$(0.25m)^3$, 0≤$(0.5m)^3$, -1≤$(0.75m)^3$, -2>$(0.75m)^3$
Mass under 10kg	5	+2≤1kg, +1≤5kg, 0≤10kg, -1≤20kg, -2≤20kg
Direction control	10	+1=yes, -1=no
Obstacle height cleared 0.5m	10	+2≥1m, +1≥0.75m, 0=0.5m, -1≥0.25m, -2<0.25m
Gap cleared 0.25m	5	+2≥0.6m, +1≥0.4m, 0≥0.25m, -1≥0.15m, -2<0.15m
Slope capability of 30°	2	+2≥60°, +1≥45°, 0≥30° -1≥15°, -2<15°
Un-toppleable (self-righting yes/no)	7	+1=yes, -1=no
Speed ~1m/s	6	+2≥4m/s, +1≥2m/s, 0≥1m/s, -1≥0.5m/s, -2<0.5m/s
Modes of movement (>1 gives more possibilities)	13	+1=multiple modes, -1=single mode
Cost (<$1000)	12	+2≥$100, +1≥$500, 0≥$1000, -1≥$5000, -2<$10000
Payload over 0.25kg	6	+2≥0.55kg, +1≥0.4kg, 0≥0.25kg, -1≥0.15kg, -2<0.15kg
Robust (yes/no)	5	+1=yes, -1=no
Control type (remote minimum)	5	+2=autonomous, +1=remote, -1=tethered, -2=none
Must use batteries (yes/no)	4	+1=yes, -1=no
Range >2km	3	+2≥6km, +1≥4km, 0≥2km, -1≥1km, -2<1km
Lifetime >4hrs	3	+2≥24hrs, +1≥10hrs, 0≥4hrs, -1≥2hrs, -2<2hrs

Table 18 – Category score assignment for proposed exploration application (Steps 3 and 4)

The final step, where scores are calculated, is shown in Chapter 7, after the production of a multimodal jumping and rolling robot.

Chapter 4 Jollbot 1: A simple jumping sphere

The production of a novel working prototype was a key aim of this work, and such production required fabrication of physical models complemented by theoretical study. The existing purely-jumping devices presented in Section 2.6.7 (p.74), although offering suggestions, did not appear to offer a solution that would allow the integration of additional modes of movement without adding entirely new systems. Similarly, apart from a single device, the multimodal jumping robots, although achieving multi-terrain versatility, did not do so within one structure. The only device (The deformable jumping and rolling robot) that achieved multimodal movement within one structure was under developed, tethered, and of limited performance (see Section 2.6.7.5.5).

Instead of showing only the results of a single final device, the next three chapters present the detail of a series of evolving developmental prototypes. The completeness of each individual prototype was determined by its evaluated performance and potential for minor/major improvements. This resulted in three prototypes, similar in form, but dissimilar in many areas. Each was a result of lessons learned from the former.

Gat (Gat 1995) argues that current mobile robot engineering practice “places emphasis on getting things to work, resulting in widespread use of iterative design, interleaved with ad hoc evaluation”. This approach “often results in working systems, but does not yield an understanding of the limitations of these systems. In particular, it provides little assurance that a system will continue to operate when environmental parameters are changed”. Gat’s observation is interesting, but it is likely that this “getting things to work” approach is a result of the cross-discipline requirements of mobile robot development (McBride, Longoria & Krotkov 2003). In contrast to Gat, the belief here is that “getting it to work” is important when producing new devices. Theoretical optimised design studies may produce what look to be potential solutions, but there is no substitute for working physical prototypes. The general approach to the design process within this thesis is similar to that of Bares, who believes “that it is more expedient to overdesign components and thus permit integration to proceed rapidly and with less concern for equipment damage” (Bares 1999) with the knowledge that standard engineering design optimisation techniques are always available incrementally to

improve performance once a sufficient baseline has been achieved. Achieving this baseline is regarded within this thesis as “getting it to work”.

Producing physical devices is limited by the usual resources of any project, whether it be industrial, academic or defence. No matter the required goal, there is always a limit to the budget and time available. These limitations, whilst restricting potential, do provide a suitable starting point and, ultimately, a necessary ending point too. Here these limitations were accepted and the prototypes were produced as quickly and inexpensively as possible. The discussions and conclusions of this work (see Section 7.8, p.316) contain suggestions as to what direction the research could take were time and money in greater supply.

4.1 Inspiration

The design of the multimodal jumping device within this research was initially inspired by a toy – the Phlatball (Figure 91). This toy was marketed as a Frisbee-come-ball which surprises children when they throw it to one another. A child could squeeze the poles of the hollow ball together into a flat disc shape, storing energy in its springy outer leafs in the process, and a suction cup beneath one pole adhered to a flat area beneath the other, holding the poles together. This meant it could be thrown as a Frisbee until such time that the suction cup released and it rapidly returns to a ball shape. It was never intended as a jumping device, but it did perform jumps from hard surfaces upon the rapid release of energy stored in its outer leaves. These jumps occurred by accelerating the top half of the sphere away from the bottom half. However due to similar “head” and “foot” masses, the cleared height was small. The jumps were equal in height no matter which side it jumped from.

Figure 91 – Jumping Phlatball in Frisbee form with strain energy stored leafs, and in ball form with energy released.

What was appealing about basing a multimodal rough terrain robot on this structure was that the spherical form lent itself to a rolling type movement, in addition to a jumping one. Using a single structure or system for two modes of movement is common within nature.

Further investigation revealed that there was already a jumping device operating under a similar principle to the “jumping” Phlatball, but without a multimodal solution to movement. The Micro Jumping Robot produced by an undergraduate student at the Swiss Federal Institute of Technology (Burdet 2001) achieved unreliable jumps, and the unpublished work makes little mention of performance, operation or design detail. The device did not roll, but again its spherical form would lend itself to rolling.

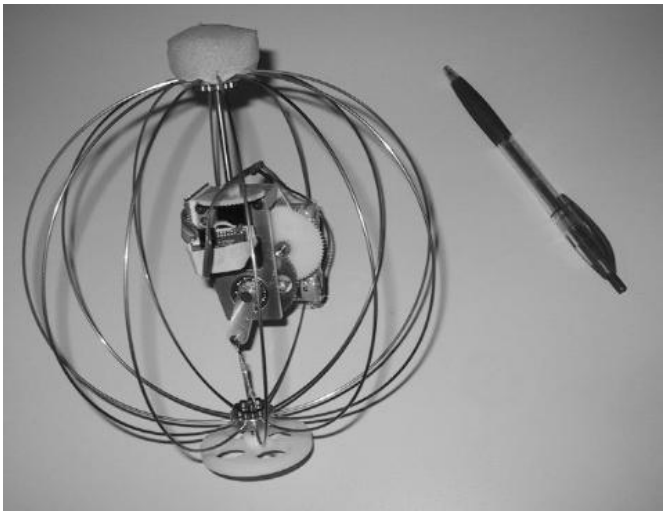

Figure 92 – Micro Jumping Robot (with pen to illustrate approximate size) (Burdet 2001). Its spherical form lends itself to rolling, but it cannot achieve such multimodal movement.

Visual inspection of illustrations and photographs (Figure 92) show that the device was spherical in form made of spars of wire material, with an internal mechanism to compress the outer structure using a short crank. Jump direction control was achieved through rotation of this internal mechanism around an axis between the poles. Similar conceptual work was subsequently carried out at the University of Bath (Lerat 2004), but no prototype was manufactured. Although a pause-and-leap jumping device based on such a form was interesting, it was believed to be a wasted opportunity to not utilise the additional and more conventional mode of movement for a round object – rolling. Thus the aim of this research was to create a multimodal spherical jumping and rolling device for movement in a variety of terrains. The main benefits of a solution based on such a structure were as follows:

- Any delicate control components can be protected from impacts on all sides by the flexible and springy outer sphere.
- The device has no top and bottom orientation and it should therefore be possible to make it jump from either pole of the sphere requiring less reorientation between jumps.

- The spherical form allows for tumbling on landing enabling extra distance to be covered with no additional energy input.
- The spherical form has potential for powered rolling movement across open and smooth terrain. This would allow for a multi-modal motion enabling large distances to be covered quickly with less energy required per unit distance travelled. This additional movement potential resulted in the device's name – JOLLBOT originating from Jumping and rOLLing RoBOT.

4.2 Design

For simplicity in this preliminary investigation, the initial prototype was developed to achieve only jumping. The design consisted of two interacting elements; the spring sphere in which the jump energy was stored, and the compression and release mechanism which converted electrical energy into stored potential energy in the sphere, before allowing it to be released as a jump.

The way in which such a device was intended to jump is shown in Figure 93. A compression mechanism was fixed between the two poles of the sphere. This mechanism was based upon a simple lever arm that slowly pulled the two poles of the sphere toward one another using a motor and electrical energy, in turn storing potential energy in the sphere. When fully compressed, the lever arm was then allowed to rotate freely, explosively releasing the energy as a jump. It was important that the centre of gravity of the complete device was not along a centreline between the two poles to ensure that the jump was not straight upward, as that would be no use when attempting to jump over an obstacle. It was also important that the centre of gravity of the complete device was slightly below the equator line of the sphere to ensure that it rolled back to its base upon landing as it was unable to jump from either pole of the sphere.

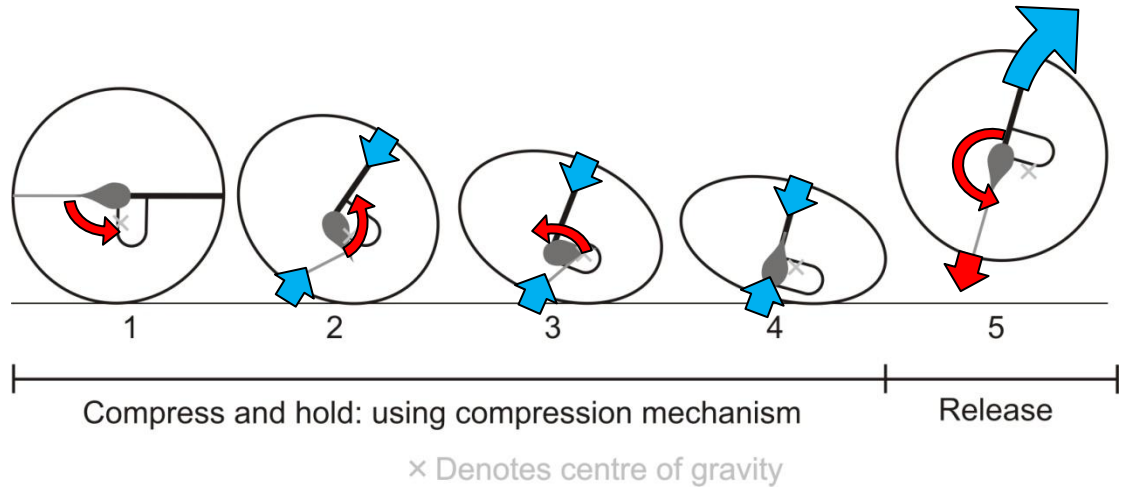

Figure 93 – Jollbot 1's jumping method. Steps 1-4: the compression mechanism rotates slowly to squeeze the sphere into a squashed shape, storing strain energy in its elements and rotating to have its pole downward in the process. Step 5: the compression crank freely over-runs once >180° rotation has occurred, allowing the sphere to rapidly release its stored energy as a jump.

4.2.1 Theoretical study of circular springs

In order to have an idea of the approximate design details of the proposed device, some analytical study of the energy storage mechanism was required. The theory developed here, concerning a sphere made of hoop-like springs, was based on work by Brewer regarding circular calibration rings (Brewer 1961). Circular calibration or proving rings are used to check the performance of testing machines used to apply loads to structures. They consist of a complete ring of material with suitable fixings for a linear displacement measure and for test machine mounting. Although the deflections involved are small as a proportion of ring diameter, the equations may provide a suitable way of determining the spring constant of a sphere constructed of multiple similar rings, and in turn through the use of standard equations the resulting energy stored (Equation 6, p.52) and vertical jump height achievable (Equation 13, p.93).

The design of the each proving ring is critical: it must exhibit the maximum possible deflection for a given load without permanent plastic deformation. When using such a ring as an energy storage device it is important to note that the force deflection curve for a complete ring under certain conditions is Hookean in its response.

The vertical deflection of a circular ring is approximated by the following (Equation 16) (Roark & Young 1975):

$$\delta = \frac{\left(\frac{\pi}{4} - \frac{2}{\pi}\right) \times P \times R^3}{E \times I}$$

Equation 16 – vertical deflection of circular ring under load

Where: δ = deflection (m), P = external compression load (N), R = Radius of ring curvature (m), E = Young's Modulus (N/m), I = 2nd Moment of Area of cross-section (m^4). This equation makes the assumption that [quoting Roark and Young (Roark & Young 1975)]:

1. *The ring is of uniform cross section*
2. *It is of such a large radius in comparison with its radial thickness that the deflection theory for straight beams is applicable*
3. *It is nowhere stressed beyond its elastic limit*
4. ***It is not so severely deformed as to lose its circular shape***
5. *It's deflection is due primarily to bending*

Some of these assumptions may be at odds with the proposed spherical structure. For practical reasons the elements were likely to be of uniform cross section and the radius of the structure would be much larger than the thickness of each element. Certainly stressing the structure beyond its elastic limit was undesirable for energy recovery reasons; however in practice the deflections involved would result in a non-circular shape and this would introduce other loading patterns. For this reason this analysis is approximate.

Equation 16 can be rearranged such that the equivalent spring stiffness for one ring (k_1) is shown in Equation 17:

$$k_1 = \frac{P}{\delta} = \frac{E \times I}{0.14878 \times R^3}$$

Equation 17 – stiffness of circular ring

Multiplying this spring stiffness by the number of rings (n) in a complete sphere results in the stiffness of the sphere (k). This, in turn, can be used to determine how much strain energy can be stored within a sphere compressed by a distance x using $kx^2/2$ (Equation 13). Assuming a vertical jump and perfect transfer of stored strain energy to gravitational potential energy results in a predicted vertical jump of height (h) (Equation 18):

$$h = \frac{kx^2}{2mg}$$

Equation 18 – jump height in terms of stored strain energy in a spring and the total mass of the device

Where g is the gravitational constant and m is the total mass of the jumping device (the sum of the mass of the sphere and the mass of the compression mechanism delivering the force P). It should be noted here that h is the change in the height of the centre of gravity from its position within the sphere when fully loaded to its peak at the top of its flight. With a deforming structure this could result in h being somewhat larger than the actual height of an obstacle over which it could jump. Equation 18 also assumes that no strain energy within the compressed ring is translated into horizontal velocity upon take-off. Obviously for practical purposes, a jumping device must achieve range to jump over an obstacle, in which case a ($1–cos2\theta$) multiplier should be applied to the right of Equation 18 (θ being the launch angle from horizontal).

Making the suitable substitutions in Equation 18 leads to the following relationship between jump height h and known values (Equation 19).

$$h = \frac{EIx^2}{0.29574mgR^3}$$

Equation 19 – jump height in terms of circular ring properties

It is from this equation that it is possible to deduce the properties required to maximise jump height:

- The choice of material for the spring elements gives a value of E, and has influence on m due to material density (ρ). It is therefore important that the chosen material should have a maximum E/ρ value.
- Maximising the second moment of area, I, would maximise jump height implying that tall narrow sections, and hollow tubes would be more suitable than wide strips or solid bar.
- Maximising the deflection, x, has a square impact on jump height.
- Minimising mass, m, would produce higher jumps, but it should be remembered that the total device mass is made up from a whole series of components – the mass of the springs and the mass of the mechanism used to compress them. The mass of the springs is influenced by the physical size of the structure, element section, and material density. The mass of the compression mechanism will increase as the force required to achieve the required deflection increases, but what that mass-to-force relationship for that mechanism is, is difficult to predict. If only the ring structure is considered, then the height to which any number of similar rings will jump when released, is the same as that to which one ring will jump. The force developed and energy stored will be larger, but the mass of the multiple rings will equalise the resultant height.
- Gravitational constant g is constant on Earth as it is on other planets, but the smaller it is, the higher the device will jump.
- The radius of curvature of the rings, R, should be minimised to maximise height, and since the mass of each rings is influenced by R then this is doubly important.

Producing a physical device based upon this ring spring theory will place practical limitations on some of these requirements and these will be discussed later (see Section 4.2.1.6, p.172).

To give some idea of how these equations relate to sphere design for a jumping (and rolling) device, a series of figures have been produced. Each is based on nominal assumptions arising from anticipated material availability and device size.

4.2.1.1 Material influence

The first illustration (Figure 94) shows how the material and round cross-section size can have an effect on anticipated performance. Materials chosen are steel, glass fibre reinforced plastic and, for practical prototyping reasons, brazing rod[2] (~30% copper, ~30% zinc, ~30% silver). Here it has been assumed that 1/3 of the sphere's diameter is a suitable compression distance given that some internal mechanism has to achieve it, and that a sphere diameter of 0.3 m was reasonable due to practical and application considerations. The choice of six hoops to make up the sphere was made arbitrarily and the influence of the number of hoops will be discussed later. A constant compression mechanism mass of 0.25 kg was assumed to be sufficient for developing all the forces required. This compression mechanism mass was based upon the use of a standard size modelling servomotor, standard batteries and an estimate of associated chassis components' masses. As the frequency of each jump was not critical, it was possible to use lightweight plastic geared gearboxes to increase torque (and therefore compression force) by decreasing speed, and without adding substantial mass. However in general the actual compression mechanism mass will increase as the force required increases.

[2] Brazing rod was selected due to suitable section size and lengths being readily available from university stores.

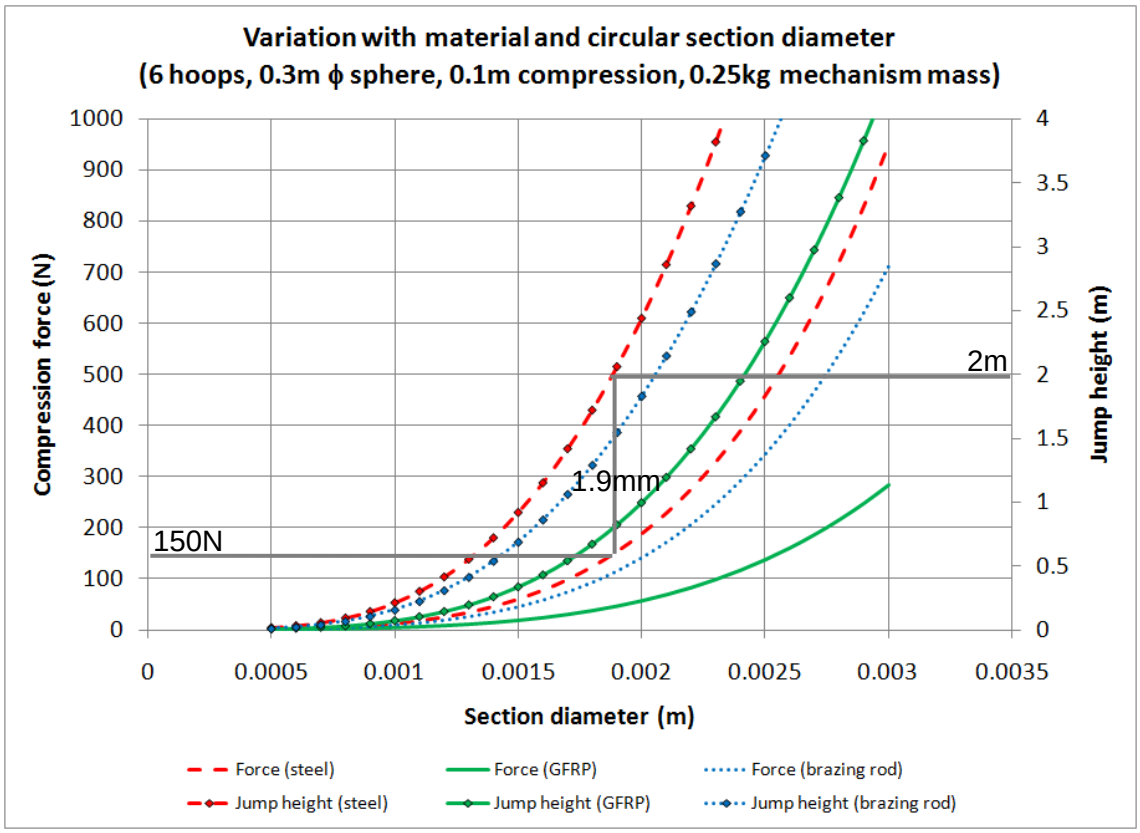

Figure 94 – How the element material and section diameter affect jumping performance for a sphere made of 6 hoops. The lines with markers illustrating jump heights and the plain lines illustrating the force required. The grey lines illustrate one way of reading the graph for a steel sphere jumping to a height of 2 m.

If a 2 m jump height is required, some anticipated properties for a 6 hoop sphere of 0.3 m diameter can be determined:

- Steel requires elements of 1.9 mm ϕ and a mechanism force of 150 N
- GFRP requires elements of 2.4 mm ϕ and a mechanism force of 115 N
- Brazing rod requires elements of 2.1 mm ϕ and a mechanism force of 160 N

For a given jump height, steel and brazing rod require similar compression forces. However, the potential for glass fibre reinforced plastic and other fibre composites should not be ignored, especially as the required jump height increases.

4.2.1.2 Cross-section influence

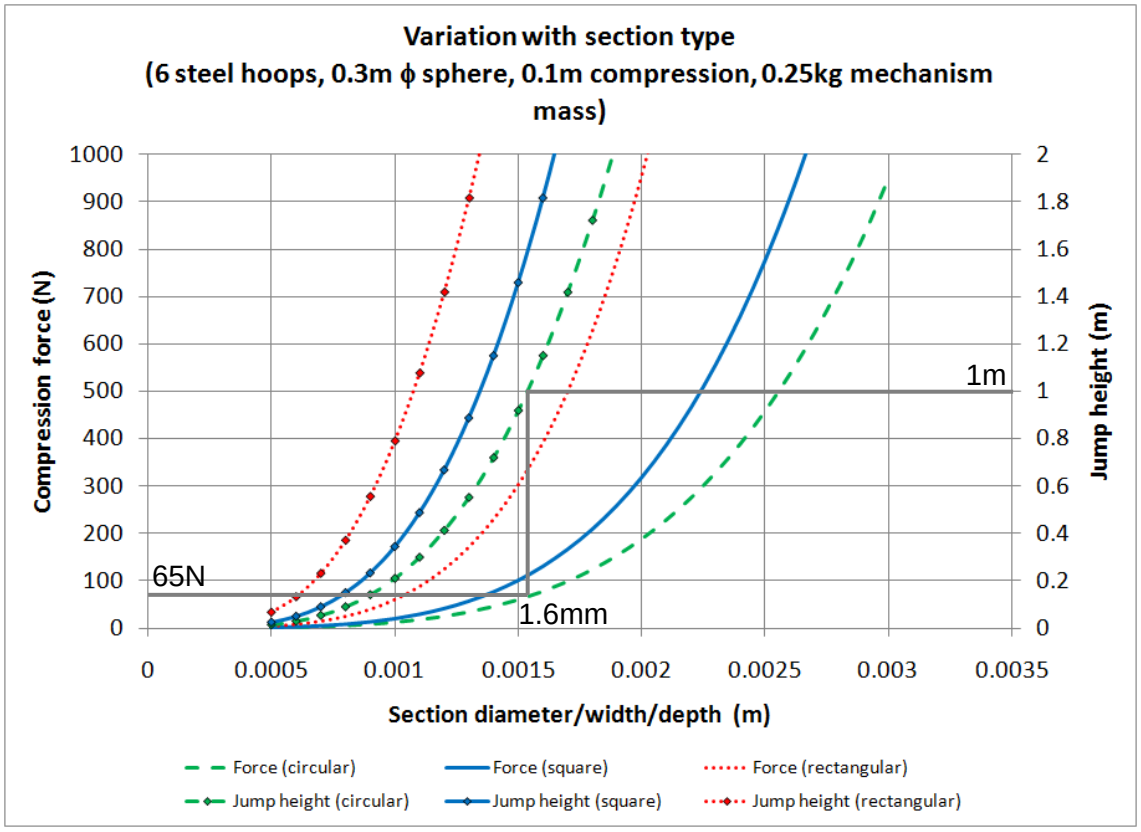

Figure 95 – Variation of jump height and required compression force with section type. The lines with markers illustrating jump heights and the plain lines illustrating the force required. The grey lines illustrate one way of reading the graph for a sphere made of circular cross-section elements jumping to a height of 1 m.

Secondly a graph (Figure 95) has been produced illustrating how the section type and size affects the achieved jump height and the required peak compression force for a series of 0.3 m diameter spheres consisting of six hoops, being compressed by 0.1 m and having an additional internal compression mechanism mass of 0.25 kg. The section types are; round, having a particular diameter; square, having the same depth and breadth; and rectangular, having a breadth three times the depth. To highlight how the section type changes the jump height and peak force required, a series of readings need to be taken. For clarity a jump height of 1 m has been chosen which results in the following peak forces:

- Circular section of 1.6 mm ϕ and a peak compression mechanism force of 65 N
- Square section of 1.3 mm x 1.3 mm and a peak compression mechanism force of 65 N
- Rectangular strip section of 1.1 mm deep and 3.3 mm wide and a peak compression force of 87 N

This quickly illustrates that circular and square sections would produce similar devices (actually with circular elements requiring slightly more force for the same performance due to the proportionally larger amount of material away from the radius of the centre of cross-section available with square sections). Flat wide strips would require larger forces to be generated within the compression mechanism. It can then be deduced that deep and narrow elements of large second moment of area (precurved I-beams or tubes for example) that have more material away from the radius of curvature might produce even better results. However, producing or obtaining such precurved elements is not trivial.

4.2.1.3 Deflection distance influence

As anticipated, Figure 96 shows that deflection distance has a square effect on jump height. Thus for any given device, the deflection should be maximised. The internal mechanism achieving this deflection must be able to produce the required force (also shown in Figure 96) and it is clear that operating at over 50% deflection gives the most increase for smaller increases in force. Note that this is where the analysis very definitely parts company from the requirements that the rings remain circular. For this reason empirical tests on an actual device were done under realistic conditions. The results of these are reported in Section 4.3.1 (p.183), Section 5.2.2 (p.207) and Section 6.2.1 (p.233).

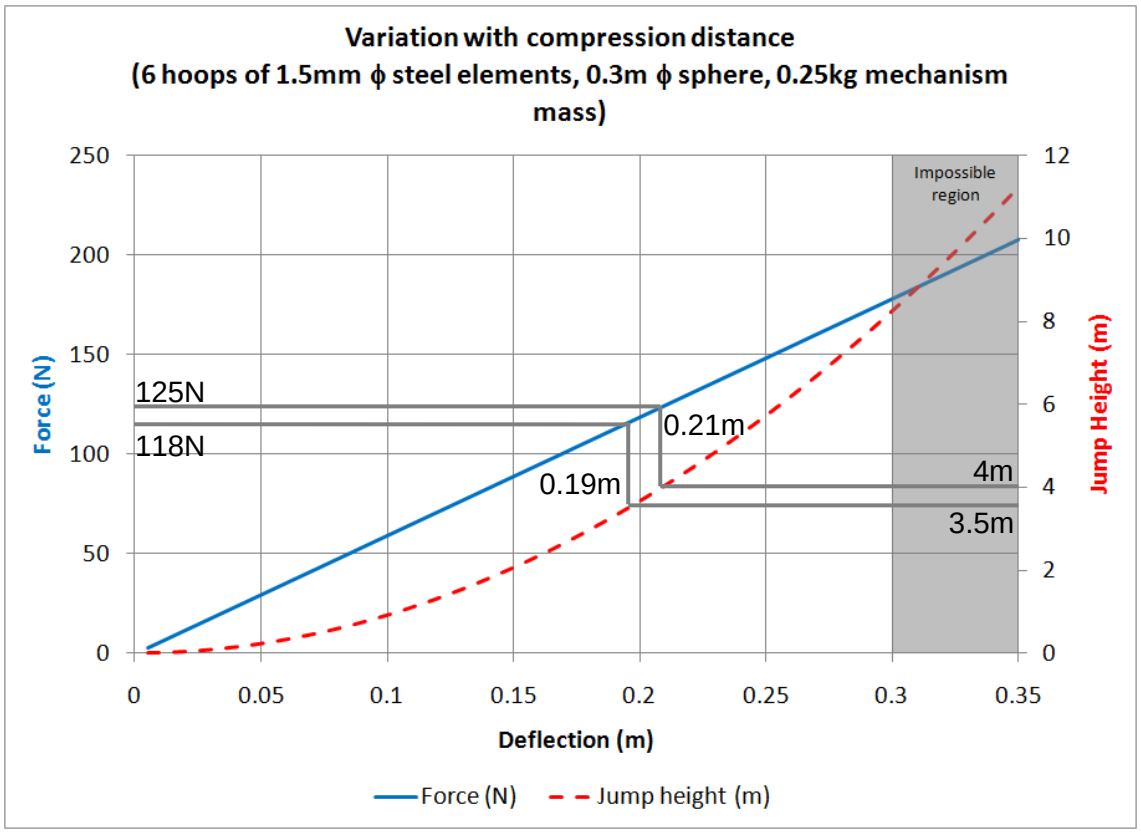

Figure 96 – Variation of jump height with deflection distance. Deflecting the hoop further than its own diameter is not possible. The idealised force-displacement profile of a sphere is Hookean (blue line), so operating above 50% compression gives a higher jump for a smaller increase in the ability of the compression mechanism. For example an improvement of 7 N in the capability of the compression mechanism results in an increase of 0.5 m in jump height, assuming an increase in deflection of 0.02 m is possible.

It should be remembered here that the deflection distance is also going to be equal to the distance through which the "head" of the sphere will accelerate before the whole sphere leaves the ground. As discussed in Section 2.6.8.1.1, p.93, maximising this distance means that more strain energy would be available in the sphere for a given peak force (less stiff spheres would allow more strain energy to be stored for a given peak force if displacement were unlimited).

4.2.1.4 Mass influence

The two factors that affect mass in Equation 19 are the number of hoops making the sphere, and the weight of the compression mechanism within the sphere delivering the force required to compress it. Figure 97 shows both how varying the number of hoops and how a series of different weight mechanisms affect jump height. It is important to remember in all cases that an assumption has been made that the selected weight compression mechanism is able to deliver the entire range of forces required.

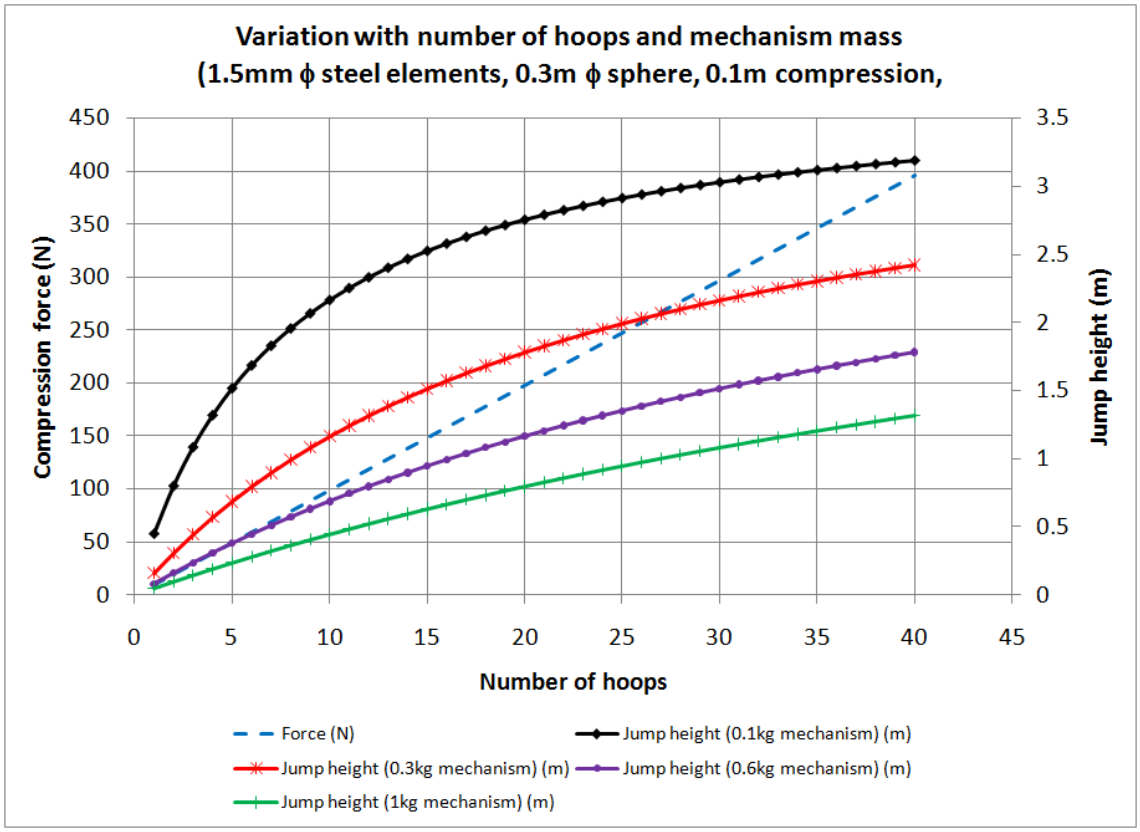

Figure 97 – How number of hoops and mechanism mass affect jump height

Figure 97 shows how varying the number of hoops alters the performance for a sphere consisting of 1.5 mm ϕ steel circular section elements and of 0.3 m in size and with a mechanism mass of 250 g. What is most important to remember here is that, were there no compression mechanism mass at all, the jump height would be the same for each number of hoops; every additional hoop adding the same weight and energy

storage capacity, this would result in a sphere of more and more rings requiring more and more force to achieve the same jump height. Given enough hoops, every device would eventually reach a jump height of 3.8 m (a height which is dependent on individual circular spring geometry, material and section type). The lighter the compression mechanism, the fewer the hoops required to reach that ultimate peak, but until a relationship between mechanism mass and its delivered force is known, then the optimum number of hoops cannot be determined.

4.2.1.5 Size influence

The final figure (Figure 98) shows how required force and jump height vary with changing sphere diameter. Here, like the first case, it is again assumed that 1/3rd of the sphere's diameter is a suitable compression distance, and that the compression mechanism will again weigh 250 g no matter the peak force required. The hoop elements are fixed at 1.5 mm ϕ and made of circular section steel.

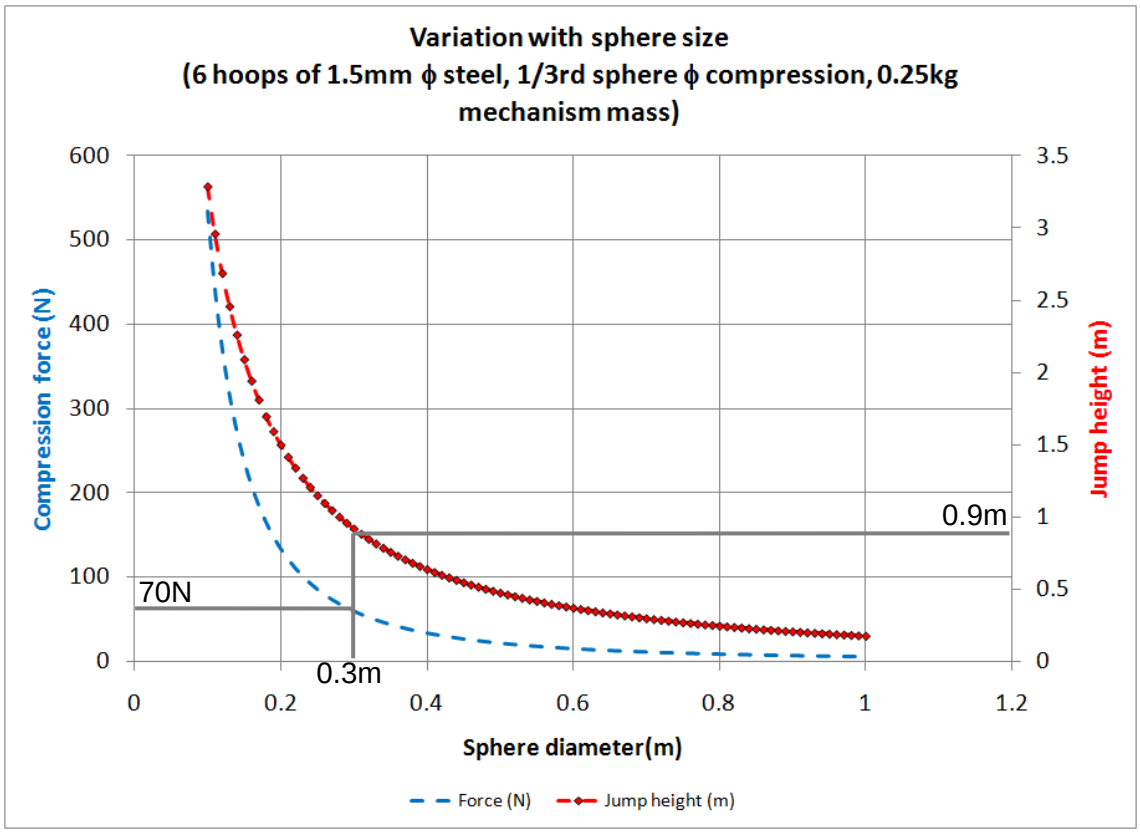

Figure 98 – Variation of force and jump height with sphere diameter. Selecting a sphere of approximately 0.3 m in diameter results in a jump of 0.9 m and a required compression force of 70N. Increasing the sphere diameter reduces the force required but also the jump height. Decreasing the diameter rapidly increases the force required and the jump height. The aim of maximising jump height while reducing the compression force required results in a 6 hoop sphere of 1.5 mm steel elements having a diameter of around 0.2 - 0.4 m.

Figure 98 shows that as sphere diameter increases, so the force required to compress it by 1/3rd reduces, and that as sphere diameter becomes very small then the force required to compress it by a 1/3rd becomes very large. Similarly, as the sphere diameter becomes large, the achievable jump height reduces. In this specific case of hoop material and mechanism mass, this results in an appropriate sphere diameter where the peak force required is minimised and the jump height is maximized in the range of 0.2 m - 0.4 m diameter.

4.2.1.6 Practical limitations

The first and most important practical limitation comes from the requirement to produce a sphere made of circular springs. Although a sphere could be machined or fabricated from one solid piece of material, where material at the pole is common to every ring, this would be expensive and time consuming. The realities of prototyping mean that either complete rings would need to overlap and interleave at the poles resulting in non-concentric hoops, or each ring would be made of two halves joined by a suitable clamp securing each element in-line with its opposite at the poles. The assumption was therefore made that two separate semi-circular elements, securely meeting at their ends will produce the same Hookean response as a continuous circular calibration ring. Thus a sphere of semi circular elements is proposed.

The study on pages 160 to 172 suggests:

1. *Choose the best material possible.*
2. *Choose the cross-section with the biggest second moment of area.*
3. *Maximise the deflection distance.*
4. *Minimise the mass of the compression mechanism.*
5. *Minimise the number of rings.*
6. *Small is better.*

The first two suggestions were practically limited by the material available to produce the elements of the sphere. Lightweight composite fibre rods were available from the university stores, but, as they were straight, they would be significantly pre-stressed when formed into a spherical shape. They appeared to be in danger of fracturing when further deformed, as they would be during the device's operation. Their smooth circular cross-section and straight form at the ends also meant that fixing would be a problem. The availability of custom pre-curved composite tubes and rods of a variety of sections was looked into, but no suppliers produced the small diameters/sections required within a reasonable budget and at quantities suitable for an individual piece of work. Manufacturing such elements was considered, but the time taken, the uniformity required between each element, and the knowledge that the spring sphere could

always undergo conventional materials and engineering optimisation at a later time meant that metal round section elements were deemed satisfactory for this work.

Using semi-circular pre-curved elements results in a ring, or sphere that was unstressed when round and at rest. The metal wire-like elements used to build a sphere were likely to be straight when sourced and required plastic bending to produce the curved shape required. Building a sphere from straight un-bent elements would pre-stress the structure. The strain energy developed within these now curved elements would not be recoverable until the sphere was disassembled, but the effect would be to produce a sphere that required some non-zero minimum applied force before it began to deflect (Figure 99). The overall stiffness of the structure was unlikely to be affected and thus, for a given force limit, less energy could be stored. This is true for all stiffnesses, but the effect can be exploited if displacement were the limiting factor, rather than force.

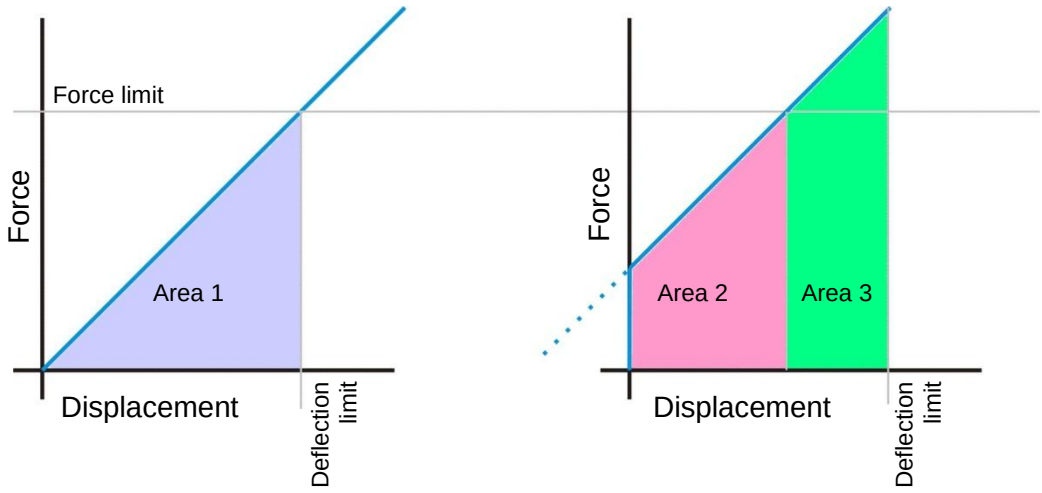

Figure 99 – Pre-stressed elements result in a non-zero force requirement at zero displacement (right figure). This results in less energy (Area 2 < Area 1) being able to be stored for a given force limit. For deflection limited systems, more energy (Area 2 + Area 3 > Area 1) could be stored with a pre-stressed structure.

The third suggestion was to maximise the deflection distance. To maximise the deflection distance as a proportion of the diameter of a particular sphere required that the sphere's diameter-to-element section size ratio was very large. Small spheres with elements of thick sections would buckle when compressed by a large proportion of

their diameters. The deflection distance was also limited by the capabilities and design of compression mechanism.

As mentioned, the assumption that the ring was “not so severely deformed as to lose its circular shape” means that the equations above are unlikely to hold true at large deflections when each ring is no longer circular. This would occur almost immediately after loading a slender ring, and thus it was unlikely that the load displacement curve of the sphere would remain perfectly Hookean. A simple theoretical model highlights the potential forms as the applied force and deflection increases (Figure 100) and indicates that at large deflections the stress arrangements in each ring are complex. Producing and testing a physical sphere made of semi-circular elements would provide more details.

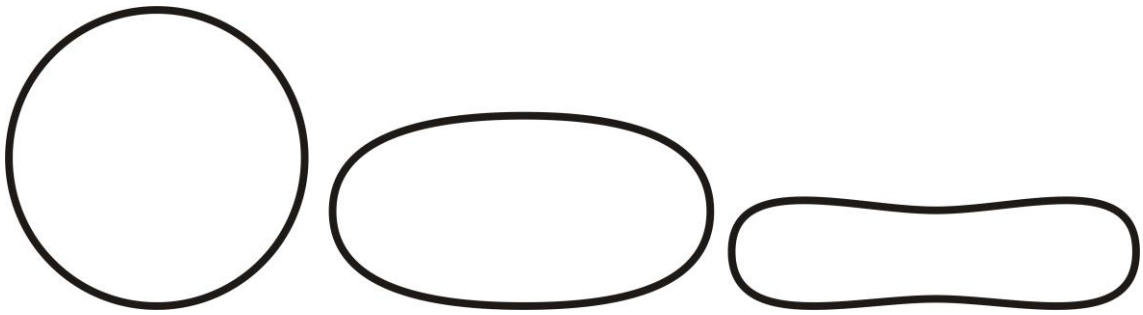

The pre-formed semi-circular elements form a ring. When loaded under small deflections the structure stores strain energy following a Hookean response based upon circular spring theory.

As the force and deflection increase, sections toward the poles of the pre-curved ring are straightening (storing strain energy as they do so), while other areas are continuing to deflect and their radius of curvature tightens.

Once a minimum radius of curvature has been achieved at the equator (at maximum stress before deformation) the straightening areas of the ring begin to bend backward as the loads reorganise into a minimum energy structure forming an S shaped bend from the pole to the equator

Figure 100 – Large deflections of circular springs

An additional model investigates the possible response of large deflections of a semi-circular hoop spring. Substituting a semi-circular element with a leg of two perfectly stiff elements joined with a torsion spring at the ‘knee’ produces the response shown in Figure 101 for one half of a hoop spring under large deflections. The result appears almost Hookean at very low deflections (up to ~10 %) and again Hookean after

approximately 30 % deflection. Between 10% and 30% the structure's stiffness decreases.

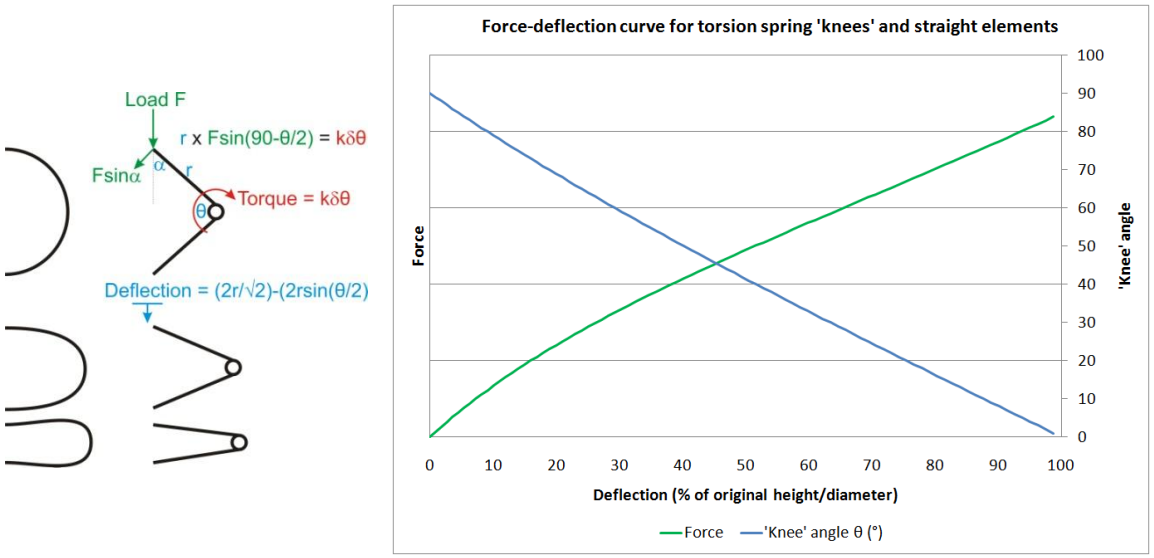

Figure 101 – Study of high deflections in torsion spring system results in an approximately Hookean response at very low deflections and after ~30% deflection. Calibration ring theory deals with only small deflections.

The fourth suggestion (p.172) was to minimise the mass of the compression mechanism. Utilising a mechanical advantage system such as a gearbox means that a given low torque motor of a particular weight can produce more torque at a lower speed. Given that the frequency of jumps was not of high priority then this was a reasonable design choice. (The "pause" part of "pause-and-leap" can be fairly lengthy if ultimately a particular obstacle is overcome.) The materials and components making up the complete compression mechanism (motor, power supply, mechanical advantage system etc.) determine whether the force delivered varies directly with mass or not. Other mechanism masses, such as direction control components and those components required for an additional powered rolling ability, mean that the entire mass of the internal compression mechanism within Jollbot cannot all be devoted to energy storage.

The fifth suggestion was to minimise the number of rings. Since combining many springs of a given construction produces a device that jumps to the same height, but

requires more force, then it would be expected that minimising the number of rings was of benefit. However since the sphere itself provides some secondary functions (providing impact protection, self-righting ability, and a rolling surface) then a sphere made of a series of hoops was required.

The sixth and final suggestion was that small is better from an optimum jump height perspective. However, small size puts limits on the internal volume available for a compression mechanism and was at odds with maximising deflection distance. In addition, a small rolling device would have more difficulty moving around with even tiny bumps in a surface.

4.2.2 Physical design

The CAD model of Jollbot 1 was made using Solid Edge 17 (Figure 102) and included twelve semi-circular spring elements, a manually-adjustable-length crank compression mechanism, and an off-axis centre of gravity that had the potential to enable jump direction control with additional actuation. The possible powered rolling capability was not considered at this stage, although physical space was available on the mechanism chassis plates for it to be included later. The main mass of the compression mechanism was fixed to the upper half of the ~300 mm diameter sphere such that it was part of the mass that was accelerated. This meant that the momentum of the top half of the sphere was high after the spring delivered all its stored energy, and would reduce only slightly when the light-weight base was subsequently lifted off the surface.

Figure 102 – CAD model of Jollbot 1

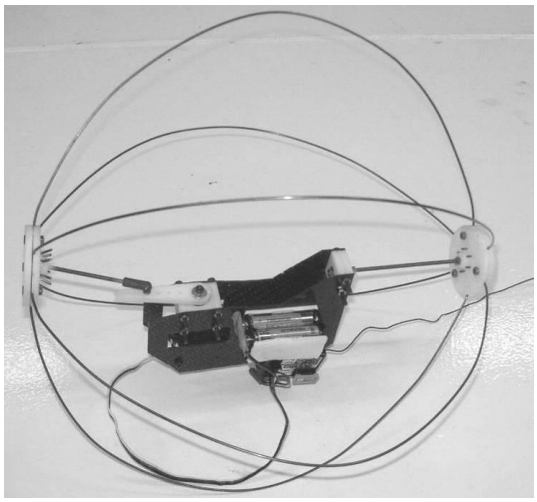

Figure 103 – Photograph of Jollbot 1

The Centre for Biomimetic and Natural Technologies at the University of Bath had access to a Fused Deposition Modelling (FDM) Rapid Prototyping (RP) machine so intricate prototyped engineering components could be made from ABS (Acrylonitrile butadiene styrene) plastic directly from the CAD models. This process allowed for design alterations to be carried out quickly, and for broken or damaged components to be redesigned and relatively cheaply replaced. Rapid prototyping enables a high speed of development and its purpose is for quickly-evolving trial-and-error prototypes.

The two main chassis panels were manufactured from carbon fibre plate, their shape being dictated by clearances for the rotating crank, compliance in the elements linking to the sphere, possible interference with the sphere's structure, and in an effort to minimise the weight along the sphere's polar axis. For centre of gravity adjustment purposes along the axis, M3 threaded bar was used for the links from the mechanism to the top and bottom pole of the sphere. Rapid prototyped components supporting the upper thrust bearing, crank shaft and bearings, and compression servomotor, were all sandwiched between the two chassis plates. The separation and unused area of the chassis plates close to the upper thrust race mount would allow for a second motor to be fitted when required. A spur gear connection to the upper threaded bar would provide some rotation of the centre of gravity around the sphere's polar axis for jump steering and powered rolling (this idea is discussed in detail in Chapter 5). The whole device (Figure 103) was assembled using M3 machine screws and nuts.

Some consideration of the assembly and adjustability of the device was made at the design stage to cater for any discrepancies between the calculated and actual spring and compression mechanism performance. These included the possibility of removing some of the spring elements, adjusting the position of the compression mechanism within the sphere using the threaded link elements, changing the compression crank length depending on the actual motor torque, and replacing the compression servomotor with a higher torque version.

The device was powered by an onboard rechargeable Ni-Mh battery pack delivering a rated 4.8 V (~5 V in practice) and 600 mAh. Control was achieved using a simple Acoms 2-channel model radio control handset and receiver, in this case driving a single model servo (Towerpro MG995) adapted for continuous rotation. This gave a method for wireless control of the mechanism.

4.2.2.1 Spring sphere

The sphere was constructed from metal semi-circular hoop spring elements joined at an upper and lower pole assembly manufactured using rapid prototyped ABS plastic components. For initial testing, the most readily available metal rods suitable for the springs were 0.5 m lengths of 1.5 mm diameter brazing rod. Given the materials performance chart in Figure 67, and the theoretical results in Figure 94, brazing rod does not give the best weight to strain energy storage relationship, but would however allow for the main principles and mechanisms to be tested. Metal rods were chosen as the initial spring material as they can be permanently bent without inducing additional stresses in the material, and the possibility of tight radius bends at their ends allows for secure location and fixing. The semi-circular spring elements are clamped between a pair of rapid prototype ABS plates which were manufactured to include slots and holes for secure location. An example of this is fixing is shown in Figure 104.

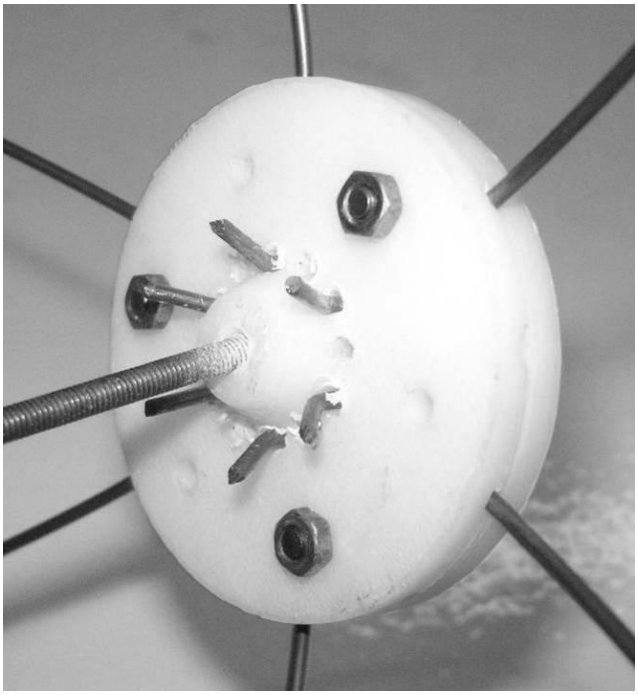

Figure 104 – Semi-circular spring element clamp. The two disc portions mated together leaving a locating path for the wire elements which were tightly bent at their ends to provide secure location and minimise twisting.

As some idea of the sphere and device construction was available, it was now possible to use the previous theory (see Section 4.2.1) to predict performance. Inserting the known values of the metal elements produced a predicted sphere stiffness of 445 N/m from twelve semi-circular elements 1.5 mm in diameter and weighing a predicted 7.15 g each. With the additional mass of the polar clamps, compression mechanism and mounting link elements of around 250 g this would achieve a jump height of 0.28 m.

4.2.2.2 Compression and release mechanism

The compression mechanism was based on a fixed length crank (fixed at 32 mm, but adjustable in 6 mm increments depending on motor performance and sphere stiffness) driven by a motor with a simple interlocking over-running clutch that allowed the crank to be driven for 180° during compression, and to rotate freely for 180° for quick release. This is shown in Figure 105. The compression mechanism was driven by a 6 V rated

model servo (Towerpro MG995) operating at 4.8 V that had been modified to work as a simple motor and reduction gearbox providing continuous rotation. This was achieved by removing the connection between the position feedback potentiometer and the output shaft, and by removing the mechanical end stops which restriced the movement of the output drive gear.

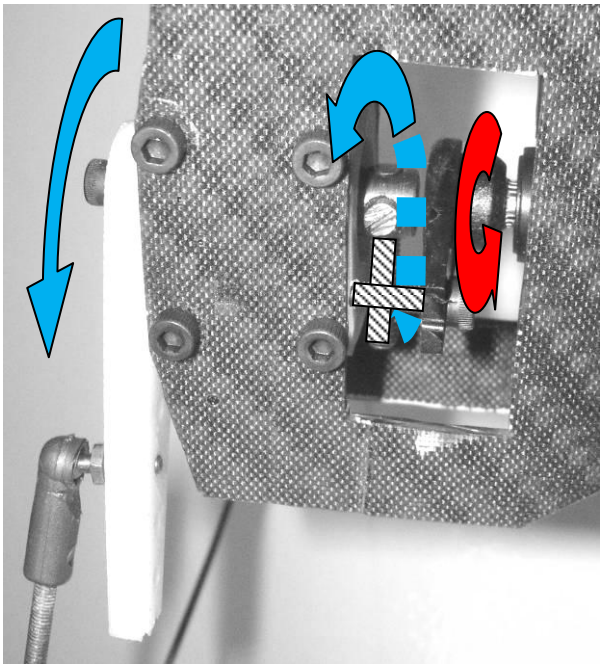

Figure 105 – Photograph of the over-running clutch. The darker arrow highlights the drive action and the lighter arrows show the resulting motion of the crank axle. The hatched areas show the interlocking pins, the one behind being driven by the one above before being able to freely move away after 180° of rotation. The crank axle was supported on a pair of rolling-element bearings and in-line with the axle of the servomotor.

A modified servo assembly, whilst not necessarily smaller and lighter than a separate DC motor and gearbox, does have the advantages of being simple to control remotely using a conventional model radio control system, and that it was inexpensive and readily available and in a variety of torques and speeds, all within the same physical size and fixing locations. This provided an easy upgrade path if required. Modified servomotors are commonly used by roboticists due to these factors.

The servo was powered by four 1.2 V 600 mAh Ni-MH rechargeable batteries, the mass of which contributed to the larger accelerated mass (in an effort to maximise accelerated mass to trailing mass ratio – Section 2.6.1) and would ultimately provide an off centre mass for controlling the direction of a particular jump.

The sales documentation for the Towerpro MG995 servo listed a claimed torque of 13 kgcm (1.27 Nm) at 4.8 V. The theoretical sphere stiffness of 445 N/m was used to produce the following illustration (Figure 106) of the torque required as the fixed length crank rotates.

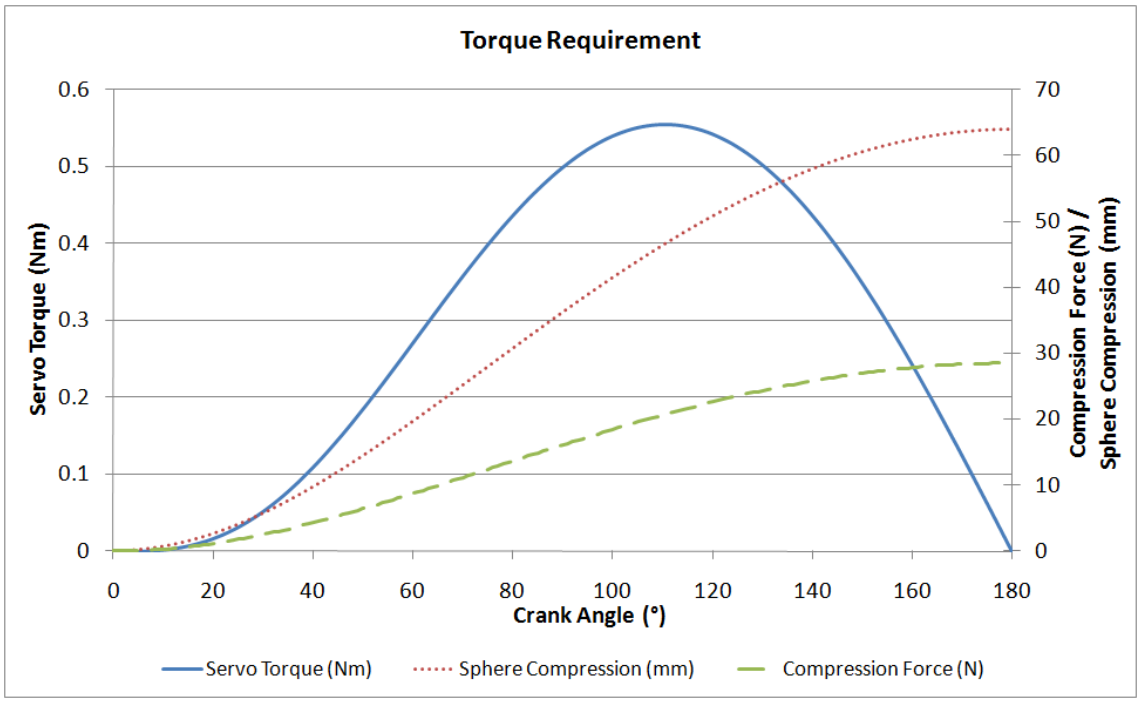

Figure 106 – Required motor torque for prototype sphere consisting of 12 elements (6 hoops)

Figure 106 shows that the predicted peak torque required was 0.555 Nm and occurred at a crank angle of 111° from bottom dead centre when the sphere was at its unloaded diameter. The selected motor should easily achieve this requirement. The peak force developed in the sphere was predicted as 28.5 N after it had been compressed by 64 mm (twice crank length). This results in theoretical 0.9 J of stored strain energy ready to be released as a jump.

4.2.3 Jollbot 1 mass

The mass of the robot and its components is shown in Table 19.

Component	Mass
Compression Servo	50 g
Batteries and Battery box	65 g
Receiver	20 g
Half-hoops (6 @ 7 g each) Note that 12 could not be compressed by mechanism (see Section 4.3)	42 g
Sphere Top & Bottom Clamps	52 g
Jollbot 1 mechanism and chassis	86 g
Total Mass of Robot	**315 g**

Table 19 – Jollbot 1 mass

Table 19 results in an accelerated “head” mass to trailing “foot” mass ratio of 5.7:1, making the simplifying assumption that the top half of the sphere contributed to the “head” and the bottom half to the “foot”. Maximising the accelerated to trailing mass ratio would result in improved jump height.

As predicted, each individual element of the sphere was indeed 7 g. However, the remaining masses weren’t quite as proposed, and totalled 273 g. This results in a predicted no-loss jump height of 0.26 m using a sphere of twelve elements.

4.3 Experiments

In order to evaluate the performance of the prototype device, various physical factors needed to be measured and video recordings of jumps made. The results from these experiments could then be used to find numerical efficiencies and qualitative observations of areas of improvement. After preliminary testing it was clear that the motor was not capable of compressing the sphere using a 32 mm crank lever if all twelve elements were fixed in place. This was due to a difference between the

calculated sphere stiffness and actual sphere stiffness (see below), a difference between the servomotor's actual torque and that mentioned in the sales literature, and the frictional losses in the compression mechanism itself. Adjusting the crank length did improve the peak applied force of the compression mechanism, but the deflected distance was small, meaning that the resulting jumping force was applied for only a short time. Removing a few spring elements was another way of enabling the compression mechanism to achieve full sphere-compression of 64 mm.

4.3.1 Spring sphere characterisation

The spring performance of the assembly of the working device was evaluated by testing the sphere, comprising only six semi-circular spring elements (three complete hoops) and excluding the internal mechanism, in an Instron desktop materials test machine (Figure 107). The desktop test machine compressed the sphere by 130 mm at a test speed of 1 mm/s whilst measuring the load. A graph of the output from the test is shown in Figure 108.

Figure 107 – Instron desktop materials test machine

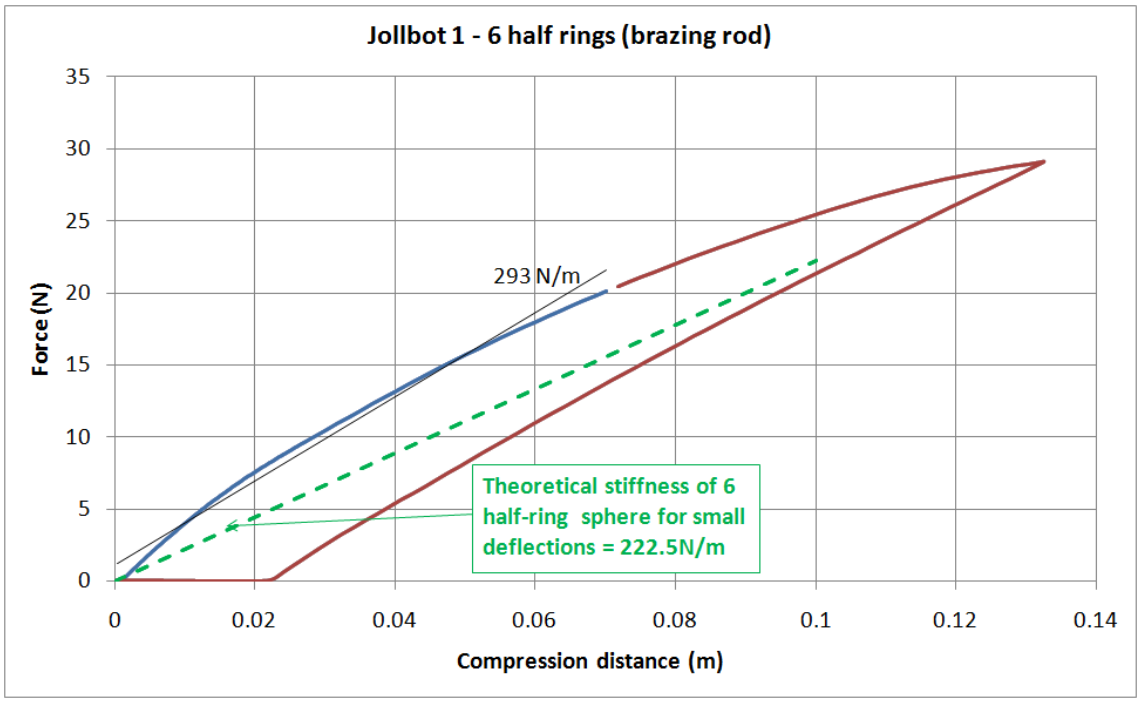

Figure 108 – Compression test data for Jollbot 1. The brazing rod deforms plastically during the test and does not recover its original shape. This is a result of compressing the sphere beyond the yield point of its elements. Repeated cycles at double the crank length (64 mm) resulted in almost no plastic deformation. The theory suggests that the stiffness should be 222.5 N/m for such a sphere, which is substantially less than the 293 N/m achieved experimentally.

The force/displacement curve shown in Figure 108 is far from linear and therefore is not Hookean. It is clear that the brazing rod deforms plastically during the test and does not recover its original shape. However, from continued experimental tests of the working prototype, the springs exhibited far less plastic deformation with the repeated cycles of 64 mm delivered by the compression mechanism. This force/displacement curve is at odds with theory, but the elements making up the sphere must reach their plastic deformation limit soon after 60mm of compression. Although a non-linear response was found, for approximation purposes at this early stage, a straight line was fitted over the first 75 mm of compression (the separate segment in Figure 108) to give a spring stiffness of approximately 300 N/m. The theoretical stiffness of such a sphere was predicted as 222.5 N/m.

4.3.2 Jumping performance

It was clear even after the first few experimental jumps that this device was far from optimised and the design needed substantial development if it was going to be able to achieve a useful jump. However, preliminary quantitative experiments were conducted in an effort to determine what areas of the design required attention.

The jumping performance of the prototype was recorded on a simple handheld KonicaMinolta X50 digital camera at 30 frames per second (fps). Captured images from a typical video are shown in Figure 109. The robot jumped very much around its centre of gravity. This means that the release of stored energy was not along a line from the contact point with the ground through the centre of gravity of the whole device. The centre of gravity must therefore lie far away from the sphere's polar axis – perhaps by as much as 60 mm. This was far from ideal for maximising the jump height, but did show that jump direction can be controlled by having the centre of gravity away from the axis of compression. The resulting cleared jump height was estimated at approximately 0.05 m, however the centre of gravity of the entire robot appeared to rise only by around 0.01-0.02 m.

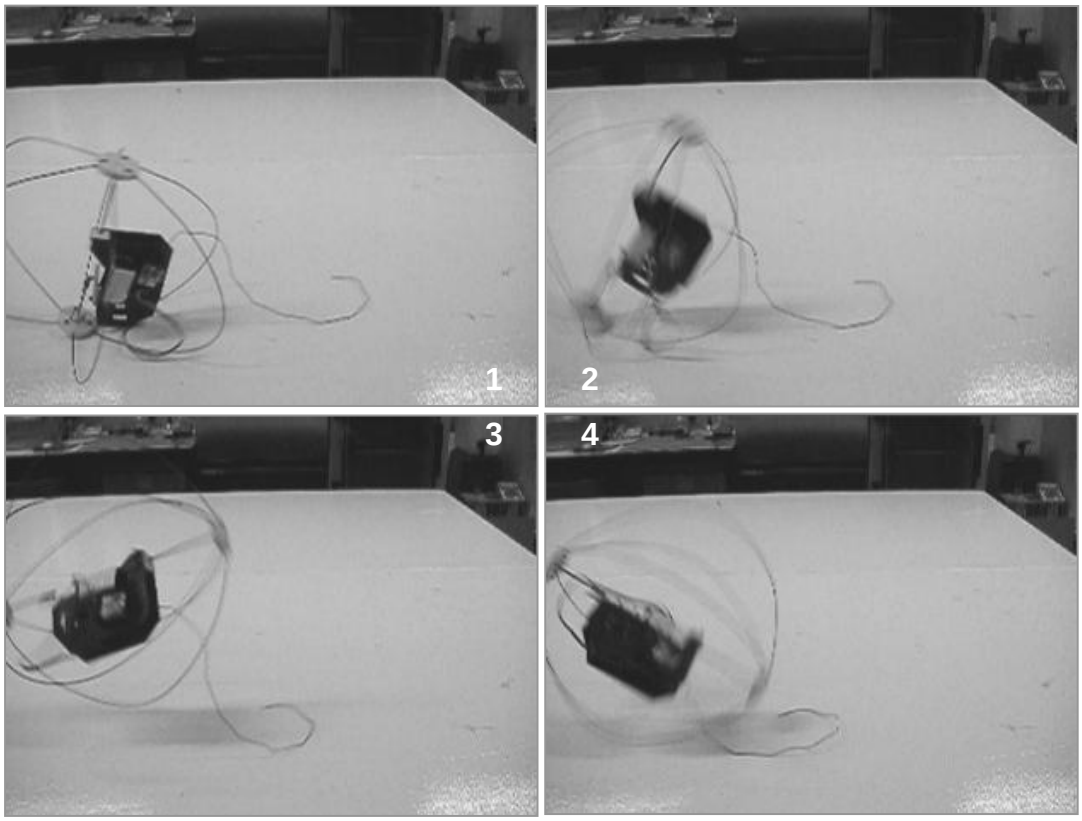

Figure 109 – Jollbot 1 Video Stills Jump 1

4.3.2.1 Jumping efficiency

Using kinetic and potential energy equations allowed for some efficiency calculations to be made.

4.3.2.1.1 Potential energy stored in compressed robot

The compression crank was 32 mm long which meant that the sphere was compressed by 64 mm (double the crank length). Using Equation 13, the measured spring constant and the deflection, the energy stored was:

$$PE = \frac{1}{2} \times 300 \ \ N/m \times (0.064\ m)^2 = 0.61J$$

Due to the non-Hookean spring value of the sphere, this energy was likely to be slightly different from the actual amount of energy stored.

4.3.2.1.2 Gravitational potential energy of robot at peak of flight

Substituting values for an apparent change in height of centre of gravity (0.015 m) and robot mass (0.315 kg) into Equation 6 gives the potential energy of the device at peak jump height.

$$PE = 0.315kg \times 9.81kgms^{-2} \times 0.015m = 0.046J$$

4.3.2.1.3 Mechanism release efficiency

Comparing the potential energy stored in the sphere with the potential energy of the device at its peak height gives an efficiency of 7 %.

4.4 Evaluation

Whilst not giving impressive jumps, the low density electrical energy provided by the batteries was successfully converted and stored as strain energy in the outer sphere. The release and subsequent jump was a result of the amplification provided by its spring structure.

This measured stiffness of 300 N/m for the sphere of Jollbot 1 was larger than expected from theory. One would expect a sphere of three complete hoops to have a stiffness of only 222.5 N/m. This was a difference of almost 35%, and implies there was a large discrepancy between theory and practice. This could come from inaccuracies in the material data, or that the construction of the physical sphere had the effect of stiffening the structure, or, most likely, from the fact that there were large deflections as mentioned in Section 4.2.1.6.

Using the measured sphere stiffness allowed a value of the motor's delivered torque to be estimated. The mechanism theory suggests that the peak torque delivered by the servomotor was 0.373 Nm. This was significantly lower than the manufactures claimed torque at 4.8 V of 1.27 Nm. Some of this discrepancy could be frictional losses in the crank assembly (although, as that was supported by a rolling-element bearing, it was unlikely to account for the entire remainder). It can therefore be deduced that the

manufacturers claimed torque was achieved under ideal conditions. Ultimately this particular motor failed during the testing of Jollbot 3a (see Section 6.2, p.233).

Although designed for twelve semi-circular spring elements, the compression mechanism was only capable of compressing six elements. Any more than that would cause the motor to stall and stop the device from reaching maximum compression and the point at which the stored energy could be released. Thus only after testing the working device could the spring performance be matched to the capability of the compression mechanism, or visa versa. The peak force developed by the compression mechanism was determined as 19.2 N for a weight of 273 g. This resulted in a compression mechanism force to mass relationship of 70 N/kg.

The compression mechanism's integral over-running clutch provided a low resistance quick release mechanism, but not a reliably functioning resting-state catch position enabling the device to remain ready without requiring additional energy to hold it there. However, the relatively short compression time of around two seconds meant that a catch wasn't required.

The sphere stiffness and compression achieved resulted in 0.61 J of stored strain energy. Using the actual mechanism masses suggested a potential jump height of 0.2 m. This was far greater than the achieved 0.015 m. The implied 7% mechanism release efficiency could not all result from friction in the over-running catch mechanism so must have been due to another source. This loss was mostly due to the fact that the strain energy was released through a line far from the centre of gravity thus rotating the device rather than launching it upwards. The centre of gravity of the device needed to be located much closer to the compression axis for improved performance, whilst still enabling potential jump direction control by being a small distance away from it.

4.5 Future considerations

The main conclusions to be taken from this initial prototype were:

- The position of the centre of gravity should have been much closer to the axis of the device for useful jumping.

- The compression mechanism could not deliver the force required to compress all the available springs, so further jump energy could not be stored no matter what spring material was used. A compression mechanism delivering more force for less weight (improving on the 70 N/kg) would be required to improve jumping performance.

Jollbot 1 had quickly shown that a spherical jumping device has potential, but it needs to have some control over where it jumps before it could be considered useful. This could be achieved by moving the centre of gravity around the axis between the poles of the sphere, which in turn would give the possibility of providing the rolling required for a multimodal device. Space within the existing chassis was available, but the positioning of an additional motor would move the centre of gravity further from the polar axis of the sphere hindering jumping ability. The jump steering requirement, along with the important issue of improving the delivered force of the compression mechanism resulted in a significant redesign – Jollbot 2 (Chapter 5).

Chapter 5 Jollbot 2: Adaptive compression mechanism

After it was proved that the first prototype spherical jumping robot was able to jump, albeit poorly, the main aim of the subsequent version, Jollbot 2, was substantially to improve jumping performance by developing more compression force, integrating an element of direction control and considering an additional rolling capability. Although the elements of the existing sphere were not made of an ideal material, the sphere was not the main performance limiting factor of Jollbot 1 and remained largely unchanged for Jollbot 2.

5.1 Design

The second prototype of Jollbot attempted to tackle some of those issues of the first device and integrate jump direction control and an element of powered rolling.

Direction control of the jump was achieved by adjusting the centre of gravity of the device around its polar axis, thereby slightly leaning the compressed doughnut-like shape to one side before launch. The subsequent release of jump energy along the now-tilted polar axis, resulted in a jump in that pre-selected direction (Figure 110).

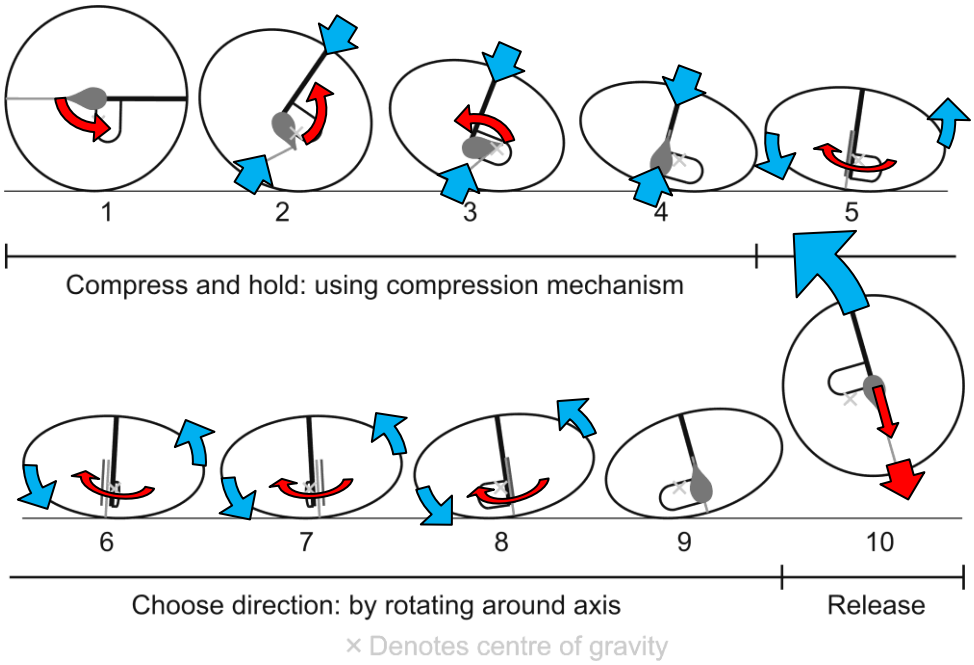

Figure 110 – Jumping method for Jollbot 2. Energy was stored in the sphere by the compression mechanism (1-4). The jump steering mechanism rotated the centre piece around the polar-axis choosing the jump direction (5-9).

Rolling was achieved by orienting the central axis parallel to the ground, and rotating the off-axis centre of gravity of the sphere around it using a “ballast mass fixed axis” mode of rolling (R.H. Armour & J.F.V. Vincent 2006). Although not implemented within this prototype, direction control of rolling would be possible by moving the centre of gravity laterally out of line with the ground contact area. This is summarised in Figure 111. Having an entirely driven outer surface of the device would help it roll over uneven terrain, and the low ground contact pressure would enable it to traverse soft surfaces such as sand, snow or brush. The further potential of sealing the ball with a waterproof material would allow it to paddle across lakes and rivers if mass and volume displacement were carefully considered. To stop the spherical device from rolling uncontrollably down hills, either the ballast mass could be used to brake the rolling motion, or by compressing the outer sphere, a stable squashed form could be adopted, discouraging unwanted tumbling. If downhill motion was subsequently required, then a spherical form could be adopted. If uphill motion were required, then a jumping strategy could be used.

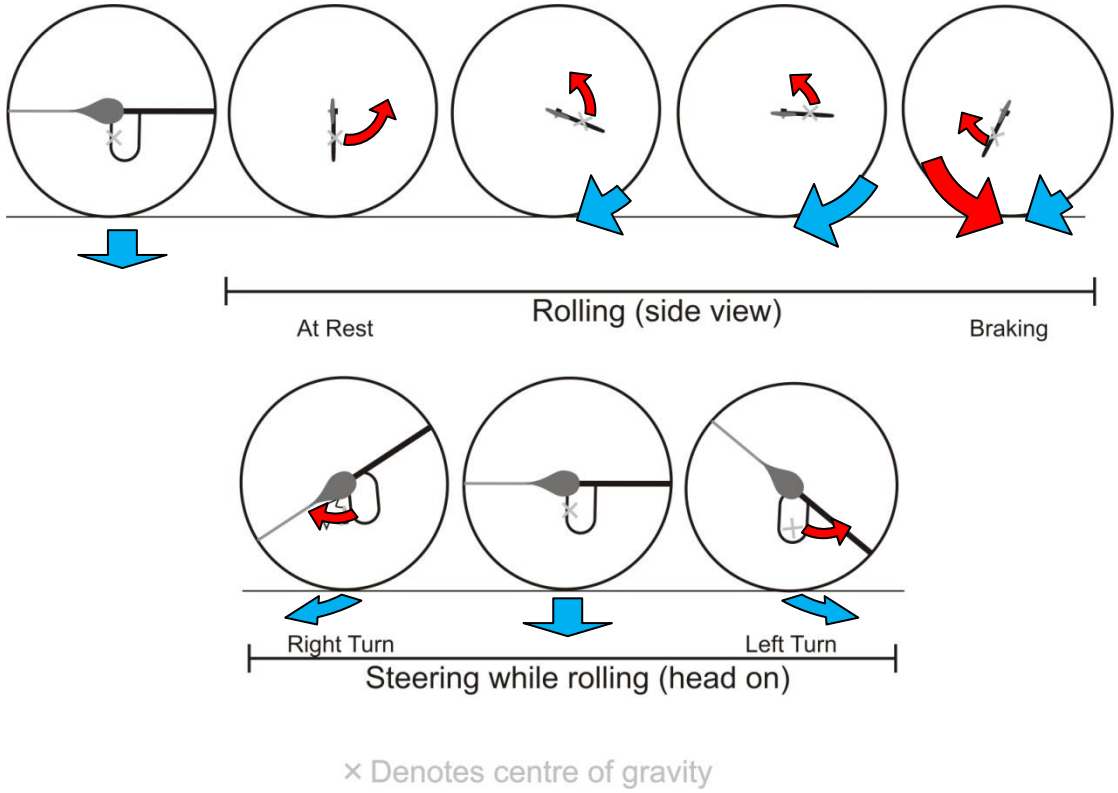

Figure 111 – Rolling method for Jollbot 2. Having the centre of gravity inline with the sphere's equator and away from polar axis ensured that the axis was horizontal and ready for powered rolling. Running the dual-purpose jump steering motor (now the rolling-motor) causes the centre of gravity to move outside of the sphere's contact patch with the ground and starts it rolling (out of the page in the lower part of the figure). Braking can be achieved by slowing the motor. Direction control of rolling can be achieved by moving the centre of gravity towards one pole or the other out of line with the equator, leaning the main axis over, and producing a turn.

5.1.1 Theoretical study of rolling

Combining the existing jumping motion of Jollbot 1 (Chapter 4) with the proposed additional rolling motion (see Section 2.7, p.105) could prove complicated, presenting some significant trade-offs between the types of motion. However, the potential benefits of a mobility system that was able to both jump over obstacles and achieve controlled active rolling over a wide variety of terrains, gave sufficient incentive to persevere.

Using simple geometry, and assuming perfect traction, rigid structures and substrates, and no momentum, the sizing and distribution of the wheel and ballast masses within a wheel-shaped or spherical rolling device could be determined if it were to roll over a small step or up a slope. Two theoretical studies were undertaken through the development of a pair of spreadsheets to help to clarify the problem and to indicate the properties required if a rolling device were to roll over a step or up a slope. In both cases a complete rigid wheel form was assumed, so no account was made of paddles or treads that may be on the surface of the resulting device.

5.1.1.1 Rolling over a step

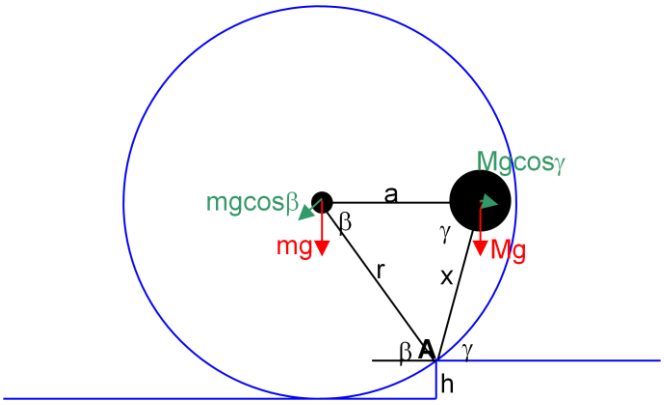

Figure 112 – Diagram of ballast rolling up step

The first study determined the required ballast mass given the rolling robot's details (size and mass of sphere, and anticipated off-axis radius for ballast). Taking moments around the contact point with the step edge (A) makes it simple to determine if the device would continue to roll clockwise and over the step given these criteria. As long as the selected value for length a is greater than some minimum value, then the ideal device would surmount the step. The simulation then gives the value of the ballast mass, M. Results of this are best shown visually taking a specific example of a 50 mm high step (Figure 113).

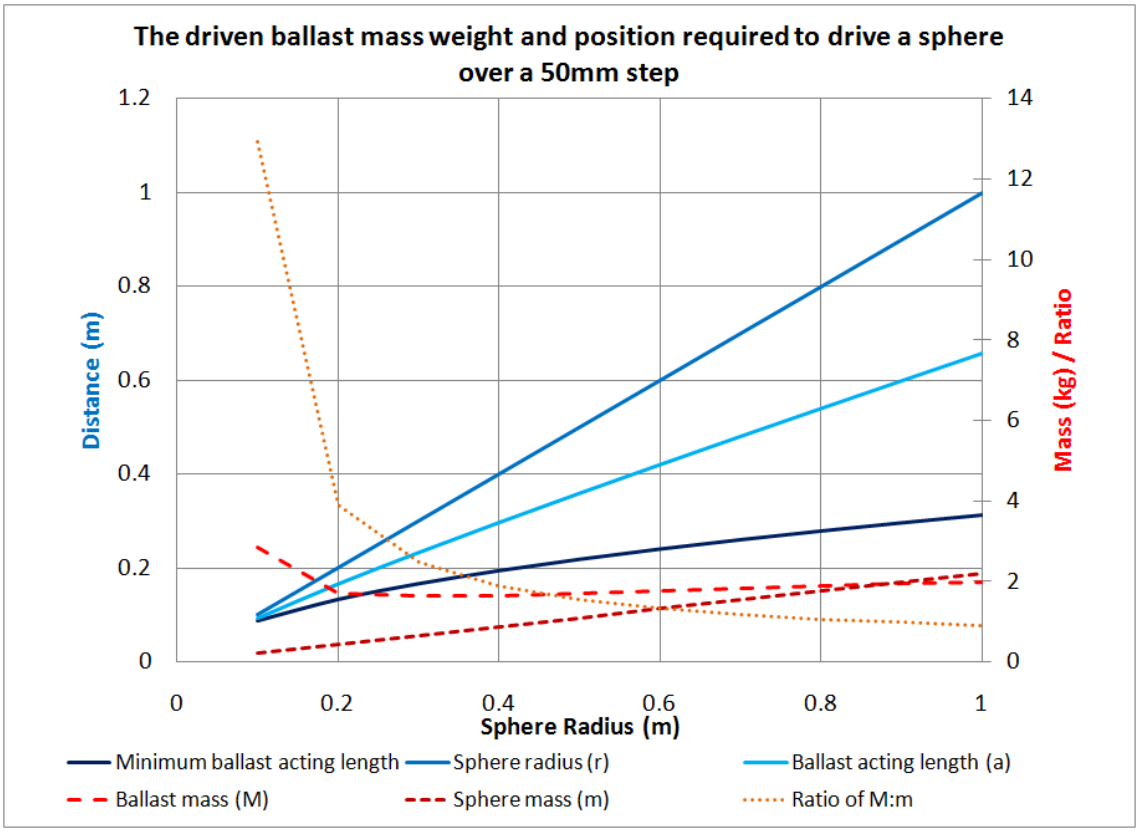

Figure 113 – Graphical representation of how ball radius affects ballast mass for a given step height. The illustration assumes that the mass of the sphere, m, increases at a given rate proportional to radius, r, (x2.2 - calculated from a Jollbot-type sphere of six elements of 1.5mm ϕ steel), and that the ballast mass, M, is a point mass offset by a value, a, halfway between the radius of the sphere and the minimum possible for clockwise rotation. For example, a sphere with a radius of 0.4 m and weighing 1 kg, with a ballast mass acting at 0.3 m would require the ballast mass to have a weight of approximately 2 kg to overcome a 0.05 m (50mm) step.

The solid lines in Figure 113 show the physical dimensions of each hypothetical powered rolling spherical robot that is able to overcome a 50 mm step. The light blue line indicates on the vertical axis the radius, a, at which the ballast mass acts for a given sphere. The blue line shows the radius, r, of the sphere. The darkest blue line highlights the minimum value of a for rotation. The dashed lines show the masses of the sphere (dark red) and ballast (red). The mass of the sphere was assumed to be directly proportional to its radius due to Jollbot's sphere construction. The calculated

ballast mass comes as a result of the other values. The remaining dotted line shows the ratio of ballast mass, M, to sphere mass, m. As might be expected, a wheel of small radius, where the step height is comparatively large (25 % of its height) the $M{:}m$ ratio is also large (13:1). This ratio decreases rapidly until the step becomes <10 % of the wheel height where the $M{:}m$ ratio is ~3:1 and continues to gently fall as the sphere increases in size. It can be quickly seen that for overcoming a particular stepped obstacle, the diameter of the ball should be maximised to allow for a relatively lightweight ballast mass. If a small rolling device is required, then the ballast mass will be comparatively heavy, and should therefore act as close to the circumference of the wheel as possible to generate the largest torque. Similarly, large torques are possible by maximising the ratio of ballast mass to sphere mass.

5.1.1.2 Rolling up slope

The second study determined similar details for a device being powered up a smooth sloping surface. An example graphical output (Figure 115) is shown below with a diagram of the problem's construction (Figure 114). Similarly to the step problem, rolling up a slope requires that the moment provided by the ballast mass around the contact point (C) is greater than the moment opposing it as a result of the wheel mass.

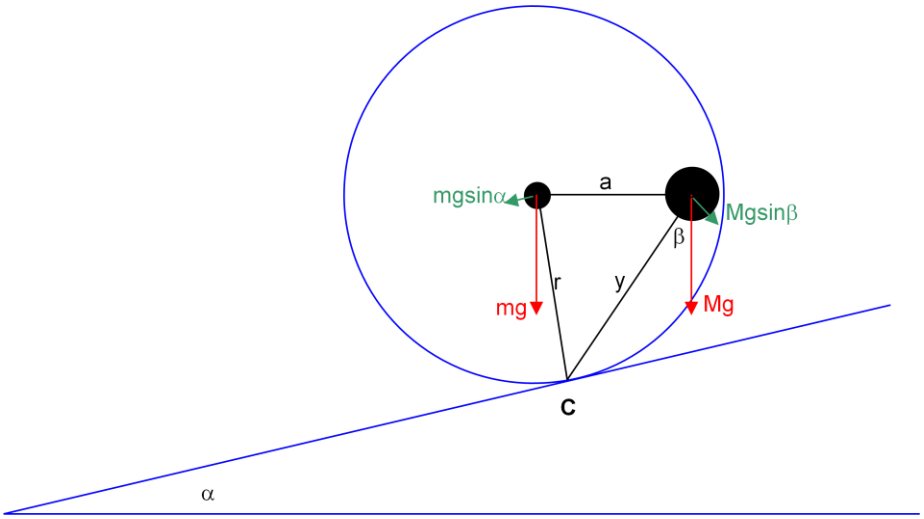

Figure 114 – Diagram of slope problem

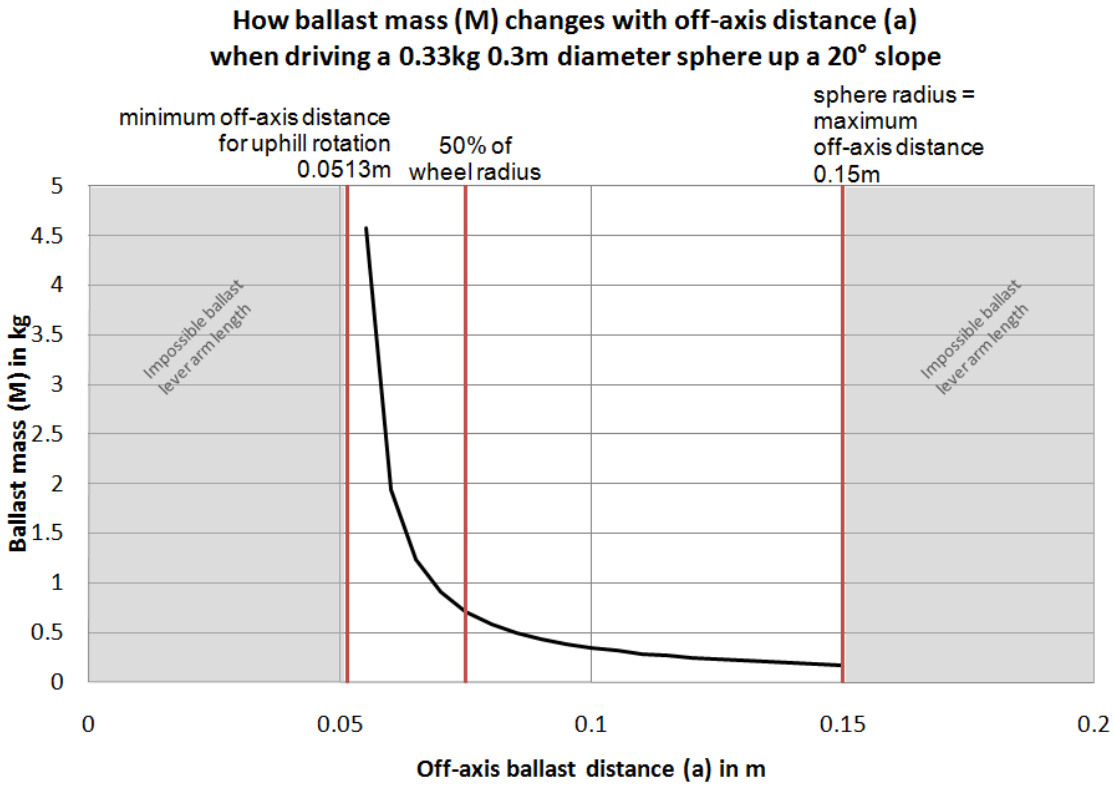

Figure 115 – Uphill rolling ballast mass variation with off-axis distance

For a given ball of a particular size and weight (Figure 115 shows the results for a sphere of 0.3 m diameter and 0.66 kg), there is a minimum lever length (off-axis distance) value that any ballast has to work at to achieve up-slope rotation. This value is related to the geometry of the slope and the size of the sphere, and in this case is 0.0513 m. The black line shows the required mass of the ballast for a given acting lever arm length, a. As expected the required mass of this ballast needs to be very large when it is acting close to the minimum off-axis radius value, and falls rapidly as its acting length approaches 50% of the sphere radius. An acting length of greater than the sphere radius is impossible. That would be ≥0.15 m in this case. Taking a specific example, the mass of ballast acting at 50% sphere radius (of a sphere weighing 0.33 kg) needs to exceed 0.7 kg for upslope driving. This is a $M{:}m$ ratio of 2.12:1.

5.1.1.3 Rolling summary

Comparing the challenges of rolling over a step, and up a slope, determines which is the more difficult. To drive a sphere of 0.3 m diameter up a slope of 20° with a lever arm length of 50% sphere radius (0.075 m) requires a ballast mass, M, to sphere mass, m, ratio of 2.12:1. Overcoming a step of 50 mm with a sphere of the same size and weight requires a $M{:}m$ ratio of ~7:1 and this assumes a different lever arm length of almost the maximum possible (~0.14 m). If the lever arm length was the same 0.075 m as in the slope case, then the 50 mm step would require a much greater ratio of ballast mass to sphere mass. For a 0.3 m diameter sphere, the challenge of achieving driven rolling over a 0.05 mm obstacle is far more difficult than rolling up a 20° slope. For larger diameter spheres this difference would decrease.

The above cases are based on many assumptions, including the relationship between sphere size and mass, the selection of the off-axis acting point of the ballast mass, ignoring momentum and run-ups, and taking no consideration of the friction, traction and the true form of the prototype sphere.

In Jollbot's case, the sphere viewed in its intended rolling position with its polar axis horizontal, would have many radial elements. This form would allow for the centre of gravity of the entire device to approach closer to the edge of stepped obstacles. This would improve obstacle surmountability, but also leads to the potential for a single spar to become stuck in the nook at the base of a step, halting progress. The springy and compliant form also results in a larger-than-idealised contact patch, meaning that rolling on smooth and sloped surfaces may require a larger ballast mass than anticipated, acting at a greater off-axis distance, and combined with a more spherical form consisting of more hoop elements. In general, however, for all powered rolling considerations, the off-axis mass should be maximised and should act at a distance as far from the polar axis of the sphere as possible. This results in a significant contradiction: where for jumping, the centre of gravity of the complete device should be close to the polar axis (but not on it to allow for jump steering control); and that for rolling, the centre of the gravity of the complete device should be as far as possible from the polar axis of the sphere. However, as rolling was considered a secondary form of movement, it was intended that powered rolling would be used only on smooth and

level surfaces. Thus the powered rolling ability need only require the ability to overcome small obstacles and shallow slopes.

5.1.2 Physical Design

The outer shape of Jollbot 2 came from a sphere made of metal semi-circular hoops. These hoops were the springs that provide the energy for jumping and made up the outer rolling surface. A photo and CAD model of the device is shown in Figure 116.

Many of the components for Jollbot 2, particularly the main chassis components, were manufactured directly from the CAD models using rapid prototyping in ABS.

Jollbot 2 was powered by a 4.8 V 600 mAh Ni-Mh battery pack. This supplied two 6 V rated model servos (the high torque Towerpro MG599 and standard Acoms AS12) and the radio control receiver. As with Jollbot 1, the servos were modified to allow continuous rotation. They had integral gearboxes allowing sufficient torque to be developed for storing the jump energy within the hoop springs, and for rotating the slightly off-axis centre of gravity for jump steering and powered rolling control.

(a) 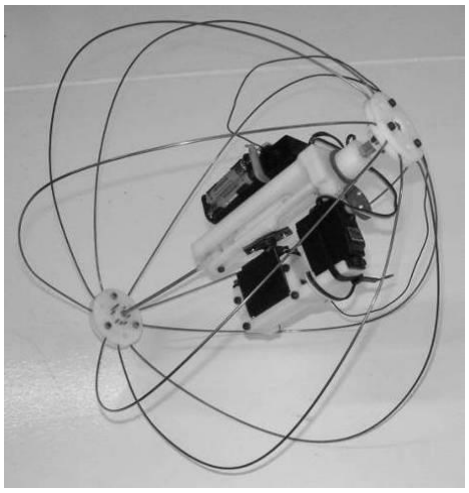 (b) 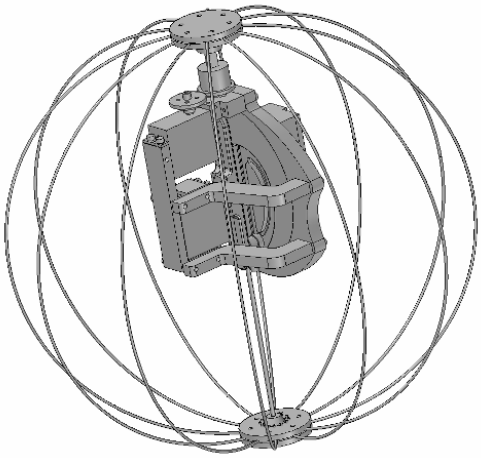

Figure 116 – Photograph (a) and CAD model (b) of Jollbot 2

5.1.2.1 Spring sphere

The spring sphere for Jollbot 2 was based on the same spring elements, materials and structure as that of Jollbot 1. However, due to the improved force capacity of the new adaptive compression mechanism (see Section 5.1.2.2), the stiffness of the sphere could be increased. By adding three additional wire elements, making a total of nine, a sphere that was considerably stiffer was produced. Its characteristics are determined experimentally in Section 5.2.2. Using the sphere theory from earlier (see Section 4.2.1, p.160), resulted in a theoretical sphere of nine elements having a stiffness of 334 N/m. But this was expected to be quite different from the physical sphere after the discrepancy between theory and practice found in Jollbot 1.

5.1.2.2 Adaptive compression mechanism

Jollbot 2 involved a re-designed compression mechanism that would allow the same size motor from Jollbot 1 to store more strain energy in the springs. The compression mechanism sat on a chassis. This was fixed to the uppermost pole or “head” of the robot, and consisted of a model servo rotating a continuously-variable-length crank with its connecting rod attached to the “foot” at the opposing side of the sphere. As the servo rotated, the head and the foot of the robot were pulled toward one another storing strain energy in the springs.

To maximise the stored energy, the compression system, powered by a constant-torque motor, should adapt to the required compression force. As the hoop springs are compressed, the force required increased with displacement. Therefore, when using a fixed length crank, the required rotary torque increased as the displacement increased. By introducing a crank that varied in length as it rotated, the output force of the compression mechanism could vary while the input torque remained almost constant. This was achieved by using a guide, face-cam and slider-roller as shown in Figure 117 and Figure 118. This revised mechanism outperformed the fixed-length crank mechanism as it was able to compress more hoop spring elements using the same model servo as Jollbot 1.

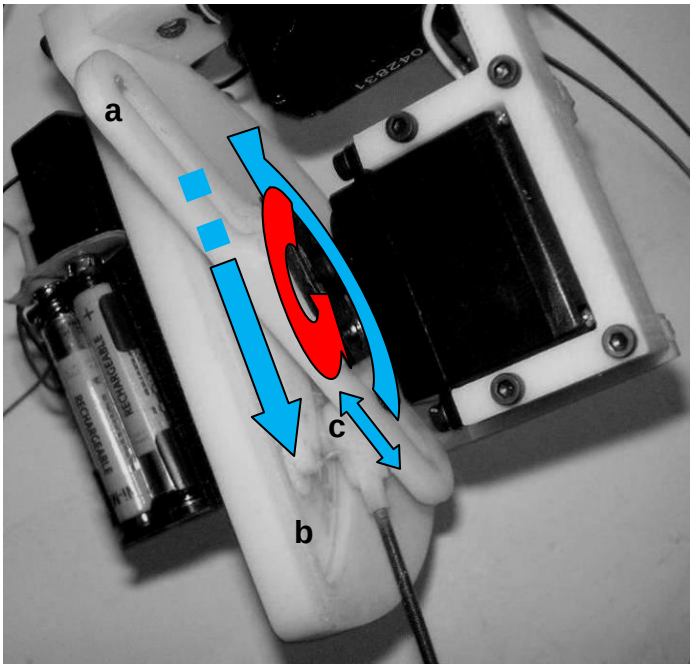

Figure 117 – Photograph showing detail of guide (a), face-cam (b), slider-roller (c) in Jollbot 2. The red arrow highlights input from motor. The slider-roller (c) follows path in face-cam (b) and slides along a variable length guide.

As the motor rotated the guide, the face cam ensured that the slider-roller moved in a specific path, and therefore at a variable crank length around the servo axle. The design of the cam profile was critical to the operation of the mechanism: the face cam surface could not be sloped too steeply as then the slider roller would lock the mechanism causing failure.

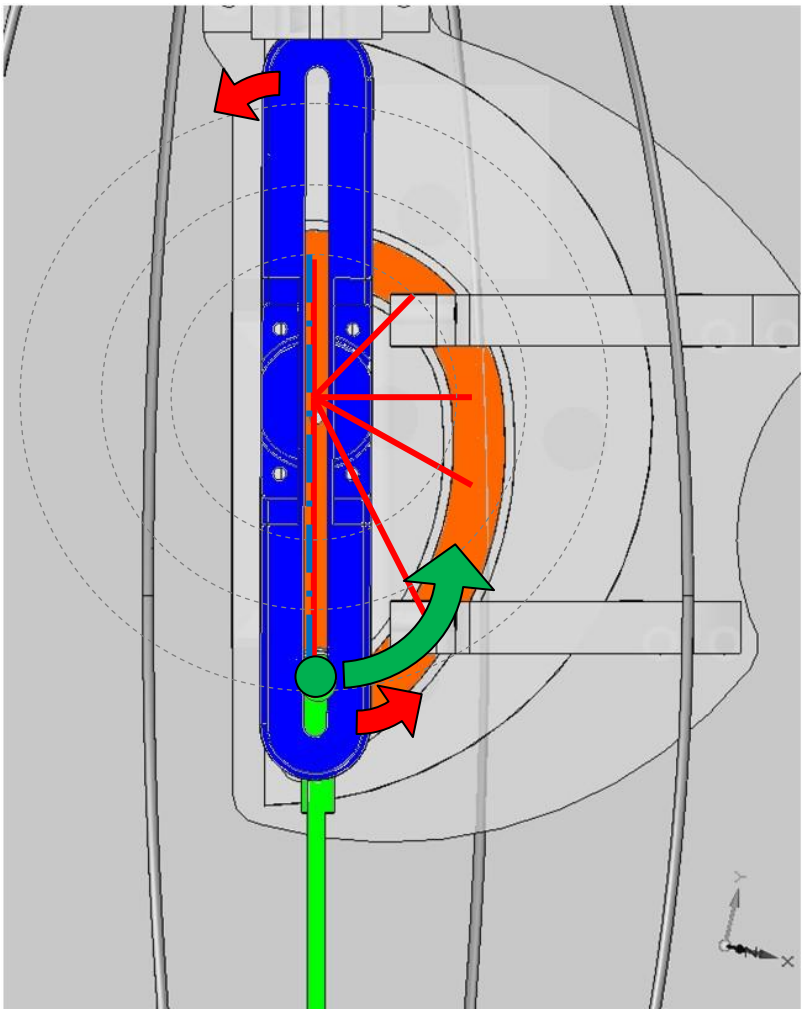

Figure 118 – Diagram illustrating the variation in effective crank length (solid red lines) due to the cam profile (orange shading). Dotted concentric rings are marked around the centre of rotation of the compression motor for length visualisation. The red arrows show rotation of the guide and the green arrow indicates the movement of the slider roller that was connected to lower pole of sphere. Once the guide (shaded blue) had rotated by 180°, the slider roller (green) was allowed to travel along the guide and the face-cam as the energy stored in the outer sphere was released.

The face-cam was designed to be readily replaceable for tuning purposes. The cam that worked the best kept the slider-roller at a constant radius for a short time initially. As the guide rotated toward 90°, the radius of the cam reduced slightly, and between 90° and 180° the radius reduced further to ease the loading on the motor. As soon as the 180° position was reached (after a total of 65 mm of compression), the slider-roller

was free to move in the axial direction because of the cam profile and the slot that ran all the way along the guide. This straight axial release of the spring energy ensured that none was wasted unnecessarily as would be the case with a rotating fixed length crank. Once the slider-roller had reached the bottom of the cam, the guide then continued to rotate, beginning another energy storage phase. Figure 119 shows the compression phase of Jollbot 2, illustrating how the crank length continuously varied throughout the rotation of the servo. Figure 120 shows the jumping phase.

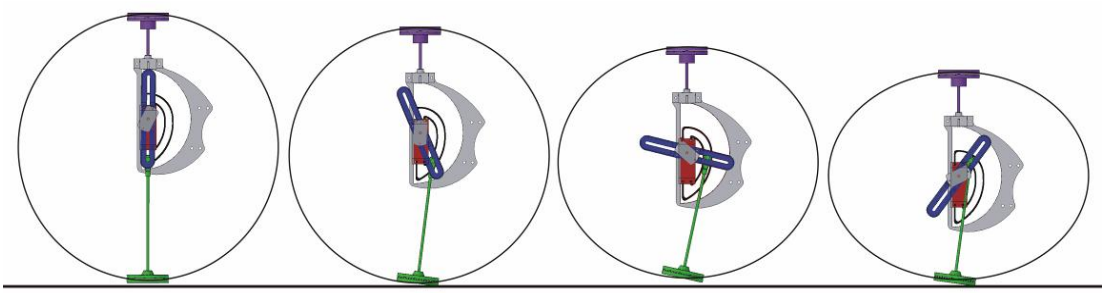

Figure 119 – Compression phase of Jollbot 2

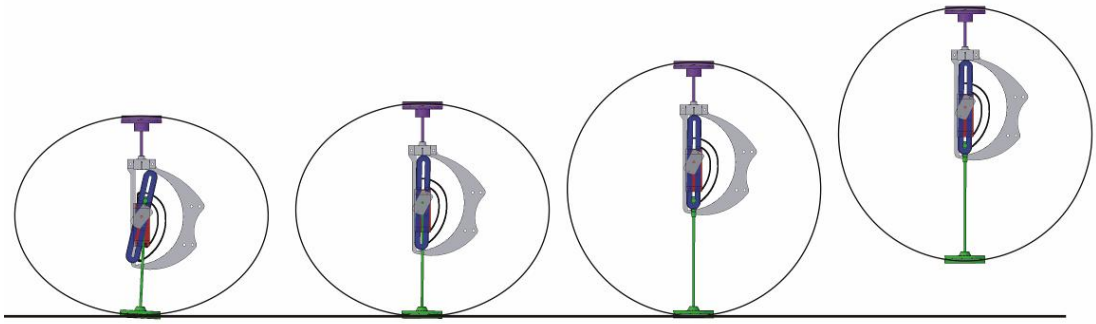

Figure 120 – Jumping phase of Jollbot 2

5.1.2.3 Jump direction control

To achieve direction control, a second servo (Acoms AS12) rotated the compression mechanism around the axis of the sphere. The movement of the slightly off-axis centre of gravity would enable the jump direction to be chosen by tilting the axis of the robot in the required jump direction. The servo was mounted onto the main chassis and drove itself around a gear fixed to the sphere of the robot (Figure 121). This enabled the

entire central chassis and its associated components to twist, adjusting the centre of gravity, and therefore the lean of the main jumping axis. The semi-spherical form of the foot and hoop springs when compressed allowed the robot to lean in any direction.

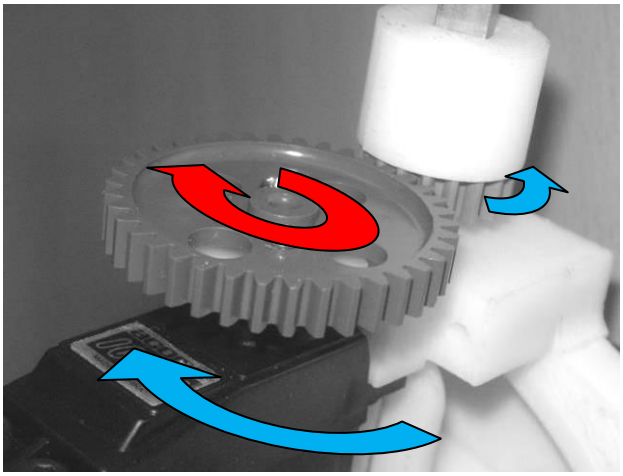

Figure 121 – Jollbot 2 jump direction and rolling mechanism. The darker arrow shows the rotation of the large spur gear which results in the rotation of the entire motor around the smaller spur gear.

5.1.2.4 Powered rolling capability

The same motor that controlled jump direction was used to rotate the intentionally off-axis centre of gravity of the whole device, and thus produce a powered rolling moment. The whole mechanism was secured to the outer sphere using manually-adjustable length links so that the point at which the centre of gravity acted could be tuned to be in-line with the contact patch when the robot was in its rolling orientation with the polar axis horizontal.

Steering control during rolling was not implemented in Jollbot 2 as it was thought that achieving steady straight-line rolling was of higher priority.

5.1.3 Jollbot 2 mass

The masses of the Jollbot 2 and its components are shown in Table 20.

Component	Mass
Compression Servo	50 g
Rotational Servo	40.5 g
Batteries and Battery box	65 g
Receiver	20 g
Half-hoops (9 @ 7 g each)	63 g
Sphere Top & Bottom Clamps	52 g
Jollbot 2 mechanism and chassis	174.5 g
Total Mass of Robot	**465 g**

Table 20 – Jollbot 2 mass

These masses resulted in an accelerated "head" mass to trailing "foot" mass ratio of 7.1:1 making the simplifying assumption that the top half of the sphere contributed to the "head" and the bottom half to the "foot".

Combining the theoretical sphere stiffness of 334 N/m, the above masses, and a compression of 65 mm, resulted in a predicted no-loss jump height of 0.15 m. This was less than that predicted for Jollbot 1, but larger than the experimental results of Jollbot 1. It is true that a sphere of greater stiffness, when compressed by a similar amount, would produce a jump higher than that possible with a less-stiff sphere. However, the additional mass of the new compression mechanism and jump steering components in Jollbot 2 meant that the predicted jump height was less than that predicted for Jollbot 1. The stored energy in the sphere of Jollbot 2 would be more than in the previous prototype.

5.2 Experiments

In order to evaluate the performance of Jollbot 2, various physical factors needed to be measured and high speed video recordings made of jumps. The results from these could then be used to find numerical efficiencies and qualitative observations of areas of improvement.

5.2.1 Centre of gravity position

The position of the centre of gravity of the robot was determined by combining the centre of gravity of the spring sphere (at its geometric centre) and that of the control mechanism determined by hanging it by a thread and taking photographs (Figure 122). The centre of gravity of any object suspended by a thread lies inline and below the thread. By suspending an object from different points, the centre of gravity can be determined.

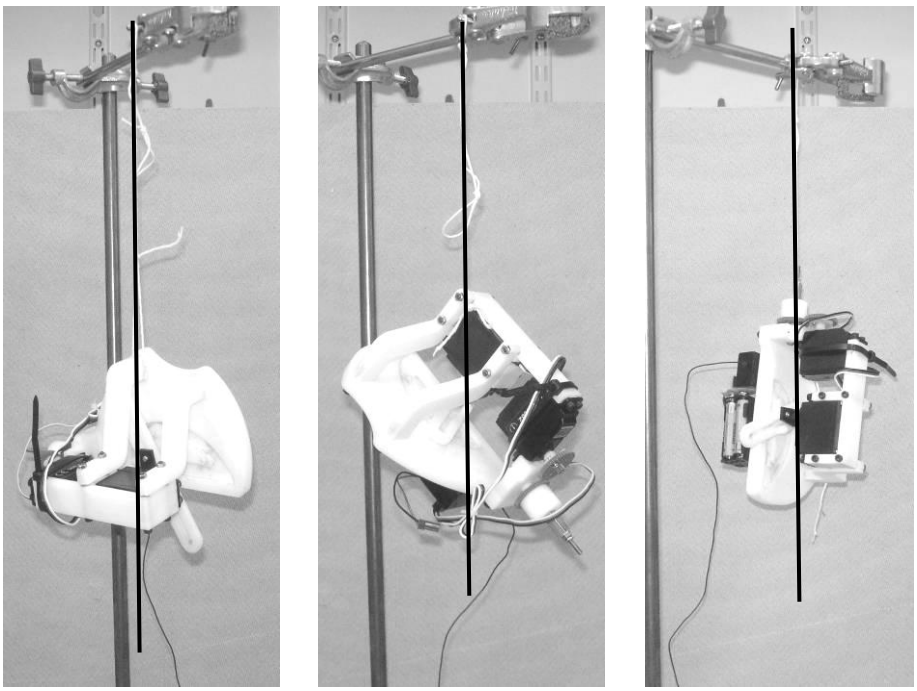

Figure 122 – Determining CofG of control mechanism by hanging it from 3 different points and intersecting the results.

Owing to the different masses of the spring sphere and the control mechanism, the centre of gravity of the entire robot was approximately in the location shown in Figure 123. This was substantially toward to upper half of the sphere and would result in difficulties achieving powered rolling.

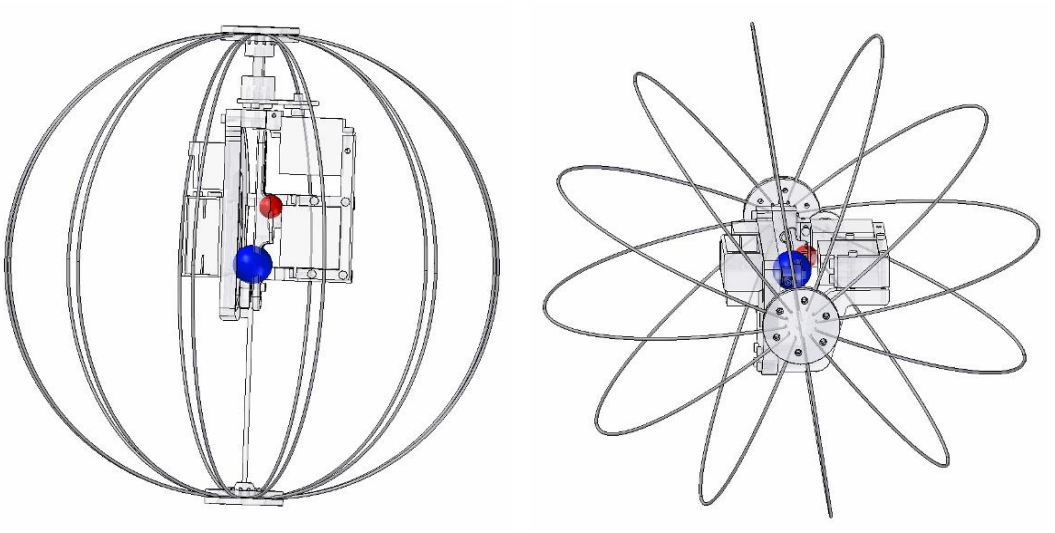

Figure 123 – Image showing centre of gravity location; small red marker is centre of gravity, larger blue marker is geometric centre of device

5.2.2 Sphere characterisation

As for Jollbot 1, a force-displacement curve for the revised sphere was obtained through testing in an Instron desktop test machine. The results of this are shown in Figure 124.

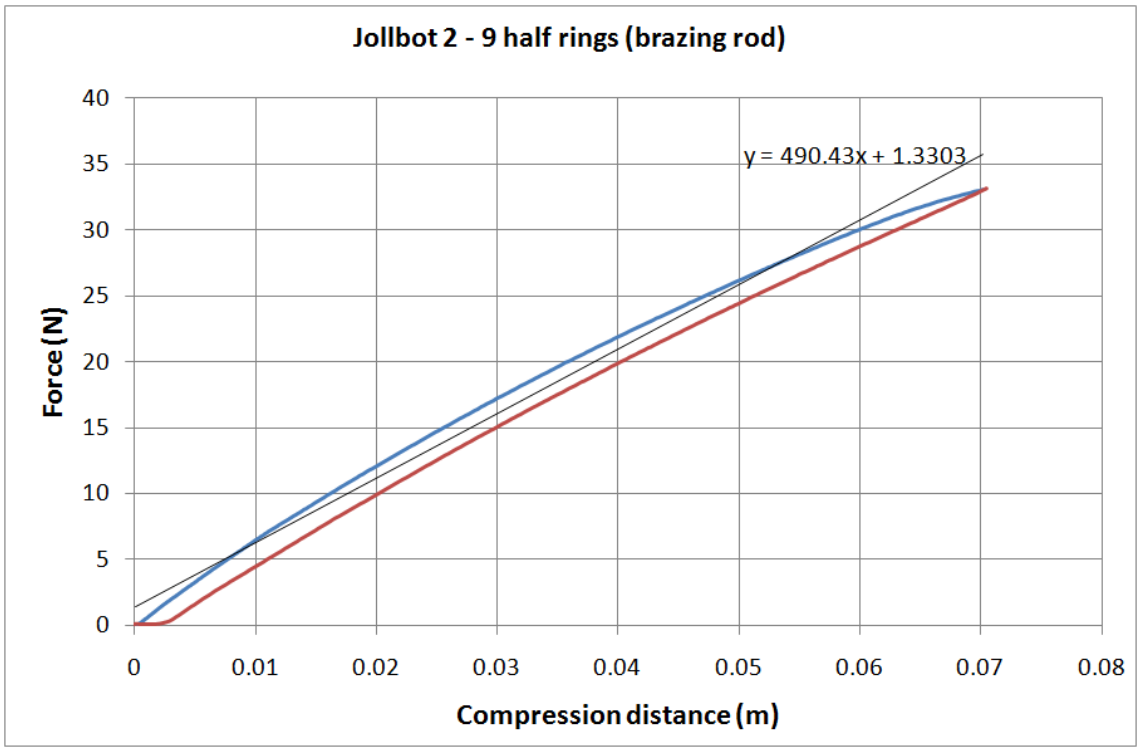

Figure 124 – Jollbot 2 sphere characterisation

Once again, the nine brazing rod elements and the fixing clamp assembly display not very linear behaviour. This could be due to a number of factors, including the plastic deformation (implied by the hysteresis in the return extension path) of the brazing rod elements, compliance in the clamping mechanism, and the proportionally large deflections involved. However, fitting a straight line through the first 70 mm of compression, gave some indication of the energy stored in the sphere when fully compressed. The slope of this line gave the stiffness of the sphere as ~500 N/m. Unexpectedly, the nine element sphere was 67% stiffer than the six element one from Jollbot 1, meaning that after compression of 65 mm, the sphere stored ~1.1 J of energy (using Equation 13). Applying theory here resulted in a predicted no-loss jump height of 0.24 m. This is different to the 0.15 m predicted previously as the physical sphere's stiffness of 500 N/m is substantially more than the 334 N/m predicted by theory for a nine element sphere.

5.2.3 Jumping performance

Jollbot 2 was originally designed for twelve semi-circular spring elements, but even after the development of a reliably working cam, the mechanism was only capable of compressing nine elements. Any more than that would cause the motor to stall and stop the mechanism. The available torque from the Towerpro MG995 servo was again insufficient (see Section 4.2.2.2).

In order to measure the jumping performance of the robot, a Redlake Images Motionscope high-speed camera was used to film each jump at a pre-selected frame rate of 50Hz. ImageJ software (Rasband 2010) was used to determine the position of different components of the robot in each frame. In order for this method to be valid, the robot was always placed such that it jumped in a plane parallel to the camera lens, and both a horizontal and a vertical calibration was performed using graduated markers.

The jumping performance of the 0.3 m diameter Jollbot is illustrated in the high speed camera images in Figure 125. From the images, it was determined that the robot raises its centre of gravity by 0.218 m through the course of the jump, which is approximately 2/3 of Jollbot 2's height. The robot can clear a height of 0.184 m which was just over half its own height. As mentioned above, the theoretical best jump would have been 0.24 m, so Jollbot 2 had a ratio of 91%. This was much better than Jollbot 1 (7%).

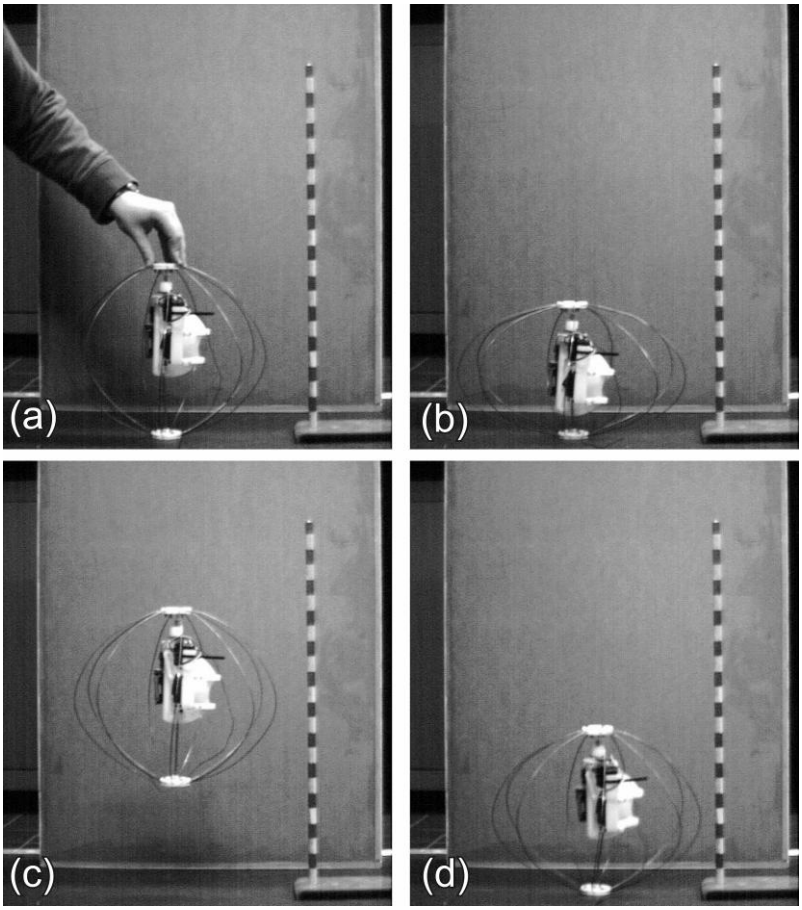

Figure 125 – High speed camera images illustrating the jumping performance of Jollbot; (a) Resting state of Jollbot (hand in place to avoid toppling), diameter = 294 mm, (b) 1.44 s later, Jollbot is ready to jump after compressing 65 mm, (c) 0.24 s later, Jollbot is at its peak jump height, clearing 184 mm, (d) 0.22 s later Jollbot hits the ground and absorbs impact energy in the slight compressing of the sphere.

The output from ImageJ was logged in a spreadsheet and the position data presented in graphical form (Figure 126). Figure 126 indicates the resting diameter of Jollbot on the far left, the compressed diameter in the middle of the graph and its response during release and subsequent jump beneath the peaks.

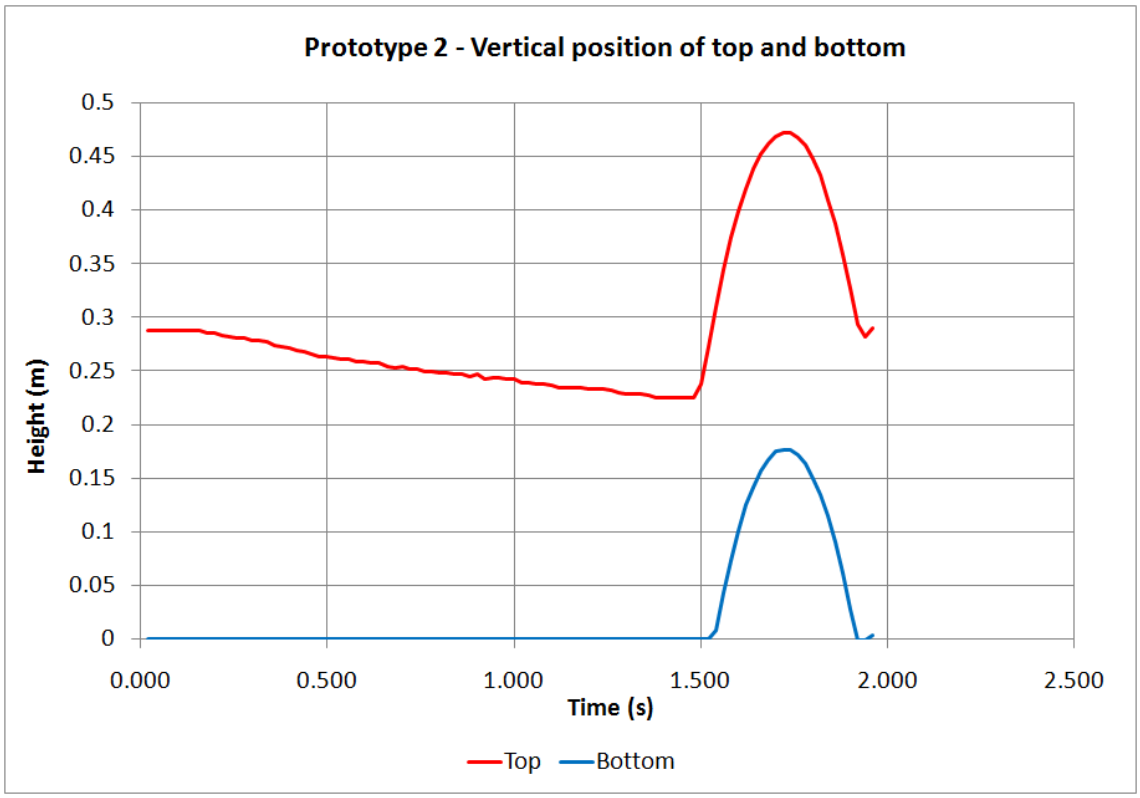

Figure 126 – Position of top and bottom of Jollbot 2 during compression (0 – 1.5 s) and subsequent jump (1.5 – 2 s)

Differentiating this position data twice results in acceleration data for the top and bottom of the device. This is given in Figure 127. This shows a steep increase in acceleration to over 10 m/s^2 of the top of the device after release, followed shortly after by the base accelerating as it leaves the ground. At the peak of the flight, the acceleration is obviously zero, and afterwards it becomes approximately -10 m/s^2 as expected when acted on only by gravity. The small number of frames covering the jump itself made it difficult to determine the relative accelerations of the head and foot. But it can be seen that the head achieves a peak vertical acceleration of 1.2 g, and the foot a peak vertical acceleration of 1 g, ~0.05 seconds later.

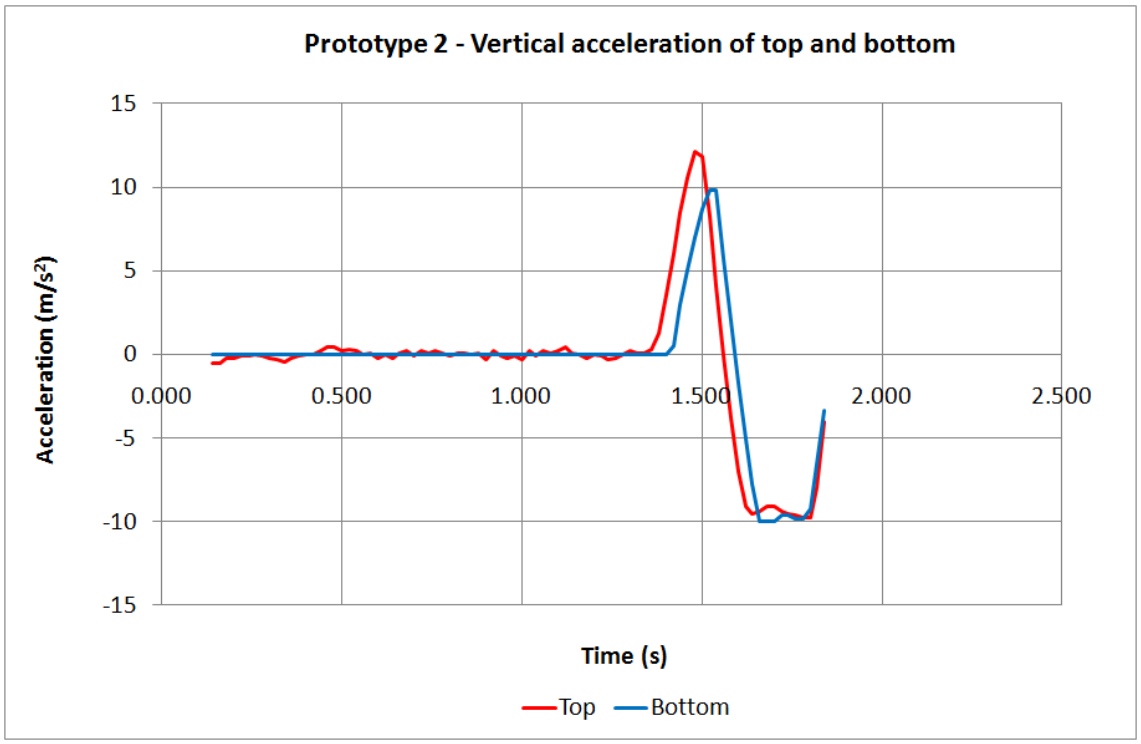

Figure 127 – Acceleration of top and bottom of Jollbot during compression and subsequent jump

5.2.3.1 Jump efficiency

The efficiency of various mechanisms within the robot could be determined by comparing the energy of the device in different states. A comparison between the electrical energy consumed and the energy stored within the system gives a conversion efficiency for the compression mechanism. Comparing the energy stored with the potential energy of the robot at peak jump height illustrates the efficiency of the jump mechanism.

The electrical energy consumed was found from Equation 20.

$$Electrical\ Energy\ (J) = Voltage\ (V) \times Current\ (A) \times Time\ (s)$$

Equation 20 – electrical energy

The potential energy stored in the spring-based jumping system was equivalent to the area under the force-displacement curve (Equation 13, p.93). The potential energy stored in a mass suspended at a height is defined in (Equation 6, p.52).

In Jollbot 2's case, the servo drew a peak current of ~1.2 A from the 4.8 V battery pack over the 1.44 s compression. This equated to a power of 5.76 W. From Equation 20, this gave a total energy consumption of 8.3 J per jump. As the current increased throughout the compression, reaching a peak at maximum compression, this estimate was larger than the actual energy consumption, and logging of the current values throughout the short compression time would have given a more accurate value.

The energy stored within the robot's spring system was estimated from the area under a force-displacement curve from the testing carried out with the materials test machine (see Section 5.2.2). This resulted in approximately 1.1 J of stored energy (Figure 124).

The potential energy of the device was determined using Equation 6, where the mass of the robot is 0.465 kg and the change in height of the centre of gravity is 0.218 m. This resulted in 0.9 J of potential energy.

Comparing the first two energy measurements with one another resulted in a conversion efficiency of 14 % for the compression mechanism. This low value was due to friction in the entire mechanism including the servo's gearbox and between the face cam, slider and guide, along with a contribution from the overestimation of the average current draw. Comparing the second two energy measurements resulted in a mechanism release efficiency of 81 %, indicating that energy was lost due to friction of the slider as it moved through the guide and across the cam, as well as due to factors such as noise, the sphere elements not being perfect springs, and the oscillations and vibrations of the structure during flight. This 81 % efficiency was much higher than the equivalent 7 % efficiency achieved in Jollbot 1.

5.2.4 Jump direction control performance

The semi-spherical form of the foot and hoop springs when compressed, allowed the robot to lean in any direction as shown in the video stills in Figure 128. This feature

allowed for the direction of each jump to be chosen. However, full testing of this jump steering mechanism could not be undertaken as it proved difficult to control both servos accurately to ensure the “compress and hold”, “choose direction”, and “release” stages occurred in a suitable series without the robot toppling over. The absence of a “primed for jump” catch was the main contributing factor to this. A modification to the cam profile would allow for such a position to be available.

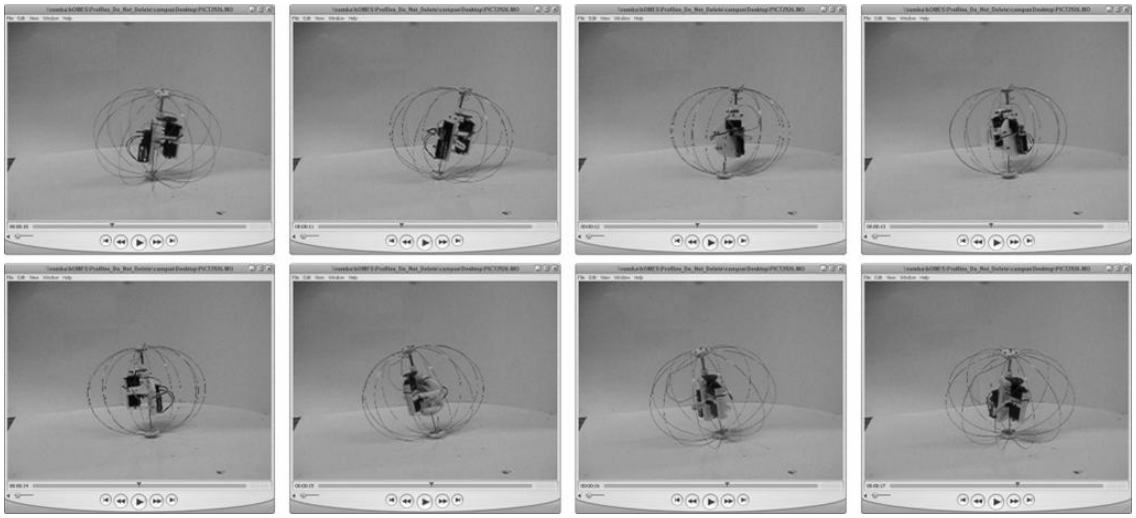

Figure 128 – The jump direction control of Jollbot 2 as the central mechanism moves around an axis between the poles of the outer sphere.

5.2.5 Rolling performance

The spherical form of the device naturally allowed for passive rolling (see Section 2.7.2.1), but active rolling (see Section 2.7.2.2) proved impossible with the device as prototyped. The centre of gravity of the device within the sphere was almost in line with the main axis. This meant that the turning moment of the off-axis centre of gravity was not sufficient to rotate the entire device on the large contact patches made as a result of small number of hoop springs. Additionally, keeping the main axis horizontal for stable rolling was very difficult as the centre of gravity was closer to one pole than the other. Jollbot 2 did not have any provision for direction control whilst rolling.

5.3 Evaluation

Jollbot 2 performed a jump of around half its diameter. This was achieved by accelerating 88 % of the weight of the device away from the remaining 12 %, and through a distance of approximately one quarter of the diameter of the sphere. This distance should be maximised to maximise take-off velocity, but minimise the forces involved. With design optimisation of Jollbot 2, it could be possible to increase the compression length to around half the diameter of the sphere. However significant re-design of the compression mechanism was required to enable a distance larger than this, and the next prototype aimed to do that (see Chapter 6).

The revised compression mechanism was able to compress a sphere with a stiffness of 500 N/m by 65 mm. This resulted in a peak force delivery of 32.5 N, but came at the expense of additional masses. Including the jump direction and rolling mechanisms masses, the new compression mechanism delivered 93 N/kg: a significant improvement over the 70 N/kg delivered by the fixed length crank mechanism of Jollbot 1. Jollbot 1 was also missing any additional components for direction control.

Jollbot 2 had a simple mechanism which relies on an unstable equilibrium point at complete compression and just before release. With the manual remote control system, it proved very difficult to stop the mechanism at the required point on the cam, but with minor modification to the cam profile, a stable stop point could be created. This missing ‘catch’ position made it difficult to test the direction control of jumps fully. Preliminary testing suggested that the proposed system would work, but repeatable experiments were impossible to undertake.

Like the first prototype, Jollbot 2 could only jump from one pole of its sphere. The heavier masses making up the “head” of the device were fixed to one pole, meaning that, after landing, the sphere was required to rotate back to its base. This was a solution others have used (Kovač et al. 2010; Weiss 2001) and whilst it would work with suitable centre-of-gravity locations, it did require some open area for reorientation. Being able to jump from both poles of the sphere would remove this area requirement.

The powered rolling ability was severely limited by the few elements making up the sphere. This resulted in a large contact area between the few spring elements and the substrate. The positioning of the centre of gravity close to the axis between the poles of the sphere meant that sufficient moment could not be generated outside of the large contact area with the ground. The position of the centre of gravity toward one end of the sphere also meant rolling in a straight line, with the main axis horizontal, was impossible to achieve.

Owing to the spherical shape of the robot, Jollbot 2 could passively roll down surfaces, and bounce off obstacles, particularly after a jump. The springs on its outer surface would also absorb much of the impact energy from collisions and landing, thus protecting any sensitive equipment from damage. However, if the robot were to land directly on its “head” then the chassis would take much of the impact force, but it was thought that that would be an uncommon occurrence.

5.4 Future considerations

Jollbot 2 made an improvement over Jollbot 1, but left a fully-working rolling capability underdeveloped. The main aims of Jollbot 3 were therefore to concentrate on developing the rolling performance while still making improvements in jumping capability. This would require substantial adjustment to the design.

Chapter 6 Jollbot 3: Combined jumping and rolling movement

The results from the previous two prototypes clearly suggested that a step-change increase in performance was required to produce a device that could usefully jump over obstacles whilst also successfully achieving powered rolling over smoother surfaces.

There were five main differences between Jollbot 3 and the Jollbot 2. These were:

1) **A winch-cable based sphere compression mechanism;** This winching mechanism allowed the sphere to be compressed by a much higher percentage of its diameter (about 90 %), but also introduced complications due to possible tangling of the cables – especially during rolling;
2) **A solid square section axle** positioned pole-to-pole within the sphere, but allowed to move through either end; this gave the control mechanism a fixed component to react against when rolling;
3) **An additional mechanism** to steer the robot when rolling and to attach the control mechanism to the suitable pole of the sphere when jumping;
4) **An increase in the diameter of the sphere** to increase the size of obstacles that could be overcome when rolling, to increase the percentage of compression and resultant amount of energy that could be stored by the same power motor as Jollbot 2, and to provide more volume to allow for additional mechanisms to be incorporated within.
5) **A change to spring steel sphere elements**

A pair of new designs was developed in series – each with more attention to the combination of rolling and jumping ability than any previous prototype. Each of the new

designs were based around a powered-rolling-and-steering-with-jumping principle represented pictorially in Figure 129 and Figure 130. The main differences between Jollbot 3a and 3b came from the assignment of the three dual-use motors in each device. The assignment of the motors changed due to the different speeds required to perform each of the functions of jumping, rolling, and direction control.

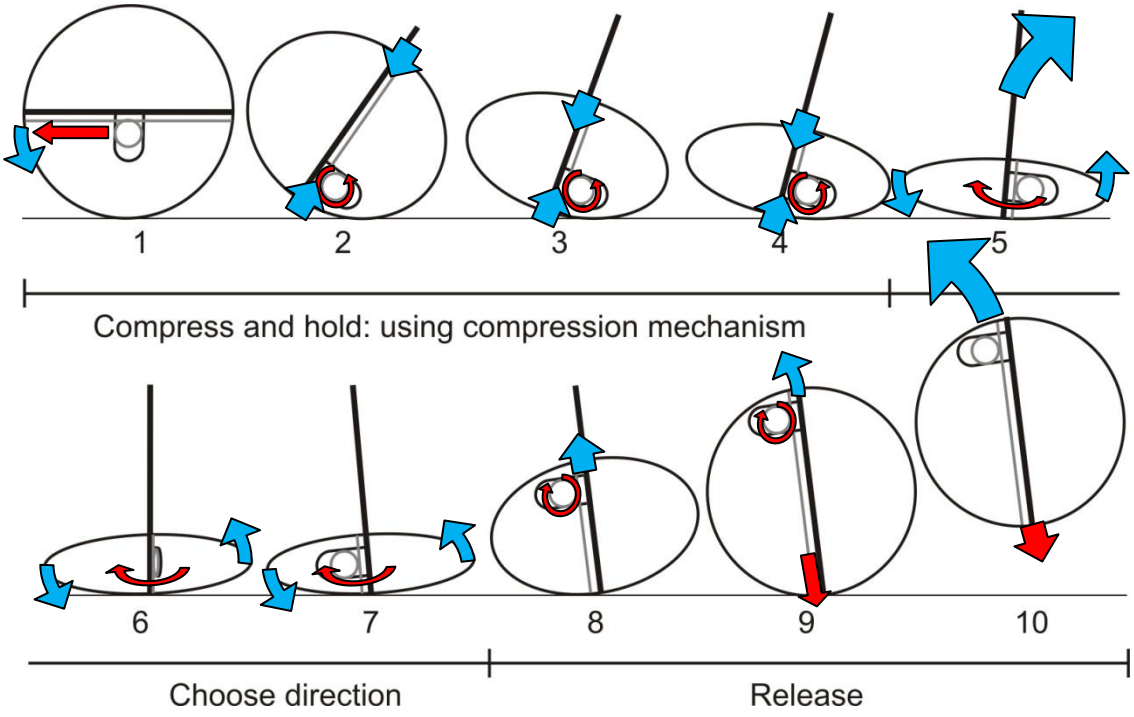

Figure 129 – The jumping method for Jollbot 3a and 3b. Moving the central mechanism along the square section axle (1) encouraged the sphere to roll onto one of its poles no matter what its previous orientation. The compression mechanism wound the two poles of the sphere slowly toward one another (2-4). Rotating the compression mechanism around the square section axle allowed for the jump direction to be controlled (5-7). Releasing the correct side of the cable allowed for the sphere to quickly expand and jump (8-10).

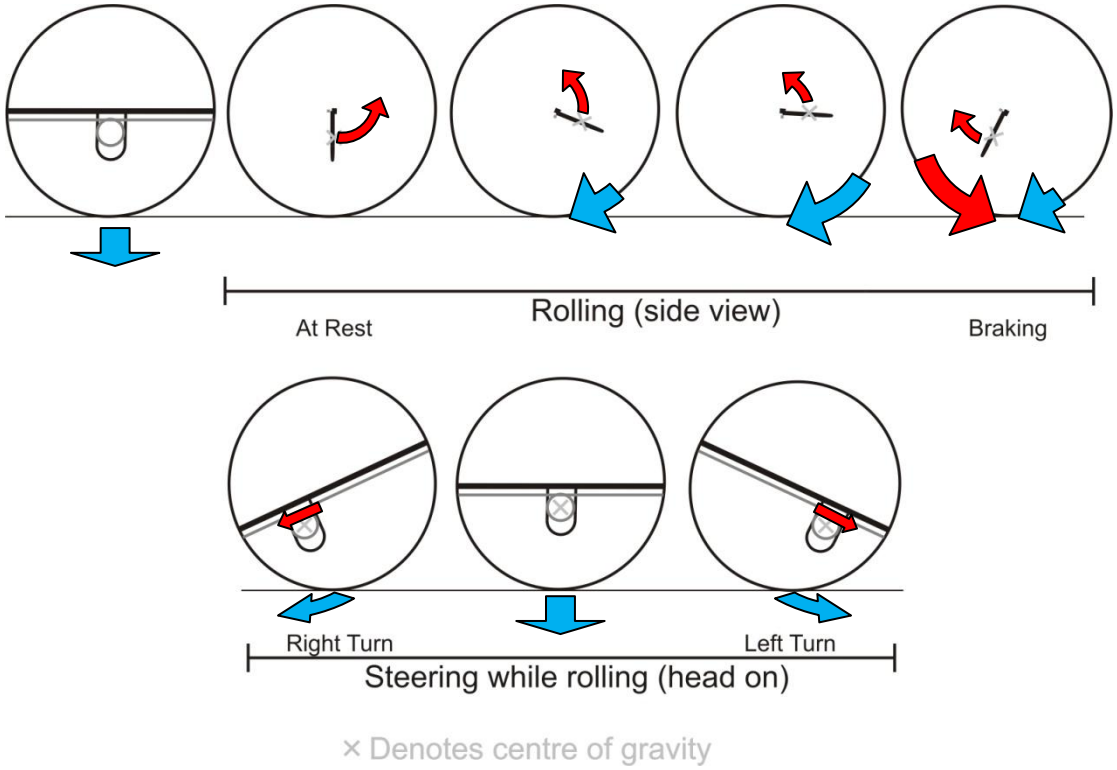

Figure 130 – Rolling method for Jollbot 3a and 3b. Rolling control was achieved by rotating the central mechanism around the square section axle. Straight line movement could only occur with the polar axle horizontal. To control where the powered rolling takes the device, the central mechanism was moved along the axle, leaning the sphere over and enabling turns. Jollbot is rolling out of the page in the lower portion of the diagram.

Both versions of Jollbot 3 used three motors in their operation. Each of these were modified model servos adapted for continuous rotation (see Section 4.2.2.2). The main advantage of this choice of motive power was that quicker and more powerful servos were available for the same size and fixing locations, easily allowing for motor replacements if required. A high torque servo (Towerpro MG995, as used for compression in Jollbot 2) was specified to provide the rotation of the weighty mechanism around a solid centre axle, whereas standard power servos (Acoms AS12, as used for direction control in Jollbot 2) were used for the other functions. The control of each version of Jollbot 3 was carried out remotely using a conventional model radio control system.

Jollbot 3a used one 'rolling' motor to provide the power for rolling, and two 'compression/steering' motors to provide both the compression of the sphere and the side to side movement of the centre mechanism for rolling direction control. Compression of the sphere was achieved by winding these two latter 'compression/steering' motors in opposite directions. Whereas steering was achieved by rotating them in the same direction. This is best described pictorially (Figure 131), and further discussion of the operation and performance of Jollbot 3a is made in Section 6.1.

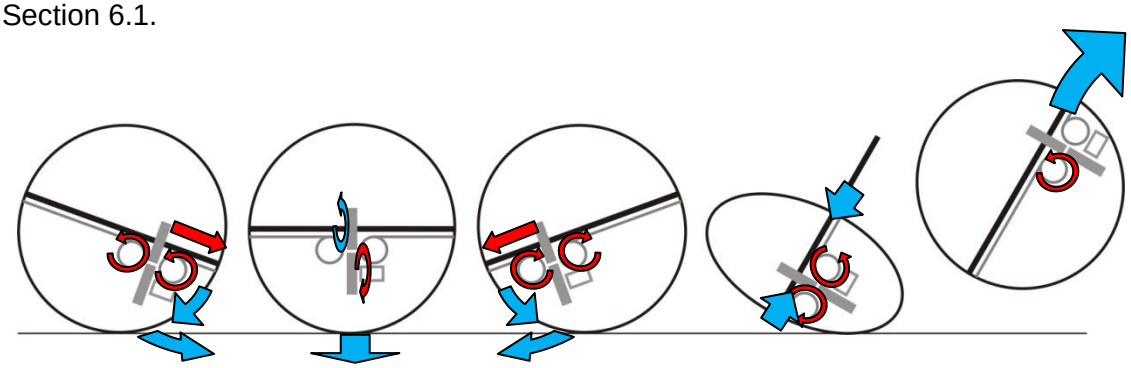

Figure 131 – Jollbot 3a operating principle. The leftmost image shows how rotating the compression/steering motors in the same direction caused the mechanism to slide along the axle and the sphere to tilt over for rolling direction control resulting in a left turn. The next image shows how the rotation of the rolling power motor caused the sphere to roll out of the page. The third image shows rolling direction control making a right turn. The fourth image shows how sphere compression was achieved by winding the compression/steering motors in opposite directions. Releasing a cable connecting one compression/steering motor to the lowermost pole enabled jumping: the mechanism slides quickly along the central axle (jump direction control being achieved between the fourth and fifth image using the motor that provides rolling).

Jollbot 3b also used three motors, but they are each devoted to a specific task. The first was a 'rolling' motor as in Jollbot 3a, the second enabled the compression of the sphere, and the final motor allowed for steering during rolling and the attachment of the mass to the suitable uppermost pole of the sphere when jumping. Figure 132 shows this. A detailed discussion of its operation and performance begins at Section 6.4.

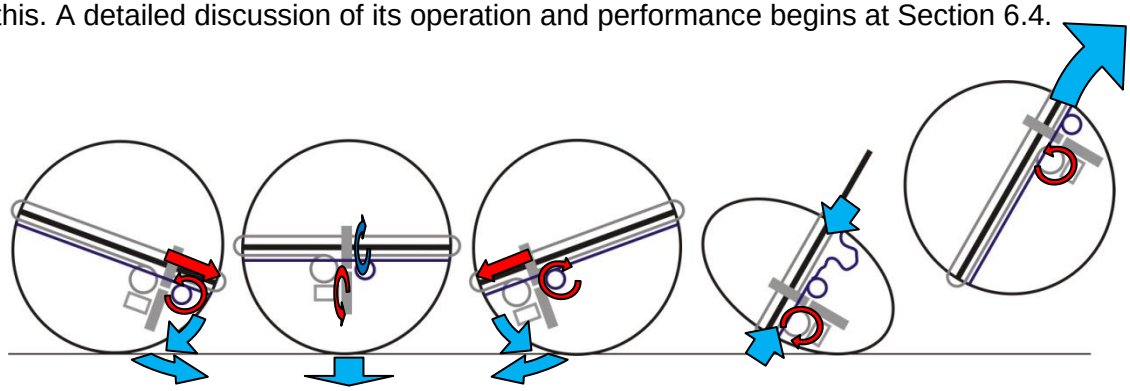

Figure 132 – Jollbot 3b operating principle. The leftmost image shows that rotating the roll steering motor in one direction caused the mechanism to move along a taught toothed belt, tilting the sphere over to start a left turn. The next image shows how running the "rolling" motor drove it along (out of the pace) with the subsequent image showing a right turn. A separate compression motor pulls the poles of the sphere together on a single thread connected to the poles at each end. Just before jumping the roll-steering motor needed to take up the slack in the belt from above the mechanism and transfer it below. When the compression motor released, the thread unwound and the mechanism was accelerated along the axle resulting in a jump.

6.1 Jollbot 3a design

The design of Jollbot 3a (Figure 133) consisted of 3 interacting elements which are discussed individually below.

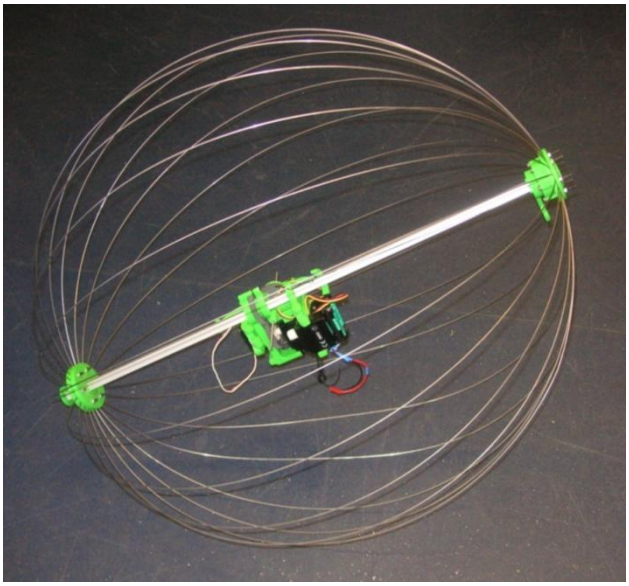

Figure 133 – Jollbot 3a

6.1.1 Design of sphere

One of the most critical changes to the device was in the outer sphere itself. Swapping the brazing rods that exhibited plastic deformation for spring steel elements, ensured that the spherical form was maintained jump after jump, and that the sphere could be compressed by a much larger proportion of its diameter without permanent deformation. Each spring element of the sphere was 1.4 mm in diameter and ~900 mm long.

To improve the rolling performance, the roundness around the equator needed more contact points, so the number of elements was increased to twenty-four from the original sphere's proposed twelve (actually six and nine in practice for Jollbot 1 and 2 respectively). Other section shapes were considered for the spring elements. Flatter strip-shaped elements could potentially improve the rolling performance by improving the rigidity of the contact patch, but the increase in mass associated with this profile would have a large impact on jumping performance (see Section 4.2.1.2, p.166 previously). Square-section elements would increase mass slightly. However, since there would be a material increase away from the curved neutral axis, there would be an increase in stiffness and therefore the amount of energy stored as described in

Section 4.2.1.2. However, the reader will recall that this difference has been determined previously to be negligible. For the purpose of this research, simple circular section elements were selected owing to their availability and ease of assembly.

The size of the sphere was also increased to around 580 mm diameter as rolling performance would be improved with a larger sphere, and more space would be required due to the complexity of a revised central mechanism capable of compression and jump direction control, and rolling and steering. The theory of circular shaped rings (see Section 4.2.1) had proved inaccurate for the large deflections produced in Jollbot 1 and 2, and Jollbot 3 was going to further increase the percentage of compression. The decision was therefore made to use experimentation to determine the sphere's force-displacement properties.

The clamping mechanism at the sphere's poles were similar in form to the previous sphere, with 90° bends at the end of each spring element securing it to a two piece rapid-prototyped spring clamp at each pole. A square section aluminium axle was positioned pole-to-pole through the centre of the sphere to allow for powered rolling (see Section 6.1.2).

Table 21 shows the weights of this new spring sphere.

Component	**Weight**
Spring Clamp 1	34.5 g
Spring Clamp 2	34.5 g
24 x Spring Elements	262 g
Axle and Endcaps	59.5 g
Total	**390.5 g**

Table 21 – Jollbot 3a spring sphere weights

6.1.2 Powered rolling mechanism

6.1.2.1 Forward motion

The rolling of Jollbot 3a was achieved by fixing an aluminium square section axle through the sphere in a pole-to-pole orientation. It was important to have a non-circular section centre axle to easily enable the rolling mechanism to react against it whilst it still slid freely along the axis of rotation for rolling direction control. The axle fitted in square holes that go right through both poles of the sphere. This allows the poles of the sphere to slide along this rigid axle which protruded when the sphere was compressed before a jump.

The rolling mechanism was driven by a modified model servo (Towerpro MG995) coupled to a 38-tooth Module1 gear. A final 1:1 ratio was produced by combining this driven gear with a similar Module1 gear (Figure 134). This was fixed to the centre axle, but free to slide along it. This fixed rotation and sliding capability was achieved by mounting the Module1 gear within two rapid prototyped components with bearing surfaces upon which the main chassis can rotate (Figure 134).

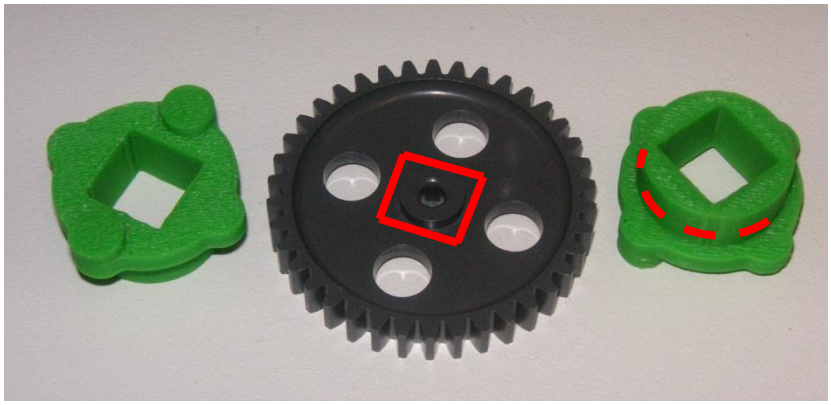

Figure 134 – Sliding rolling gear. The solid lines mark the cut-away area in the Module1 gear. The dashed line illustrates the bearing surface.

As the motor ran it moved around the central axle, and thus rotated the off-axis mass of the chassis and associated mechanisms, moving the centre of gravity of the complete

device and thus producing torque for rolling. This is illustrated in Figure 135 and Figure 136.

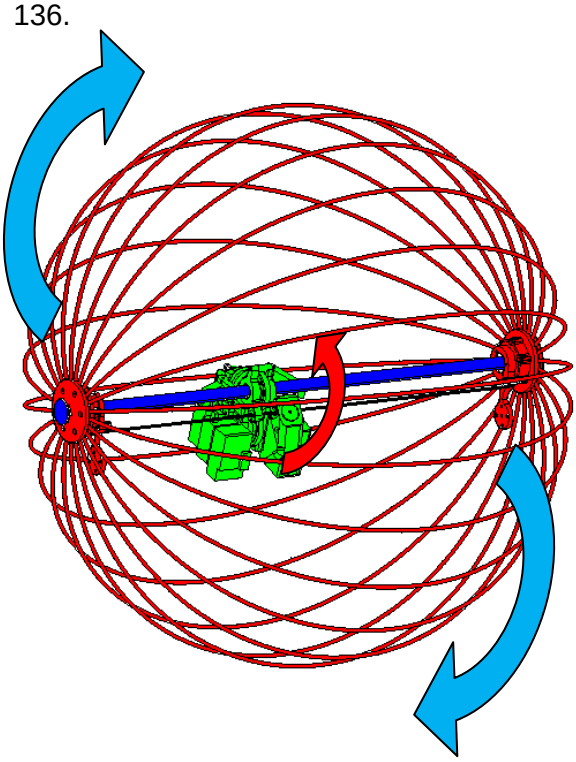

Figure 135 – Rolling principle. Rotating the central mechanism around the axle fixed to the sphere (red arrow), caused the device to roll forward (blue arrows).

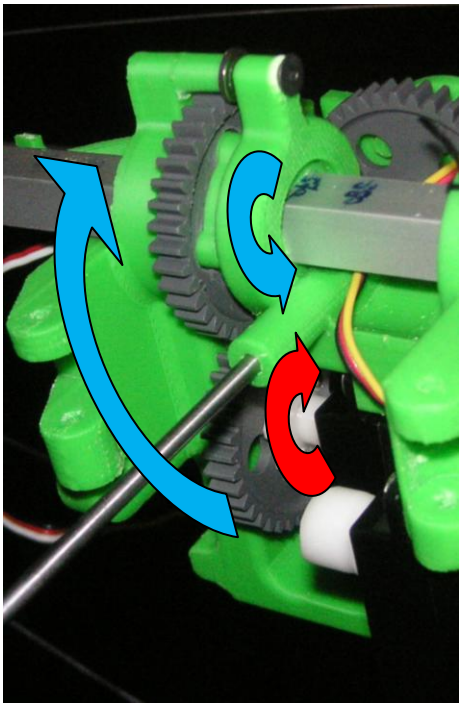

Figure 136 – Rolling mechanism operation (some components removed for clarity). Red arrow indicates motor input, with the blue arrows indicating the resulting rotary motions around the square-section central axle.

6.1.2.2 Direction control

Although powered rolling is interesting, it cannot be considered useful until some sort of direction control is achieved. As such, a method to move the compression mechanism along the central axle was developed. This was based entirely on the compression method discussed in the following section (6.1.3), but with the difference that for rolling-direction control, the motors turn in the same direction – thus alternately winding or unwinding the corresponding compression-thread. This moved the whole mechanism along the central axle, thus moving the centre of gravity toward one pole or the other.

This tilted the central axle, which meant the device rolled forward in an arc rather than in a straight line (Figure 137).

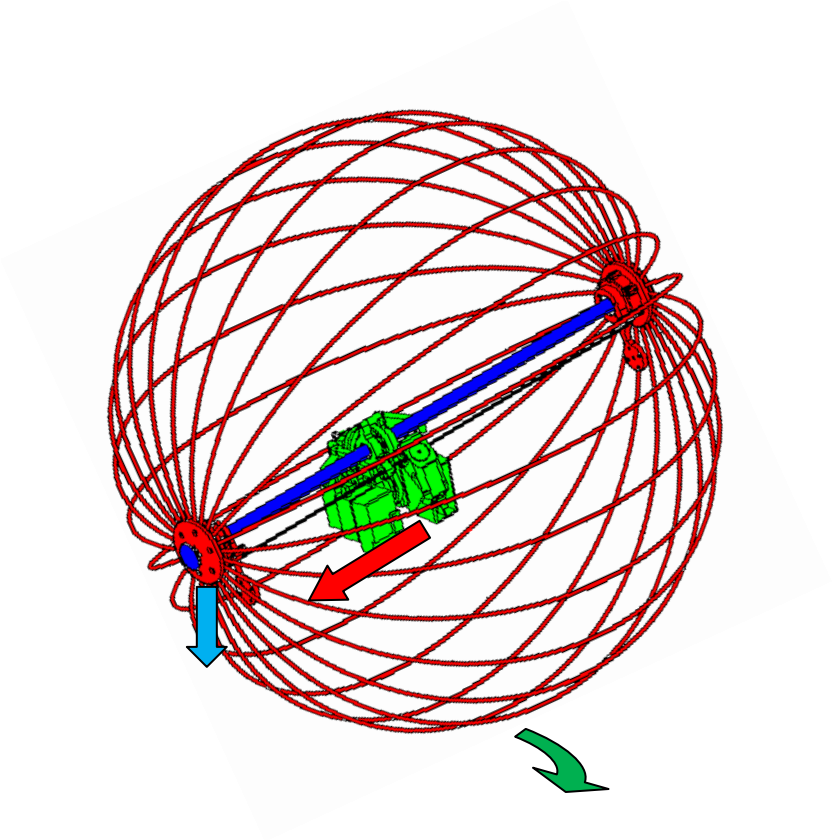

Figure 137 – An illustration of the principle used to achieve rolling direction control. Moving the central mechanism toward one pole (red arrow) caused the sphere to tilt over (blue arrow). As the mechanism continued to rotate, the sphere rolled forward, and a turn would be performed (green arrow).

6.1.3 Compression and release mechanism

The sphere compression mechanism of Jollbot 3a relied on the combined operation of two modified model servers acting as continuously rotating motors with integral gearboxes. Each motor was coupled to a Module1 worm gear which in turn drove a 38 tooth spur gear. Attached to this spur gear was a spool that wound a length of thread to compress one side of the sphere. A similar mirrored mechanism appeared opposite this to compress the other side of the sphere.

Once compressed, levers were used to force the spool away from its engagement with the worm driven spur gear. The levers were interlocked with one another such that they could only move when both poles of the sphere were in contact with them. This only occured at maximum compression (Figure 138). Which spool was released was very important to the jumping operation of this design. Enlarged elements of the axle end caps were used to actuate the appropriate levers. Just before a jump, the axle end-cap on the lower side of the device would always be nearer to the main chassis than that at the other end of the axle. The interaction between this lower axle end-cap protruding through the polar-clamp, and the lever, determined that only the spool connecting the bottom of the sphere to the central mechanism was released. This meant that the central mechanism would be accelerated away from the “foot” of the sphere.

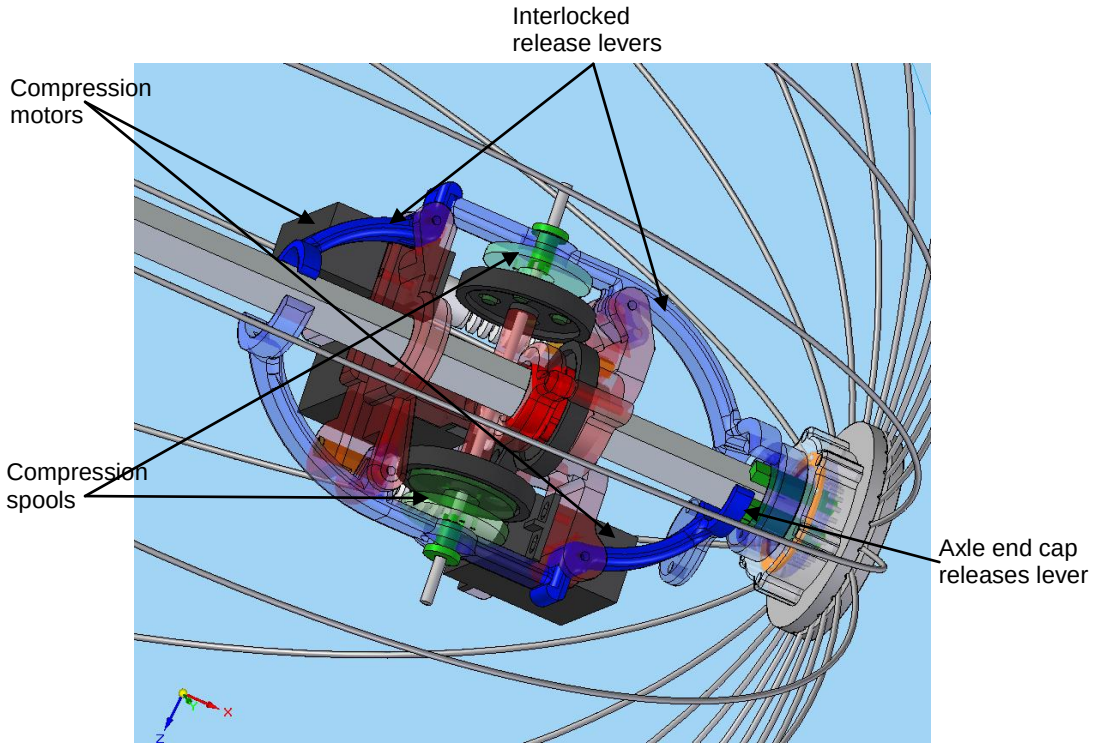

Figure 138 – CAD image illustrating release levers and enlarged axle end cap protruding through pole of outer sphere.

6.1.3.1 The anti-tangle mechanism

As compression was achieved by winding of a length of thread, it was critical that the thread needed to be managed so as to not get tangled either when compressing and releasing, or particularly while rolling along. Considering only one side of the designed compression mechanism, if a single off-axis fixing point for the compression thread were used at the sphere's pole and central mechanism, then the resultant loading would cause the mechanism and pole to twist. This load, inline with the axis of the central axle, would substantially increase friction, reducing possible jump performance and steering capability whilst rolling (Figure 139).

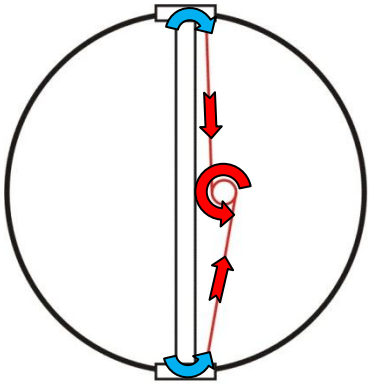

Figure 139 – As the compression mechanism wound the thread, the tension generated in the thread at its single-point off-axis fixing on the polar-clamps would cause them to twist in relation to the central axle. This would increase the friction both during compression and release.

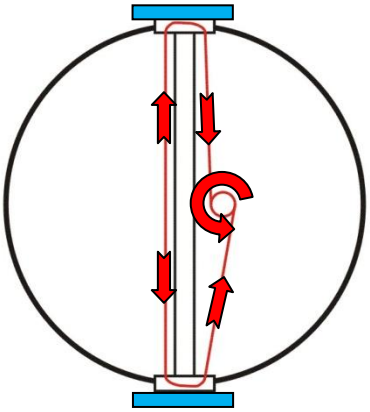

Figure 140 – Routing a single thread through each polar-clamp would give two fixing points at each side of the central axle at the sphere's pole. This would keep the polar-clamps parallel with one another and perpendicular to the central axle.

A design with two thread fixing points either side of the main axle on both the sphere's pole and central mechanism would minimise this twisting (Figure 140). In addition, as the central mechanism needed to rotate around the main axle during rolling, the single thread also needed its fixing points to rotate around this axle. This made for a very interesting and complicated problem (Figure 142). The fixing points needed to be

mounted on a bearing to allow for rotation around the axle at the sphere poles, and a single thread running from a fixed point on the central mechanism, via the pole of the sphere and back to the winding spool needed to pass through the geometric centre of the centre axle without touching it (Figure 141 and Figure 142).

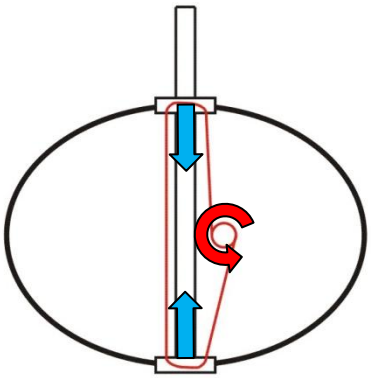

Figure 141 – The requirement for the polar-clamps to move along the solid central axle meant that the thread must be carefully routed whilst appearing to pass through the geometric centre of the axle.

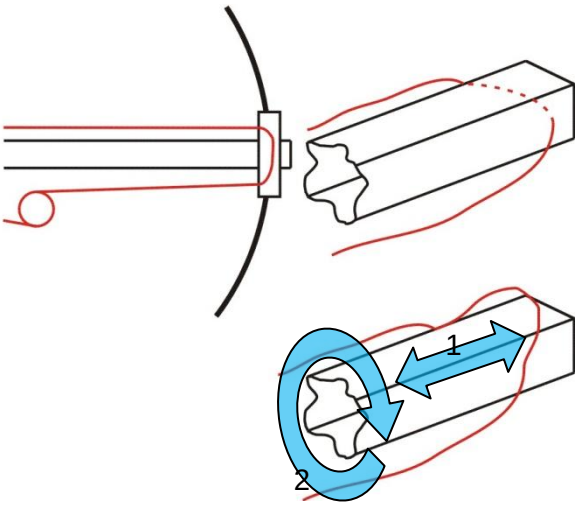

Figure 142 – The thread was therefore carefully managed by an anti-tangle mechanism that allowed the central axle to move through the clamps (1) and to rotate within the thread surrounding it (2)

The solution developed relied on a bespoke thrust bearing and a “top-hat” component through which the compression thread was allowed to pass. The mechanism is best show as a CAD illustration in Figure 143, and as a photograph in Figure 144.

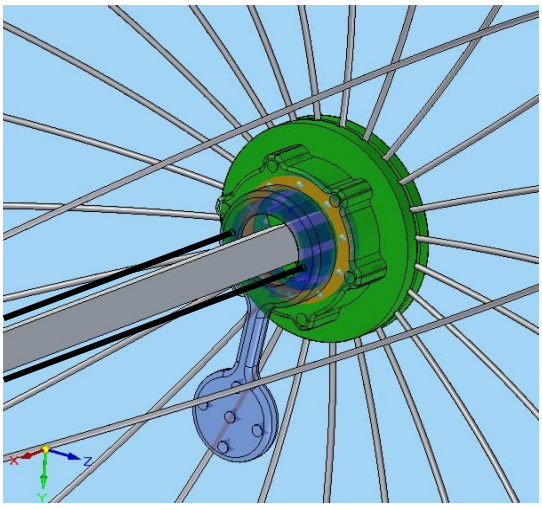

Figure 143 – CAD model of thread anti-tangle mechanism with some translucent components allowing a view of bespoke thrust bearing

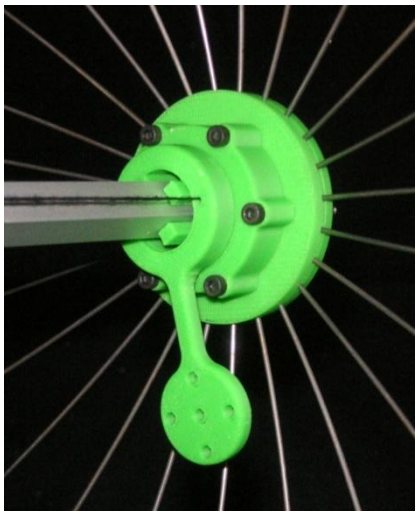

Figure 144 – Complete anti-tangle mechanism

The thrust bearing allowed the thread-entry and exit points to rotate around the central axle. It consisted of 4 elements, the housing which was fixed to a pole of the sphere (Figure 145a), a series of steel ball bearings and a ball-bearing holder (Figure 145b), and the moving “top-hat” component with a guide hole for the thread to pass through (Figure 145c). In addition there was a cover plate with integral off-axis mass (and holes for attaching additional tuning masses) to ensure that the assembly, and therefore the apparent thread fixing locations, were always in the same orientation with respect to the ground when rolling along.

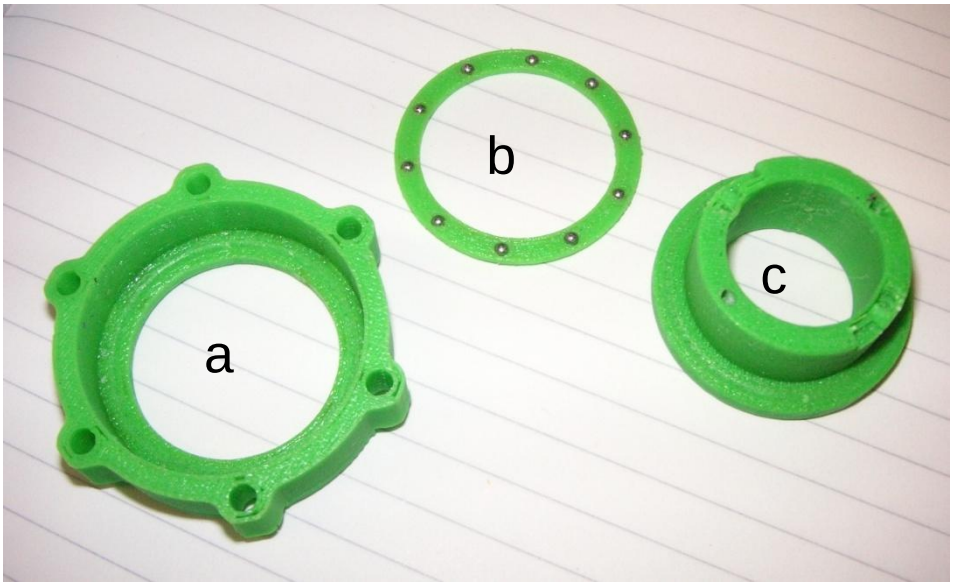

Figure 145 – Anti-tangle mechanism; a) housing, b) bearing holder and steel bearings, c) "top-hat" thread guide

The “top-hat” had a fairly complex hole through it following a path best described as a quarter-turn reflected helical tunnel. This sort of component was an ideal example of the benefits of rapid prototyping, as it would be impossible to machine a similar component from solid using conventional engineering processes. An investment casting would allow for such a component to be made in numerous quantities at relatively low cost, but for the purposes of this work a rapid prototyped component was made directly from the CAD model. This required special consideration during its design. The FDM rapid prototyping method relies on the layering of fine filaments of material and there are some limitations in what designs can be produced without using additional support material. Support material is not part of a final rapid-prototyped component, but is required to ensure that the component can be built up in layers. Overhanging areas at greater than 45° therefore require support material beneath them. The support material needs to be removed after manufacture. It would be almost impossible to remove the support material used within a complicated tunnel following a helical path in a component like the “top-hat”, so the design needed to be adjusted to allow for the limitations of FDM rapid prototyping.

If you take for example a horizontal round hole through a component, the overhanging top side of the hole needs support once its angle is more than 45° to the vertical, and thus the rapid prototyping machine lays support material under the middle section of the hole. If the hole had a teardrop profile (with a 45° sloping upper surface) then no support material would be required (Figure 146). For some rapid prototyped components to work as anticipated, careful design needs to be undertaken within a CAD package.

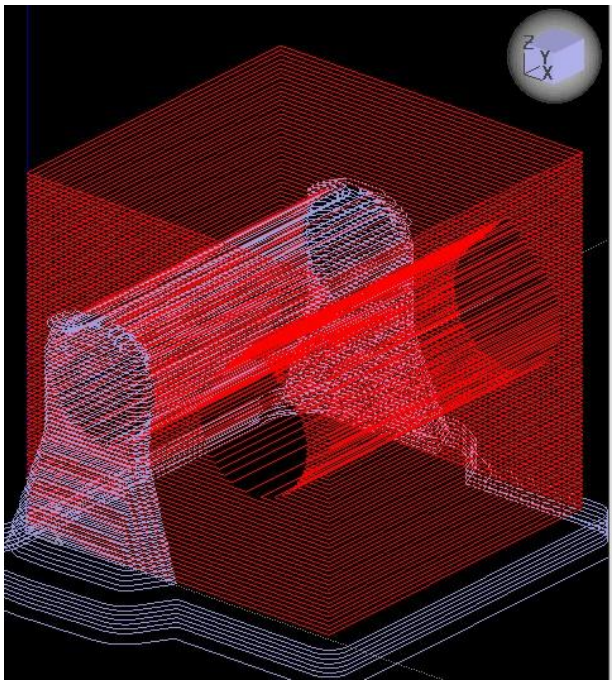

Figure 146 – Rapid prototype print path for round section (left) and teardrop section (right) through-holes indicating supporting material deposited inside the round hole to support its low-angle roof.

Thus the “top-hat” component had a teardrop profile swept along an internal path to ensure that no support material was deployed within the through-hole. The complete path revolved 180° around the geometric centre axis and consisted of two segments, the first being 90° of helix downward, and the second being the same but upwward. This resulted in path where the compression thread appeared to pass through the centre of the main axle. Figure 147 shows an illustration of the CAD model of the “top-hat”.

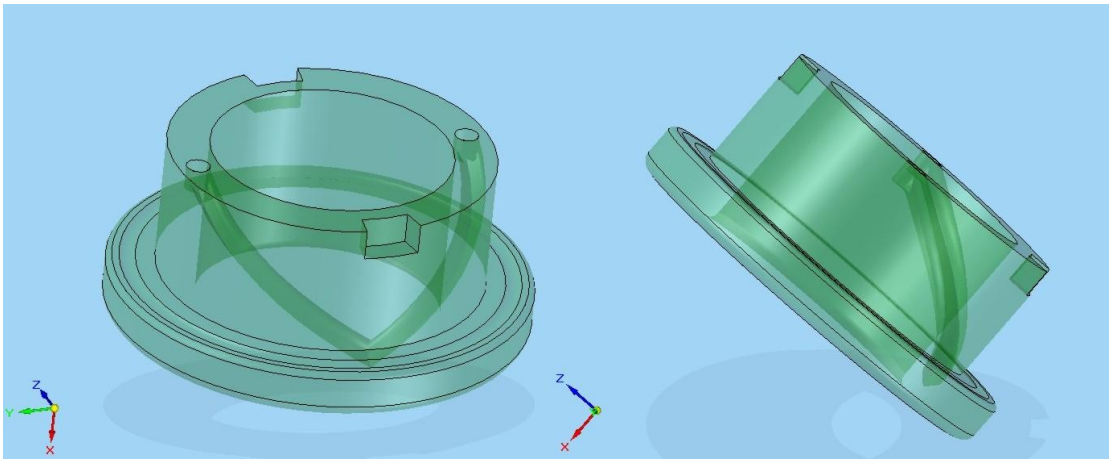

Figure 147 – CAD model of the anti-tangle "top-hat" component. Particular attention should be made to the continuous path through it along which the compression thread moves.

6.2 Jollbot 3a experiments and evaluation

6.2.1 Sphere characterisation

As the deflection of this new sphere was expected to be very large as a proportion of its diameter, the previously presented theory (see Section 4.2.1) will not apply. Low deflection theory suggested that the sphere would produce a spring Hookean in response and with a stiffness of around 125 N/m. Experience of the previous spheres suggested that this would not be the case in practice.

Owing to the physical size of the complete sphere, it was impossible for the force-displacement curve to be determined using the available desktop materials test machine (Instron), so another method was developed. By adapting a conventional 5 kg capacity kitchen scale, it was possible to use it as a makeshift spring balance. This spring balance was attached to the upper side of the sphere while being loaded from beneath via an extended square section axle. Photographs illustrating the experimental setup are shown in Figure 148. The sphere was loaded to known measured intervals by hand (11 mm intervals as a result of 11mm thick masking tape), by holding the spring balance. Readings of the force at each position were recorded.

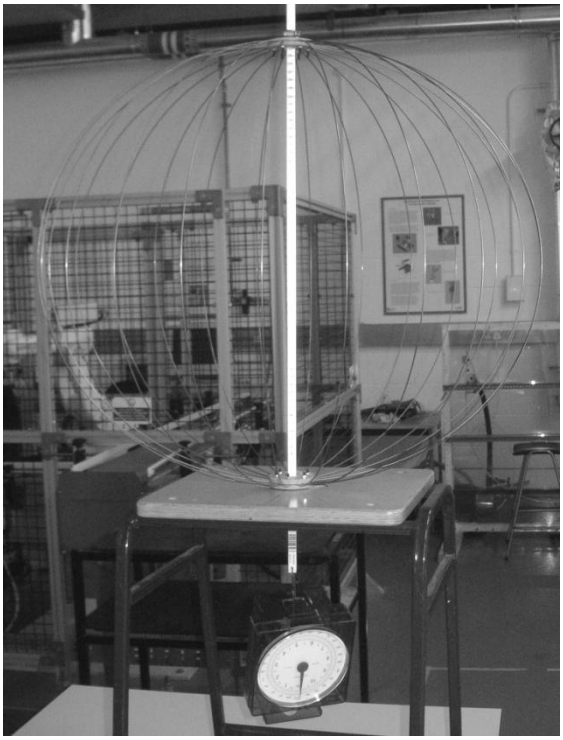

Figure 148 – Experimental set-up for evaluating sphere elasticity

The accuracy and linearity of the spring balance was determined by adding known masses and taking readings from the scales. This resulted in a 0.94x under-reading throughout the range of the scale. The corrected force-displacement results for the two passes of the test are shown in Figure 149.

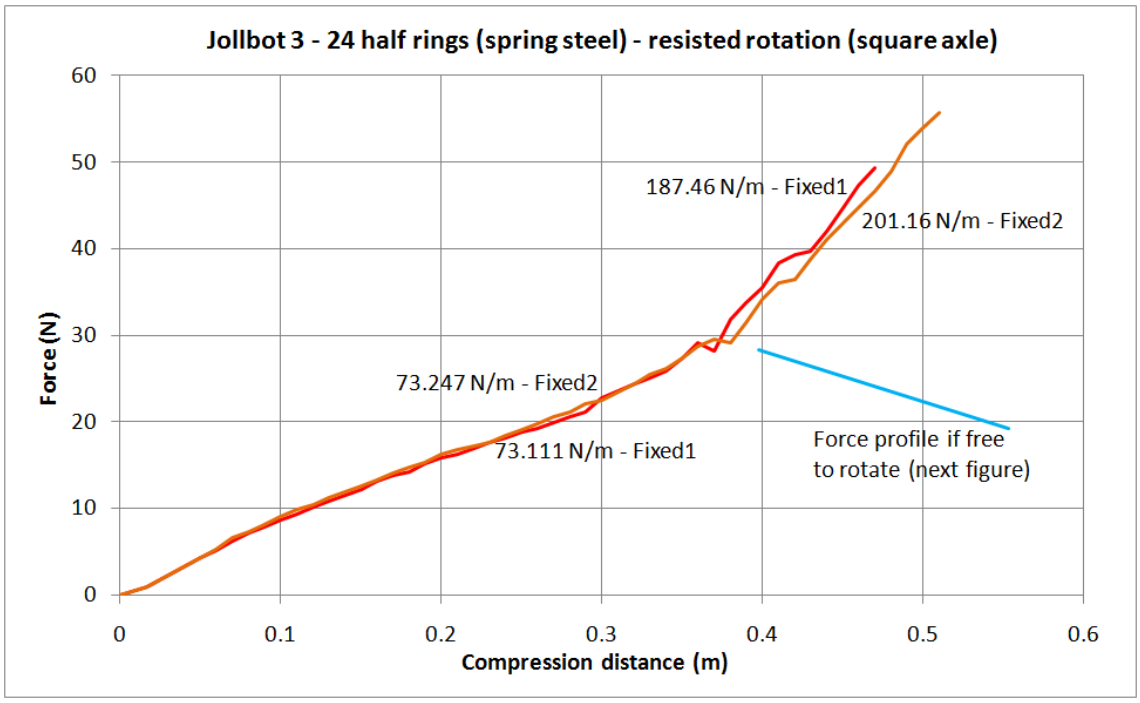

Figure 149 – Force-displacement curve with square section centre axle resisting relative rotation of the poles of the sphere resulted in a stiffening of the sphere as the compression distance increases. The force profile when the sphere is allowed to twist is illustrated for comparison (see Figure 150).

What is most interesting about Figure 149 is that it occurs in two stages, both of which appear almost linear. The change in element material and increase in the percentage of compression of the sphere, appeared to result in this characteristic – theories on large compressions were discussed in Section 4.2.1.6, but are revisited below in Section 6.2.1.1. It appeared that at large compressions, after about 75% of maximum compression (or 63% of sphere diameter), the sphere underwent significant stiffening. A quick test without the square central axle in place showed that this was due to an axial twist occurring after a large amount of compression - a photograph of a similar twist is shown in Figure 152. During the non-twisting compression, the sphere's poles were unable to rotate relative to one another due to the square axle. The friction and resistance to twisting resulted in a step change in stiffness at around 370 mm compression - from 71.5 N/m to 194.3 N/m (an increase of ~170 %). The first few compression data points are not inline with later data. This was probably due to the internal friction and low accuracy of the modified kitchen scales at low load levels. The

data points around the transition point were also not reliable owing to the onset of stick-slip friction around the square section centre axle. Lines of best fit were added automatically using Microsoft Excel for each of the two separate stages of mostly linear response (leaving two data points separation at the point of change).

Given this unexpected variation in stiffness, a similar hand-powered characterisation test was conducted with a small round section central axle that allowed for the poles of the sphere to twist independently of one another. The results for the two loading passes are shown in Figure 150.

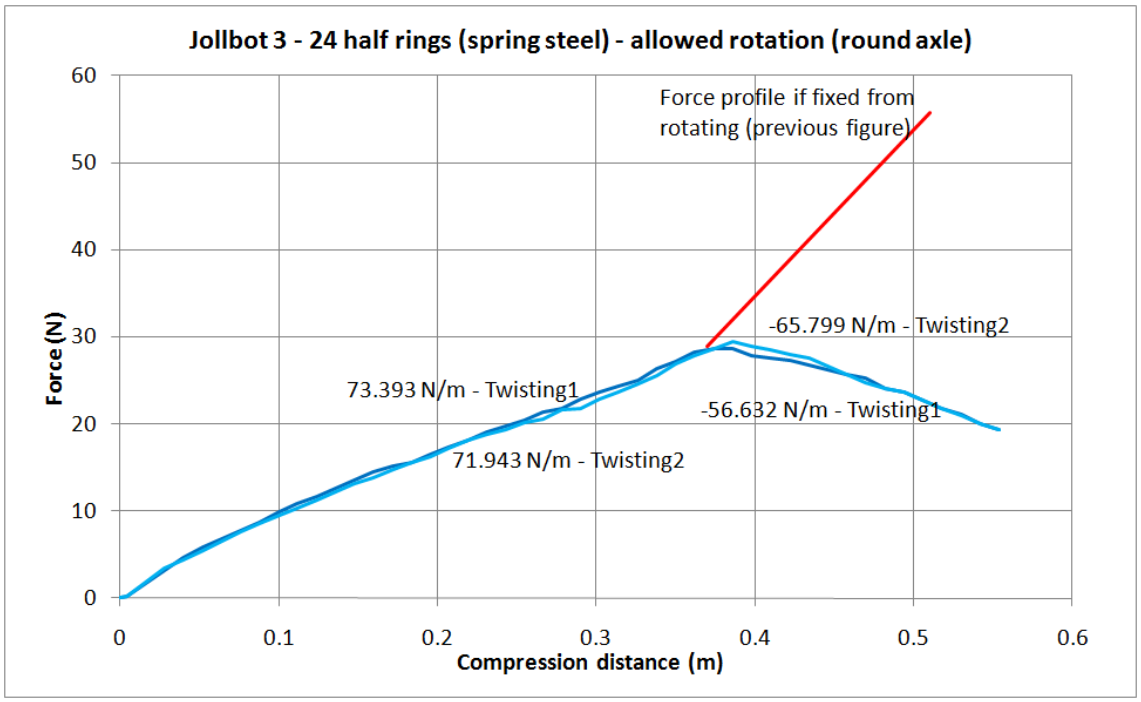

Figure 150 – Force-displacement curve with round section centre axle allowing for relative rotate of the sphere poles and resulted in a softening of the sphere as compression distance is increased above 63% of sphere diameter. The force profile when the sphere is stopped from twisting is illustrated for comparison (see Figure 149).

Here there is no similar increase in stiffness as the poles of the sphere are allowed to rotate. The graph illustrates a step change decrease in sphere stiffness at approximately 75 % of full compression. What is most interesting here is that there is a negative stiffness after this peak, creating a softening spring when fully compressed.

This property could be exploited by a jumping device, since for a given peak force capability, a particular compression mechanism could be utilised to store more energy (area under the curve) if it were able to compress the sphere by around 85-90 % of its diameter. This is analogous to the compound bow (see Section 2.6.8.2.2), where additional energy can be stored for a given peak draw force, and that the holding force is lower than the peak draw force.

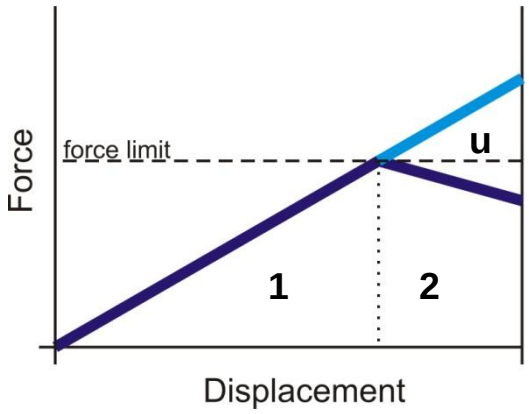

Figure 151 – Energy storage in non-Hookean hoop spring sphere. Area 1 indicates the amount of energy that can be stored by a Hookean spring for a given force limit available by a compression mechanism, even if a longer displacement was possible. The non-Hookean spring sphere can store an additional amount of energy, area 2, for the same force limit as it allows the displacement to continue. The area marked u is unavailable as it is outside of the force limitation of a compression mechanism.

Area 1 in Figure 151 shows the maximum possible energy that can be stored in a Hookean spring for a given force. Even if additional displacement were possible, the force capability of the compression mechanism would stop additional energy storage. For the same given force, more energy could be stored within the non-Hookean spring sphere produced here as additional displacement is available (area 1 added to area 2). Additionally, any catch mechanism required to contain this energy, does not need to restrain a peak force but a smaller force.

It was unknown as to whether this variability in stiffness was due to the combination of the numerous elements, so to find out, additional tests were conducted using an Instron desktop materials test machine. These tests were carried out on an incomplete

sphere ranging from one complete hoop to four complete hoops. The incomplete sphere was positioned within the columns of the test machine and beneath the moving crosshead containing an integral 1 kN Load Cell. The polar spring clamps were each positioned on a ball bearing or conical support to allow for any natural twisting of the assembly (a centre shaft was not present during loading in this instance). Photos illustrating the experimental set-up and during test twisting are shown in Figure 152. A graph illustrating the performance of the incomplete sphere along with actual and interpolated (from simple multiplication) complete sphere data is shown in Figure 153.

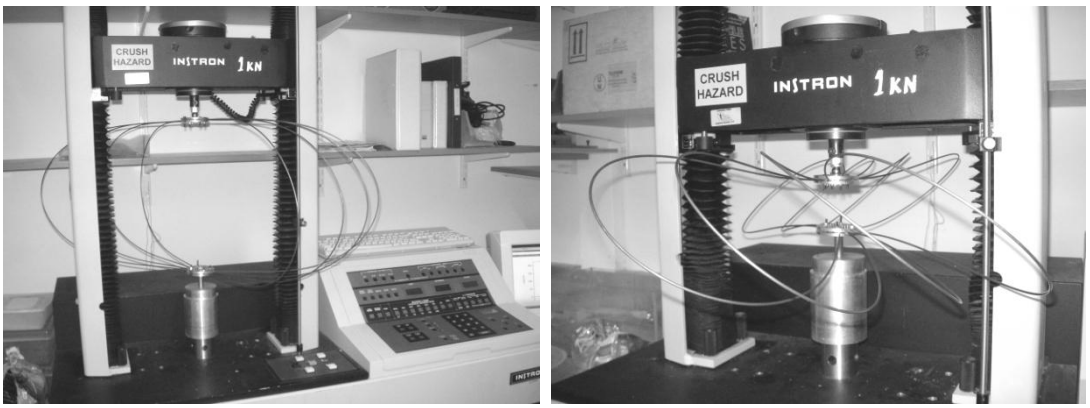

Figure 152 – Photos illustrating Instron test machine experimental set-up with 4 complete hoops and mid-test twisting at maximum deflection.

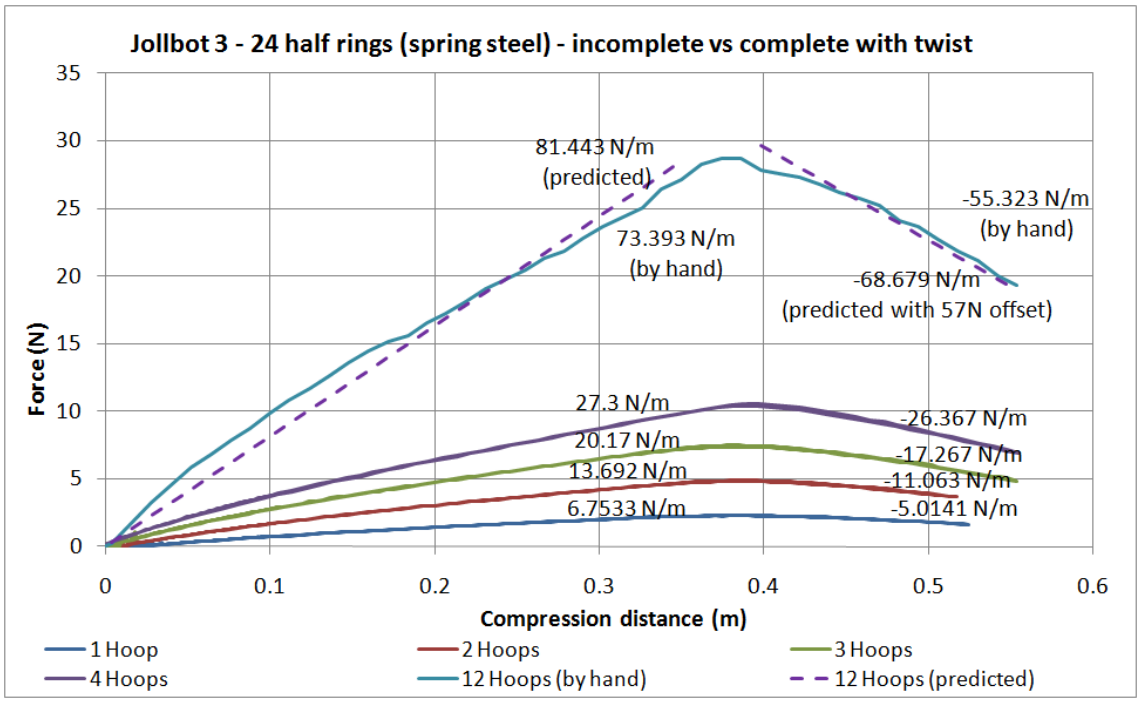

Figure 153 – Force-displacement curve (with twisting) for incomplete (Instron data) and complete sphere (hand compression). The figure also illustrates a predicted complete-sphere stiffness (81 N/m and -69 N/m) estimated from multiplying the Instron data.

Lines of best fit were added to each series of data and the slopes of each calculated, producing an average stiffness increase of 6.8 N/m for each additional complete hoop. It can be seen from Figure 153 that the predicted stiffness of the entire sphere (81.4 N/m) is within 11 % of the measured value from the previous experiments (73.4 N/m). It should also be noted that even with a single hoop, a twist in the assembly occurs; however the relation between a predicted and the actual softening performance is poor as the predicted negative stiffness of the entire sphere is 25 % more negative than as measured (-69 N/m verses -55 N/m).

For experimental purposes (see Section 6.5.1), the cumulative area under the force-displacement curve for the complete sphere, both with and without twist, and after every mm of compression, was created to allow for the reading off of stored potential strain energy at any point during compression or release (Figure 154). For example, after a compression of 380 mm, i.e. 68 % compression, 6.5 J of energy is stored in the sphere's structure if the twist is allowed.

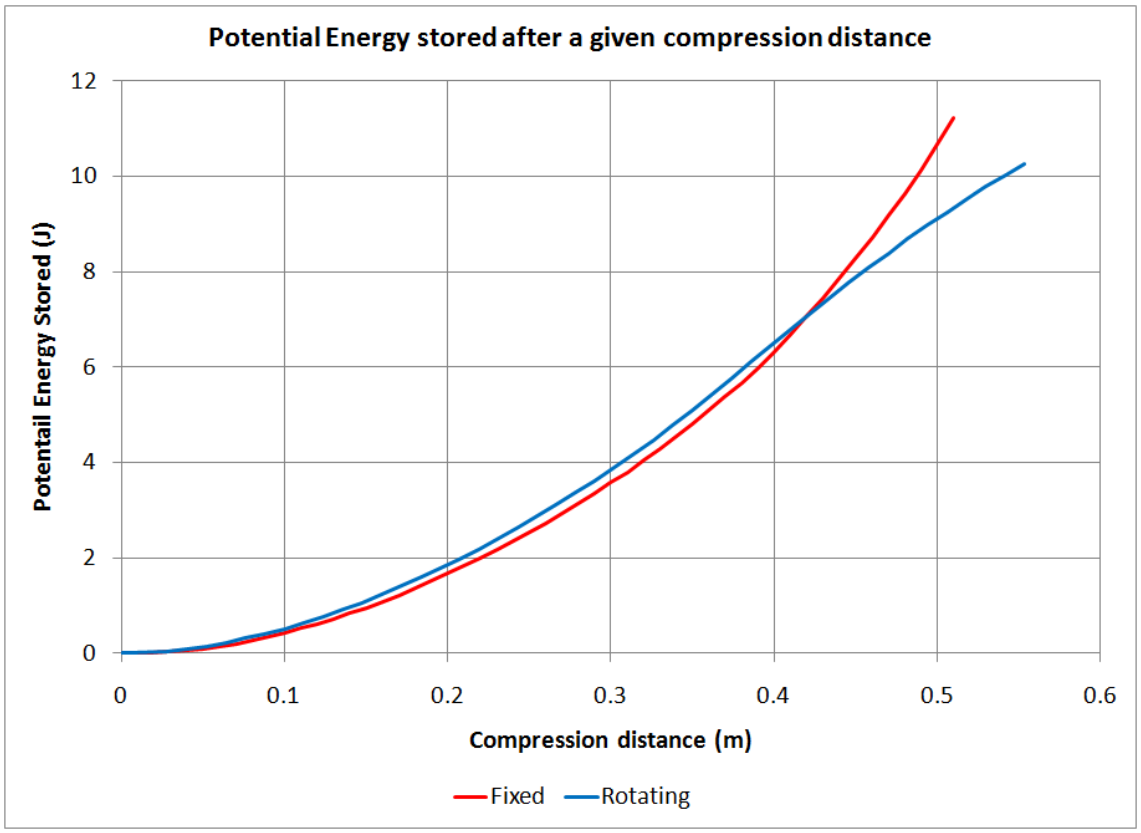

Figure 154 – Lookup-graph for amount of potential energy stored for a given compression distance in the sphere when fixed or free to twist.

6.2.1.1 Theories of non-linearity

As a result of the characterisation of this spherical structure, the discussion on large deflections of circular rings (see Section 4.2.1.6, p.172) can be expanded. The non-linearity of the sphere's force-displacement curve was not evident in previous prototypes mainly owing to either the smaller percentage sphere compression (up to ~25%), or the plastic deformation of the relatively thick brazing rod elements. The larger more slender sphere, constructed of more elastic elements undergoing bigger deflections, appeared to produce this twisting feature.

At all deflections, the structure comprising metal elements and plastic clamps making up the sphere would organise itself into a minimum energy configuration. The plastic clamps themselves were rigid and would contribute little to changing stress

rearrangement (unless they fail). Ultimately the twist was a result of each element maximising the radius of curvature for any given end to end positional arrangement (vertical deflection and rotation). The two cases are discussed below in Figure 155.

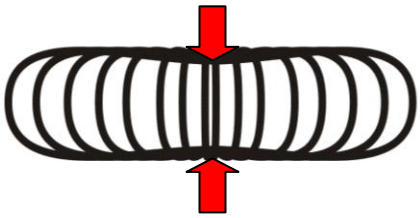

Stiffening structure - No twisting allowed

The first case, where the poles of the sphere were unable to rotate relative to one another, resulted in a stiffening sphere with a step change in stiffness occurring at a certain percentage compression (~63%). As the poles of the sphere were squeezed closer to one another, the curvature required along the entire length of each element produced a bulbous profile with strain energy being stored all the way along its length – the re-curved portion toward the polar clamps, and the curved portion along the rest. The fixed relationship between the polar clamps restricted the easiest way to minimise the energy in the arrangement – a twist. The twisting moment applied at the poles resulted in high levels of friction between the square central axle and the clamps.

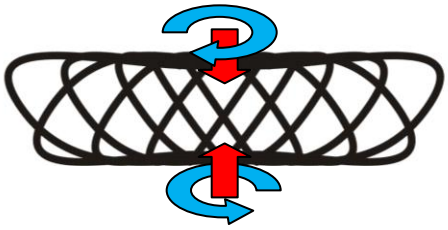

Softening structure – Twisting evident

If the poles of the sphere were able to rotate relative to one another, a softening force-displacement response was produced. After a certain amount of compression, the radius of curvature at the equator of each element is smaller than one that would be achieved if the element lay diagonally. The relative rotation of the clamps allowed such a form to be adopted, and thus each mm increase in deflection mainly resulted in a more flattened system storing only a small amount of additional strain energy in bending.

The elements were securely fixed at the poles with a 90° bend. This ensured that they could not twist at the poles, so more energy was stored in torsion in each element as the sphere twisted and flattened. Again this arrangement would balance out to give minimum total energy.

Figure 155 – Non-linearity of spring sphere

In order to exploit this discovery of a non-Hookean response (similar to that of the Compound Bow, p.100), the next prototype of Jollbot (3b) allowed the sphere to twist as it was compressed.

6.2.2 Rolling experiments

The tested version of Jollbot 3a was not entirely complete with respect to its CAD model. As there were two mirror images of a single compression mechanism, only one was assembled for initial functional testing. This was the first time that rolling of the

robot had been considered from the outset, so it was first tested as a simple rolling device with little consideration as to its jumping capability. (The missing half of the compression mechanisms meant that automatic jumping was not possible.) It was clear from early on that there were some deficiencies in the design – specifically the speed of direction control while rolling. The compression mechanism provided both the large force for jump energy storage, and the direction control while rolling. However, the high gearing and low speed resulting from the worm gear arrangement, meant that during steering, the winding and unwinding of the thread was slow, leading to a very unresponsive steering system. It was thought that it would be impossible to use this type of arrangement to create a workable rolling device that could be steered by the same system that provided the jump energy storage. It will be shown in Jollbot 3b that a toothed belt solution with a dedicated steering motor offers substantial improvements (see Section 6.4.2.2).

6.2.3 Jumping experiments

Before moving on to the next design, the opportunity was taken to test the force capability of the motor-driven compression mechanism. By securing the compression mechanism to one pole of the outer sphere with a spare length of thread, and rotating the compression spool with the remaining motor, it was clear that both the thread and motor were capable of compressing the sphere by the amount required. This included the large increase in force due to the resistance to twisting provided by the central axle (see Section 6.2.1). The unsuccessful “jump” that occurred after release of the compressed sphere also illustrated that the increase in friction between the axle and the sphere’s poles coming as a result of the tendency to twist, would destroy any opportunity explosively to release the stored jump energy.

The jump direction control system could not be tested directly with Jollbot 3a, but it was noted that at large compressions, the “foot” of the device became very large in area as the spring elements came into contact with the ground (Figure 156). This meant that there was no unbalanced pole around which the device could lean. Direction control of jumping with such a sphere would be difficult. Much larger dome-shaped axle end caps would resolve this issue, at the expense of more mass.

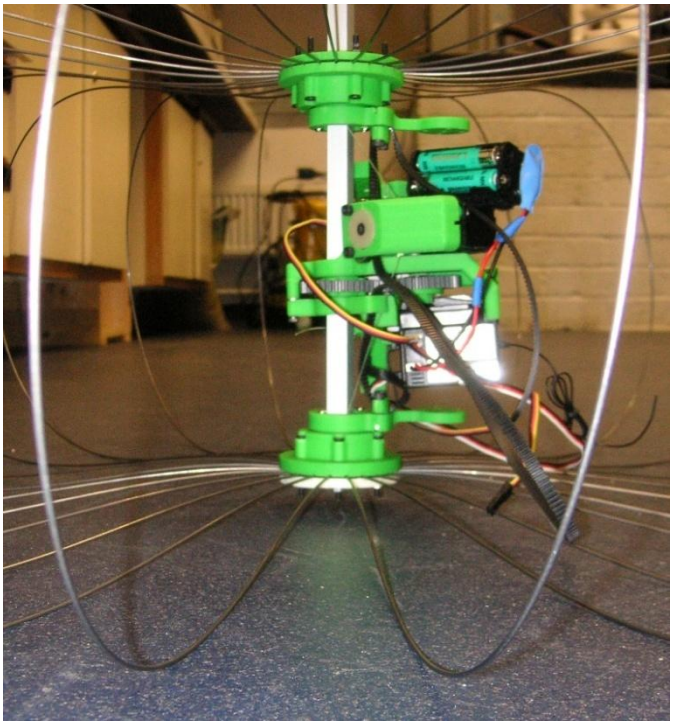

Figure 156 – The spring elements caused the pole of the sphere to leave the ground at large compressions when the outer sphere was restrained from twisting. The resulting large footprint would make jump direction control difficult.

6.3 Jollbot 3a future considerations

Several points of design deficiency were noted during the assembly and testing of Jollbot 3a, all of which needed to be considered and mitigated in Jollbot 3b:

- The design was generally missing cut-outs for outlets of wires from servos.
- The high torque (Towerpro MG995) servo was slightly larger than the standard servos (Acoms AS12).
- The steering mechanism for rolling was too slow to enable accurate control. The three motors needed to be reassigned to 1-compression, 2-rolling, 3-roll-steering – this meant a complete redesign.

- The 1.4 mm diameter spring elements were floppy in the lateral directions meaning that the sphere contact patch was very large when rolling.
- The 1.4 mm diameter spring elements were not powerful enough to enable a jump of significant proportion given the friction involved on the central axle at high deflections.
- After further component testing, the Acoms AS12 servo could lift 5 kg using a 10 mm diameter pulley wheel resulting in a torque of 0.24 Nm at 5 V (manufacturer's published torque was 3.2 kg/cm or 0.313 Nm at 6 V). The force available from using the 10 mm diameter pulley meant that peak required compression force could be raised to 50 N from the sphere's 30 N at ~400 mm compression. This meant a sphere that is 67 % stiffer could still be compressed using the existing motor and batteries. (The thread used broke at a little more than 5 kg load, so another thread material would be required).
- The worm to spur gear axle separation was slightly too large by a fraction of a millimetre resulting in slippage between the gears.
- The catch mechanisms did not work. In general they were too flexible.

6.4 Jollbot 3b design

The main failing of Jollbot 3a was the use of two motors working in tandem for either compression or the control of rolling direction. As they were integral to the design, the mechanism could not be modified to make it work. A completely new mechanism design was therefore required with the sphere, axle and thread anti-tangle elements mostly remaining the same. The major difference between Jollbot 3a and 3b (Figure 157) was the assignment of the motors used. The three interacting components of the complete device are discussed below.

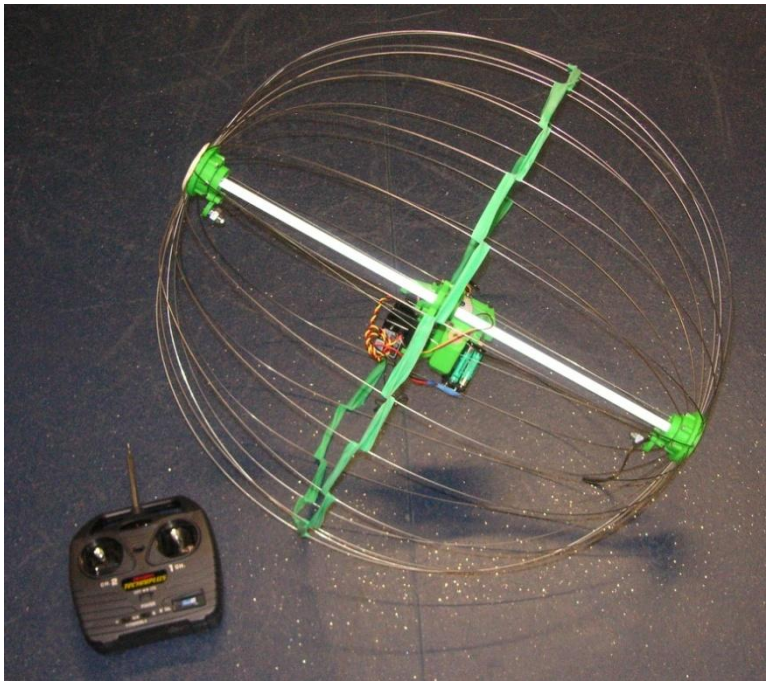

Figure 157 – Jollbot 3b complete with radio control transmitter

6.4.1 The Spring sphere

The sphere used was based upon that used in Jollbot 3a. The spring elements were the same 1.4 mm diameter x 900 mm long spring steel wires. The only difference was that one of the poles of the sphere has a round hole supporting the square central axle (Figure 158). This feature allowed the sphere to twist freely as it was being compressed, meaning that the force-displacement profile followed that shown previously in Figure 150.

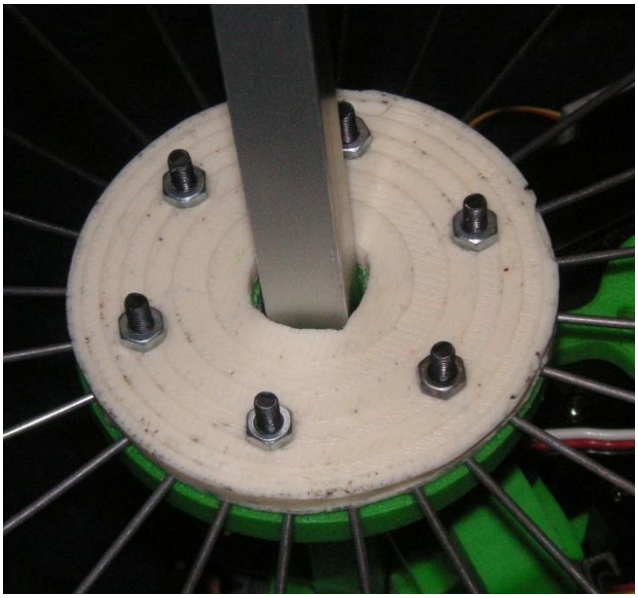

Figure 158 – Round axle support hole in one pole allowed the sphere to twist as it was compressed

Allowing this twist meant that, unlike Jollbot 3a, the foot of the sphere remained in contact with the ground surface throughout the compression and that the peak holding force at maximum compression, and in turn the force required to release the catches, was smaller than with Jollbot 3a.

In addition, the sphere was ultimately fitted with a latex band around its equator with the aim of controlling the separation of each spring element so that they did not splay laterally when rolling. This is discussed in more detail below in Section 6.5.2 and the influence of the band on jumping performance is discussed in Section 6.5.1.6.

Table 22 shows the weights of the sphere and components.

Component	Weight
Spring Clamp 1 (rotating)	38.5 g
Spring Clamp 2 (fixed)	30.5 g
24 x Spring Elements	262 g
Axle and Endcaps	56.5 g
Latex Band	15.5 g
Total	**403 g**

Table 22 – Jollbot 3b spring sphere weights

6.4.2 Powered rolling mechanism

6.4.2.1 Forward motion

The forward rolling mechanism of Jollbot 3a worked well and so was implemented in Jollbot 3b (see previous Figure 135 on p.225 for an illustration). Again an aluminium square section axle through the sphere was used to re-act the torque of the rolling-motor.

The rolling mechanism was driven by a modified model servo (a HiTec HS-965MG replaced the Towerpro MG995 servo after failure) coupled to a 38 tooth Module1 spure gear. A final 1:1 ratio was produced by combining this driven gear with a similar Module1 gear. This was fixed to the central axle, but free to slide along it. As the motor ran, it moved around the axle and rotated the overall off-axis mass. This moved the centre of gravity of the complete device and thus produced a rolling-torque. This mechanism is shown in Figure 159.

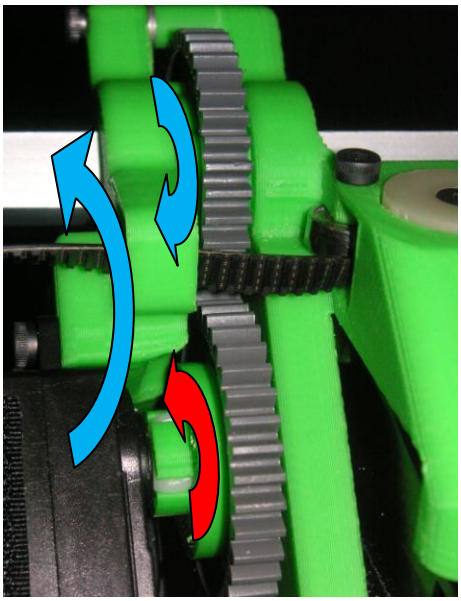

Figure 159 – Complete rolling mechanism

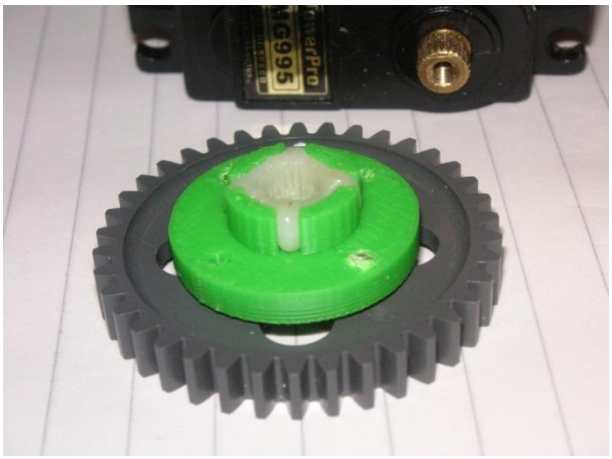

Figure 160 – The motor coupling. It consists of a larger rapid-prototyped component fixed to the Module1 spur gear, and a deformable thermoplastic Polymorph element that matches the splines on the motor-shaft

Particular attention was given to the coupling between the model servo and the driven Module1 gear. A low temperature thermoplastic [Polymorph - Polycaprolactone (PCL)] was used to connect the splined output shaft of the model servo to a custom made rapid-prototyped gear mount. While warm and therefore deformable, a Polymorph blob was sandwiched between the gear mount and the motor using a threaded bar to ensure alignment. The assembly was allowed to cool before the threaded bar was replaced with a securing screw. The resultant coupling (Figure 160) proved reliable with no slippage. The thermoplastic nature of the Polymorph allowed for it to be remoulded when, after failure, the original servomotor was replaced.

6.4.2.2 Direction control

Direction control of the rolling motion required substantial changes for Jollbot 3b. Jollbot 3b used a dedicated motor to move the central mechanism quickly along the central axle, and tilt the sphere while rolling. This was achieved by driving a pulley wheel along a toothed belt fixed pole-to-pole in the external sphere. Again the drive motor was a model servo modified for continuous rotation driving a pulley wheel along

a belt extracted from a broken computer printer. Another novel Polymorph based coupling (Figure 162b) was used to join the pulley wheel to the output of the drive motor, and two roller bearings were used to ensure that the belt remained tightly wrapped around approximately 180° of the pulley wheel (Figure 162a) even when the belt was not under tension (i.e. when the outer sphere was compressed and the poles were close together). The belt was fed through the main chassis, around the drive wheel and securely clamped at either end to modified elements of each of the previously discussed anti-tangle mechanisms (see Section 6.1.3.1). This ensured that the belt did not become wrapped around the central axle as the device rolled along.

Rotating the drive motor one way or the other moved the entire central mechanism along the axle (Figure 161). This roll-direction control mechanism was also used to fully enable jumping, and this will be discussed later in Section 6.4.3.

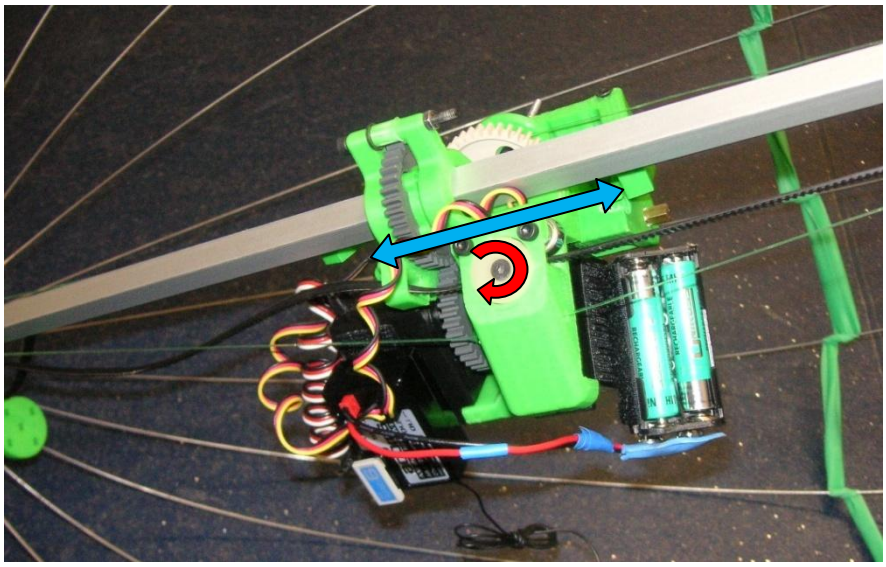

Figure 161 – Rolling direction control mechanism (see previous Figure 137 on p.226 for illustration of the principle of rolling direction control).

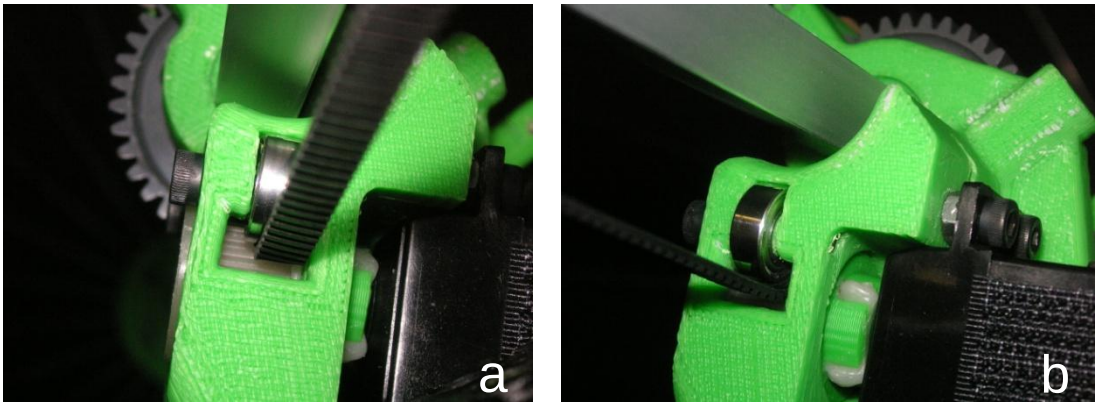

Figure 162 – Rolling direction control; a) with pulley wheel visible, b) with coupling visible

6.4.3 Compression mechanism

In contrast to Jollbot 3a, Jollbot 3b used a single dedicated motor for compressing the sphere. This time a length of lightweight and strong fishing line was used rather than the original thread that showed signs of fraying and wearing. The fishing line ran from a securing point on the central mechanism, to one pole of the sphere and through its anti-tangle mechanism, back through a guide in the central chassis and to the opposing pole and anti-tangle mechanism, finally returning to the main compression spool (Figure 163).

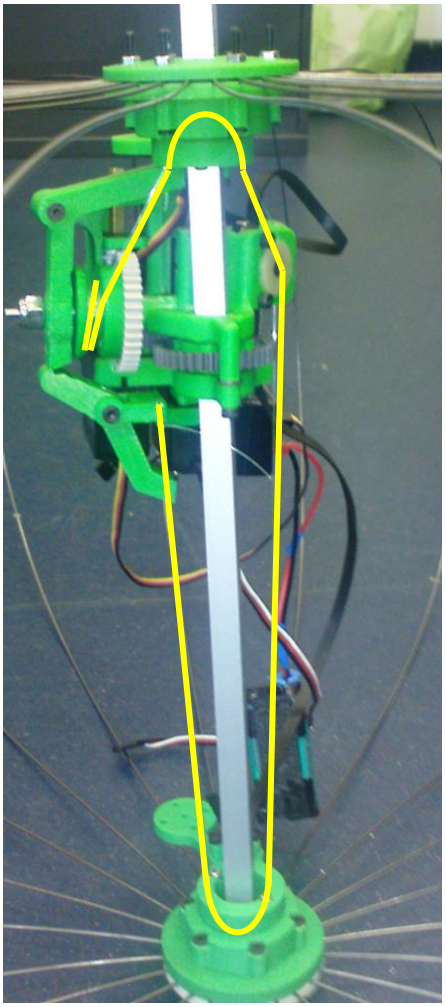

Figure 163 – Path of the single compression thread within Jollbot 3b

The compression spool was driven by a model servo through a Polymorph coupling, and a Module1 worm gear and spur gear combination (Figure 164). This gear combination gave a suitable reduction in speed (38:1) and increase in torque, and as any gear system consisting of a worm gear cannot be back-driven, the system did not need a ratchet mechanism to maintain compression when the motor was not receiving power. This feature would be particularly useful if the electrical power source for the device was of intermittent supply and low density – perhaps directly from photovoltaic panels.

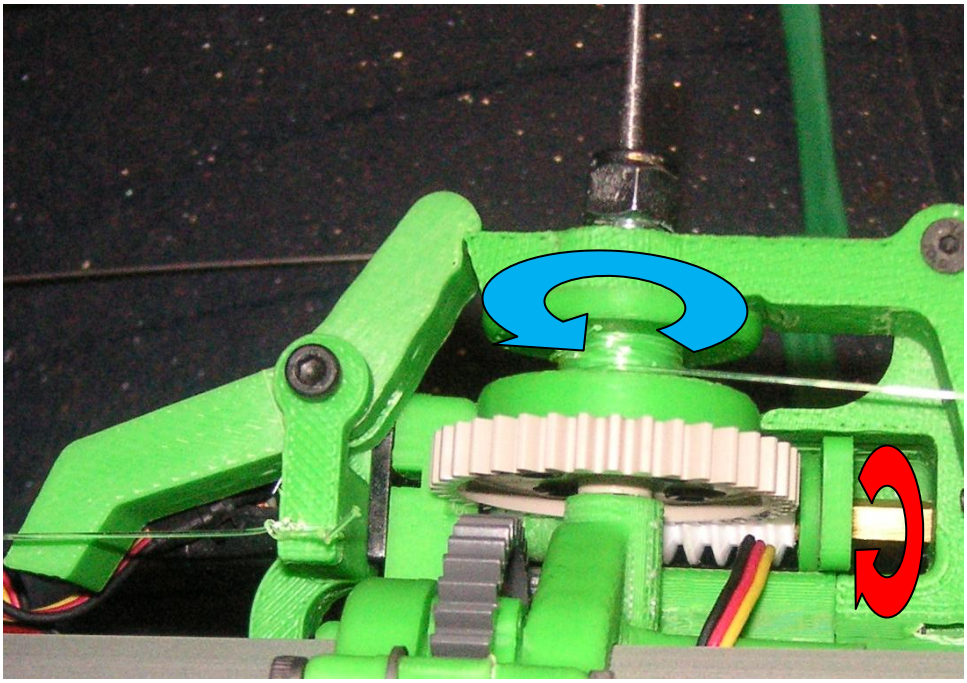

Figure 164 – Worm driven compression mechanism

As the compression spool rotated, the thread was shortened, compressing the spring sphere. The thread path itself resulted in a 2:1 mechanical advantage over the sphere. This again slowed the rate of compression and reduced the continuous power requirement.

Before a successful jump could be initiated, it was critical that the mass associated with the central mechanism was attached to the uppermost pole of the sphere. This is the main requirement of any jumping device – to accelerate the most weighty part of the body away from the lightest possible "foot" (see Section 2.6.1). The attachment of the central mechanism was achieved using the Rolling Direction Control Mechanism described in Section 6.4.2.2. After compression was completed, the mechanism was run such that the central mass of the device was almost touching the upper pole of the sphere. The belt was therefore short in length, but taught above the mechanism and long and slack below it.

The device was then ready to perform a jump.

6.4.4 Release mechanism

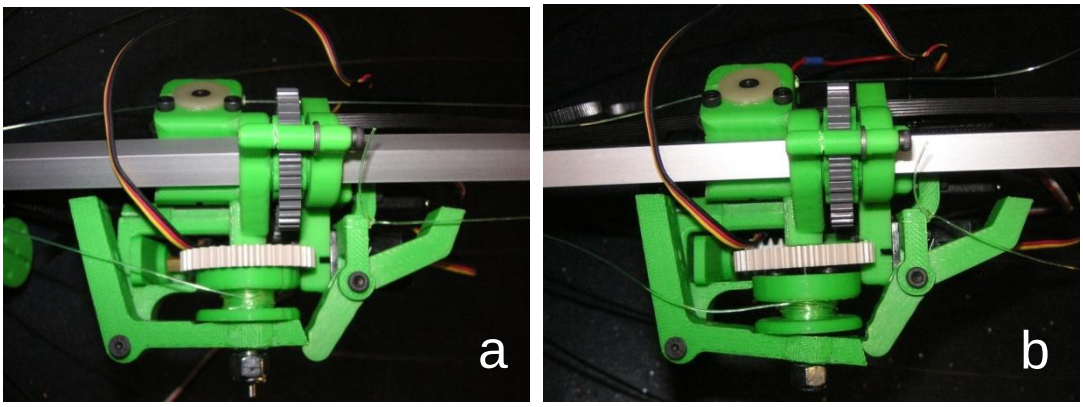

Figure 165 – Release mechanism; a) closed, b) released

To ensure that the stored potential energy in the spring sphere could be usefully used for jumping with minimal losses, a low friction quick release mechanism was required. This mechanism relied on the disengagement of the compression spool from the main Module1 gear. This was achieved by using a series of levers to provide the mechanical force to pull the spool away from the gear (Figure 165). Some of the ideas for this release mechanism were taken from a similar mechanism designed by Dr Keith Paskins (Paskins 2007).

The spool made engagement with the spur gear through 4 locking pins (here made from M3 cap head screws). The smooth round heads of the pins fitted neatly in the 4 holes in the spur gear and provided an adjustable release point by tightening or loosening them. The spool was mounted on an M6 bolt that had a 3.4 mm diameter hole machined through it. This allowed the spool to rotate freely on its 3 mm diameter shaft whilst also allowing the spool to slide along it when pulled by the release lever. To make secure engagement with the release lever, a locking Nyloc nut was screwed on the protruding end of the bolt. Figure 166 illustrates these features.

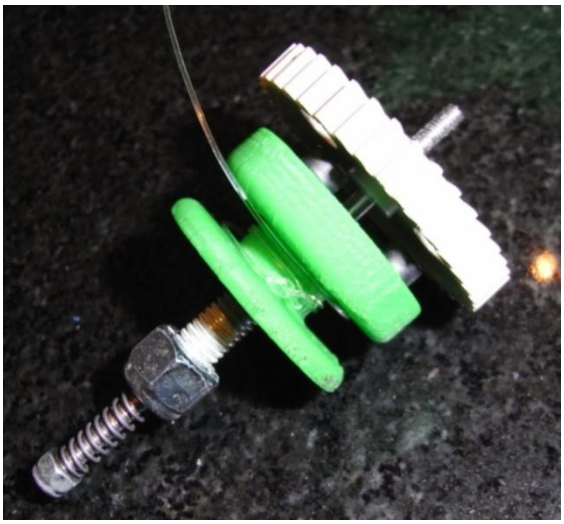

Figure 166 – Compression spool sliding and engagement mechanism

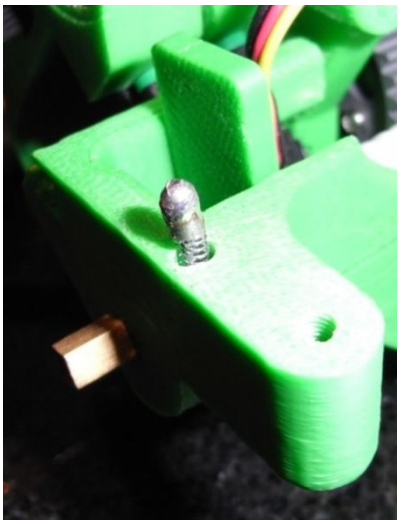

Figure 167 – Spring loaded catch resulting in a two-position state for the release lever

Each of the two levers was actuated by touching a single pole of the sphere (or more specifically, the surface of the anti-tangle mechanism on each pole). The smaller lever was spring loaded and used as a safety catch, ensuring that the main release lever could not be depressed until both poles of the sphere were in contact with the main chassis. This feature guaranteed that release could only occur at maximum compression (~190 mm pole-to-pole, after ~380 mm / ~68 % compression).

The main “L” shaped release lever contained a hole through which the spool mounting bolt and axle passed. The locking nut secured the two components loosely together. The release lever had a spherical profile to ensure that as one side of the lever was pressed, the spool was pulled linearly along its axle (Figure 168).

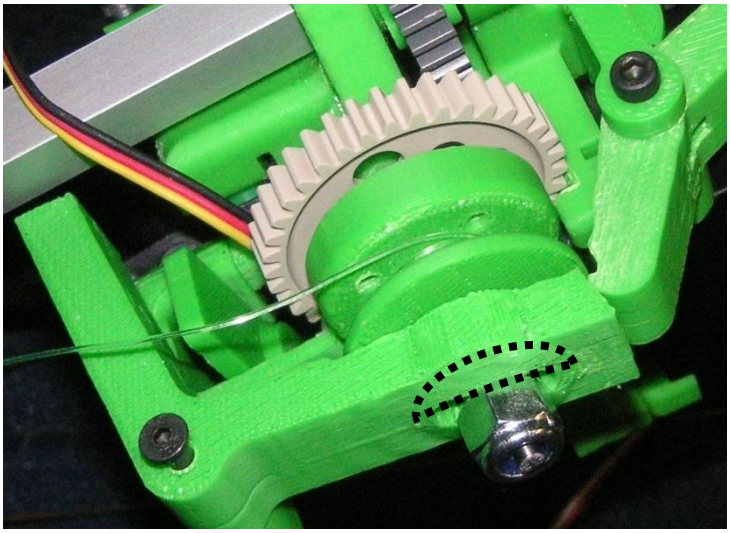

Figure 168 – Release lever (spherical profile highlighted)

It was critical that the spool was securely located in the fully engaged position for compression and in a fully disengaged position during release. Any movement of the spool along its axle while rotating would cause energy to be wasted due to premature disengagement when winding in, or premature engagement while rapidly releasing. The release lever was held gently in an either open or closed position by a spring loaded catch consisting of a solder blob at the end of a short length of M3 threaded bar, and a small coil spring positioned within a hole in the main chassis (Figure 167). A pair of matching dimples was incorporated in the surface of the release lever to provide a two-position state for the spring loaded catch.

The combination of the sliding spool, and the catch and release levers, allowed the energy in the sphere to be released explosively with little frictional loss.

6.4.5 Jump direction control mechanism

Controlling the direction of a particular jump was critical to the usefulness of a jumping and rolling robotic mobility system. This direction control was achieved by positioning the centre of gravity of the device slightly away from the line along which the jump energy is released (i.e. a line along the central square section axle), and in the direction in which a jump was intended to take the device. As designed, a mechanism already existed within the device for moving the centre of gravity around the central

axle to any chosen position – the rotary motion capability of the Powered Rolling Mechanism (see Section 6.4.2.1). Once the device was fully compressed, this mechanism meant that the centre of gravity could be moved in such a way so as to lean the axle of the device toward the intended direction and promote a jump in that direction (Figure 169).

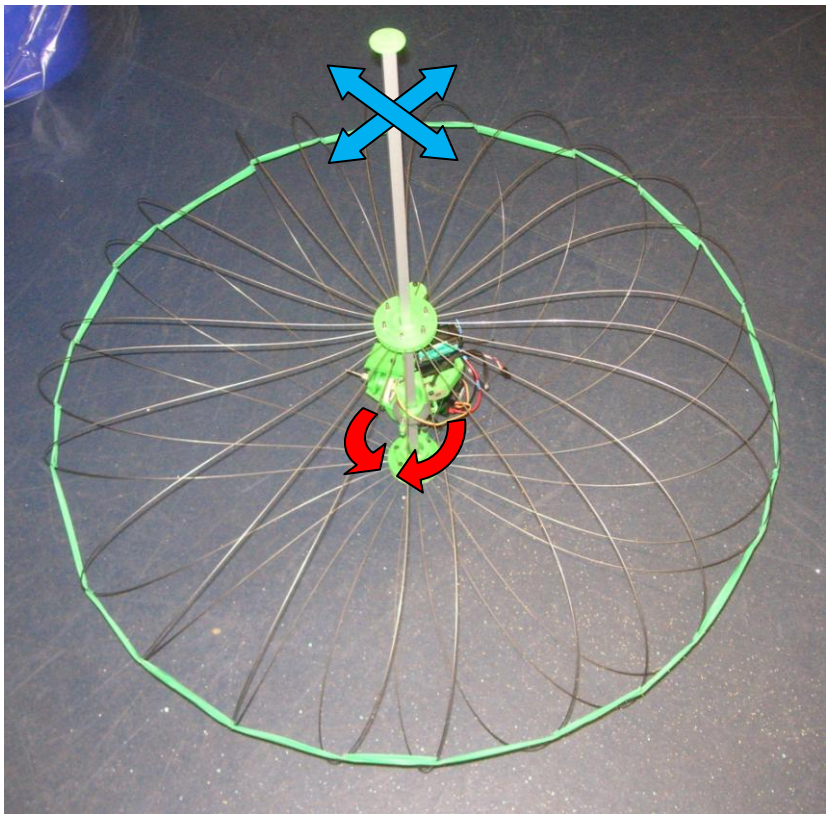

Figure 169 – Jump direction control. Red arrows show movement of central mechanism. Blue arrows show resultant lean of the compressed sphere providing jump direction control.

6.4.6 Reset mechanism

Once a successful jump has taken place, the device needed to be readied for either rolling or another jump. Rolling could take place immediately, although the compression thread was likely to get entangled unless it was rewound a little onto the spool after being slack after a jump. Jumping required that the spool was re-engaged with its drive gear using a reset mechanism. As the release lever was attached to the

spool, it could also be used to re-engage the 4 locking pins. However, the force of the spring-loaded catch needed to be overcome to allow the release lever to move. This was achieved by using a by-product of a worm and spur gear combination. When a worm gear is driven against a spur gear, if the spur gear is under load and the worm is free to slide along its drive axle, then the worm moves in a linear direction along its axle. This is seen in Figure 170.

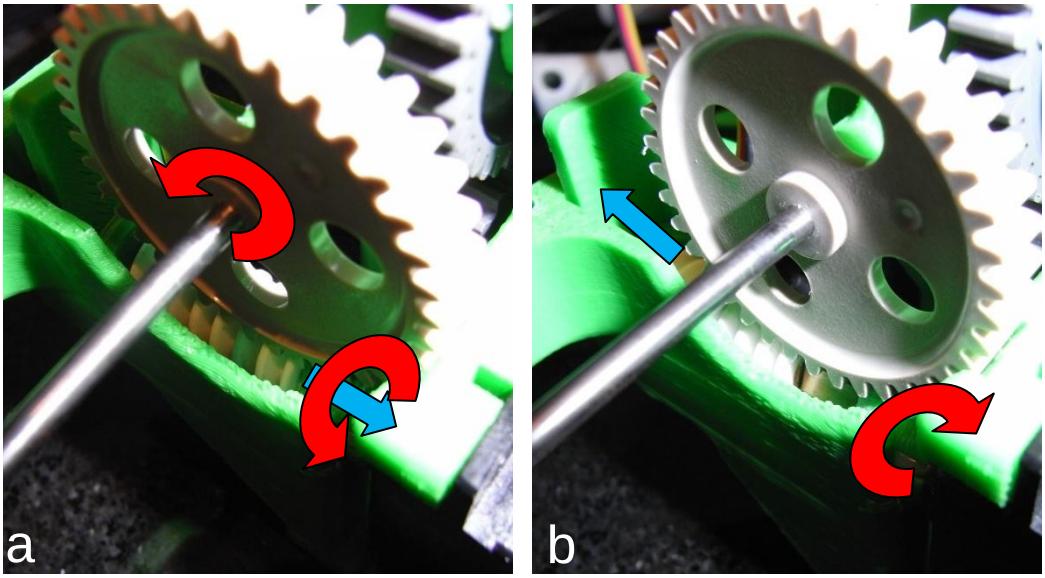

Figure 170 – Sliding worm gear reset mechanism. a) Standard position where rotation of motor forces worm gear against the coupling and results in the rotation of the spur gear. b) A sliding reset movement would be produced when counter rotating the motor which forces the worm gear to slide along the shaft leaving the spur gear stationary.

In the case of Jollbot's mechanism, the worm gear was able to slide since it was mounted directly on a 4 mm square-section tube. This tube was in turn able to slide along a 3.5 mm square-section drive-axle coupled to the motor using a Polymorph coupling. The worm gear could only slide in a direction away from the drive motor due to the position of the coupling in relation to the spur gear. This could only occur when the compression motor was rotated in the "loosening" direction. Co-axial with the worm gear was a small rapid prototyped component that made contact with the underside of the release lever as the worm gear moved. This was the component that applied load to the lever to re-engage the spool. In addition, a tuneable coil spring was applying a

load directly to the spool along its axle to ensure complete engagement. It was not a problem if the 4 locking pins were not in alignment with the holes in the spur gear, as when the compression motor was first rotated in the usual “compression” direction, the worm would begin to move back along the stationary spur gear until a point where it stopped moving, and then would begin to turn the spur reaching a position where the locking pins could re-engage and then compression would continue.

6.4.7 Jollbot 3b mass summary

Table 23 shows a summary of the main masses of Jollbot 3b. Appendix A has more detail of the masses, material, and photographs of individual components.

Component	Mass
Spring sphere	411.5 g
Removable central axle and end caps	56.5 g
Central mechanism	352 g
Removable anti-tangle rolling weights	33 g
Total Mass of Robot	**853 g**

Table 23 – Jollbot 3b mass summary

Jollbot 3b’s masses resulted in an accelerated “head” mass to trailing “foot” mass ratio of 2.1:1 making the simplifying assumption that the top half of the sphere contributed to the “head” and the bottom half to the “foot”. This ratio improved to 2.7:1 with the central axle removed (see Section 6.5.1.3), but was still far less that the equivalent ratio in the jumping only Jollbot 2 (7.1:1).

From theory and the known details of the spring sphere (stiffness of 75 N/m compressed by 400 mm), the predicted no-loss jump height for Jollbot 3b was 0.72 m. This was a change in centre of gravity height only and would likely result in a smaller cleared height due to the shape change from ready-for-take-off to peak jump height.

6.5 Jollbot 3b experiments

Since Jollbot 3b was capable of both jumping and rolling, the testing phase could focus on the performance of each mode of motion. In addition, the combined jumping and rolling performance could also be considered. Throughout the experimental phase, simple hypothesis and subsequent modifications were considered and tested where appropriate.

6.5.1 Jumping experiments

Numerous experiments were conducted with the aim of quantifying Jollbot's jumping performance. These are broken down into the sections below each testing a particular feature.

6.5.1.1 Power consumption during compression

The first aspect of jumping that required testing was to measure details about the compression phase of a jump. After repeated experiments, it was determined that it takes around nineteen minutes to compress the sphere automatically using the onboard 4.8 v 600 mAh battery pack. This compressed the sphere by 400 mm from its resting diameter of 590 mm (Figure 171a) down to a pole-to-pole doughnut shape of 190 mm (Figure 171b).

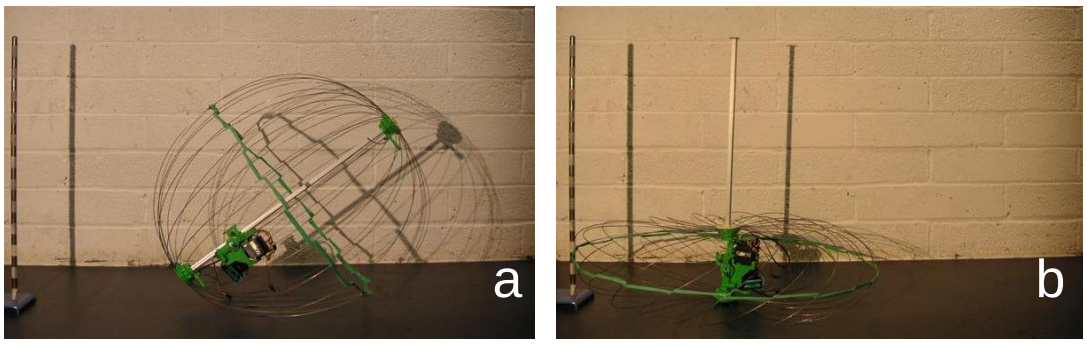

Figure 171 – Compression of Jollbot 3b; a) start, b) finish

Throughout a single compression, the current draw on the batteries was measured at 20 Hz using a USB datalogger (Measurement Computing PMD-1208LS) and the results are presented in Figure 172. The average power consumption during this period was 1.24 W. Even though the hobby servomotor had been modified for continuous rotation, the controller still provided pulse width modulated power (~2 ms in length) at a set frequency (~50 Hz). Thus the instantaneous power measurements recorded at 20 Hz fluctuated by a large amount. Figure 172 has therefore been produced using a moving average over a period of ten seconds. The area of low power level came about as a result of slowing the motor for thirty seconds due to a problem with the management of the compression cable. However, the average power consumption during compression remains fairly unchanged over the nineteen minute period.

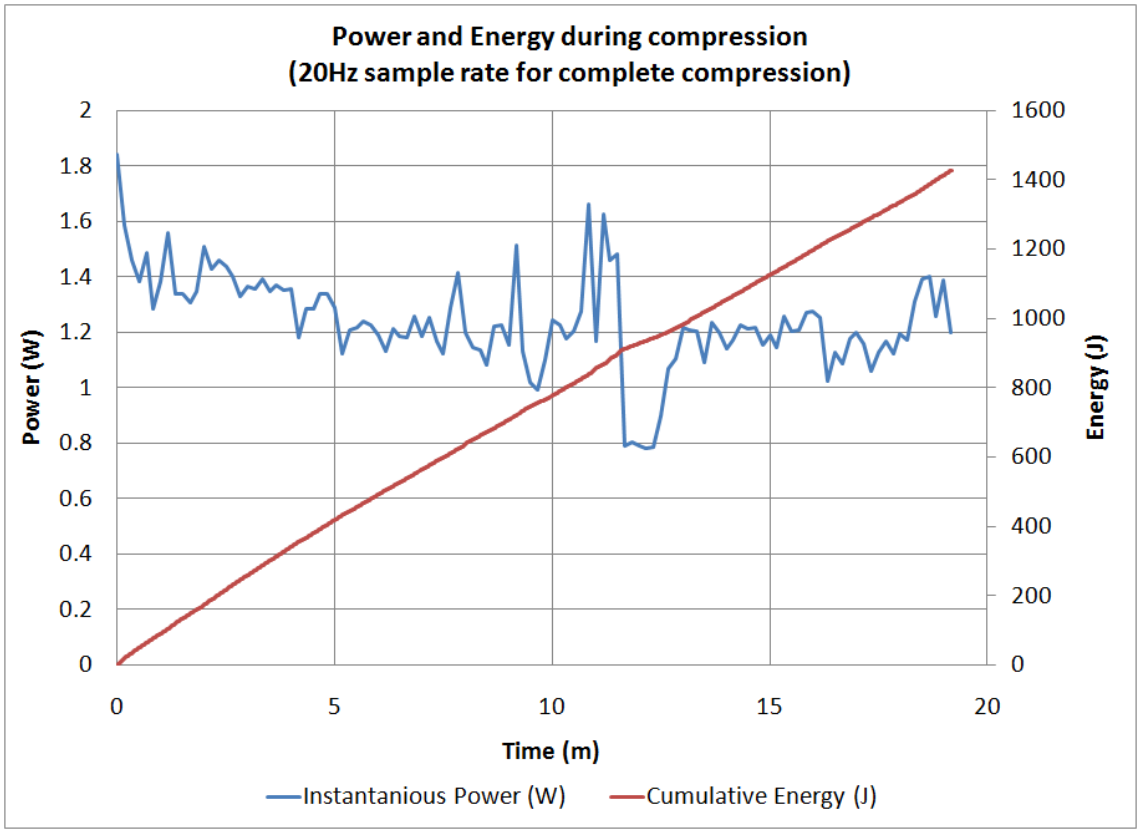

Figure 172 – Electrical power consumption during compression (moving average over 10sec period)

The red line in Figure 172 shows the cumulative energy used throughout compression, and totals approximately 1400 J. This was an enormous amount when compared to Jollbot 2, but this came mainly as a result of the lengthy time taken to perform the compression and substantial energy losses during the conversion of the stored chemical energy in the batteries to mechanical motion of the motors and finally to elastic potential energy stored within the strained spring elements. The continuous power requirement of 1.24 W for Jollbot 3 was however substantially less than the 5.76 W of Jollbot 2. To determine the operational life on a single set of batteries an equation relating battery capacity (q in Ah), current draw (i in A) and draw time (t in hrs) was required (Equation 21).

$$t = \frac{q}{i}$$

Equation 21 – battery lifetime

The existing 600 mAh capacity batteries would provide approximately 2.2 hours of use at 0.27 A current draw, enabling Jollbot to perform around 6 jumps on one charge.

6.5.1.2 Jumping

A black and white video of each jump was recorded using a Redlake Imaging high speed camera and the associated Motionscope software package. The frame rate was selected depending on the light available and the lens chosen for each experiment. The camera was fixed to a tripod and filming took place from the same height as the centre of the uncompressed Jollbot. Jumps were recorded using a 100 % trigger such that frames over the last 3-5 seconds (depending on frame rate) were stored on the attached computer once the trigger was activated. This meant that the moment of jump need not be predicted in advance.

The stored frames were reduced to a selection including only those that were of interest. This typically meant those frames ranging from initial movement to peak jump height were retained. The position of both the upper and lower pole of the sphere was obtained by gathering calibrated pixel positions using ImageJ (Rasband 2010) which

output X,Y coordinates to an Microsoft Excel file. A known size object in each frame allows for each image to be calibrated. A typical screen capture of ImageJ is shown in Figure 173.

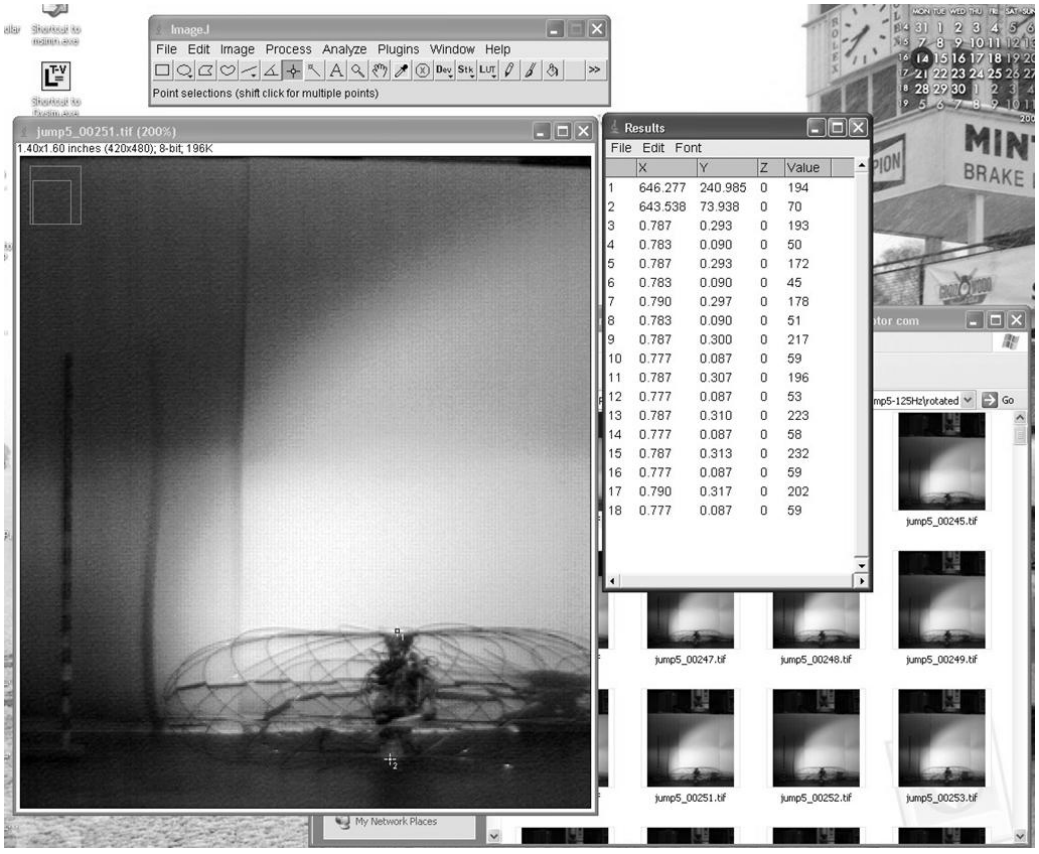

Figure 173 – Screen capture of ImageJ data gathering software

The initial jumping experiments took place with Jollbot 3b in its “as designed” form. To save time, the majority of the compression was performed by turning the spool by hand with only the final stages of compression and subsequent automatic release being powered by the onboard batteries. The off-axis mass was positioned to the rear so that the device would appear to jump vertically within the frame when in reality it was jumping slightly away from the camera.

Still images taken at 250 frames per second (fps) from the first jump are shown in Table 24, along with a summary of the performance of Jollbot 3b.

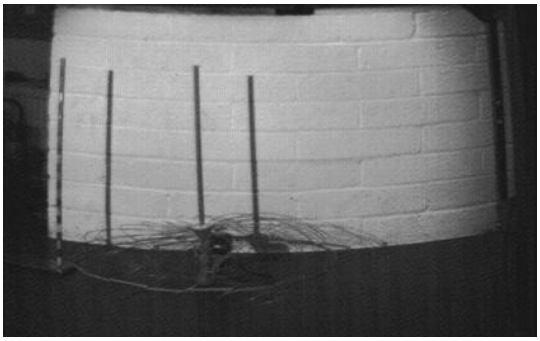

At Maximum Compression

Minimum compressed diameter = 170 mm
Stored Potential Energy = 6.46 J

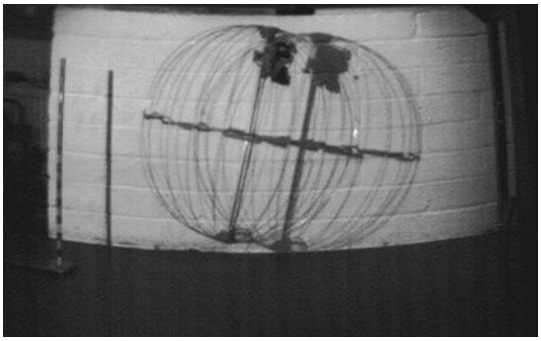

At Peak Height

Maximum diameter = 642 mm
Cleared jump height = 113 mm
Potential Energy at peak height = 3.33 J
% Efficiency = 52%

Table 24 – Performance of a jump with main axle in place

The data file created with ImageJ was imported into Microsoft Excel and manipulated such that all points were re-centred with respect to the initial position of the bottom point of the robot. The positions of the top and bottom, and estimated centre of gravity of the robot could then be plotted against time as shown in Figure 174.

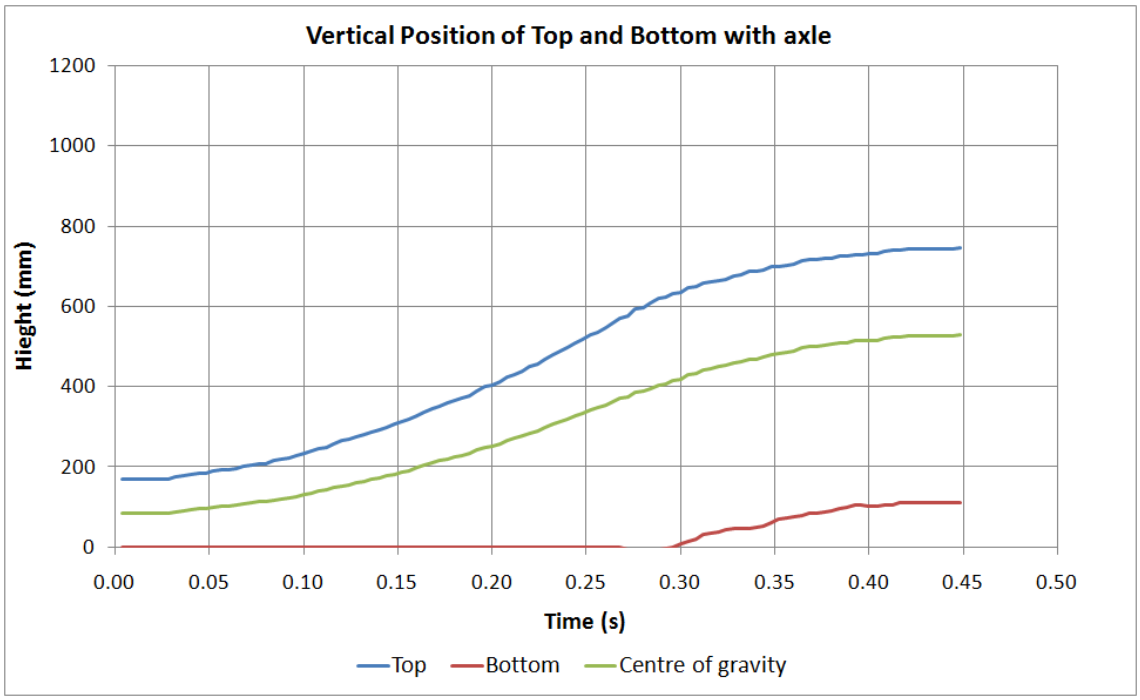

Figure 174 – Jump with main axle top, bottom and CofG vertical positions

Figure 174 illustrates some interesting aspects. The difference between the “top” and “bottom” data series on the far left of the figure shows the minimum compressed height of ~170 mm. When released, the top of the device (and therefore the main chassis components) moved with increasing speed away from the base, until a point where it hits the end-cap of the main central axle. At this point, the kinetic energy gathered by the moving components was redistributed around the device to include the now moving main axle and bottom pole of the sphere. This is evident as the slowing of the top of the device when the bottom first begins to move at ~0.3 s. The difference between the data series at this point should equal the length of the main central axle. The axle measures 612 mm and the difference at this point is 642 mm. As the push-fitted shaft end cap was loose after this jump, the length difference was likely to indicate the point at which this loosening occurred and energy was therefore lost.

The middle line in the figure represents an estimate of the position of the centre of gravity of the complete device during the jump using the centre positions of the sphere and the central mechanism and a proportional representation of their masses. The line gives a useful estimate of the change in height of the centre of gravity (446 mm) which can be in turn used to predict the change in potential energy as a result of the stored strain energy.

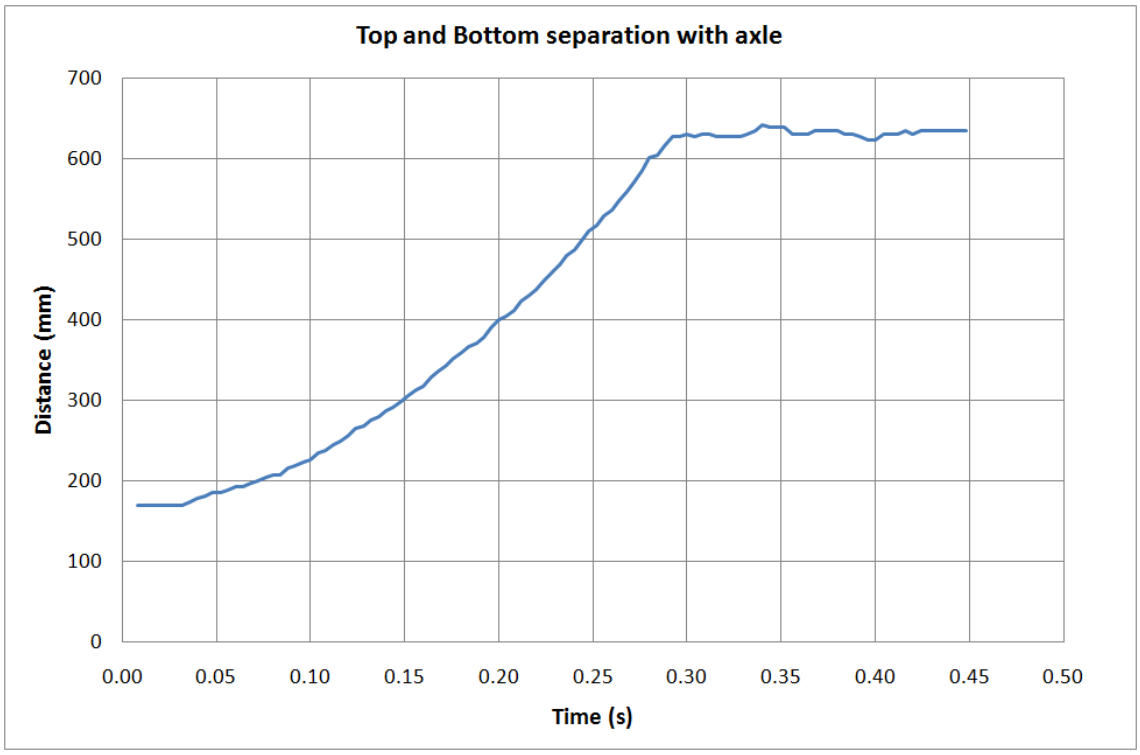

Figure 175 – Jump with main axle top and bottom vertical separation

Figure 175 shows the distance between the top and the bottom of Jollbot throughout the course of this first jump. After ~0.3 s when the device leaves the ground, the distance between the top and bottom varies in a slightly oscillatory way, finally settling at approximately 612 mm. If the "head" and "foot" of a jumping device are connected only by a spring, then oscillation of the head of the device with respect to the foot just after take-off is expected. The effect of oscillations can be minimised by increasing the ratio of the mass of the head to the foot. As mentioned above, in Jollbot's case, the ratio of the "head" mass (557.75 g) to "foot" mass (262.25 g) was 2.1:1. The friction on the central axle also significantly dampened these oscillations, but damping equates to lost energy.

The data for the raw positions of the top and bottom of Jollbot during a jump were differentiated to give the velocity of each of the points, and further differentiated to give the acceleration at each of those points. Owing to the low resolution (420 x 480 pixels) of the video, and the requirement to see the whole device during a jump, there are very small positional changes between sequential frames at 250 fps, sometimes less than

one pixel in width. Thus the initial velocity and acceleration data taken between neighbouring frames was extremely noisy. To smooth the results, data 7 frames apart were differentiated to give the following graphs of velocity and acceleration shown in Figure 176 and Figure 177.

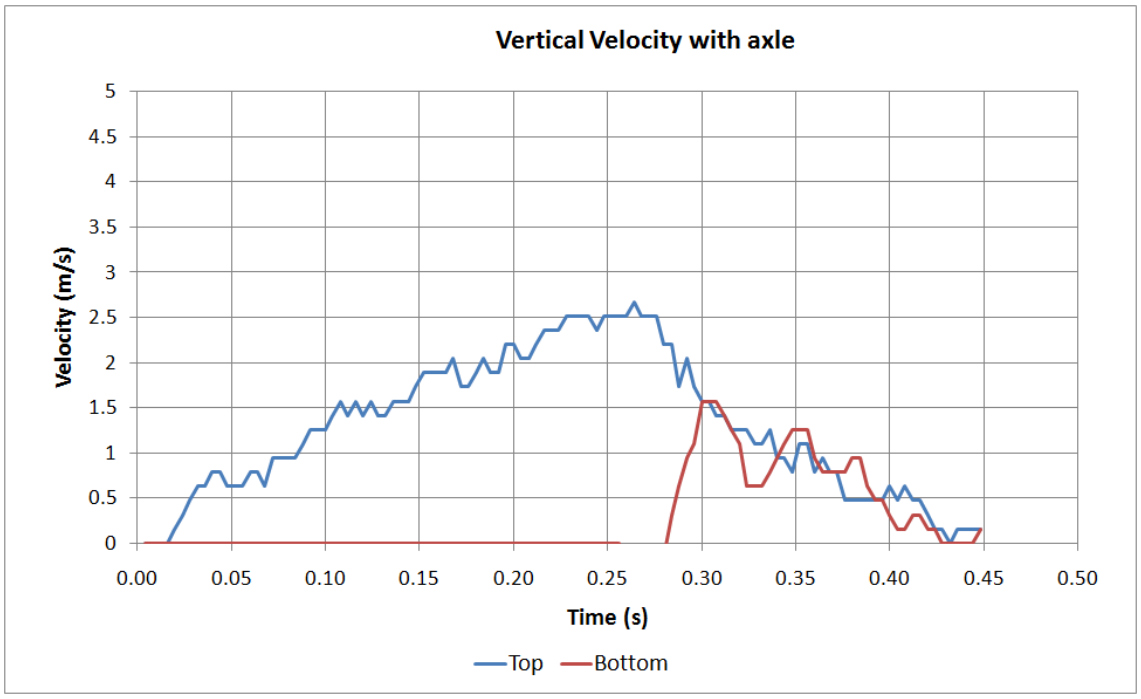

Figure 176 – Jump with main axle top and bottom vertical velocity

The velocity figure shows an almost linear increase in velocity of the top part of Jollbot until ~0.27 s at which time it was travelling at 2.5 m/s. At this point the velocity rapidly decreases as the bottom of the device left the ground. The velocity of the top continued to decrease, but at a lower rate once the bottom, and thus the entire Jollbot, had achieved ~1.5 m/s. The bottom of the device underwent an almost step change in velocity at 0.3 s between 0 m/s and 1.5 m/s. After the entire device had left the ground and achieved a common velocity, it was acted on only by gravity, thus the combined velocity falls to zero at the highest point of the jump after 0.45 s.

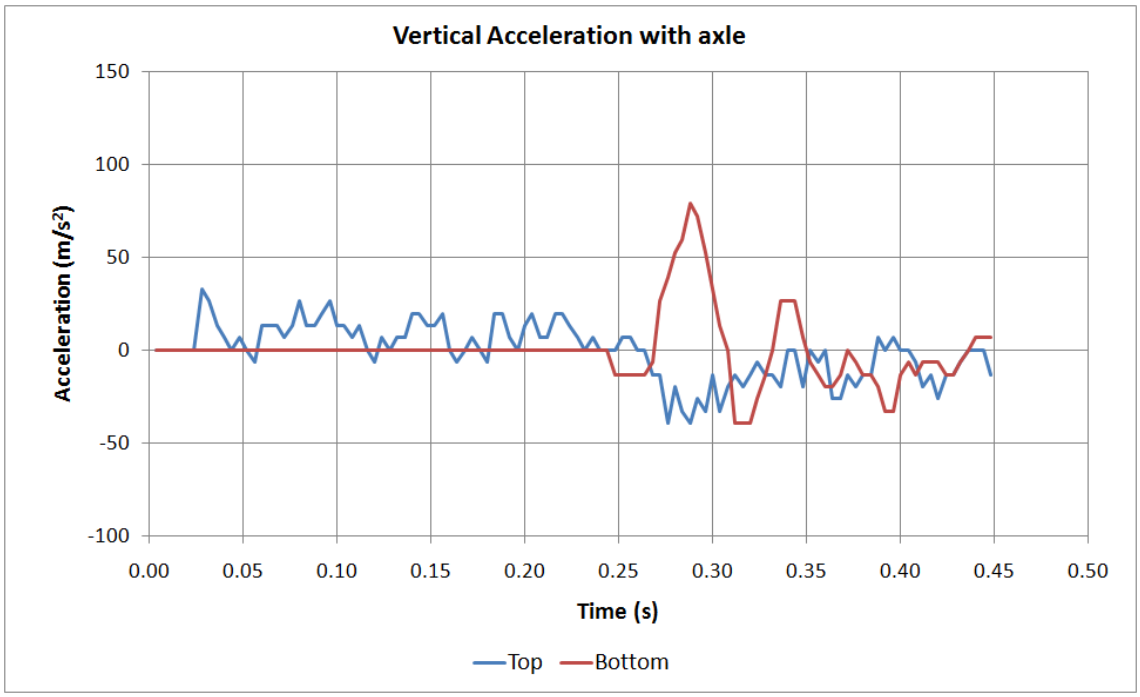

Figure 177 – Jump with main axle top and bottom vertical acceleration

The vertical acceleration figure (Figure 177) further highlights the approximately constant acceleration of 10 m/s^2 of the "top" of the device during release, and the constant deceleration of -10 m/s^2 after take-off. The oscillation of the entire sphere after take-off is also clearly evident with the alternating sign of the acceleration of both the top and bottom of the device.

Summary pages for this and all subsequent vertical jumps are shown in Appendix B and the enclosed DVD has full videos of numerous jumps.

6.5.1.3 Jumping without central axle

The initial jumping performance did not live up to expectations. There appeared to be large losses of energy due to friction between the main chassis mechanism and the central square section axle. As Jollbot should still be able to automatically jump without this central axle in place, a subsequent experiment was conducted without it. A short lightweight (3 g) extension had to be fitted to the main release lever as without the central axle as a guide, the lever would often miss the contact point on the inside of the

polar clamp. As the axle was removed, the central mechanism was no longer rigidly attached to the device as only the flexible belt fixed it to the upper pole of the sphere. This resulted in substantial movement of the central mechanism, particularly just after take-off where it continued upward even though the rest of the sphere is slowing due to the additional drag of the foot of the device. This had an impact on the oscillations during early flight as there were three masses connected with springs and dampers of different properties.

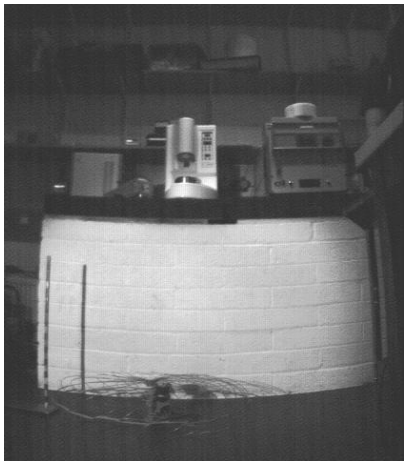	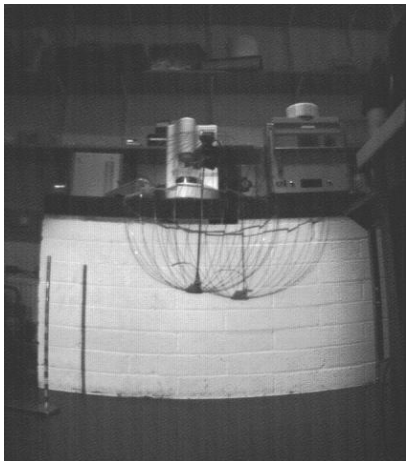
At Maximum Compression	**At Peak Height**
Minimum compressed diameter = 171 mm Stored Potential Energy = 6.43 J	Maximum diameter = 643 mm Cleared jump height = 504 mm Potential Energy at peak height = 6.23 J % Efficiency = 97%

Table 25 – Performance of Jump with main axle removed

Table 25 shows images and a summary of the important performance details of a jump with the main axle removed. It is clearly apparent that the jump height was far larger without the friction associated with the central axle. Again, four figures were produced from the raw data illustrating the position (Figure 178), velocity (Figure 180), and acceleration (Figure 181) of the top and bottom of the device during a jump, along with a figure illustrating their vertical separation over this same time (Figure 179).

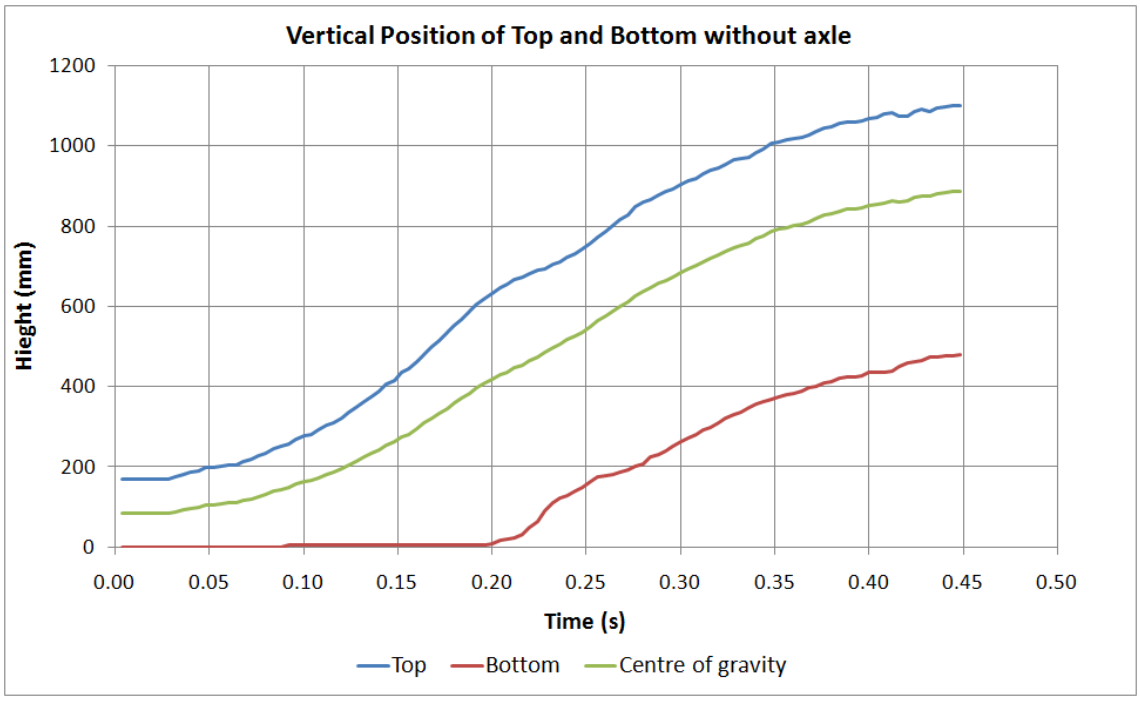

Figure 178 – Jump without main axle top, bottom and CofG vertical positions

It is clear from Figure 178 that the jump height achieved was far greater than that achieved in the jump where the axle was in place (Figure 174). The time taken to reach the resting diameter of the sphere was approximately 0.2 s, only two-thirds of the time it took in the first jump, indicating greater power output from the sphere. The flight time taken to reach peak height was around twice that of the first jump indicating a greater take-off velocity.

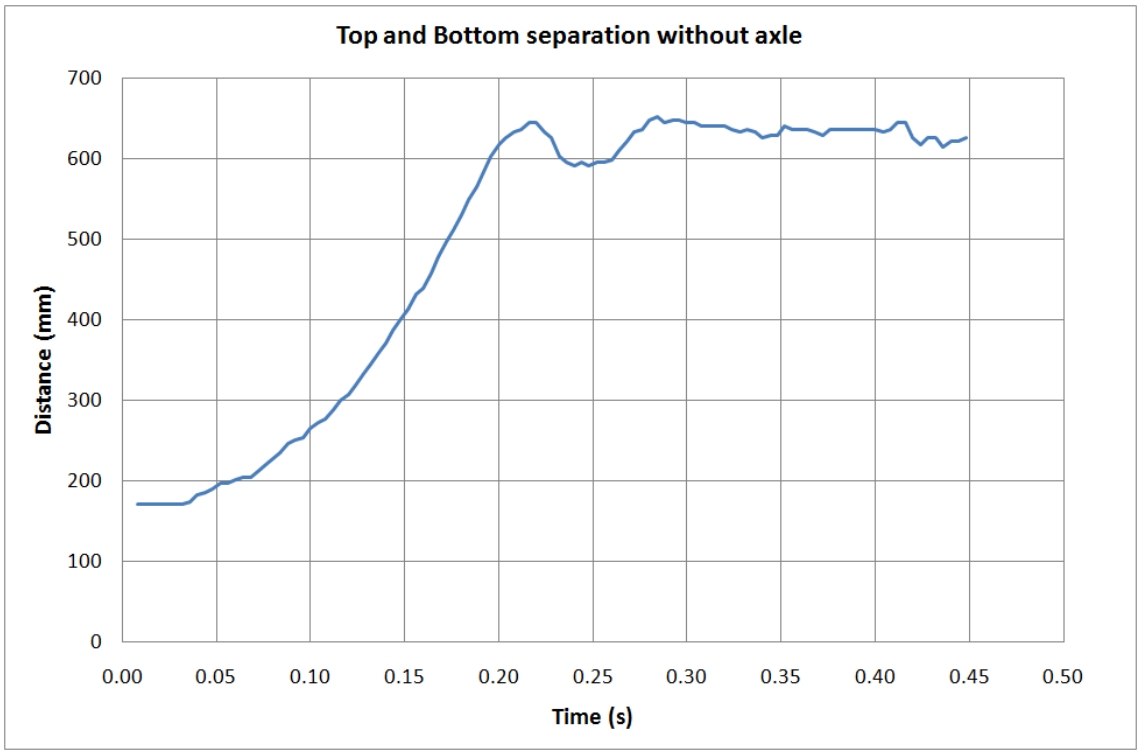

Figure 179 – Jump without main axle top and bottom vertical separation

Figure 179 shows a large oscillation when the device was fully extended and this was only lightly damped for the first cycle, after which point it appeared that some other factor contributed to quickly damping this oscillation. It was highly likely that this was a result of the freely swinging central mechanism.

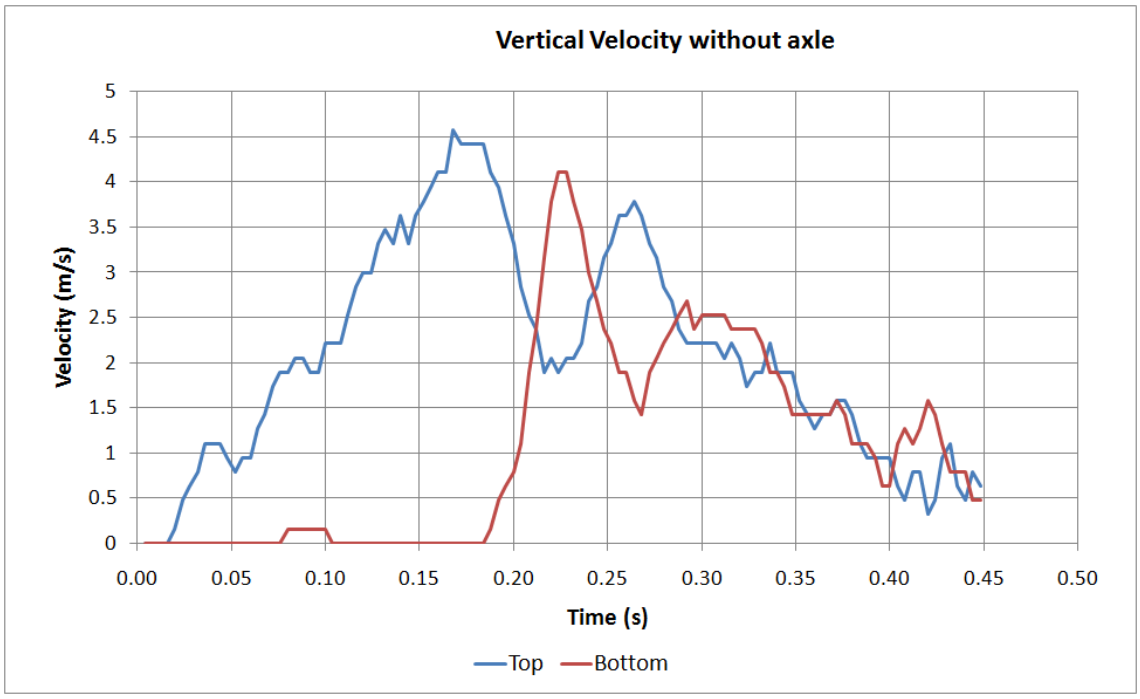

Figure 180 – Jump without main axle top and bottom vertical velocity

Figure 180 shows an almost linear increase in velocity of the top as energy was released over the first 0.17 s after which time the top was travelling at ~4.5 m/s – far faster than the 1.5 m/s achieved during the first jump. Again the velocity of the top reduced dramatically when the bottom began to move, until the entire device was moving at approximately 3 m/s. Gravity then slowed the device until it reached its peak height at 0.47 s.

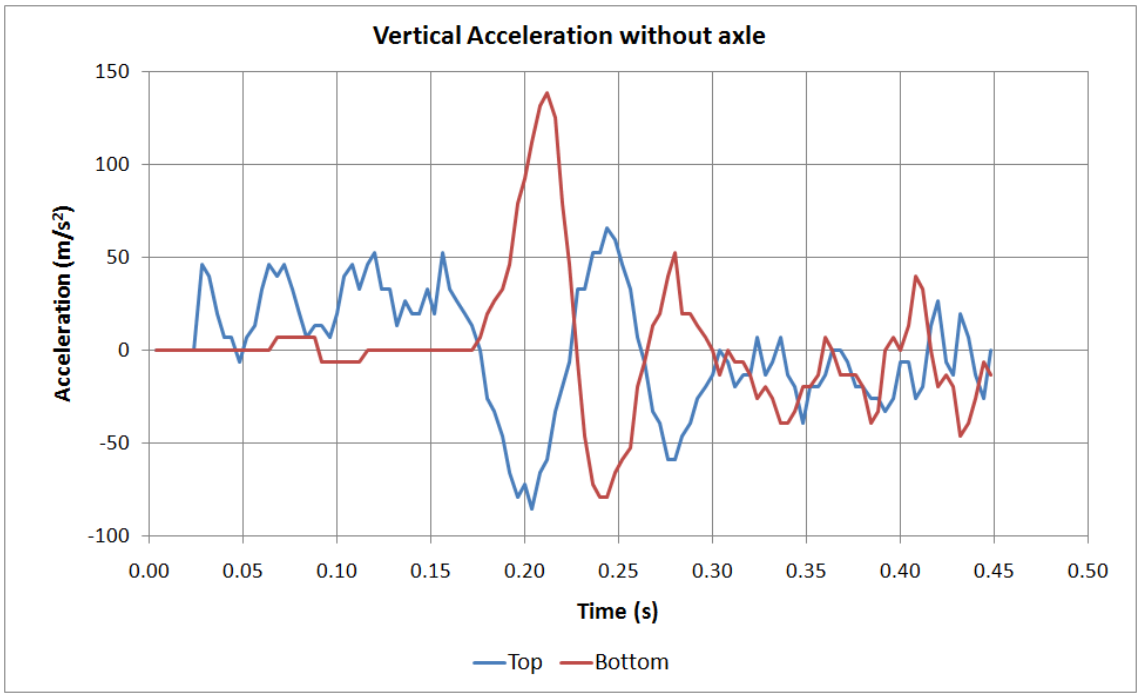

Figure 181 – Jump without main axle top and bottom vertical acceleration

The acceleration of the top was approximately 30 m/s^2 during release (Figure 181) – far more than the 10 m/s^2 achieved in the initial jump with the main axle in place. The large oscillation at take-off can be easily seen and the acceleration levels are therefore much larger than in the first jump.

6.5.1.4 Further jumps without the central axle

The much-improved jumping performance with the central axle removed meant that additional jumps were conducted to find the repeatability of vertical jumping performance. From the early videos, it can be seen that there was a significant change in perspective toward the edges of the video frame. This was due to the 12 mm lens chosen resulting in the camera having to be positioned very close to the jumping device. Analysis of the affected video would have naturally resulted in overestimated distances as the device approached the edge of the frame (at peak height for example). Therefore subsequent high speed camera experiments were conducted using a 25 mm lens which meant that the camera could be placed approximated 7-8 m

from Jollbot, ensuring that this perspective issue did not significantly affect the subsequent analysis.

Five additional jumps were conducted, although the start of the first jump was missed by the recording system. Table 26 summarises the main findings of the series of jumps with the results from jump 5 being presented in full in Figure 182, Figure 183, Figure 184, and Figure 185. Jump 5 was selected for further illustration as it delivered the highest jump performed at maximum frame rate of 250 fps.

Jump	Compressed Size (mm)	Energy stored (J)	Time to peak (s)	Cleared Height (mm)	Energy at peak (CofG height) (J)	Release efficiency %
2	176	6.26	0.48	494	5.71	91
3	181	6.14	0.46	426	5.41	88
4	188	5.94	0.45	420	5.32	90
5	170	6.43	0.47	454	5.67	88
Avg	**179**	**6.00**	**0.47**	**449**	**5.52**	**89**

Table 26 – Summary of additional jumps without axle

The average cleared height from this series of jumps was 449 mm. This equated to almost 80 % of the resting diameter of Jollbot 3b. The sphere stored around 6 J and transferred around 5.5 J to the jump height with the remaining 0.5 J being lost. This loss was likely to be the result of friction of the spool unwinding on its shaft, along with the friction of the thread as it moved through the anti-tangle mechanism of the lower pole. Also, some discrepancy will result from the estimated position of the centre of gravity calculated for each jump.

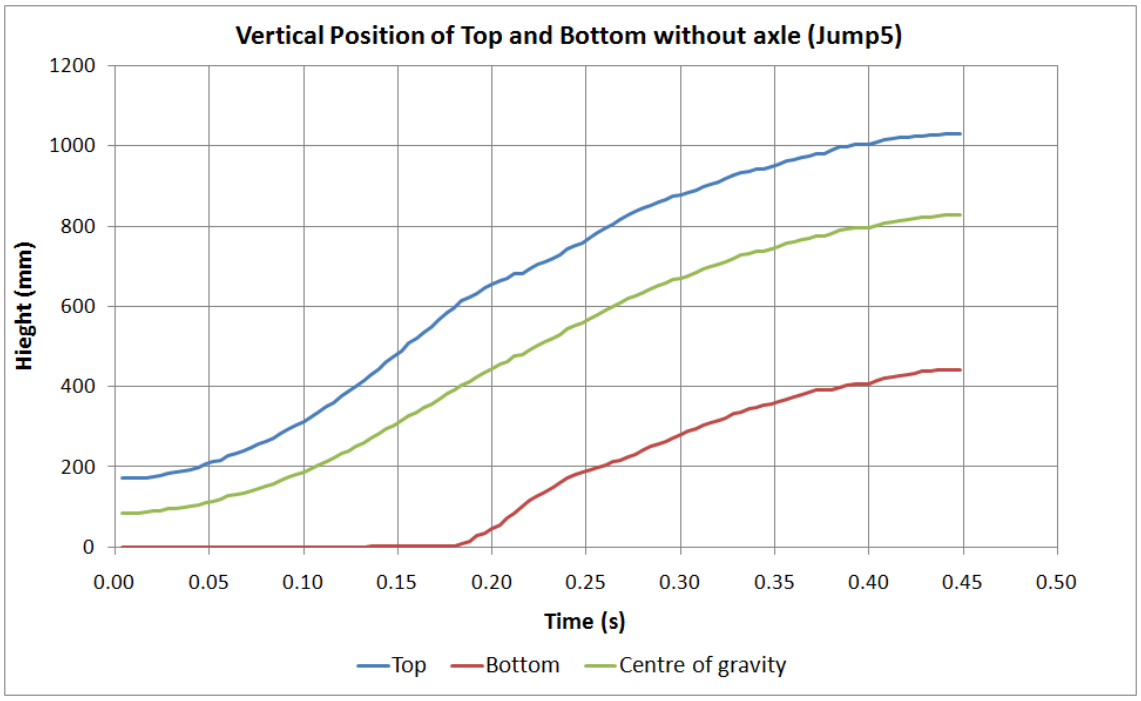

Figure 182 – Jump 5 top and bottom vertical position

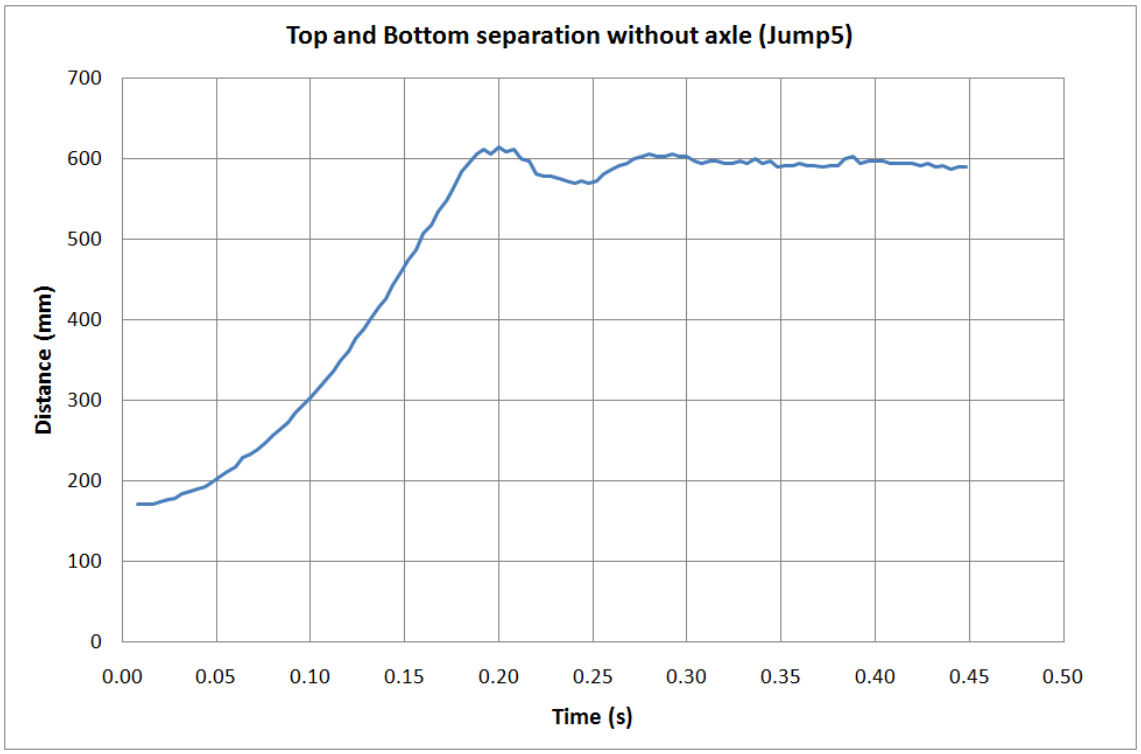

Figure 183 – Jump 5 top and bottom vertical separation

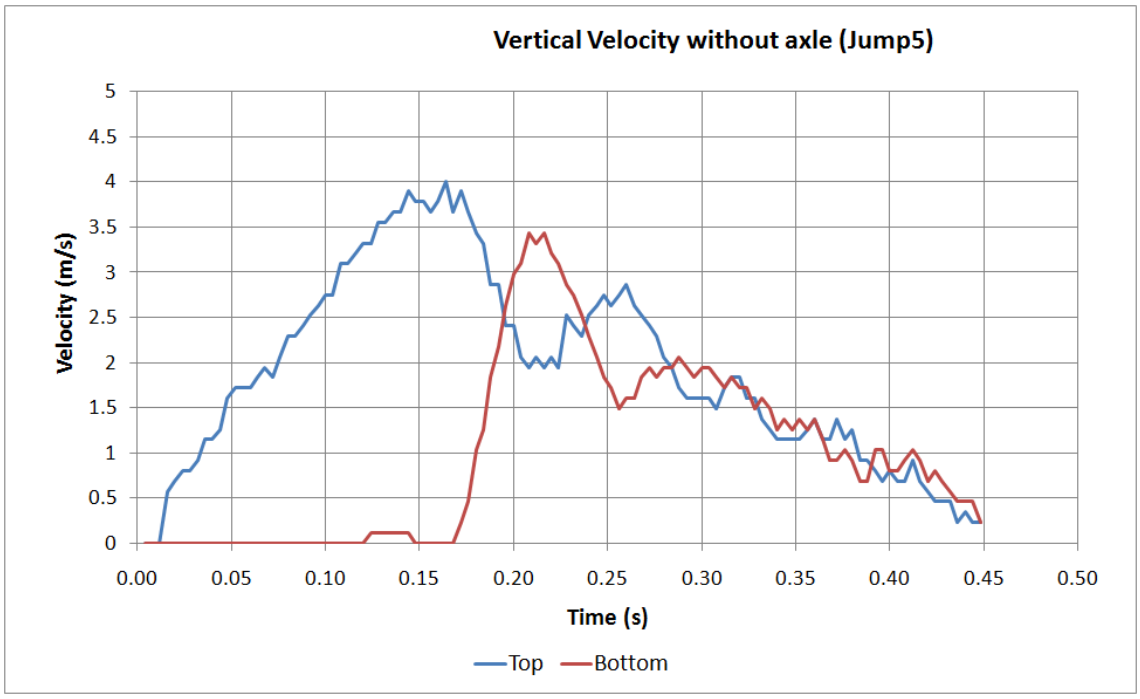

Figure 184 – Jump 5 top and bottom vertical velocity

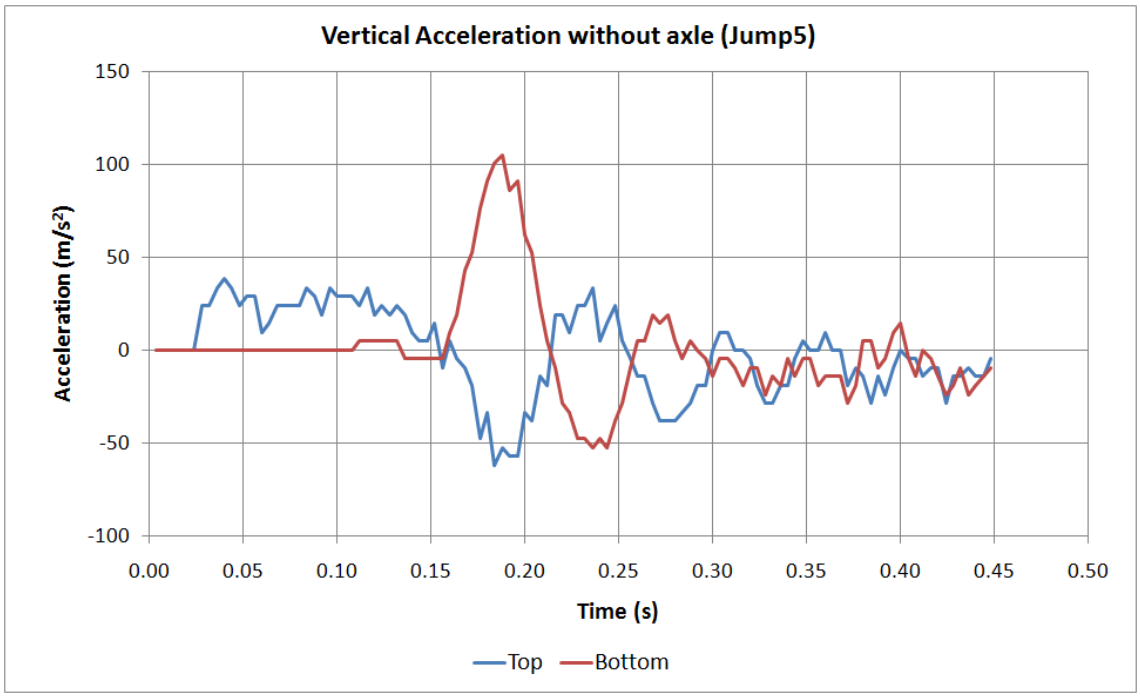

Figure 185 – Jump 5 top and bottom vertical acceleration

The high jump and more accurate results from Jump 5 show the potential energy stored in the sphere released over 0.18 s and a flight time from take-off to peak height of 0.29 s. The oscillations of the top and bottom relative to one another are clearly seen from both the vertical velocity and vertical acceleration graphs. Velocity and acceleration data indicates that just before take-off, the accelerated "head" of the device accelerated at 25 m/s^2 to almost 4 m/s, before rapidly slowing at a peak rate of -50 m/s^2 to 2 m/s as Jollbot transferred its momentum into the trailing "foot" portion. The "foot" underwent rapid acceleration at a peak rate of 100 m/s^2 to 3.5 m/s at full device extension, before a couple of oscillatory cycles where the foot slowed and head accelerated and then visa versa, resulting in an overall device speed of 2 m/s that decayed as expected due to gravity at approximately -10 m/s^2.

6.5.1.5 Upside-down jumping

Jollbot was designed to operate with either pole uppermost, but all of the previous jumps took place with the rotating pole at the top, and the spool unwinding through only the lower anti-tangle mechanism. An experiment was conducted to ensure that "upside-down" jumping was possible. Four further jumps were conducted, two of which were upwards as before and two were "upside-down". Images and values for the peak height of each are shown in Table 27.

Normal orientation	
Jump 1	Jump 2
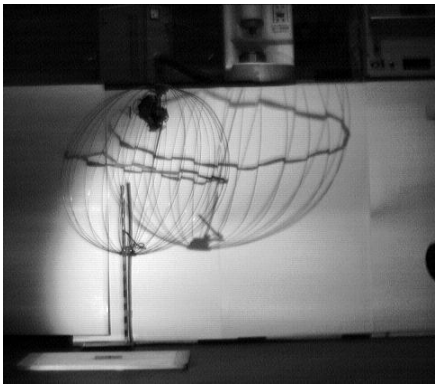	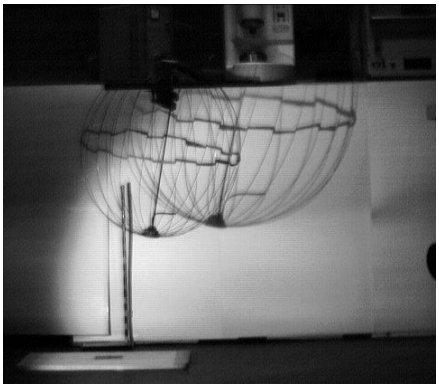
384 mm	444 mm
Upside-down	
Jump 1	Jump 2
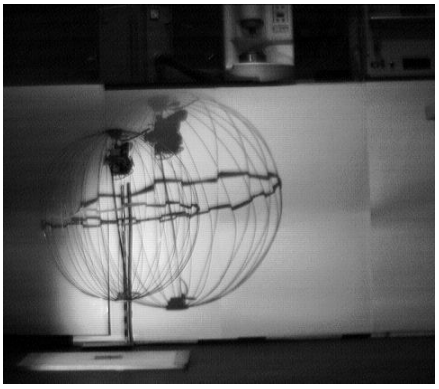	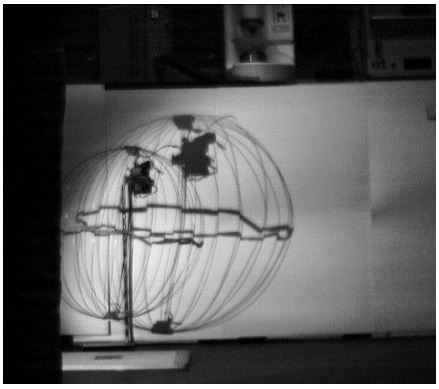
209 mm	141 mm

Table 27 – Comparison of normal and upside down jumps

The performance of Jollbot when jumping from the other pole was not quite as expected. Jumping “upside-down” resulted in a 58% decrease in achieved jump height. This could only be due to the asymmetric friction arrangement coming from the compression cable running rapidly through both anti-tangle mechanisms at each pole. When jumping from the usual pole, the cable needed to unwind only from the spool and travel quickly through one anti-tangle mechanism. Modifications of the profile of the path through the anti-tangle mechanism could provide some efficiency improvements, but ultimately there would be differences in jumping performance dependent on which pole was uppermost.

6.5.1.6 Influence of equatorial latex band

The equatorial latex band that was initially added to assist in rolling by preventing the splaying of the elements (see Section 6.5.2 below), was likely to provide additional energy storage over and above that contained within the compressed spring steel sphere. For any analysis of the energy conversion efficiency of the release mechanism, the influence of this stretchable band needed to be determined.

Four experiments were conducted with the high speed camera: two jumps with the latex band and two without. The results are presented in Table 28.

Jump	Compressed Height (mm)	Cleared Height (mm)	Time Taken (s)
With Band 1	182	467	0.496
With Band 2	179	458	0.448
Without Band 1	185	354	0.416
Without Band 2	169	350	0.432

Table 28 – Influence of equatorial latex band

Even with such a small number of samples, a substantial difference can be seen in the cleared jump heights. After averaging both ‘with’ and ‘without’ the band, the cleared height difference was 110.5 mm or a 24 % reduction. Therefore it can be determined that the equatorial latex band had a significant contribution to the peak jump height.

The additional energy storage capacity of the latex band was not considered in the jumping experiments above. It therefore seems that the stored energy within the fully compressed device was more likely to be around 7.5 J rather than 6 J, making release efficiencies 73 % rather than the original 90 %. Changing the length and material of the central band, or considering an entire covering that is stretchable, may allow for fine tuning of the energy store and matching it to the capabilities of the compression mechanism (see Section 7.8.1.4).

6.5.1.7 Influence of payload

For a device such as Jollbot to be useful in exploration, it must be able to carry additional payloads. This would typically include equipment to automate the device (control modules and sensors) as well as sample-recovery devices or other scientific payloads. Jollbot was therefore tested with additional masses (Figure 186) attached to the main chassis to see how a given weight would affect performance.

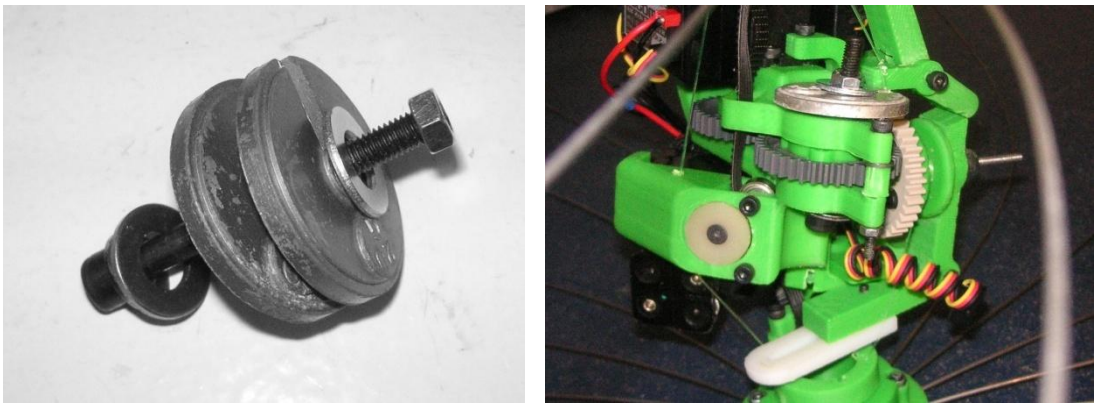

Figure 186 – An additional mass and its attachment to Jollbot

Again, data was gathered from high speed video recordings of individual jumps and is presented in graphical form in Figure 187.

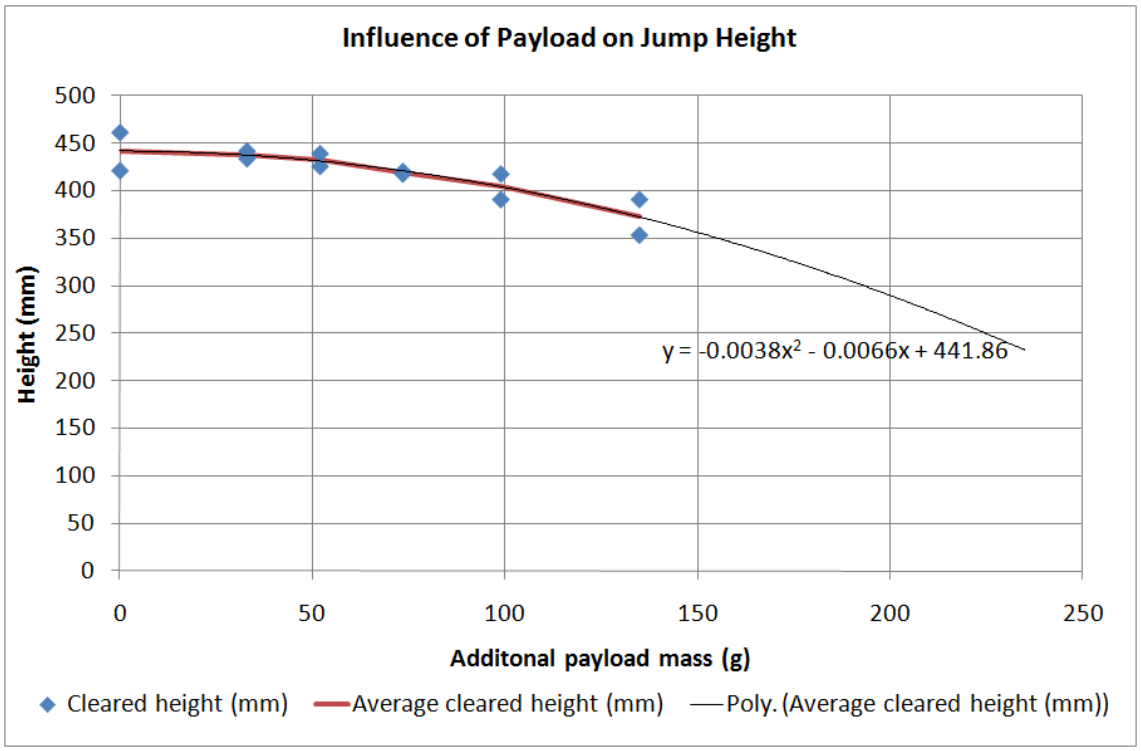

Figure 187 – Influence of payload on cleared jump height

Figure 187 shows how the cleared jump height decreased as the payload increased. A line joining the average cleared jump height for each payload mass is shown in red. A forecasted second-order order polynomial trend line was fitted to the data of averaged cleared height using a Microsoft Excel function. A second-order polynomial was selected as it most closely matched the experimental data. From Equation 9 (p.53) it can be expected that the jump height will decrease as the mass increases. This forecasted line adequately shows that as the mass increased, the jump height decreased more and more. However, even with an additional 250 g, it was predicted that Jollbot would still be able to clear 200 mm.

6.5.1.8 Trajectory performance

Jumping vertically is not useful unless the object to be cleared is very narrow. If Jollbot was to successfully cross rough terrain, then each jump would need to have some forward motion as well as height, allowing the device to overcome a barrier or climb up onto an obstacle. With the main axle in place, Jollbot did make a slightly angled jump

with some range to it. However, since the jump was so low (~110 mm), this range was also small. Unfortunately, without the main axle, where Jollbot achieved reasonable heights, it would jump almost vertically even with the off-axis direction control mass. This was due to the large area of contact with the surface at the pole of the device when fully compressed. This is shown in Figure 188 where the spring steel elements are in contact with the ground in addition to the lower pole of the sphere. This problem could be overcome by adding additional domed components to the poles (or to the axle end-caps if the axle were present) ensuring that the device would always jump from a significant angle (see Section 7.8.1.1).

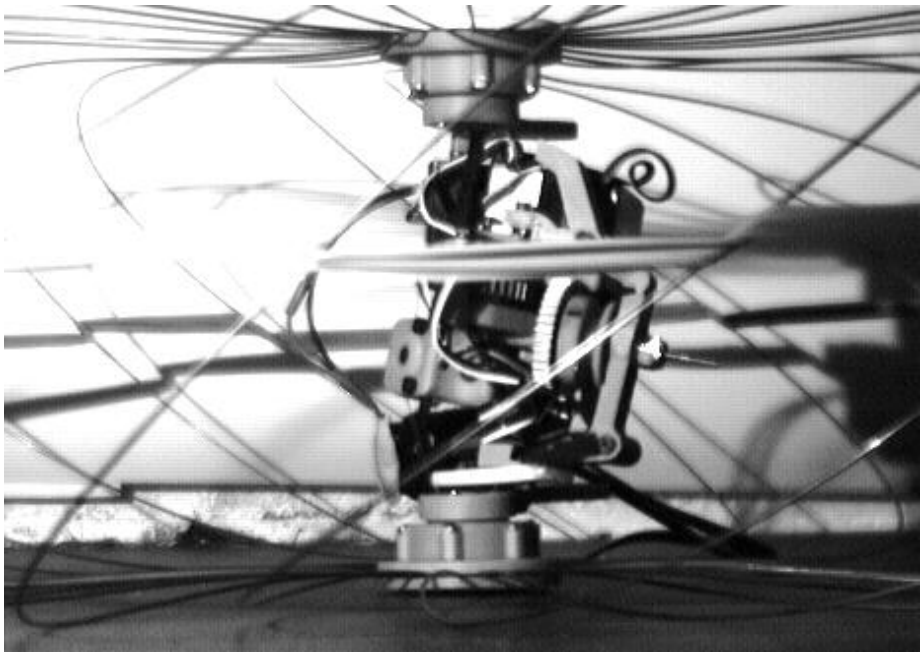

Figure 188 – Jollbot before launch with numerous ground contact points. The twisting of the sphere is clearly evident.

However, making Jollbot jump from an inclined surface (Figure 189) would give an idea as to its potential trajectory performance.

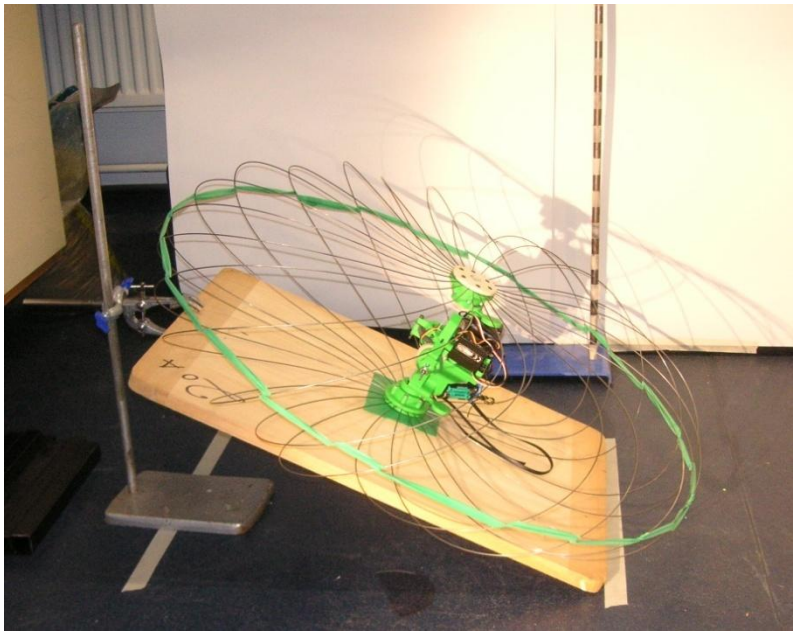

Figure 189 – Experimental setup for trajectory jumps

A pair of jumps were conducted from an inclined surface at each of the following angles to the horizontal; 0°, 5°, 10°, 20°, 25° with an additional single jump at 23°. A small piece of latex was attached to the smooth sloping surface to ensure that the device did not slide either when compressing itself or during energy release. High speed video recordings were made of each jump and the positions of various points recorded:

- X,Y coordinates of the top and bottom of the device at release and take-off – to provide the actual launch angle from horizontal. This was not the same angle as the inclined surface and was closer to 90° minus the angle of the inclined surface and the not-quite-vertical trajectory of Jollbot.
- Coordinates of the lowest point of the device at peak height – to give a cleared height measurement
- Coordinates at first contact with the ground – to give a range measurement
- Coordinates of two points on the sloping surface – to calibrate the rotation of the videos (the error was generally ±1°).

The data was arranged so that jump range and peak height against launch angle could be plotted as shown in Figure 190. The variation in height and range is known from trajectory equations, so $x\sin^2\theta$-height and $y^2\sin 2\theta$-range lines were added and adjusted by varying x and y such that they approximately fitted the data obtained. This is to illustrate where the performance might lead if tests were conducted with Jollbot jumping at a series of angles ranging from 0° to 90°.

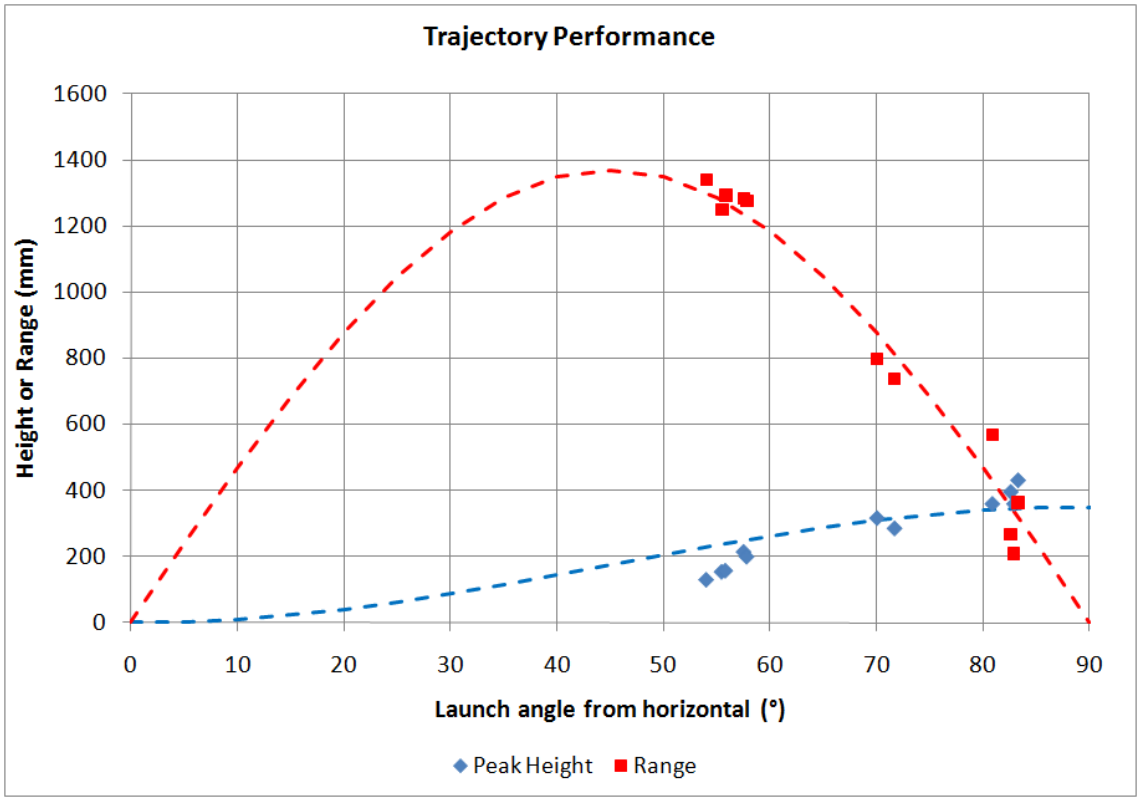

Figure 190 – Trajectory performance of Jollbot

As expected, Jollbot's range continually improved as the launch angle approached 45°. Its maximum height also decreased accordingly as the launch angle left vertical. However, obstacles of 200 mm height could still be overcome at a launch angle of 62° to the horizontal, while achieving a range of around 1.2 m. This may be sufficient for terrain of regular roughness (a ploughed field for example), but it would be ideal if the launch angle could be varied for each jump. Even if fixed-angle jumps were achieved with modifications to the sphere, varying the launch angle would require additional mechanisms.

6.5.1.9 Reset mechanism

Evaluation of the reset mechanism was critical if Jollbot were to be able to continuously move across a variety of terrains. In practice, the designed reset mechanism did not work as expected. The main spur gear was so lightly loaded that when reversing the direction of the compression motor, the worm gear did not move along its shaft. Instead the spur gear just rotated in the opposite direction. This did not achieve the linear movement of the worm gear and the subsequent re-engagement of the compression spool with the spur gear. By applying a load by hand to the spur gear, the mechanism did work as intended. A modification to the design would be required to load or restrict the movement of the spur gear.

6.5.1.10 Practical points of note from jumping experiments

Some notes were made during these experiments that should be considered in any future prototype. They are presented below:

- Movement of both the spur gear and therefore the spool along their axle meant automatic lever-induced release didn't always work. The steel spool axle also bended as it was loaded.
- Jump energy release often required manual intervention to ensure it actually released. This was because without the axle in place, the thread pulled at an angle holding the spool against the spur gear.
- The off-axis mass of the anti-tangle mechanism was broken off during a particular jump when the belt pulled hard against its fixing point.

6.5.1.11 Jumping performance summary

Jump Height (with central axle) Cleared / change in centre of gravity	Jump Height (without central axle) Cleared / change in centre of gravity	Jump Range (from 55° angled launch surface)	Power Consumption during compression	Payload
113mm / 446mm	449mm / 800mm	1.3m	1.24W	250g for 50% reduction in jump

Table 29 – Jollbot3 rolling performance summary

6.5.2 Rolling experiments

Initial testing of the rolling capability of Jollbot 3b highlighted an important issue. The complete weight of the device, combined with the side-to-side instability of the circular section spring elements in the sphere, meant that the sphere flattened and splayed when Jollbot was in its rolling orientation. If it was to roll, then some additional support need to be added to stop the lateral movement of the spring elements. This was achieved by weaving a flat 30 mm wide latex band through each of the 24 spring elements and securing the ends together using latex adhesive. This small modification immediately improved the rolling capability.

In addition, the high torque Towerpro MG995 model servo was becoming unreliable. It no longer responded accurately to forward and backward commands and that made controlled rolling difficult. The servo was replaced with a similar capability one (HiTec HS-965MG) also converted to continuous rotation and quickly fitted as a result of the Polymorph coupling system (see Section 6.4.2.1).

With these modifications, Jollbot's rolling capability could be quantified. This involved determining the slope angle up which Jollbot could roll, the step height over which it could climb and its speed across level ground. In each instance guide rails were used to ensure that Jollbot did not lose its balance and turn off course. This was because

accurate direction control in confined areas proved difficult. Although video was not specifically required for these tests, it was felt that they would enable further analysis. However the high speed camera system, with its very limited recording time, could not be used due to the time taken for Jollbot to undertake a specific experiment. In this case the camera used was a Konica Minolta handheld digital camera set to 30 fps video mode (320 x 240 pixels). Videos of Jollbot rolling are available on the attached DVD.

6.5.2.1 Speed

To determine the speed over flat ground, markers were set up in the test area spaced 1140 mm apart (the distance between the guide rail supports). The device was allowed a short run-up to gather speed and the time taken to travel between the markers obtained from video (Figure 191). The video was then used to determine an average speed of 0.69 m/s (2.48 km/h) from 15 trials. The maximum recorded speed was 1.07 m/s.

Figure 191 – Still image from video recording of speed experiment

6.5.2.2 Slopes

To determine the capability of Jollbot to climb slopes, the robot was positioned on a board mounted with guide rails and supported at variety of angles to the horizontal (Figure 192). Jollbot was then powered forward from a standing start in an attempt to

move up the slope. Videos of each test were recorded although it was easy to determine which slopes were possible to climb and which were impossible.

Figure 192 – Jollbot rolling up a slope (photograph of standing start)

Jollbot 3b struggled, but managed to climb a 4° slope. However a 5° slope was too steep. The device also had trouble stopping itself rolling backward after over rotating the central mechanism. This was because the moment around the contact area quickly changed direction accelerating Jollbot down the ramp. Over longer length slopes this tumbling could be a significant problem.

6.5.2.3 Obstacles

To test Jollbot's capability to roll over obstacles, a step arrangement was constructed using a wooden board. This time, the board was positioned horizontally, but lifted at both ends to give a step of varying height onto which Jollbot could climb (Figure 193). These steps were at 26 mm, 30 mm, 37 mm, 44 mm and 52 mm determined by the availability of spacing material. It was clear from the outset that Jollbot could not climb over any step without some momentum generated from a run-up. The device was therefore allowed a run-up over a distance of 1.2 m. Jollbot was able to roll up a step of 44 mm. The increase to 52 mm proved too high for Jollbot to overcome. It should be

noted how much the outer sphere of the device was able to deform when overcoming a step. This deformation allows the centre of gravity of the device to get closer to the edge of the step than would be possible with a rigid outer sphere.

Figure 193 – Jollbot rolling over a step

6.5.2.4 Power consumption during rolling

The power consumption during rolling was determined by driving and steering the device in the laboratory for fifteen minutes repeatedly around a four corner course of 7 m in length. The course varied in width between 1 m and 1.5 m and was littered with numerous obstacles to become caught upon. The current was measured using a USB datalogger (Measurement Computing PMD-1208LS) and standard equations applied to determine that Jollbot 3b consumed an average of 2.4W during smooth surface rolling operations. A typical two minute capture is given in Figure 194 shown with a moving-average power consumption over a three second period.

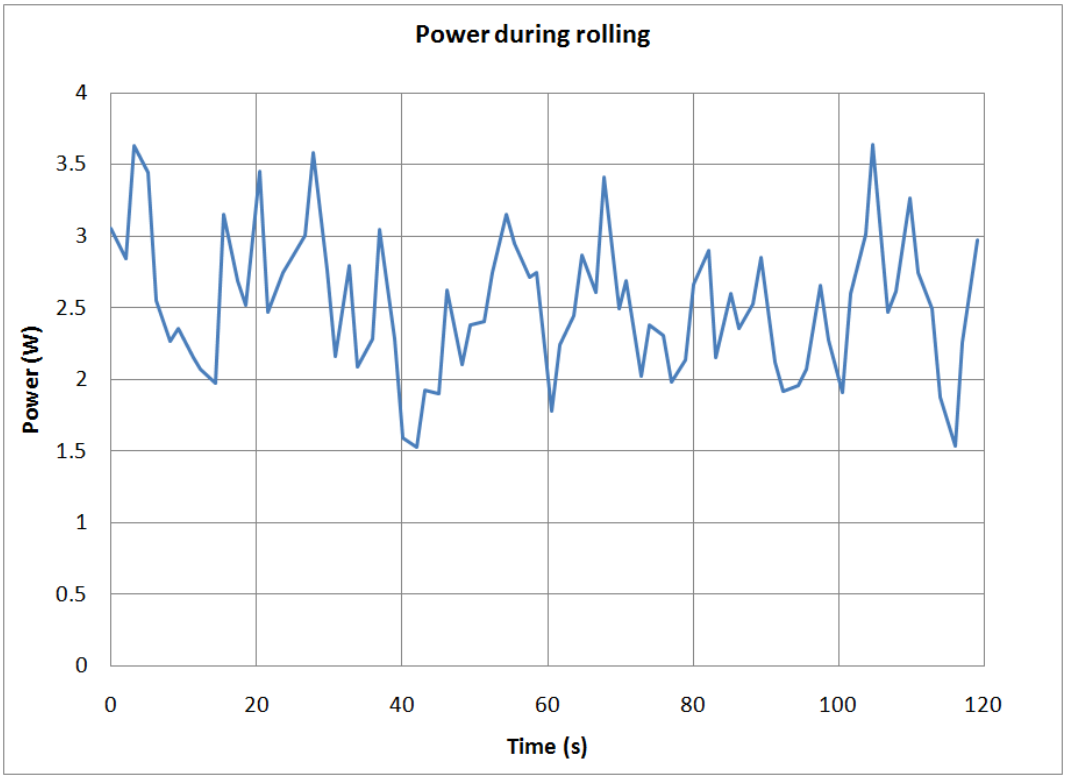

Figure 194 – Power consumption during rolling

An additional result of this test also produced an in-use speed of around only 1 m/min (0.017 m/s). This is much slower than the peak rolling speeds recorded earlier (see Section 6.5.2.1), but gives a better representation of actual capability in a smooth environment filled with obstructions. The complexity of route, and numerous obstacles, illustrated the difficulty of accurately controlling such a device indoors. However, the average rolling speed in larger open spaces was expected to be substantially faster.

6.5.2.5 Rolling performance summary

Rolling Speed	Slope Climbing Ability	Step Climbing Ability	Power Consumption
0.7 m/s	4°	44 mm with run-up	2.4 W

Table 30 – Jollbot3 rolling performance summary

6.5.3 Outdoor environment multimodal experiments

To give an overall impression of Jollbot 3b's multimodal capabilities, the device was tested in a pair of outdoor environments. These included a level and open grass field scattered with trees Figure 195, and a multi-terrain rock garden Figure 196.

Figure 195 – Grass testing area

Figure 196 – Rock garden testing area

Movement across wide open areas such as a grass field, would rely entirely on the rolling capability of Jollbot. The main aim of such a test was to qualitatively evaluate the devices ability to roll in a straight line over long distances, and the steering capability when required. At slow speeds, and therefore while accelerating, the device moved in a far from linear path until sufficient momentum and gyroscopic stability was achieved. This was evident during indoor testing (see Section 6.5.2.4) where insufficient space was available to create gyroscopic stability. In open spaces, after this stability had been achieved, tens of meters could be covered with little steering control input. The speed of the response to steering inputs immediately made Jollbot 3b far easier to control than Jollbot 3a. However, the near-spherical form of the contact patch made stable straight-line control difficult, with the device tending to make a turn in one direction or the other. A wider, more rectangular contact patch would improve this stability (see Section 7.8.1.2).

The rock garden multi-terrain test route consisted of rolling down a sloping path over a series of steps of different heights spaced at varying intervals, before moving across a

flat paved area toward a collection of rocks onto which Jollbot would jump. The entire scene was captured on video from a tripod mounted handheld KonicaMinolta X50 digital camera and is available to view on the attached DVD.

The device was remotely controlled throughout the test with no manual input apart from at the changeover between rolling and jumping. As the simple Acoms radio control system used was capable of controlling only two channels at a time, Jollbot's three motors could not all be used simultaneously. Therefore the rolling phase had the abilities of only the powered-rolling motor and the rolling-direction-control motor. The jumping phase included the use of only the compression-motor and the mass-attachment motor (also known as the rolling-direction-control motor). Owing to the much improved jumping performance after the central axle had been removed, the decision was made to remove it at the point of changeover between rolling and jumping. Obviously removing the axle could not occur during a remote mission, but with future design improvements the friction issues between the central axle and mechanism could be reduced (see Section 7.8.1.2), or the axle could be designed out completely (see Section 7.8.2.2). For the sake of a proof of concept, it was felt that removing the axle was justifiable.

When rolling downward over steps, Jollbot moved very much in the prevailing direction of the sloping path, whether the main axle was parallel to the ground or not. Jollbot dealt with the impacts with the ground after each step and showed no signs of damage after negotiating all three steps and colliding with a rock. Progress was negligible for almost five minutes when Jollbot became stuck in a depression in the path that had raised areas on three sides. Jollbot eventually managed to recover itself after multiple rolling and steering attempts. Escape may have been quicker if the compression motor could have been driven to adjust the shape of the device – including performing a jump. It was clear during this incident that the amount of position monitoring, sub-system state observation (particularly the orientation of the anti-tangle mechanisms), and control that was carried out by the human operator, would make it difficult to automate Jollbot as a multi-terrain robot without additional mechanical optimisation. However, remotely controlled operation had been achieved.

Figure 197 – Jollbot 3b readying itself for a jump.

Once rolling to a stop at the jump site (Figure 197), Jollbot was manually changed over to a jumping configuration. The main axle was removed and the rolling-motor was disconnected in favour of the compression-motor. The device was left to compress under battery power alone before it automatically released its stored energy as a jump. Owing to the close to vertical take-off trajectory of Jollbot (see Section 6.5.1.8), it failed to jump up onto the rock obstacle. It did achieve sufficient height to land on the surface of the rock, but the outer sphere collided with the top edge as it descended, and therefore it tumbled backward off the rock.

These outdoor tests provided a proof of concept for a multimodal spherical jumping and rolling device. However, substantial performance improvements would be needed before Jollbot could be considered as a useful remotely controlled robotic platform. Although Jollbot 3b makes significant improvements over Jollbot 2, a future Jollbot 4 would require a similar step change.

6.6 Jollbot 3b evaluation

Jollbot 3b did perform useful jumps (in certain configurations) and was able to roll under its own power in the direction a user intended. Like previous prototypes, Jollbot 3b jumped by storing energy in its outer structure thus amplifying the low-

density electrical energy into a useful form for explosive release as a jump. Compared to Jollbot 2, Jollbot 3b accelerated its “head” through a much larger distance (around 70 % of its diameter). Jollbot 3b had a maximum ratio of accelerated (“head”) to trailing (“foot”) mass (2.1:1) as there were no components that could moved from the trailing mass to the accelerated mass. However, conventional engineering optimisation and material selection would provide small improvements. The catch mechanism did operate as expected, constraining the stored strain energy in the sphere, although it was far from reliable and would not automatically reset after a successful release. Jumping from either pole was possible with Jollbot 3b, but the performance from one side was far greater than the other due to the routing of the compression-thread. Due to Jollbot’s already significant weight, the effect of additional payloads (up to a point), did not damage the jumping performance substantially. Jollbot’s compliant outer surface isolated the central control mechanism from numerous landing and tumbling impacts. Passive rolling was possible as a function of the spherical form, but the working and steerable active rolling ability was the major achievement of this prototype, especially considering it was complemented by some jumping capability.

Chapter 7 Discussion and Conclusions

The aim of this work was to produce a prototype of a single structure remotely-controlled multimodal jumping and rolling device. The evolution of such a device has been presented in this thesis through a series of iterative prototypes. An initial evaluation of each prototype was presented at the end of the appropriate chapter making some mention of the considerations for subsequent versions. However, a full comparison between the three Jollbot devices and existing rough terrain rovers has not yet been included. Such a comparative evaluation has been made possible using the scoring system presented in Chapter 3. In addition an evaluation of the jumping capability of each prototype was made possible using the chart presented in Section 2.6.7.6 (Figure 63).

Firstly a summary of the performance of each prototype is required (Table 31). These details enabled the three prototypes to undergo Step 5 of the scoring system (Steps 1-4 occurring in Section 3.7). The final scores are shown in Table 32 and Figure 198.

	Jollbot 1	Jollbot 2	Jollbot 3b
Mass	315 g	465 g	853 g rolling 820 g or 763 g jumping
Diameter	0.3 m	0.3 m	0.58 m
Sphere stiffness	~300 N/m	~500 N/m	~75 N/m
Compressed through	~21% (64 mm)	~22% (65 mm)	~68% (380 mm)
Strain energy stored	0.6 J	1.1 J	6.5 J (7.5 J inc band)
Electrical power required (jump/roll)	-	5.76 W / -	1.24 W / 2.4 W
Consumed electrical energy per jump	-	8.3 J	1400 J
Cleared jump height	50 mm (est.)	184 mm	449 mm
Height through which Centre of gravity is raised	15 mm (est.)	218 mm	686 mm
Potential energy at peak height	0.05 J	0.92 J	5.52 J
Efficiency of release mechanism	7%	84%	73%
Approximate ratio of accelerated to trailing mass during jumping	5.7:1	7.1:1	2.1:1 / 2.7:1
Force/mass ability of mechanism	70 N/kg	93 N/kg	67 N/kg
Range of jump	0 m	0 m	1 m at 70°
Time between jumps	~1 s	~2 s	~1200 s
Load carrying capability	No	No	0.25 kg
Powered rolling capability	No	No	yes (0.7 m/s, 4° slopes, 44 mm steps)
Evaluation score	-38	-21	52

Table 31 – Performance summary of Jollbot prototypes

Robot	Score	Certainty %	Type
Jollbot Proto3	**52**	**93.8**	**Multimodal**
University of Bath Glumper	50	75.0	Jumping
Sandia Hopper	35	68.8	Jumping
Jumping Miniwhegs	30	81.3	Multimodal
JPL Hopper Gen3	21	68.8	Jumping
Minnesota Scout	17	81.3	Multimodal
Boston Dynamics Big Dog	13	81.3	Walking
EPFL Miniature Jumping with cage	11	75.0	Jumping
iRobot Warrior 710	9	87.5	Tracked
EPFL 7g Miniature Jumper	6	68.8	Jumping
Sandia Ratler II Rover	1	87.5	Wheeled
Ritsumeikan University Deformable Sphere	0	62.5	Multimodal
iRobot Packbot 510 FasTac	-4	87.5	Tracked
RoboMotio Inc. STRV Defence R&D Canada	-8	50.0	Tracked
Utah Monopod	-12	68.8	Jumping
Foster Millar Talon	-16	81.3	Tracked
Redback	-19	81.3	Tracked
Jollbot Proto2	**-21**	**93.8**	**Jumping**
Bluebotics Shrimp	-27	75.0	Wheeled
Rhex (2001 version)	-31	62.5	Walking
ESA Prolero	-31	62.5	Walking
Jollbot Proto1	**-38**	**93.8**	**Jumping**
IMPASS Virginia Tech	-39	43.8	Walking
Tehzeeb	-39	62.5	Tracked
Sprawlita	-44	62.5	Walking
ROBHAZ-DT3	-44	75.0	Tracked
Activrobotics P3-AT	-45	81.3	Wheeled
CMU Corky	-46	56.3	Wheeled
OT4 Omnitread (UofMichigan)	-46	93.8	Serpentine
Dante II Carneige Mellon	-52	75.0	Walking
ESA ExoMars	-53	75.0	Wheeled
University of Tokyo Mowgli	-60	56.3	Jumping
OT8 Omnitread (UofMichigan)	-63	81.3	Serpentine
NASA Pathfinder Sojourner Rover	-67	56.3	Wheeled
IMT Grillo	-73	50.0	Jumping
Kagoshima Pendulum Jumper	-74	43.8	Jumping
NASA MER Spirit and Opportunity	-78	68.8	Wheeled
Tokyo Institute Airhopper	-93	75.0	Jumping

Table 32 – Scores for proposed exploration application

The scores for the three Jollbot prototypes were, -38, -21 and +52 respectively.

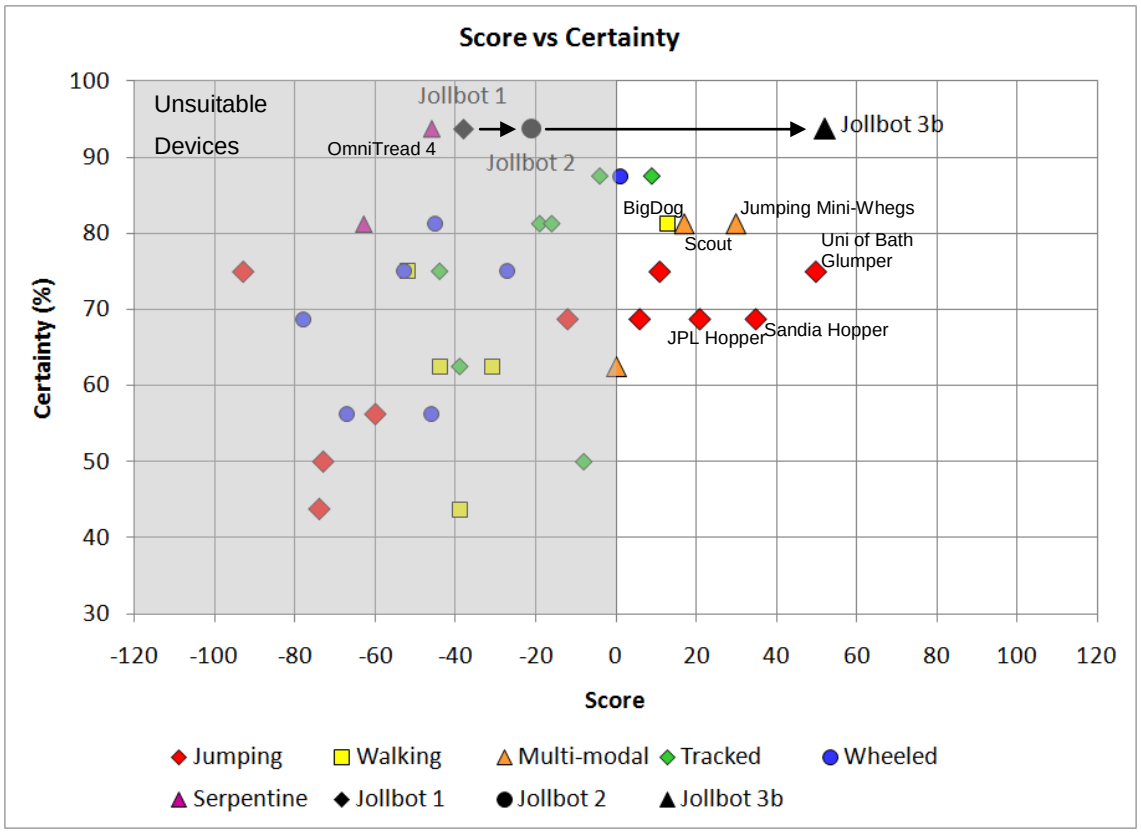

Figure 198 – A visual representation of the scores and certainty for all robots for proposed exploration application. The three Jollbot prototypes are labelled separately.

7.1 Jollbot 1 score

Jollbot 1 certainly did not meet the needs of the proposed application as it achieved a score of -38. The certainty of the score was high given the detail available. However, it was not 100%, and this came from the earlier assumption that jumping robots would be able to climb a 20° slope with repetitive jumps (this actually resulted in a negative category-score due to the 30° requirement from the application). In Jollbot 1's case this slope climbing ability was very unlikely to be true unless a very large number of jumps and lengthy time were available. However, to conform to the previous evaluation assumptions it remained. The score did suggest that Jollbot 1 outperforms some existing rough terrain devices. That was due to the remaining positive score points

resulting from its spherical shape's inability to fall over, its inexpensiveness, and its robustness resulting from simplicity. It should be noted though that the low score certainty of those devices scoring less than Jollbot 1 could result in a significant number achieving greater scores as more details become known.

When compared to the three multimodal devices, Jollbot 1 scored less than the least capable. However, Jollbot 1 was not a working multimodal device and as such should only really be compared with other jumping devices. Four of these performed equally as badly given their limitations (low jump height, tethered air supplies etc.). However, most more-evolved battery-powered jumping devices performed substantially better due to increased obstacle surmountability and jumping range.

7.2 Jollbot 2 score

Evaluating the performance of the second prototype resulted in a score of -21. Therefore, Jollbot 2 did not meet the needs of the proposed application. It did however score 17 more points than Jollbot 1 due to its ability for jump direction control. The improvement in obstacle surmountability (jump height) was not significant enough in itself to lead to an improved score. The main places where additional points could further be obtained were in the areas of jump height and jump range, and overall speed and range.

Jollbot 2 did not make a significant enough improvement over Jollbot 1 to compete with the multimodal devices – the closest is twenty-one points better. However like Jollbot 1, Jollbot 2 was not truly multimodal having an inoperable rolling ability. When compared to the other jumping devices, Jollbot 2's performance was less than average. When compared with all the other modes of movement, Jollbot 2 scored better than the average wheeled or walking robot, and achieved close to the average of the tracked robots.

7.3 Jollbot 3b score

Evaluating the third prototype with the scoring system gave a value of +52. As a score of zero would exactly meet the requirements of the proposed application, then it

appears this version did exceed that. This score was much better than the -38 and -21 achieved by the previous Jollbot prototypes. Jollbot 3b achieved the highest score of all devices, with a pair of jumping robots separating it and the best multimodal robots. It must be remembered that this score was very user-subjective and it may not reflect its true any-eventuality performance, particularly if the application definition, weighting, and value-assignment, were to change, even if only slightly (a study of how the score varies with a random assignment of weights follows the evaluation of the scoring system in Section 7.6). The main score improvements above the other Jollbot prototypes came from the fact that there was range to its jumps, and from the speed of movement coming as a result of its rolling ability and its multi-modal operation. Jollbot 3b was far from a fully optimised solution so future generations of Jollbot have potential for improved scores. Section 7.8 will discuss possible future developments and research directions.

Throughout the testing of Jollbot 3b some performance measures were produced in specific circumstances. For example removing the central axle gave the best jumps, and jumping from an inclined plane produced range. If the jump height with the central axle in place as designed was considered then it would score 10 points fewer. If no range to the jump were considered then it would lose a further 10 points. Perhaps the certainty of Jollbot 3b's score should be revised given these specific circumstances.

For additional assessment, Jollbot 3b's ability has been evaluated against the three example applications from Chapter 3. From a cursory evaluation of its actual performance compared to existing devices, it was expected that Jollbot would score reasonably well for the first example application of rough terrain exploration, but would not be the best robot. Jollbot was unlikely to meet the requirements of the military application due to its slow speed and inability to carry a large payload, but should provide a good fit to the farming/environmental example application. Jollbot 3b's scores for the three example applications are shown in Figure 199, Figure 200 and Figure 201 and tabulated below (Table 33).

Rough terrain exploration	Military	Environmental surveying
42	0	74

Table 33 – Jollbot 3b's scores for example applications presented in Chapter 3

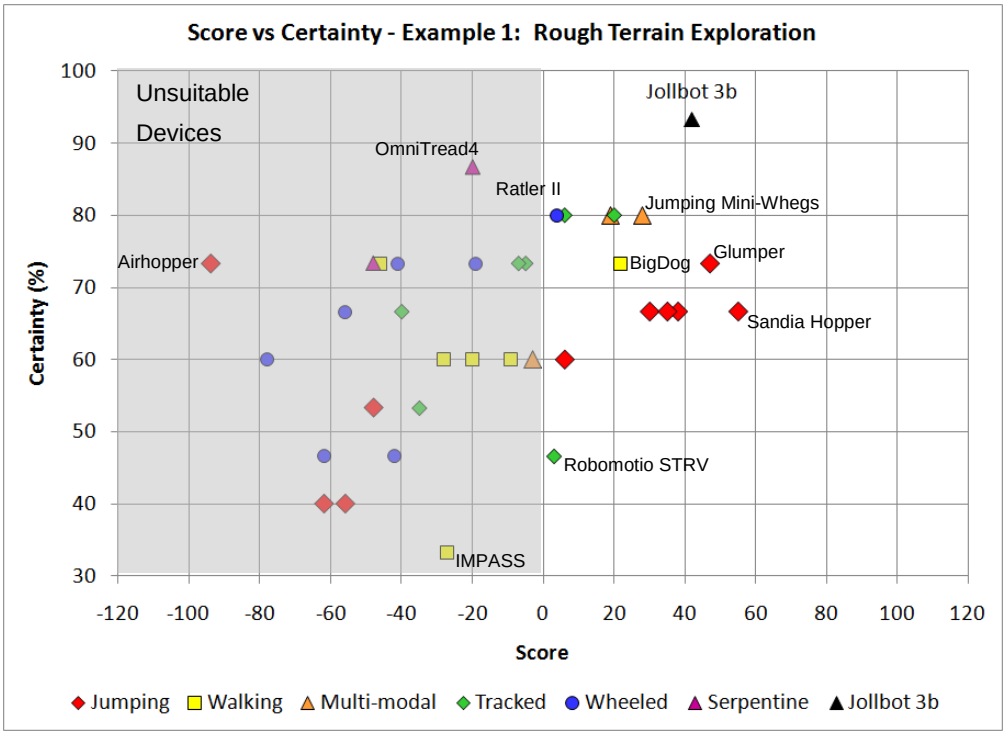

Figure 199 – Jollbot 3b achieves a score of 42 for the first example application in Chapter 3

Jollbot 3b scores well for the first example application of rough terrain exploration. This was not unexpected as the example closely resembles the selected application. Jollbot 3b compares well with some of the jumping robots and beats all of the other multi-modal devices.

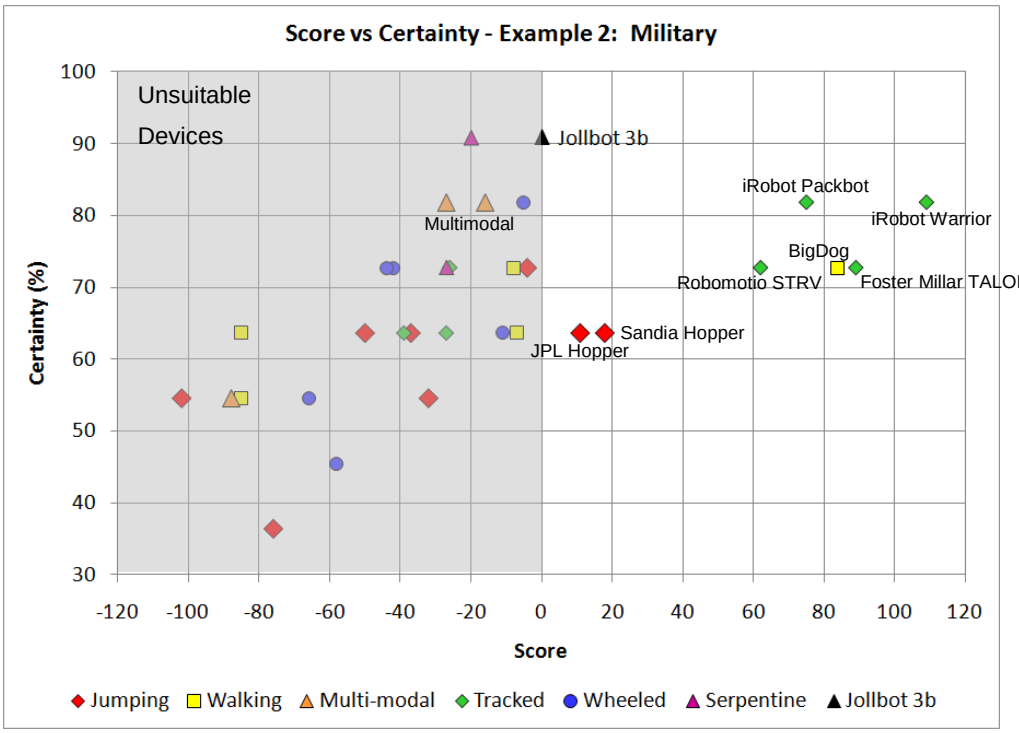

Figure 200 – Jollbot 3b achieves a score of 0 for the second example application in Chapter 3

Jollbot achieves a score of zero for the military example application. This suggests that it meets the minimum requirements although it is far from the highest scoring.

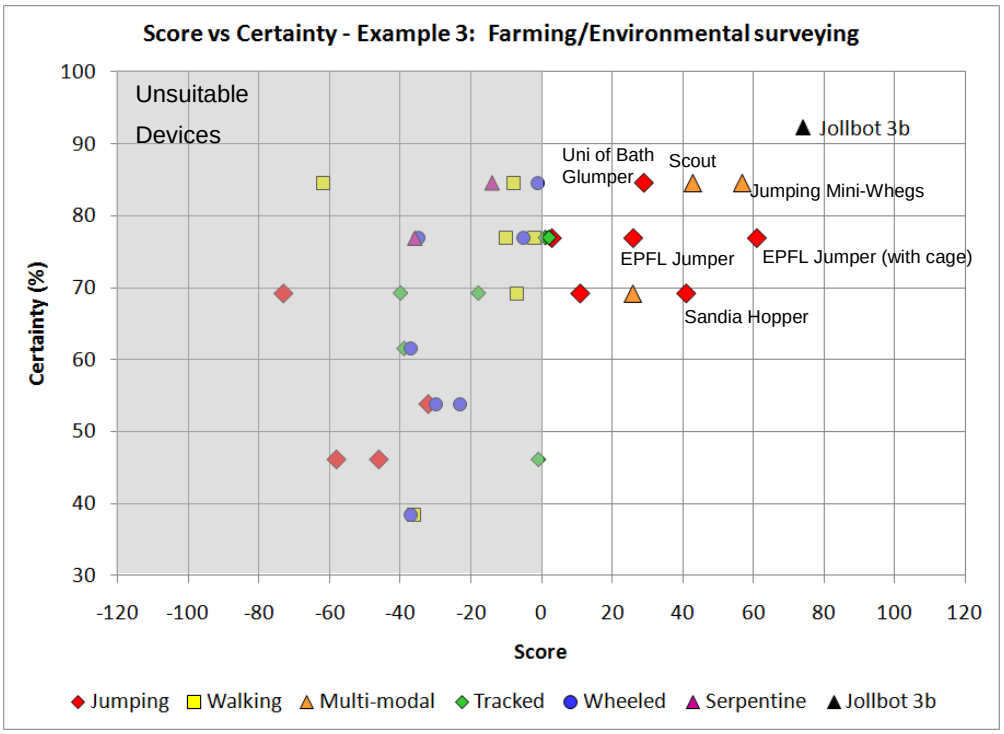

Figure 201 – Jollbot 3b achieves a score of 74 for the third example application in Chapter 3

Jollbot achieves the highest score for the environmental surveying example application. This is unsurprising due to its low cost and adequate rather than extraordinary movement abilities.

7.4 Jumping evaluation

In addition to the new scoring system, the three prototypes of Jollbot could be added to the jumping diagram from Section 2.6.7.6. This specifically illustrates only the improvement in jumping capability between prototypes (Figure 202). In each case it was the change in height of the centre of gravity that was used as the jump height, and particularly in Jollbot 3b's case due to its very changeable shape, this could substantially overestimate the true jumping "performance".

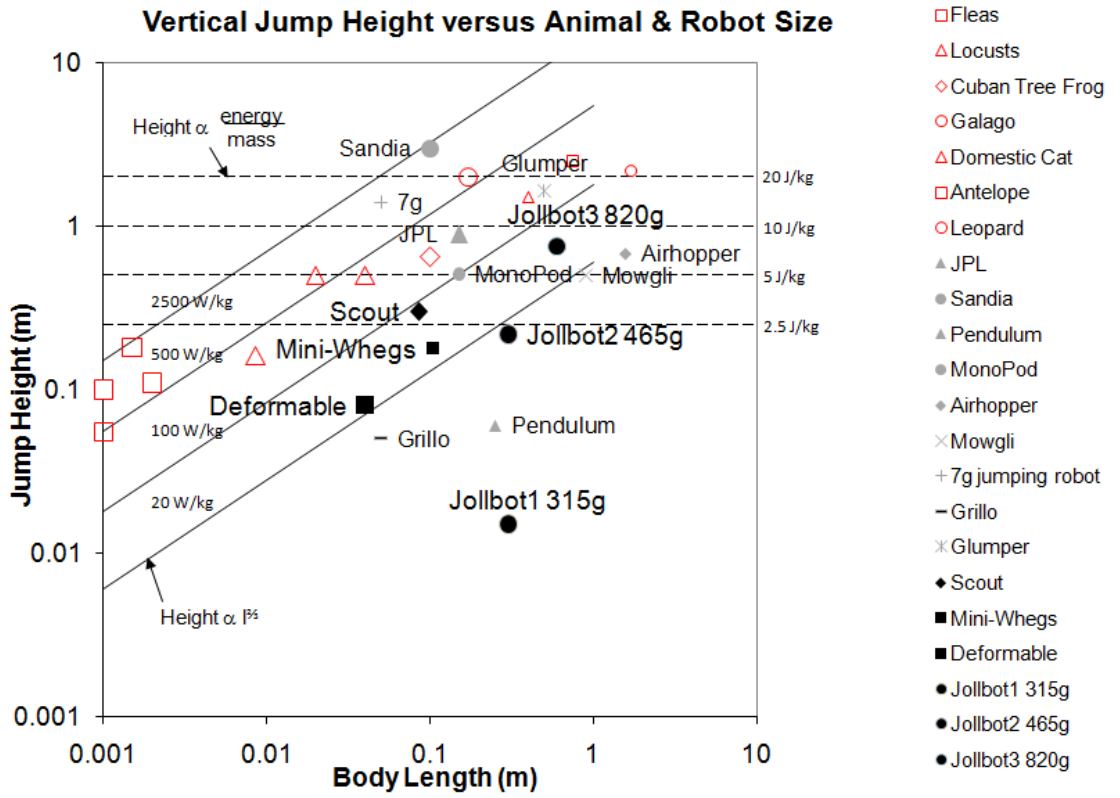

Figure 202 – Jollbot prototype jumping comparison. Animals have outline markers with robots having solid markers. Jollbot prototypes are labelled with their masses. Other multimodal devices are also highlighted with enlarged labels and heavy markers.

Figure 202 shows a substantial improvement in apparent energy density between Jollbot 1 and 2 resulting in a large increase in jump height. The graphic does not adequately show that there is an increase in mass (of ~50 %) at the expense of this improvement in height, so should be read with some discretion. The improvement between Jollbot 2 and 3b is not so marked, although more height is achieved through improving the energy capacity, this comes at the expense of increasing size and mass (by ~70 %). If mass rather than "body length" were considered in this illustration then Jollbot 2 and 3b would likely lie on similar power density lines. However, Figure 202 does not illustrate the fact that Jollbot 3b had an additional and entirely working powered rolling capability.

Comparing Jollbot 3b's jumping ability with that of other jumping devices results in fairly good equivalent performance. The energy density is similar to the majority of the jumping devices, although the apparent power density is less due to the additional size. However, as Jollbot prototype 3b was a multimodal device, it should be expected that it didn't achieve the best jumps outright. It did perform jumps higher than any of the other multimodal devices, but is substantially larger.

7.5 The usefulness of multimodal movement

To make comparisons between Jollbot 3b and the existing multimodal devices, a summary table of their performances has been produced (Table 34). As before, some entries have been assumed or estimated from video. In addition, scores are also shown; including the achieved scores if one entire mode of movement was missing. It is important to consider details such as that direction control may be a result of only one mode, and can therefore only contribute to one uni-modal score. The performances of each mode individually are based on the published results for a multimodal device. For example, they cannot take into account the possibility of improved performance from a reduced mass with unused components removed. If these devices were redesigned as single mode devices then their uni-modal scores may be better.

		Robot	Independent structures		Single structure	
			Jumping Mini-Whegs	Scout	Deformable	Jollbot 3b
Performance	Size	L (m)	0.104	0.085	0.09	0.59
		H (m)	0.05	0.05	0.09	0.59
		W (m)	0.076	0.11	0.09	0.59
	Mass (kg)		0.191	0.2	0.05	0.8
	1st Mode (jumping)	Speed (m/s)	0.003	0.025	0.0025	0.0008
		Obstacle jumped (m)	0.2	0.3	0.18	0.449
		Jump range (m)	0.1	0.25	0.01	1
	2nd Mode	Speed (m/s)	0.9	0.31	0.009	0.69
		Obstacle climbed (m)	0.04	0	0	0.044
		Gap range (m)	0.05	0.017	0.03	0.05
		Slope (°)	20	20	10	4
	Control		Remote	Remote	Tethered	Remote
	Scores	**Multimodal**	**30**	**17**	**0**	**52**
		1st Mode only	**-36**	**-39**	**-26**	**20**
		2nd Mode only	**4**	**-29**	**-28**	**-6**

Table 34 – Multimodal devices with estimated and assumed values highlighted (Hirai, Matsuyama & Nakanishi 2007; Lambrecht, Horchler & Quinn 2005; Stoeter, Burt & Papanikolopoulos 2003)

The performance measures in Table 34 show that Jollbot was considerably larger than the other multimodal robots. It was also much slower when jumping due to the lengthy time taken to store strain energy in its outer sphere. However, its open area rolling speed was comparable and the jump height and range were substantially larger.

Where only one movement or the other was available, the scores show that some devices meet the requirements of a general exploration task. Whegs when walking, and Jollbot 3b when jumping, both achieve scores above zero. The same isn't true of the other devices: the Deformable device having a negative or zero score in all cases and the Scout only achieving a positive score when multimodal. Comparing the multimodal scores with the single mode scores for the four devices does illustrate that combining two movements within one device offers an improvement in performance, as their scores are largest in that configuration.

Whether the structures used to achieve these movements should be separate mechanisms, or integrated in a single structure, is impossible to determine given the scores and small sample size, but the difference appears small. Certainly in Jollbot 3b's case, the challenges involved with achieving two movements from one structure required additional mechanisms and motors just as using a separate structure would. Although the spherical structure of the jump storage device also makes up the rolling surface, the mechanisms within had to achieve two functions: firstly to compress the sphere for jumping, and secondly to move its centre of gravity around as much as possible, to enable rolling and jump direction control. This was achieved with a single dedicated motor for compression and two additional motors that translated and rotated the centre of gravity along and around the polar axis of the sphere. There was no provision to adjust the position of the centre of gravity radially, and that would have had a big impact on the rolling ability, particularly with obstacles and slopes.

Unlike the other multimodal devices, it is possible to predict what changes the device might undergo if Jollbot 3b could only jump – "Jumpbot" perhaps. Enough detail is known of the components that are only used to enable rolling that a thought experiment can be conducted to evaluate the uni-modal performance. Jollbot 3b was carefully designed such that there were very few components dedicated to only one type of movement – the possible exceptions being the central axle (57 g) and anti-tangle mechanisms (44 g). Through more complex drive mechanisms it could be possible to remove one of the motors (60 g) enabling a single motor to control sphere compression and the other motor to control both head-attachment and direction control. With ruthless weight saving and component optimisation it is anticipated that a total of around 200 g could be saved from the overall weight of the device – thus resulting in a jumping only device weighing ~620 g. This would equate to an increase in jump height of 30 % assuming similar levels of energy loss when released (25 %). The scoring system gives a hypothetical uni-modal "Jumpbot" a score of 30: 10 points more than Jollbot 3b if it were only able to jump.

Similarly with only a rolling ability, a hypothetical "Rollbot" would lose the compression motor (60 g) and the anti-tangle mechanisms (44 g). However since a reduction in mass of the central mechanism is not desired for improved rolling ability, it is likely that

additional masses would subsequently be added to “Rollbot”. Other than additional mass, the main difference from Jollbot 3b would be a large increase in the distance of the centre of gravity away from the centre of the sphere, which would improve slope climbing ability and obstacle surmountability in that mode. Speculating that the mass of “Rollbot” would rise to 10kg, that slope climbing ability could be improved to 20°, and that obstacles of 1/5th sphere diameter and gaps of 1/3rd diameter could be overcome, would result in a score of -4 (slightly better than the original -6 when Jollbot 3b is only rolling).

These two thought experiments indicate the differences between the suitability for rolling and the suitability for jumping for the proposed rough terrain exploration application. Rolling as a mode of movement cannot be considered suitable for rough terrains. Jumping however can be considered suitable. A multimodal jumping and rolling device may not give huge benefits for the selected application, but the possibilities for other applications is far wider than those available to uni-modal equivalent devices.

7.6 Evaluation of the scoring system

The development of a scoring system to compare mobile robots was an aim of this work from the outset. The three examples appearing in Chapter 3 go some way to prove its usefulness. But now it is possible to compare the performance score generated by the evaluation method with the perceived actual abilities of the three prototype Jollbots. Without the scoring system, cursory evaluation would suggest that the first two prototypes appear unsuitable to the proposed exploration application. Jollbot 1 particularly achieved little useful forward movement and only a very small cleared jump height. The scores suggest that Jollbot 1 had a similar performance to a tethered walking device, IMPASS, and a tracked robot, Tehzeeb. It was better than the serpentine devices and a whole series of wheeled robots. This includes the most well known and successful robots – the NASA Mars Exploration Rovers. As some movement ability and direction control is critical to any mobile rover, in practice Jollbot 1 was most certainly not as capable as any of those devices. This perhaps indicates that the scoring system for the proposed application was overly generous to

inexpensiveness, small size and light weight, and gave too little consideration to actual movement ability. Jollbot 2's jumping ability meant that in practice it did not compare well with the performance of the devices achieving similar scores. The wheeled Bluebotics Shrimp and tracked Redback achieve scores either side of Jollbot 2, but in practice it is thought that both are far more capable in rough terrains. Jollbot 3b did have some useful ability and scores very well. However, when practically considered, Jollbot 3b's movement ability in the rock garden multimodal test (see Section 6.5.3) would be easily exceeded by one of the military tracked robots. Since the application specific scoring is compiled from so many different factors, including a deliberately highly-weighted multimodal requirement, it is difficult to confirm whether the system produces reasonable scores without fully testing each device on a suitable course reflecting the exact application.

Applying the scoring system to other mobile robots would provide the possibility of evaluating any of them. However, within each stage of the scoring system are possibilities for improvement. The first step, where a table of performance is produced, reports only those properties that relate to rough terrain ability. Most of the devices included in Step 1 were designed for rough terrain applications and no inclusion is made of those devices suitable for smoother surfaces. Improving the detail of the table produced would help, and this could be carried out by questioning each research group as to a device's particular abilities and traits. The production of Table 4 was a time consuming process, and to apply the scoring system to another type of application would require a similar effort. This may discourage future users of the scoring system. Defining the application in Step 2 requires that only the available factors from Step 1 are included. If a user's requirements stated that the device must be able to withstand 300 °C, then temperature tolerance for all the devices would need to be determined in Step 1. The assignment of weights (Step 3) and the grading of category-values (Step 4) are both very user-oriented and are therefore open to bias. Having those steps carried out by a series of individuals, or after consultation across a team would produce more reliable results.

It is possible to quickly give some indication as to the influence of the assignment of weights in Step 3 using a selection of random weightings. Two sets of sixteen random

weights totalling 100 were assigned at to the categories (Table 350) and result in the scores shown in Table 36 and Figure 203, and Table 37 and Figure 204.

Category	Random Weights 1	Random Weights 2
Size smaller than $(0.5m)^3$	4	5
Mass under 10kg	9	8
Direction control	11	8
Obstacle height cleared 0.5m	6	6
Gap cleared 0.25m	4	8
Slope capability of 30°	10	10
Un-toppleable (self-righting yes/no)	5	2
Speed ~1m/s	9	2
Modes of movement (>1 gives more possibilities)	3	4
Cost (<$1000)	2	6
Payload over 0.25kg	8	5
Robust (yes/no)	9	6
Control type (remote minimum)	4	8
Must use batteries (yes/no)	5	6
Range >2km	9	7
Lifetime >4hrs	2	9

Table 35 – Random assignment of category weights for an exploration application

Robot	Score	Certainty %	Type
iRobot Warrior 710	67	87.5	Tracked
iRobot Packbot 510 FasTac	52	87.5	Tracked
Boston Dynamics Big Dog	50	81.3	Walking
Foster Millar Talon	44	81.3	Tracked
RoboMotio Inc. STRV Defence R&D Canada	43	50.0	Tracked
Jumping Miniwhegs	28	81.3	Multimodal
Jollbot Proto3	16	93.8	Multimodal
Sandia Hopper	10	68.8	Jumping
Sandia Ratler II Rover	5	87.5	Wheeled
JPL Hopper Gen3	1	68.8	Jumping
Rhex (2001 version)	0	62.5	Walking
Minnesota Scout	0	81.3	Multimodal
Activrobotics P3-AT	-2	81.3	Wheeled
University of Bath Glumper	-3	75.0	Jumping
Redback	-6	81.3	Tracked
EPFL Miniature Jumping with cage	-7	75.0	Jumping
EPFL 7g Miniature Jumper	-19	68.8	Jumping
Bluebotics Shrimp	-19	75.0	Wheeled
ESA Prolero	-21	62.5	Walking
OT4 Omnitread (UofMichigan)	-26	93.8	Serpentine
ESA ExoMars	-27	75.0	Wheeled
Ritsumeikan University Deformable Sphere	-31	62.5	Multimodal
Utah Monopod	-33	68.8	Jumping
ROBHAZ-DT3	-35	75.0	Tracked
NASA Pathfinder Sojourner Rover	-36	56.3	Wheeled
Dante II Carneige Mellon	-37	75.0	Walking
Tehzeeb	-38	62.5	Tracked
CMU Corky	-41	56.3	Wheeled
Jollbot Proto2	-42	93.8	Jumping
NASA MER Spirit and Opportunity	-43	68.8	Wheeled
IMPASS Virginia Tech	-53	43.8	Walking
Sprawlita	-56	62.5	Walking
Jollbot Proto1	-62	93.8	Jumping
OT8 Omnitread (UofMichigan)	-64	81.3	Serpentine
IMT Grillo	-78	50.0	Jumping
University of Tokyo Mowgli	-82	56.3	Jumping
Kagoshima Pendulum Jumper	-91	43.8	Jumping
Tokyo Institute Airhopper	-120	75.0	Jumping

Table 36 – Scores for robots for a randomly weighted (1) exploration application

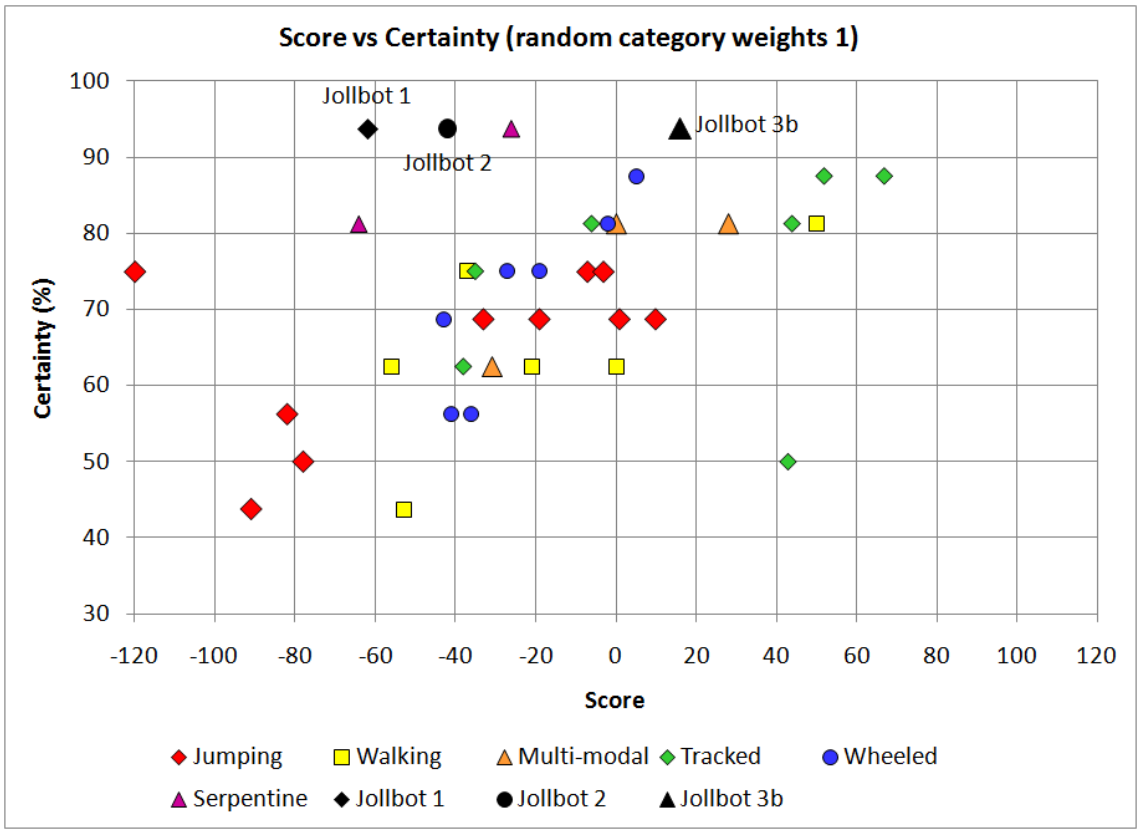

Figure 203 – Illustration of scores for randomly weighted (1) exploration application

Robot	Score	Certainty %	Type
Sandia Hopper	44	68.8	Jumping
JPL Hopper Gen3	37	68.8	Jumping
iRobot Warrior 710	32	87.5	Tracked
Jumping Miniwhegs	30	81.3	Multimodal
iRobot Packbot 510 FasTac	23	87.5	Tracked
Jollbot Proto3	22	93.8	Multimodal
Boston Dynamics Big Dog	20	81.3	Walking
Foster Millar Talon	18	81.3	Tracked
University of Bath Glumper	13	75.0	Jumping
EPFL 7g Miniature Jumper	10	68.8	Jumping
RoboMotio Inc. STRV Defence R&D Canada	10	50.0	Tracked
EPFL Miniature Jumping with cage	5	75.0	Jumping
Minnesota Scout	5	81.3	Multimodal
Sandia Ratler II Rover	2	87.5	Wheeled
Utah Monopod	-3	68.8	Jumping
Ritsumeikan University Deformable Sphere	-10	62.5	Multimodal
Activrobotics P3-AT	-10	81.3	Wheeled
Rhex (2001 version)	-14	62.5	Walking
ESA ExoMars	-14	75.0	Wheeled
Bluebotics Shrimp	-15	75.0	Wheeled
Redback	-17	81.3	Tracked
OT4 Omnitread (UofMichigan)	-19	93.8	Serpentine
NASA Pathfinder Sojourner Rover	-20	56.3	Wheeled
ESA Prolero	-21	62.5	Walking
CMU Corky	-22	56.3	Wheeled
IMPASS Virginia Tech	-26	43.8	Walking
NASA MER Spirit and Opportunity	-28	68.8	Wheeled
Dante II Carneige Mellon	-30	75.0	Walking
Sprawlita	-32	62.5	Walking
OT8 Omnitread (UofMichigan)	-34	81.3	Serpentine
University of Tokyo Mowgli	-38	56.3	Jumping
Jollbot Proto2	-38	93.8	Jumping
Tehzeeb	-42	62.5	Tracked
Jollbot Proto1	-45	93.8	Jumping
ROBHAZ-DT3	-49	75.0	Tracked
Kagoshima Pendulum Jumper	-55	43.8	Jumping
IMT Grillo	-66	50.0	Jumping
Tokyo Institute Airhopper	-88	75.0	Jumping

Table 37 – Scores for robots for a randomly weighted (2) exploration application

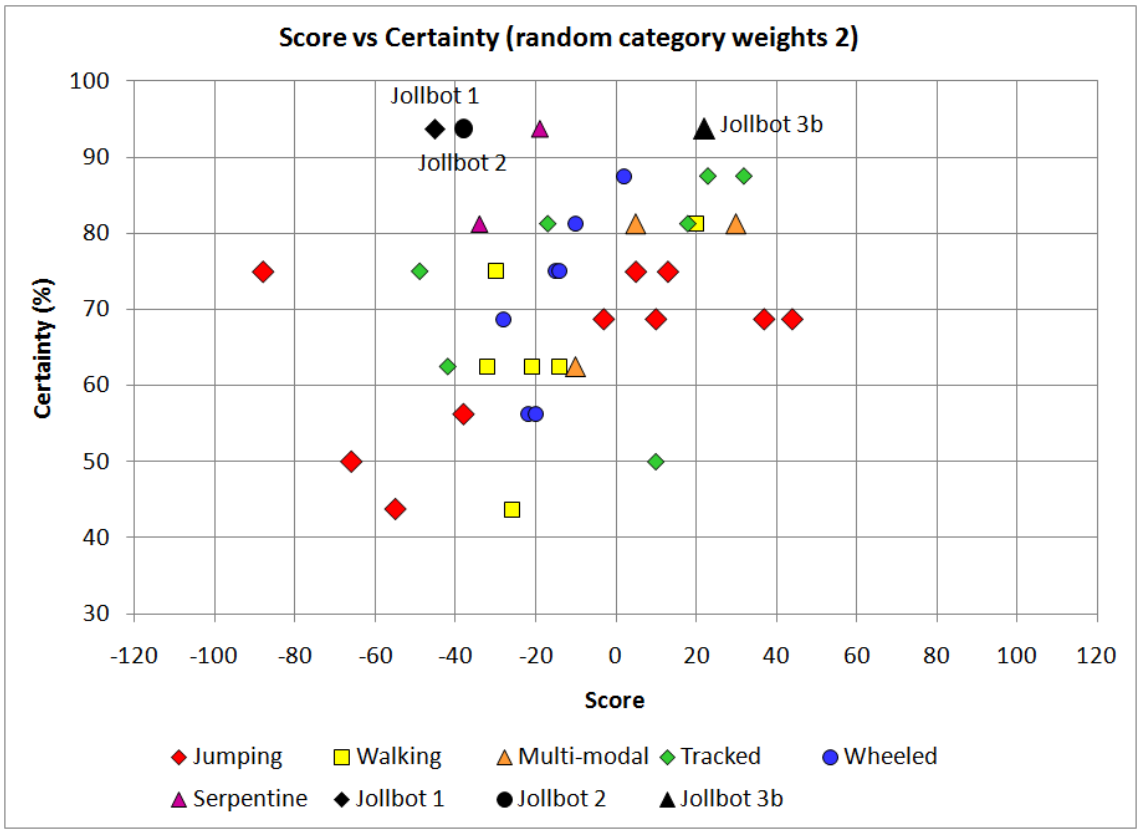

Figure 204 – Illustration of scores for randomly weighted (2) exploration application

The scores generated from random weighting assignment produces quite a different series of scores from those in Table 32 (p.297). The first random assignment favours fast, robust, and long ranging devices with good slope climbing ability such as the military tracked robots. The second random assignment favours slow, lightweight, rough terrain capable, autonomous robots with a long lifetime such as the jumping robots, multimodal robots and some tracked devices. These different "best" devices indicate that the scoring system does produce unbiased results. However, Jollbot 3b does well in both cases which shows that either Jollbot is a particularly successful rough terrain robot, or that the scoring system is somewhat biased. It should however be remembered that it is not only the weights that influence the scores. The user-created grading of category values also has an impact and such values are difficult to randomly generate.

7.7 Spring theory and spheres

With the small number of spheres produced there is little information to confirm whether the theory based upon circular calibration rings is applicable to spherical structures like those produced within this work. A summary of the properties of each sphere is shown in Table 38.

	Sphere 1	Sphere 2	Sphere 3	Sphere 4 (see Section 7.8.1.4 below)
Diameter (m)	0.3	0.3	0.58	0.58
Number of complete rings	3	4.5	12	12
Element material	Brazing rod	Brazing rod	Spring steel	Spring steel
Element cross-section diameter (mm)	1.5	1.5	1.4	2.4
Predicted stiffness (N/m)	222.5	334	125	1077
Measured stiffness (N/m)	300	500	75	550
Stiffness relationship	+26%	+33%	-67%	-97%

Table 38 – Spring theory and sphere summary

The large differences between predicted stiffness and measured stiffness across all spheres suggest that the theory is not applicable to these structures. As discussed previously this is mostly due to the large deflections, but could also be affected by the use of semi-circular rather than circular elements, whether those elements are exactly semi-circular or pre-stressed upon assembly, and the fixing method at the poles. The fairly linear force-displacement curves of the spring steel spheres do suggest that structure is somewhat Hookean until the point at which the sphere begins to twist. The brazing rod spheres are plastically deforming and do not conform to a Hookean

response. Spring theory does suggest that larger spheres for the same material and element properties are less stiff, and that is something that can be seen as a result of the size change between the second sphere and an incomplete version of the third sphere (a 580 mm diameter sphere consisting of 4.5 hoops of 1.4 mm spring steel has a stiffness of only ~30 N/m compared to the second sphere which has a similar structure apart from smaller size and achieves 500 N/m). Significant further study is required to give a full understanding of the relationship between spheres of different size, material and construction, the available energy stored within them, and the stress arrangements in each element and complete spheres at large deflections.

7.8 Future research directions

The development of a multimodal spherical jumping and rolling robotic device is naturally an ongoing process with no finite end. Jollbot 3b represents the final iteration of the process within this thesis. It illustrates that integrating a jumping movement with a powered rolling motion within a spherical device is possible and could have potential to lead to a versatile and inexpensive multi-terrain robot. The potential directions that this work could continue along are numerous. Here the possibilities have been divided into smaller incremental improvements specific to Jollbot 3b, and larger studies that that may produce greater performance improvements.

7.8.1 Jollbot 3b future considerations

The proposed research directions are presented in order of operation – jumping related suggestions first, followed by rolling suggestions, and finally universal suggestions.

7.8.1.1 Improving jump direction control

Jollbot 3b had the ability to choose jump direction, but ultimately took-off almost vertically. Modifying the design of the poles of the sphere and axle end caps such that they protrude further from the device's surface would allow for a shallower launch angle (~60° for example) (Figure 205). The ability to vary the launch angle would aid the jumping capability, but this requires substantial design revision and most likely additional mechanisms.

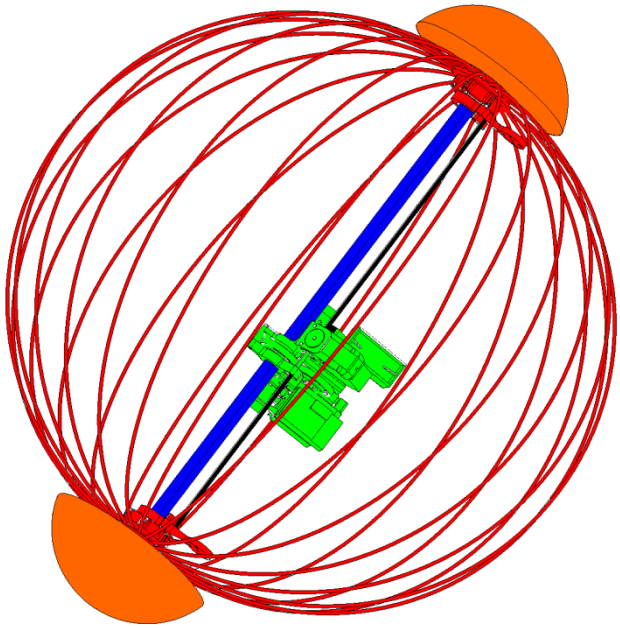

Figure 205 – Additional domed axle end-caps that would provide a non-vertical fixed launch-angle

7.8.1.2 Reducing axle friction

The main jump height limiting factor of the "as designed" Jollbot 3b was due to the friction on the main axle that is integral to the rolling capability. Subsequent versions of this prototype should attempt to tackle this point. Some friction reduction could be achieved by simply changing the material or coatings of the central axle, the sliding rolling-gear, and the sphere poles, allowing the device to jump to a considerable height without the removal of the central axle. Further friction reduction could be possible using linear and rolling element bearings at the expense of additional weight.

7.8.1.3 Maximising non-linearity of energy store

The remarkable non-linearity of the force-displacement profile of the twisting outer sphere was not fully exploited with this prototype. The force required to compress the sphere does not begin to decrease until around 75% compression. The size of the central mechanism meant that Jollbot 3b compressed its sphere by only 70%, meaning

that the reducing compression force was tantalisingly close. In future prototypes, every effort should be made to maximise this feature, resulting in around 85-90% compression and the associated additional energy stored by a single lightweight low-force compression mechanism.

7.8.1.4 Increasing stiffness of sphere

In addition to maximising the non-linearity of the sphere's force-displacement profile, building a sphere whose peak force is closely matched to the force capability of the compression mechanism would result in an increase in the energy stored. In the case of Jollbot 3b, the mechanism was capable of providing 50 N of force, but the sphere was only of about 30 N at its peak (slightly more with the additional latex band). A stiffer sphere, Sphere 4, was developed with much thicker 2.4 mm ϕ spring steel elements (rather than 1.4 mm ϕ ones) resulting in a sphere of ~580 mm ϕ. The spring clamps needed substantial revision and were ultimately produced in aluminium using CNC milling. The resultant sphere was substantially stiffer (~550 N/m) than the previous version (~75 N/m) with a peak break-point force of 220 N. Theory suggests that such a sphere should have a stiffness of 1077 N/m which is again not confirmed by experimentation. The revised sphere was more weighty (932.5 g compared to the previous sphere's 403 g excluding anti-tangle mechanisms) and it was clear that the existing compression mechanism would not be able to compress it sufficiently. Figure 206 shows the sphere characterisation produced using a similar method to those mentioned previously (see Section 6.2.1).

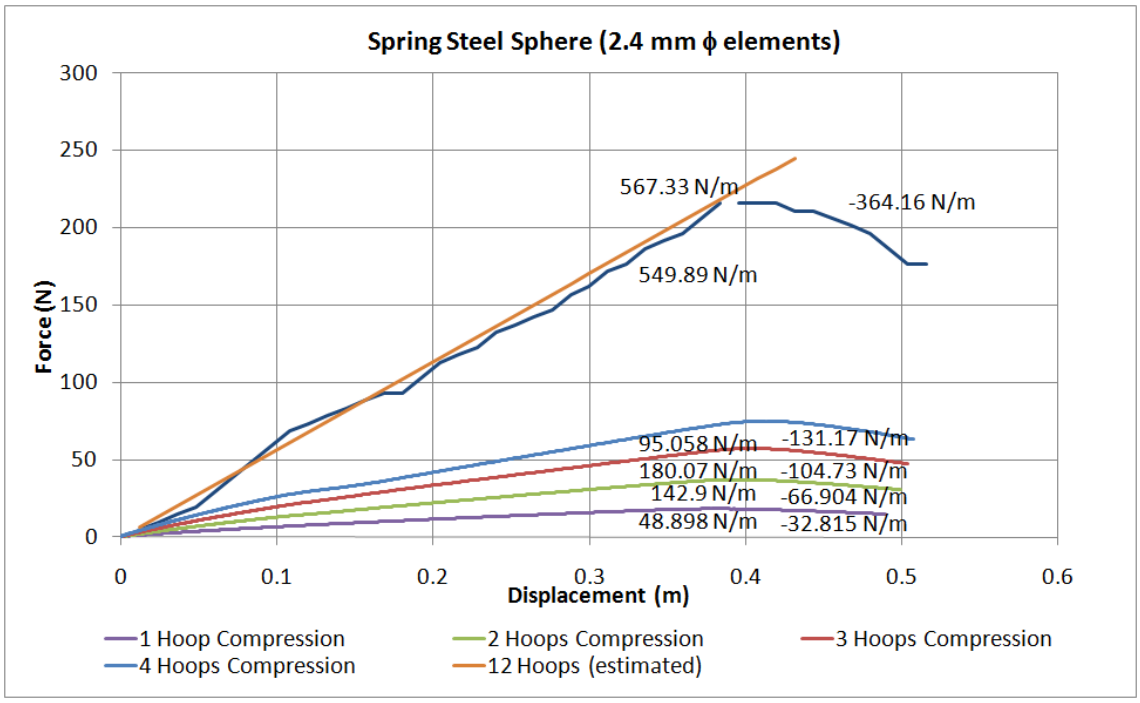

Figure 206 – Revised sphere (Sphere 4) characterisation

The possibility of changing the material and cross-section of each spring element is also an area that could deliver performance improvements, but significant in-depth study would be required (see Section 7.8.2.1).

7.8.1.1 Making sequential jumping possible

Jumps could not occur immediately after one another in Jollbot 3b due to shortcomings of the designed reset mechanism. If a ratchet system were added to the compression spool spur gear, then stopping backward rotation would allow the worm gear to slide along its axle and actuate the reset lever.

7.8.1.2 Improving powered rolling stability

Although Jollbot has achieved powered rolling, it is far from stable. The part spherical form of the contact patch of the sphere means that there is no stable resting position. Extending the sphere into an elongated form by adding a flat wheel-like section to its equator would provide a more stable rolling structure, but would have an impact on the steering ability, and the stiffness profile of the “sphere” during compression. An elliptical

form may provide a suitable compromise. The addition of a gyroscope could aid rolling stability without adjustment to the outer sphere at the expense of significant additional mass.

7.8.1.3 Adding environmental energy recovery

Full automation would require an endless energy supply and current technology dictates that this is likely to come from photovoltaic panels. Flexible panels are becoming available although the compliance required from a skin covering Jollbot may mean that there are additional problems before an environmental energy recovery system can be incorporated. The likelihood of this being possible can be determined with a quick calculation. On Earth, the sun provides 1000 W/m^2 of power under standard test conditions [clear day, sun facing 37° tilted surface with the sun at 41.81° above the horizon (ASTM International 2003)]. Off the shelf flexible photovoltaics are approximately 5 % efficient (PowerFilm 2007), and assuming that ¼ of the sphere's surface area of 1.05 m^2 is facing the sun at any given time, this results in 13.1 W of continuous power. This would be sufficient to provide the power to continuously run the device in either rolling (2.4W) or jumping (1.24W) operation. In addition, the discrepancy between the continuous power available and the existing power requirement means that there is scope for quicker charging of the jump and higher rolling speeds through the use of more powerful motors.

To retain their efficiency, photovoltaic panels must remain completely clear of surface dust and debris. This is of particular concern when applied as a covering to Jollbot. A covering over Jollbot's sphere will make up the rolling surface and will naturally come into contact with a variety of surface contaminants such as dust, mud and sand. Photovoltaic panels would therefore need to be protected and regularly cleaned. This could be achieved using a biomimetic self cleaning surface based on a lotus leaf (Barthlott & Neinhuis 1997).

7.8.1.4 Covering the sphere

Adding a skin to the surface of the sphere will obviously have an effect on the stiffness profile of the jump energy store. The length of the equator increases by around 35%

when the sphere is fully compressed and any skin should be sufficiently compliant to accommodate that increase. Whatever skin material chosen will increase the overall stiffness of the sphere, just as the latex band in Jollbot 3 does. This could perhaps be a useful way of fine-tuning the peak force required to compress the sphere, or to improve the energy storage to weight ratio. The major sheet materials suited to such a large stretch would appear to be natural rubbers and synthetic fabrics such as lycra. However, referring back to the material limitation of stress-relaxation makes their use likely to add mass with little energy storage performance benefit due to the slow "pause" of the jumping movement. Biomimetic materials could offer advantages here. In addition, although flexible, the proposed photovoltaic panels would break if stretched, so they would need to be mounted on a stretchable skin with suitably long wire links joining each panel.

Covering the sphere has both a positive and negative contribution to powered rolling performance. Using a fabric or sheet material to span the elements making up the sphere would have the effect of increasing the area of contact with the ground providing additional buoyancy in soft substrates and additional traction for overcoming obstacles. This would be of benefit. Also of benefit is the sealing effect a covering would provide. However, in outdoor environments, the wind will have a significant impact on the movement of a covered Jollbot. In Jollbot's current configuration, with individual spars, its surface area is small and thus wind has little effect on its movement, blowing directly through the device. Applying a skin around the spars of the sphere (or adding photovoltaic cells) will dramatically increase its surface area and the effective area on which wind will act. This will have a "tumbleweed" effect, and although potentially desirable for certain applications and direction requirement, would mean that Jollbot would have little control of its overall direction during both rolling and jumping. This comes as a result of its low weight and density. A deployable, sectioned, or wind-permeable skin has potential to offer tumbleweeding when required, improve traction during rolling movements and to have less of an impact on jumping ability. A wider tyre-like structure may provide a more simple solution with similar results.

7.8.1.5 Adding wind driven ‘Tumbleweeding‘

Using the wind to power rolling across open spaces could save substantial amounts of on-board energy (Figure 207). The hoop spring elements of Jollbot 3b lend themselves to having vanes or sails added to catch the prevailing wind. Very little directional control would be possible, but movement over large distances would be free. This would be useful for wide area down-wind exploration.

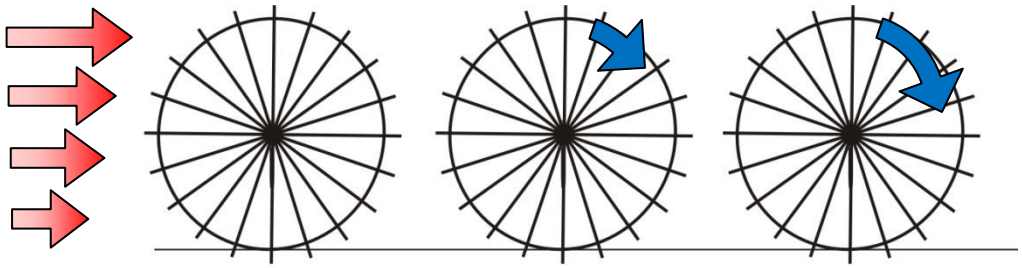

Figure 207 – Jollbot "tumbleweeding"

When the wind is not blowing in the required direction, Jollbot 3b’s ability to compress into a flattened form and hunker down close to the surface would enable it to weather out high winds in the wrong direction. When the winds direction became favourable then it could relax and take the free ride in the required direction. If the winds are too light, the Jollbot has the option of using its powered rolling ability.

A suitable wind-harvesting covering is not all that is required to tumbleweed in the winds. Apart from having to be light in weight, to “tumbleweed” in gentle winds, the centre of gravity of the device must be located at the geometric centre of the spherical form. This requirement is in contradiction to the requirements for powered rolling locomotion, making a sphere that both “tumbleweeds” and has powered rolling difficult to achieve without additional motors, even without the additional required jumping capability. A rolling and tumbleweeding device is certainly possible; as is a spherical tumbleweeding and jumping device. A device that performs all three movements would need to overcome a series of contradictions regarding mass and centre of gravity location, and the movement of that centre of gravity.

7.8.2 Future research studies

The suggestions above relate specifically to future revisions of Jollbot 3b, but here larger additional studies are suggested.

7.8.2.1 Detailed study of sphere

The sphere has two obvious areas in which performance can be improved.

The first is an improvement in energy density of a spring sphere through optimisation of the element material and cross-section, beginning with custom manufactured composites. Varying the cross section over the length of each element also has potential to reduce stresses and improve utilisation of material (Rahman & Rahman 2005) thus leading to improved stored strain energy to weight ratios.

The second improvement area is the maximisation of the energy stored for a given peak force, assuming displacement can approach 90-95% of the diameter. This would come as a result of a detailed study of the sphere's twisting: Is the twisting dependent on sphere size and slenderness, element material or cross-section profile? Can it be removed, tuned or predicted for any given sphere?

7.8.2.2 New compression/rolling control mechanism

In Jollbot, the existing mechanism resulting in the sphere's compression for jumping, and the rotation torque for rolling, relies on a solid central axle, cables, a flexible toothed belt, and complicated mechanisms at the sphere's poles to ensure the cables do not become tangled. A study of the compression/rolling mechanism would determine whether a solid axle really is required, or if another solution was possible. For example is the tension of the compression threads sufficient to re-act the torque required for rolling? Could a telescopic axle provide both the compression mechanism and the fixed rotation point for the ballast? A whole series of possibilities are available.

7.8.2.3 Adding automation

Although Jollbot is currently remotely controlled, the step up to full automation requires significant study. Firstly energy autonomy would be required – whether that comes from photovoltaic panels or not. Once energy autonomy has been achieved, the problem becomes sensory. Automation relies on sensory inputs from the environment immediately surrounding such an exploratory robot. Owing to Jollbot's spherical form, it is important that its control system knows which way is up. This could be achieved using gravitational sensors on the central mechanism. IR or laser range sensors could be mounted to the passive components of the anti-tangle mechanism as these will tend to hang downward in all situations, or they could be mounted in conventional gimballed mounts. A benefit of the existing central axle pointing skyward before a jump is to provide a suitable location for vision system cameras. This would enable terrain evaluation and direction decisions. However, the automated control of a device such as Jollbot is likely to remain complex as its movement is currently very inconsistent. A control system will need to deal with the device's constantly changing physical parameters along with those of its surroundings. It is envisaged that the expertise of a robotics control group would be required to automate Jollbot.

7.9 Conclusions

The aim of this work was to develop a new, inexpensive, remotely controlled, single structure, multimodal jumping and rolling mobility system that was able to deal with rough and varied terrains. Jollbot 3b has achieved much of that requirement and the scoring system developed as part of this work illustrates that this device has potential for use for many rough terrain applications.

Jollbot is certainly inexpensive in material cost, and remotely controlled by a conventional model radio control system. Its spherical structure provides both the storage medium for jump energy and the surface upon which it can roll. Its ability to fully deal with rough terrain is under-developed, but the device has shown potential by jumping to a cleared height of 0.5 m (80% of its own height) and rolling at 0.7 m/s over smoother terrain. As with the development of any device there will always be areas of

possible improvement and suggestions as to the future development of such a device have been presented.

The scoring method developed to evaluate a series of rough terrain robots and applications has much potential, but requires more use by independent parties to fully indicate areas in which it can be improved.

References

Aerts, P 1998, 'Vertical jumping in Galago senegalensis: the quest for an obligate mechanical power amplifier', *Philosophical Transactions of the Royal Society of London Series B - Biological Sciences*, vol. 353, no. 1375, pp. 1607-1620.

Alexander, RM 1974, 'The mechanics of jumping by a dog (Canis familiaris)', *Journal of Zoology, London*, vol. 173, pp. 549-573.

Alexander, RM 1982, *Locomotion of animals*, Blackie, Glasgow.

Alexander, RM & Goldspink, G 1977, *Mechanics and energetics of animal locomotion*, Chapman and Hll, London.

Alexander, RM & Vernon, A 1975, 'The Mechanics of hopping by kangaroos (Macropodidae)', *Journal of Zoology*, vol. 177, pp. 265-303.

Allen, HW 1969, *3486495: An archery bow with drawforce multiplying attachment*, United States patent 3486495.

Allison, J, *Monopod Jumping Robot*, University of Utah. Available from: http://www-personal.umich.edu/~jtalliso/Design/Design2.html.

Altendorfer, R, Moore, N, Komsuoglu, H, Buehler, M, Brown, HB, McMordie, D, Saranli, U, Full, R & Koditschek, DE 2001, 'RHex: A Biologically Inspired Hexapod Runner', *Autonomous Robots*, vol. 11, no. 3, p. 207.

Altshuler, DTW 2002, 'Future Landmine Systems', *Plenary briefing presented at the Fifth International Symposium on Technology and the Mine Problem*.

Amai, WA, Klarer, PR, Pletta, JB, Purvis, JW & Case, RP 1994, *Robotic All-Terrain Lunar Exploration Rover (RATLER) FY93 Program Status Report*, Sandia National Laboratories, Albuquerque, NM, USA.

Antol, J, Calhoun, P, Flick, J, Hajos, G, Kolacinski, R, Minton, D, Owens, R & Parker, J 2003, *Low Cost Mars Surface Exploration: The Mars Tumbleweed*, NASA.

Antol, J, Chattin, RL, Copeland, BM & Krizan, SA 2006, 'The NASA Langley Mars Tumbleweed Rover Prototype', *44th AIAA Aerospace Sciences Meeting and Exhibit*.

Armour, R, Paskins, K, Bowyer, A, Vincent, J & Megill, W 2007, 'Jumping robots: a biomimetic solution to locomotion across rough terrain', *Bioinspiration & Biomimetics*, vol. 2, no. 3, pp. S65-S82.

Armour, R & Vincent, JFV 2006, 'Jumping Robots: A Review', *Towards Autonomous Robotic Systems 2006*.

Armour, RH & Vincent, JFV 2006, 'Rolling in Nature and Robotics: A Review', *Journal of Bionic Engineering*, vol. 3, no. 4, pp. 195-208.

Ashby, MF 1993, *Materials Selection In Mechanical Design*, Pergamon Press, Cambridge.

ASTM International, A 2003, *Standard Tables for Reference Solar Spectral Irradiances: Direct Normal and Hemispherical on 37º Tilted Surface*.

Bares, J 1999, 'Dante II: technical description, results, and lessons learned', *The International journal of robotics research*, vol. 18, no. 7, pp. 621-649.

Barthlott, W & Neinhuis, C 1997, 'Purity of the sacred lotus, or escape from contamination in biological surfaces', *Planta*, vol. 202, no. 1, pp. 1-8.

Bennet-Clark, HC 1975, 'The energetics of the jump of the locust Schistocerca gregaria', *Journal of Experimental Biology*, vol. 63, no. 1, pp. 53-83.

Bennet-Clark, HC 1976, 'Energy Storage in Jumping Animals', in *Perspectives in experimental biology: proceedings of the Fiftieth Anniversary meeting of the Society for Experimental Biology.*, ed. PS Davies, Pergamon, pp. 467-478.

Bennet-Clark, HC 1977, 'Scale Effects in Jumping Animals', in *Scale Effects In Animal Locomotion*, ed. T.J.Pedley, Academic Press, London, pp. 185-201.

Bennet-Clark, HC & Lucey, ECA 1967, 'The jump of the flea: a study of the energetics and a model of the mechanism', *Journal of Experimental Biology*, vol. 47, pp. 59-76.

Biewener, AA 2003, 'Jumping, climbing and suspensory locomotion', in *Animal Locomotion*, Oxford University Press, Oxford, pp. 163-180.

Bluebotics, *Shrimp III - flyer*. Available from: http://www.bluebotics.com/solutions/Shrimp/Shrimp_web.pdf [25/3/2010].

Borenstein, J & Borrell, A 2008, 'The OmniTread OT-4 serpentine robot', in *Robotics and Automation, 2008. ICRA 2008. IEEE International Conference on*, pp. 1766-1767.

Borenstein, J, Granosik, G & Hansen, M 2005, 'The OmniTread OT-4 serpentine robot - Design and field performance', in *Proceedings of SPIE - The International Society for Optical Engineering*, SPIE, Orlando, FL, United states, pp. 324-332.

Boston Dynamics, 2009, *BigDog Overview presentation*, Boston Dynamics. Available from: http://www.bostondynamics.com/img/BigDog_Overview.pdf.

Brackenbury, J 1997, 'Caterpillar kinematics', *Nature*, vol. 390, no. 6659, pp. 453-453.

Brackenbury, J & Hunt, H 1993, 'Jumping in springtails: mechanism and dynamics', *Journal of Zoology*, vol. 229, pp. 217-236.

Brewer, G 1961, 'Circular Calibration Ring With Two Axes of Symmetry', in *Spring Design and Application*, ed. NP Chironis, McGraw-Hill Book Company, New York, pp. 184-188.

Brown, B & Zeglin, G 1998, 'The Bow Leg Hopping Robot', *IEEE International Conference on Robotics and Automation*.

Brown, HB, Jr. & Xu, Y 1997, 'Single-wheel, gyroscopically stabilized robot', *IEEE Robotics & Automation Magazine*, vol. 4, no. 3, pp. 39-44.

Brown, HB, Weghe, JMV, Bererton, CA & Khosla, PK 2002, 'Millibot Trains for Enhanced Mobility', *IEEE/ASME Transactions on Mechatronics*, vol. 7, no. 4, pp. 452-461.

Brown, RHJ 1967, 'Mechanism of locust jumping', *Nature*, vol. 214, p. 939.

Burdet, L 2001, *Micro jumping robot*, École Polytechnique Fédérale De Lausanne.

Burdick, J & Fiorini, P 2003, 'Minimalist Jumping Robots for Celestial Exploration', *The International Journal of Robotics Research*, vol. 22, no. 7-8, pp. 653-674.

Burion, S, Coblenz, M, Gennari, J, Koes, M, Lewis, M, Loboda, T, Manjlovich, M, Nourbakhsh, I, Oishi, K, Polvichai, J, Sycara, K, Wang, J & Yong, M 2004, 'RoboCup Rescue - Robot League Team - Team Corky, United States', in *RoboCup 2004 - US Open, Rescue Robot League Competition*, New Orleans, LA, USA.

Caldwell, RL 1979, 'A unique form of locomotion in a stomatopod - backward somersaulting', *Nature*, vol. 282, no. 5734, pp. 71-73.

Clark, JE, Cham, JG, Bailey, SA, Froehlich, EM, Nahata, PK, Full, RJ & Cutkosky, MR 2001, 'Biomimetic design and fabrication of a hexapedal running robot', in *IEEE International Conference on Robotics and Automation*, pp. 3643-3649 vol.4.

Crespi, A, Badertscher, A, Guignard, A & Ijspeert, AJ 2005, 'AmphiBot I: an amphibious snake-like robot', *Robotics and Autonomous Systems*, vol. 50, no. 4, pp. 163-175.

Dagg, AI 1977, *Running, Walking and Jumping: The science of locomotion*, Wykeham Publications (London) Ltd, London.

Dagnall, H 1986, *Exploring Surface Texture*, Rank Taylor Hobson Limited, Leicester, England.

Davis, IL, Kelly, A, Stentz, A & Matthies, L 1995, 'Terrain typing for real robots', in *Proceedings of the 1995 Intelligent Vehicles Symposium*, IEEE, Detroit, MI, USA, pp. 400-405.

Dawkins, R 1996, 'Why don't animals have wheels?' *The Sunday Times*, November 24th 1996.

Defence Mapping Agency 1994, *Planning Terrain analysis Data Base (PTADB) Scale 1:250,000*, Defence Mapping Agency, Fairfax, Virginia.

de Groot, JH & van Leeuwen, JL 2004, 'Evidence for an elastic projection mechanism in the chameleon tongue', *Proceedings of the Royal Society B: Biological Sciences*, vol. 271, no. 1540, pp. 761-770.

De Lafontaine, J & Kassing, D 1996, 'Technologies and concepts for lunar surface exploration', *Acta Astronautica*, vol. 38, no. 2, pp. 125-129.

Dunbar, B, 27/02/2008, *NASA - Moon, Mars and Beyond*, NASA. Available from: http://www.nasa.gov/mission_pages/exploration/mmb/index.html.

Edwards, J, Whitaker, D, Klionsky, S & Laskowski, MJ 2005, 'Botany - A record-breaking pollen catapult', *Nature*, vol. 435, no. 7039, pp. 164-164.

Ellery, A, Patel, N, Richter, L, Bertrand, R & Dalcomo, J 2005, 'Exomars rover chassis analysis design', *European Space Agency, (Special Publication) ESA SP*, no. 603, pp. 129-136.

Estier, T, Crausaz, Y, Merminod, B, Lauria, M, R.Piguet & Siegwart, R 2000, 'An innovative Space Rover with Extended Climbing Abilities', in *Proceedings of Space and Robotics 2000*, Albuquerque, USA.

Evans, MEG 1972, 'Jump of Click Beetle (Coleoptera elateridae) - Preliminary Study', *Journal of zoology*, vol. 167, no. JUL, p. 319.

Evans, MEG 1973, 'Jump of Click Beetle (Coleoptera elateridae) - Energetics and Mechanics', *Journal of zoology*, vol. 169, no. FEB, pp. 181-194.

Farji-Brener, AG, Barrantes, G & Ruggiero, A 2004, 'Environmental rugosity, body size and access to food: a test of the size-grain hypothesis in tropical litter ants', *Oikos*, vol. 104, no. 1, pp. 165-171.

Fiorini, P & Burdick, J 2003, 'The Development of Hopping Capabilities for Small Robots', *Autonomous Robots*, no. 14, pp. 239-254.

Fiorini, P, Cosma, C & Confente, M 2005, 'Localization and Sensing for Hopping Robots', *Autonomous Robots*, no. 18, pp. 185-200.

Forterre, Y, Skotheim, JM, Dumais, J & Mahadevan, L 2005, 'How the Venus flytrap snaps', *Nature*, vol. 433, no. 27 January 2005, pp. 421-425.

Foster-Miller 2008a, *The Soldier's Choice TALON® - Information Brochure*, Foster-Miller Inc., Qinetic North America, Waltham, MA, USA.

Foster-Miller 2008b, *TALON® IV Engineer - Information Brochure*, vol. DS08 126, ed.^eds DS08 126, Foster-Miller Inc., Qinetic North America, Waltham, MA, USA.

Full, R, Earls, K, Wong, M & Caldwell, R 1993, 'Locomotion like a wheel?' *Nature*, vol. 365, p. 495.

Furth, DG 1982, 'The Metafemoral Spring of Flea Beetles', *SPIXIANA (Supplement)*, vol. 7, pp. 11-27.

Garcia-Paris, M & Deban, SM 1995, 'A Novel Antipredator Mechanism in Salamanders: Rolling Escape in Hydromantes platycephalus', *Journal of Herpetology*, vol. 29, no. 1, pp. 149-151.

Gat, E 1995, 'Towards principled experimental study of autonomous mobile robots', *Autonomous Robots*, vol. 2, no. 3, pp. 179-189.

Giles, D, 18/03/2010, *Landslides: Rock Fall Gallery*. Available from: http://www.ukgeohazards.info/.

Granosik, GG 2005, 'The OmniTread serpentine robot for industrial inspection and surveillance', *The Industrial robot*, vol. 32, no. 2, pp. 139-148.

Gronenberg, W 1996, 'Fast actions in small animals: Springs and click mechanisms', *Journal of comparative physiology. A, Sensory, neural, and behavioral physiology*, vol. 178, no. 6, pp. 727-734.

Hale, E, Schara, N, Burdick, J & Fiorini, P 2000, 'A Minimally Actuated Hopping Rover for Exploration of Celestial Bodies', *Proceedings of the 2000 IEEE International Conference on Robotics & Automation*, pp. 420-427.

Hall-Craggs, EBC 1965, 'An analysis of the jump of the lesser galago (Galago senegalensis)', *Journal of Zoology*, vol. 147, pp. 20-29.

Halme, A, Suomela, J, Schönberg, T & Wang, Y 1996, 'A Spherical Mobile Micro-Robot for Scientific Applications', *ASTRA 96*.

Hayashi, R & Tsujio, S 2001, 'High-performance Jumping Movements by Pendulum-type Jumping Machines', *Proceedings of the IEEE/RSJ International Conference on Intelligent Robots and Systems*, pp. 722-727.

Heitler, WJ 1974, 'Locust Jump - Specializations of Metathoracic Femoral-Tibial Joint', *Journal of Comparative Physiology*, vol. 89, no. 1, pp. 93-104.

Henschel, J 2005, 'Feature Creature - The Golden Wheel Spider', *Gobabeb Times*, vol. 1, no. 1, p. 3.

Henschel, JRJ 1990, 'Spiders wheel to escape', *South African journal of science*, vol. 86, no. 3, pp. 151-152.

Hirai, S, Matsuyama, Y & Nakanishi, H 2007, 'Jumping via Deformation of a Robot Body', *Robotics and Automation Magazine*, vol. 6, no. 1.

Hollerbach, JM, Hunter, IW & Ballantyne, J 1992, 'A Comparative Analysis of Actuator Technologies for Robotics', in *The Robotics Review 2*, eds K Oussama & JJ Craig, MIT Press, Cambridge, MA, pp. 299-342.

Hong, D, Jeans, JB & Ping, R 2009, 'Experimental verification of the walking and turning gaits for a two-actuated spoke wheel robot', in *Intelligent Robots and Systems, 2009. IROS 2009. IEEE/RSJ International Conference on*, pp. 402-403.

IFR Statistical Department 2007, *World Robotics 2007: Statistics, Market Analysis, Forecasts, Case Studies and Profitability of Robot Investment*, FP6-507728, IFR Statistical Department - European Robotics Research Network.

iRobot-Corporation 2009a, *iRobot 710 Warrior® - Information Brochure*, ed.^eds 00086.1109.v4, iRobot Corporation, Bedford, MA, USA.

iRobot-Corporation 2009b, *iRobot PackBot® 510 with FasTac Kit - Information Bruchure*, ed.^eds 03/09_v1, iRobot Corporation, Bedford, MA, USA.

Jacoff, A, Messina, E & Evans, J 2002, 'Performance evaluation of autonomous mobile robots', *Industrial Robot*, vol. 29, no. 3, pp. 259-267.

Jacoff, A, Weiss, B & Messina, E 2003, 'Evolution of a Performance Metric for Urban Search and Rescue Robots (2003)', in *Performance Metrics for Intelligent Systems (PerMIS) Workshop*, National Institute of Standards and Technology, Gaithersburg, MD.

Jakubik, P, Suomela, J, Vainio, M, Yilkorpi, T & Halme, A 2004, *ARIADNA AO4532-03/6210 Biologically inspired solutions for robotic surface mobility*, Helsinki University of Technology - Automation technology laboratory, Helsinki.

James, KH & et al. 2009, 'A survey of snake-inspired robot designs', *Bioinspiration & Biomimetics*, vol. 4, no. 2, p. 021001.

Jeans, JB & Hong, D 2009, 'IMPASS: Intelligent Mobility Platform with Active Spoke System', in *IEEE International Conference on Robotics and Automation, 2009. ICRA '09.*, pp. 1605-1606.

Jensen, M & Weis-Fogh, T 1962, 'Biology and biophysics of locust flight. V. Strength and elasticity of insect cuticle', *Philosophical Transactions of the Royal Society B: Biological Sciences*, vol. 245, pp. 137-169.

Kang, S, Lee, W, Kim, M, Shin, K & Robotics, Y 2005, 'ROBHAZ-Rescue: Rough-terrain negotiable teleoperated mobile robot for rescue mission', in *Proceedings of the 2005 IEEE International Workshop on Safety, Security and Rescue Robotics*, Institute of Electrical and Electronics Engineers Computer Society, Kobe, Japan, pp. 105-110.

Kapsner, J, *Reconnaissance Robots*. Available from: http://www.it.umn.edu/news/inventing/1998_Fall/robots.html.

Kaspari, M & Weiser, MD 1999, 'The size-grain hypothesis and interspecific scaling in ants', *Functional Ecology*, vol. 13, no. 13, pp. 530-538.

Ker, RF 1977, Some structural and mechanical properties of locust and beetle cuticle: Chapter 5 - The Jump of the Flea Beetle, Oxford University.

Kikuchi, F, Ota, Y & Hirose, S 2003, 'Basic Performance Experiments for Jumping Quadruped', *Proceedings of the 2003 IEEE/RSJ International Conference on Intelligent Robots and Systems*, pp. 3378-3383.

Kimura, H & Hirose, S 2002, 'Development of Genbu: Active wheel passive joint articulated mobile robot', in *Proceedings of the 2002 IEEE/RJS International Conference on Intelligent Robots and Systems*, IEEE/RSJ, EPFL Lausanne, Switzerland, pp. 823-828.

Klaassen, B & Papp, KL 1999, 'GMD-SNAKE2: A Snake-Like Robot Driven by Wheels and a Method for Motion Control', in *Proceedings of 1999 IEEE International Conference on Robotics and Automation*.

Klute, GK, Czerniecki, JM & Hannaford, B 1999, 'McKibben artificial muscles: pneumatic actuators with biomechanical intelligence', in *Advanced Intelligent Mechatronics, 1999. Proceedings. 1999 IEEE/ASME International Conference on*, pp. 221-226.

Kovač, M, Fuchs, M, Guignard, A, Zufferey, J-C & Floreano, D 2008, 'A miniature 7g jumping robot', in *Robotics and Automation, 2008. ICRA 2008. IEEE International Conference on*, pp. 373-378.

Kovač, M, Schlegel, M, Zufferey, J-C & Floreano, D 2010, 'Steerable miniature jumping robot', *Autonomous Robots*, vol. 28, no. 3, pp. 295-306.

Kurokawa, H, Tomita, K, Kamimura, A, Yoshida, E, Kokaji, S & Murata, S 2005, 'Distributed self-reconfiguration control of modular robot M-TRAN', in *Mechatronics and Automation, 2005 IEEE International Conference*, pp. 254-259 Vol. 1.

Lambrecht, BGA, Horchler, AD & Quinn, RD 2005, 'A Small, Insect-Inspired Robot that Runs and Jumps', in *Proceedings of the 2005 IEEE International Conference on Robotics and Automation*, Barcelona, Spain, pp. 1240-1245.

Lerat, A 2004, *MSc Report: Jumping Ball Robot*, University of Bath.

Li, Z, Zhu, Q & Gold, C 2005, 'Chapter 2 - Terrain Descriptors and Sampling Strategies', in *Digital Terrain Modeling: Principles and Methodology*, CRC Press.

Lindemann, RA, Bickler, DB, Harrington, BD, Ortiz, GM & Voothees, CJ 2006, 'Mars exploration rover mobility development', *Robotics & Automation Magazine, IEEE*, vol. 13, no. 2, pp. 19-26.

Lorenz, RD, Jones, JA & Wu, JJ 2002, 'Mars Magnetometry from a Tumbleweed Rover', *IEEEAC*.

Maitland, DP 1992, 'Locomotion by Jumping in the Mediterranean Fruit-fly Larva Ceratitis-capitata', *Nature*, vol. 355, no. 6356, pp. 159-161.

Mandelbrot, BB 1983, *The Fractal Geometry of Nature*, W. H. Freeman and Company, New York.

Martin-Alvarez, A, Peuter, Wd, Hillebrand, J, Putz, P, Matthyssen, A & Weerd, JFd 1996, 'Walking Robots for Planetary Exploration Missions', in *Second World Automation Congress WAC'96*, Montpellier, France.

McBride, B, Longoria, R & Krotkov, E 2003, 'Measurement and Prediction of the Off-Road Mobility of Small Robotic Ground Vehicles', in *Performance Metrics for Intelligent Systems (PerMIS) Workshop*, National Institute of Standards and Technology, Gaithersburg, MD.

Mishkin, AH, Morrison, JC, Nguyen, TT, Stone, HW, Cooper, BK & Wilcox, BH 1998, 'Experiences with operations and autonomy of the Mars Pathfinder Microrover', in *Aerospace Conference, 1998. Proceedings., IEEE*, p. 337.

MobileRobots, *The High Performance All-Terrain Robot P3-AT*, Mobilerobots Inc. Available from: http://www.activrobots.com/ROBOTS/p2at.html.

Molfino, R, Zoppi, M & Rimassa, L 2007, 'Rescue robot module with sliding membrane locomotion', in *CLARWAR 2007 10th International Conference on Climbing and Walking Robots and the Supporting Technologies for Mobile Machines*, Singapore.

Morrey, JM, Lambrecht, B, Horchler, AD, Ritzmann, RE & Quinn, RD 2003, 'Highly Mobile and Robust Small Quadruped Robots', in *Proceedings of the 2003 IEEE/RSJ International Conference on Intelligent Robots and Systems*, Las Vegas, Nevada, pp. 82-87.

Morse, DR, Lawton, JH, Dodson, MM & Williamson, MH 1985, 'Fractal dimension of vegetation and the distribution of arthropod body lengths', *Nature*, vol. 314, no. 6013, pp. 731-733.

Mote, DC 1914, 'The Cheese Skipper (Piophila casci Linne.): An account of the bionomics and the structure of dipterous larvae occuring in human foods with particular reference to those which have been recorded as accidental parasites of man.' *The Ohio Naturalist*, vol. 14, no. 7, pp. 309-316.

Muller, UK & Kranenbarg, S 2004, 'Power at the tip of the tongue', *Science*, vol. 304, no. 5668, p. 217.

Nakamura, Y, Shimoda, S & Shoji, S 2000, 'Mobility of a Microgravity Rover using Internal Electro-magnetic Levitation', *Proceeding of the 2000 IEEE/RJS International Conference on Intelligent Robots and Systems*.

NASA-JPL, *Update: Spirit and Opportunity*. Available from: http://marsrovers.jpl.nasa.gov/mission/status.html [16/02/2010].

Niiyama, R, Nagakubo, A & Kuniyoshi, Y 2007, 'Mowgli: A Bipedal Jumping and Landing Robot with an Artificial Musculoskeletal System', in *Robotics and Automation, 2007 IEEE International Conference on*, ed. A Nagakubo, pp. 2546-2551.

Ohmiya, K 1991, 'Fractal dimensions of terrain profiles', *Journal of Terramechanics*, vol. 28, no. 2-3, pp. 155-165.

Ojeda, L, Borenstein, J, Witus, G & Karlsen, R 2006, 'Terrain characterization and classification with a mobile robot', *Journal of Field Robotics*, vol. 23, no. 2, pp. 103-122.

Okubo, H, Nakano, E & Handa, M 1996, 'Design of a Jumping Machine Using Self-energizing Spring', *Proceedings IROS 96*, pp. 186-191.

Ovaska, K 2002, 'Anatomy of the dromedary jumping-slug, Hemphillia dromedarius Branson, 1972 (Gastropoda : Stylommatophora : Arionidae), with new distributional records', *The Nautilus*, vol. 116, no. 3, pp. 89-94.

Paskins, KE 2007, The mechanics and energy economy of animal jumping and landing applied to autonomous robots, University of Bath.

Patek, SN, Baio, JE, Fisher, BL & Suarez, AV 2006, 'Multifunctionality and mechanical origins: Ballistic jaw propulsion in trap-jaw ants', *Proceedings of the National Academy of Sciences of the United States of America*, vol. 103, no. 34, pp. 12787-12792.

Patek, SNJ 2004, 'Biomechanics: Deadly strike mechanism of a mantis shrimp - This shrimp packs a punch powerful enough to smash its prey's shell underwater', *Nature*, vol. 428, no. 6985, pp. 819-820.

Paul, C, Dravid, R & Iida, F 2002, 'Design and Control of a Pendulum Driven Hopping Robot', *The IEEE/RSJ International Conference on Intelligent Robots and Systems*.

Pheasant, S 2001, *Bodyspace: Anthropometry, Ergonomics and the Design of Work*, Second edn, Taylor & Francis Ltd., London.

PowerFilm, *PowerFilm Inc. FAQs*. Available from: www.powerfilmsolar.com [26/10/2008].

Quinn, RD, *Mini-Whegs Robots*, Case Western Reserve University. Available from: http://biorobots.cwru.edu/publications/publicat.htm [3/5/2006].

Quinn, RD, Nelson, GM, Bachmann, Rj, Kingsley, DA, Offi, J & Ritzmann, RE 2001, 'Insect Design for Improved Robot Mobility', in *Proceedings of the 4th Internationl Conference on Climbing and Walking Robots*, ed. Ba Dillmann, pp. 69-76.

Quinn, RD, Offi, JT, Kingsley, DA & Ritzmann, RE 2002, 'Improved mobility through abstracted biological principles', in *IEEE/RSJ International Conference on Intelligent Robots and System*, Lausanne, Switzerland, pp. 2652-2657.

Rahman, MA & Rahman, S 2005, 'Design Parameters of a Circular Proving Ring of Uniform Strength', in *Proceedings of the International Conference on Mechanical Engineering 2005 (ICME2005)*, ICME, Dhaka, Bangladesh.

Raibert, M 2008, 'BigDog, the rough-terrain quadruped robot', in *IFAC Proceedings Volumes (IFAC-PapersOnline)*, 1, Elsevier, P.O. Box 211, Amsterdam, 1000 AE, Netherlands.

Raibert, MH 1986, 'Legged Robots', *Communications of the ACM*, vol. 29, no. 6, pp. 499-514.

Rasband, W 2010, *ImageJ*, National Institute of Health.

Roark, RJ & Young, WC 1975, *Formulas for Stress and Strain*, Fifth edn, McGraw-Hill Book Company, New York.

Roberts, TJ 2003, 'Probing the limits to muscle-powered accelerations: lessons from jumping bullfrogs', *The journal of experimental biology*, vol. 206, no. 15, pp. 2567-2580.

Rose, K 2007, 'EOD/LIC Technologies: Weaponized Bot Rolls into Battle', *The Guardian*, vol. 9, no. 3, pp. 18-20.

Rothschild, M, Schlein, J, Parker, K, Neville, C & Sternberg, S 1975, 'The jumping mechanism of Xenopsylla Cheopis III. execution of the jump and activity', *Philosophical Transactions of the Royal Society B: Biological Sciences*, vol. 271, no. 914, pp. 457-520.

Rotundus, *Rotundus Groundbot*. Available from: http://www.rotundus.se/.

Rover-Company, *Ball-shaped Robot*. Available from: http://private.peterlink.ru/rcl/iducoop.htm.

Salton, J, *Sandia hopping robots to bolster troop capabilities*. Available from: http://www.sandia.gov/news/resources/news_releases/sandia-hopping-robots-to-bolster-troop-capabilities/ [12/02/2010].

Santer, M & Pellegrino, S, November 2003, *Actuation of Multi-Stable Structures*, Deployable Structures Laboratory University of Cambridge. Available from: http://www-civ.eng.cam.ac.uk/dsl/Bistable_actuation/mjs_research.html [11/05/2006].

Scarfogliero, U, Stefanini, C & Dario, P 2006, 'A Bioinspired Concept for High Efficiency Locomotion in Micro Robots: the Jumping Robot Grillo', *Proceedings of the 2006 IEEE International Conference on Robotics & Automation*, pp. 4037-4042.

Scarfogliero, U, Stefanini, C & Dario, P 2007, 'Design and Development of the Long-Jumping "Grillo" Mini Robot', *Proceedings of the 2007 IEEE International Conference on Robotics and Automation*, pp. 467-472.

Schenker, PS, Pirjanian, P, Balaram, B, Ali, KS, Trebi-Ollennu, A, Huntsberger, TL, Aghazarian, H, Kennedy, BA, Baumgartner, ET, Iagnemma, K, Rzepniewski, A, Dubowsky, S, Leger, PC, Apostolopoulos, D & McKee, GT 2000, 'Reconfigurable robots for all terrain exploration', in *Proceedings of SPIE - The International Society for Optical Engineering*, Society of Photo-Optical Instrumentation Engineers, Boston, USA, pp. 454-468.

Schmidt-Neilsen, K 1984, *Scaling: Why animal size is so important?*, Cambridge University Press, Cambridge.

Schroll, G, *Ball-shaped robot*, Carbide Robotics. Available from: http://www.carbiderobotics.com/.

Seraji, H 2003, 'Rule-based traversability indices for multi-scale terrain assessment', in *Control Applications, 2003. CCA 2003. Proceedings of 2003 IEEE Conference on*, pp. 1469-1476 vol.2.

Sheh, R 2005a, 'The Building of REDBACK', *Rescue Robotics Camp*.

Sheh, R 2005b, 'The Redback: a low-cost advanced mobility robot', *PANDORA electronic collection.*

Shimoda, S, Kubota, T & Nakatani, I 2002, 'New Mobility System Based on Elastic Energy Under Microgravity', *Proceedings of the International Symposium on Experimental Robotics*, pp. 2296-2301.

Siegwart, R, Lamon, P, Estier, T, Lauria, M & Piguet, R 2002, 'Innovative design for wheeled locomotion in rough terrain', *Robotics and Autonomous Systems*, vol. 40, pp. 151-162.

Simons, P 1993, 'An explosive start for plants', *New scientist*, vol. 137, no. 1854, pp. 35-37.

Stoeter, SA, Burt, IT & Papanikolopoulos, N 2003, 'Scout Robot Motion Model', *Proceedings of the IEEE International Conference on Robotics and Automation*.

Stoeter, SA, Rybski, PE, Gini, M & Papanikolopoulos, N 2002, 'Autonomous Stair-Hopping with Scout Robots', *Proceedings of the IEEE International Conference on Intelligent Robots and Systems*, pp. pp. 721-726.

Studor, G 2010, *Robotic Ball Study for Planetary Surface Missions*, R Armour, NASA - Johnson Space Center Houston, Texas.

Sugiyama, Y & Hirai, S 2004, 'Crawling and Jumping by a Deformable Robot', *Proceedings of the International Symposium on Experimental Robotics*.

Sugiyama, YJ 2006, 'Crawling and jumping by a deformable robot', *The International journal of robotics research*, vol. 25, no. 5-6, pp. 603-620.

Sukhatme, GS & Bekey, GA 1996, 'Multicriteria evaluation of a Planetary Rover', in *Workshop on Planetary Rover Technology and Systems - IEEE International Conference on Robotics and Automation*, Minneapolis, MN.

Sukhatme, GS, Brizius, S & Bekey, GA 1997, 'Mobility evaluation of a wheeled microrover using a dynamic model', in *Intelligent Robots and Systems, 1997. IROS '97., Proceedings of the 1997 IEEE/RSJ International Conference on*, pp. 1506-1512 vol.3.

Suthakorn, J, Shah, SSH, Jantarajit, S, Onprasert, W, Saensupo, W, Saeung, S, Nakdhamabhorn, S, Sa-Ing, V & Reaungamornrat, S 2008, 'On the design and development of a rough terrain robot for rescue missions', in *IEEE International Conference on Robotics and Biomimetics, ROBIO*, IEEE Computer Society, Bangkok, Thailand, pp. 1830-1835.

TED Video Conferences 2007, *Robert Full on animal movement* in TED Video Conferences, TED Conferences LLC.

Trentini, M, Beckman, B, Collier, J, Digney, B & Vincent, I 2007, *Intelligent Mobility Research at Defence R&D Canada for Autonomous UGV Mobility in Complex Terrain*, Defence R&D Canada.

Tunstel, E 2007, 'Operational performance metrics for mars exploration rovers', *Journal of Field Robotics*, vol. 24, no. 8-9, pp. 651-670.

Ullman, DG 2003, 'Understanding the Problem and the Development of Engineering Specifications', in *The Mechanical Design Process, Third Edition*, McGraw-Hill, New York, pp. 127-128.

University of Minnesota Centre for Distributed Robotics, *UNM Scout Capabilities*, University of Minnesota Centre for Distributed Robotics. Available from: http://distrob.cs.umn.edu/scout.php [28/02/2005].

Vanezis, A & Lees, A 2005, 'A biomechanical analysis of good and poor performers of the vertical jump', *Ergonomics*, vol. 48, no. 11-14, pp. 1594-1603.

Vogel, S 2003, *Comparative Biomechanics: Life's Physical World*, Princeton University Press.

Wassenbergh, SV, Strother, JA, Flammang, BE, Ferry-Graham, LA & Aerts, P 2008, 'Extremely fast prey capture in pipefish is powered by elastic recoil', *Journal of the Royal Society interface*, vol. 5, no. 20, pp. 285-296.

Wei, T, Nelson, GM, Quinn, RD, Verma, H & Garverick, S 2000, 'A 5cm Autonomous Hopping Robot', in *IEEE Conf. on Robotics and Automation (ICRA '00)*, San Francisco, CA.

Weiss, P 2001, 'Hop...Hop...Hopbots!: Designers of small, mobile robots take cues from grasshoppers and frogs', *Science News*, vol. 159, no. 6, p. 88.

Yim, M, Duff, DG & Roufas, KD 2000, 'PolyBot: a modular reconfigurable robot', in *Robotics and Automation, 2000. Proceedings. ICRA '00. IEEE International Conference on*, pp. 514-520 vol.1.

Yoshimitsu, T, Kubota, T & Nakatani, I 2006, 'Operation of MINERVA rover in Hayabusa Asteroid Mission', in *AIAA 57th International Astronautical Congress, IAC 2006*, American Institute of Aeronautics and Astronautics Inc., Valencia, Spain, pp. 1199-1209.

Yoshimitsu, T, Kubota, T, Nakatani, I, Adachi, T & Saito, H 2003, 'Micro-hopping robot for asteroid exploration', *Acta Astronautica*, no. 52, pp. 441-446.

Appendices

Appendix A. Jollbot 3b's component details

Table 39 provides details for individual components of Jollbot 3b with illustrative photographs where possible.

Component	Image	Material	Weight (g)	Qty
612mm Square Section Axle		Aluminium	53.5	1
Axle Caps	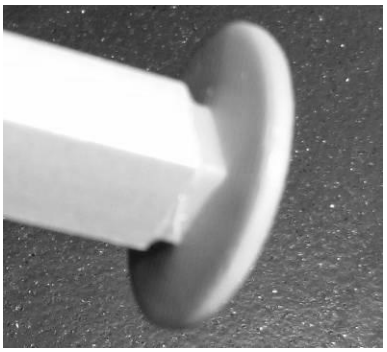	RP (ABS)	1.5	2
Rotating spring clamp inc. nuts and bolts	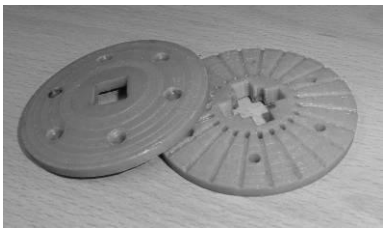	RP (ABS) & Steel	38.5	1
Fixed spring clamp inc. nuts and bolts		RP (ABS) & Steel	30.5	1

Component	Image	Material	Weight (g)	Qty
Spring elements		Spring Steel	11	24
Tyre		Latex	15.5	1
Battery pack + cable	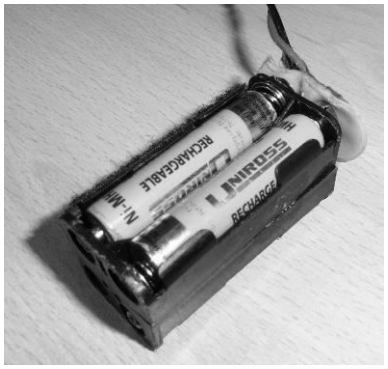		63	1
Receiver (Acoms)			19.5	1
Rolling servo (HiTec HS-965MG) & mount screws			63	1
Rolling spur gear & coupling		RP (ABS) & PVC & Polycaprolactone (PCL)	7	1

Component	Image	Material	Weight (g)	Qty
Centre gear & sliding mount		RP (ABS) & PVC	7.5	1
Main chassis		RP (ABS)	47	1
Anti-tangle mechanism including belt clamp	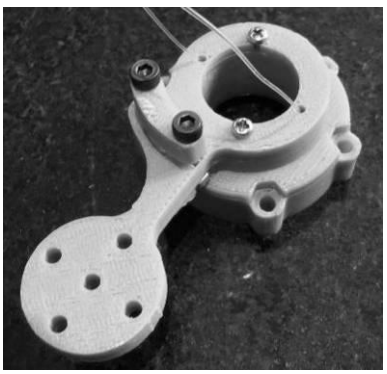	RP (ABS) & Steel ball bearings	22	2
Compression servo (Acoms AS12) & mount screw			40.5	1
Worm gear on slider & axle & coupling & reset extension		RP (ABS) & PVC & Brass	7	1

Component	Image	Material	Weight (g)	Qty
Worm axle holder & servo mount	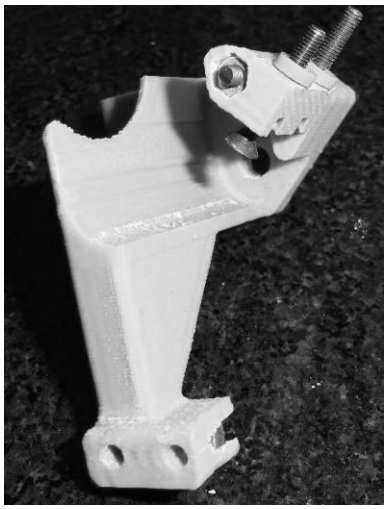	RP (ABS)	18.5	1
Fishing Line Thread			7	1
Spool & mount, axle & reset spring & gear	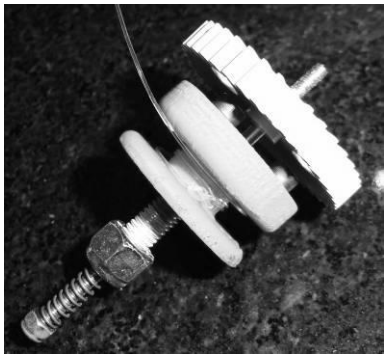	RP (ABS) & PVC & Steel	24.5	1
Release lever		RP (ABS)	12.5	1
Release lever extension	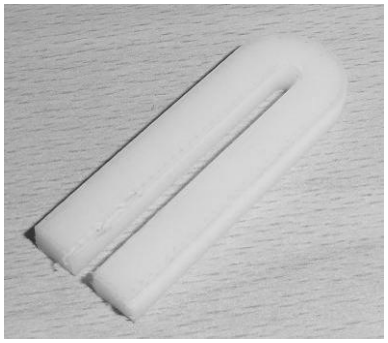	RP (ABS)	3	1

Component	Image	Material	Weight (g)	Qty
Catch lever & spring & mount		RP (ABS)	13.5	1
Belt guide bearing & screw		Steel & RP (ABS)	2.5	2
Steering servo (Acoms AS12) & mount screw			41.5	1
Belt	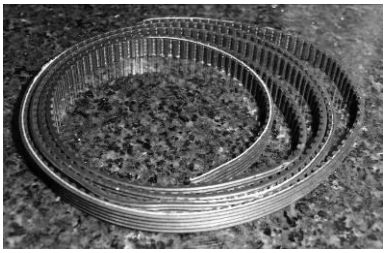	Fibre reinforced rubber	4	1
Belt pulley & coupling		RP (ABS) & Nylon & PCL	4	1

Component	Image	Material	Weight (g)	Qty
Rolling weights (removable)		Steel	16.5	2

Table 39 – Component details for Jollbot 3b

Appendix B. Detail of additional jumps

(following pages)

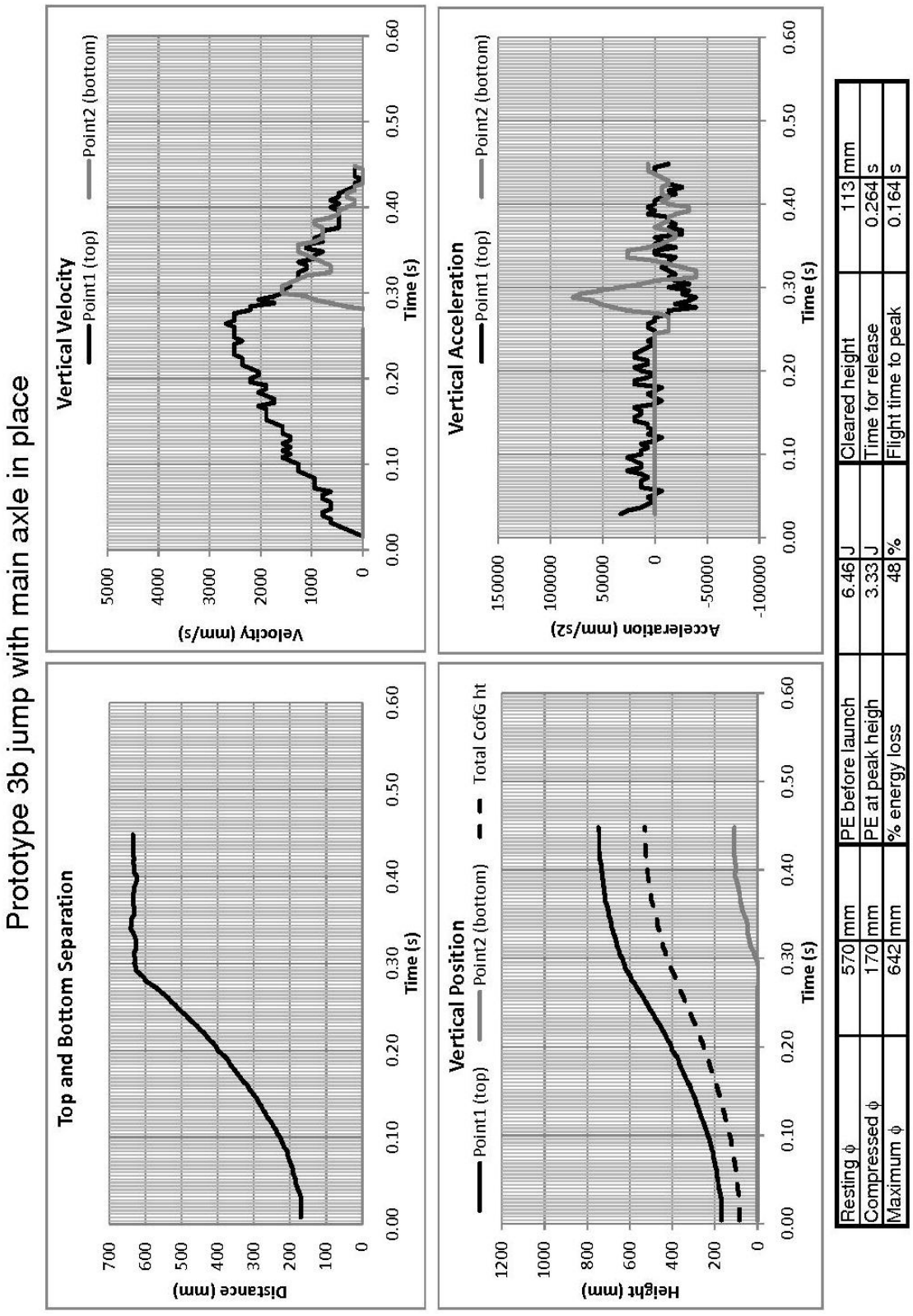

Resting ϕ	570	mm	PE before launch	6.46	J	Cleared height	113 mm
Compressed ϕ	170	mm	PE at peak heigh	3.33	J	Time for release	0.264 s
Maximum ϕ	642	mm	% energy loss	48	%	Flight time to peak	0.164 s

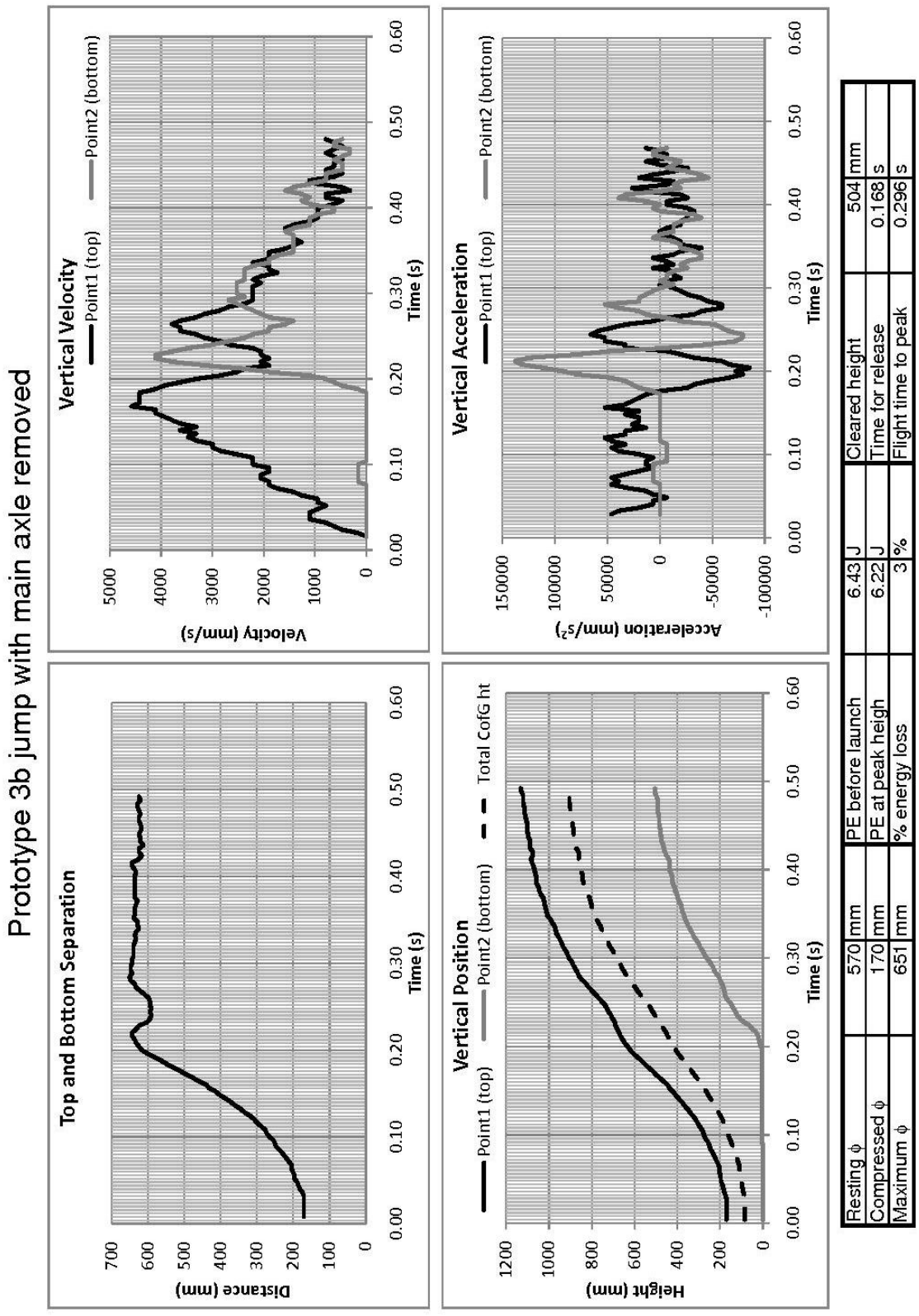

Resting ϕ	570	mm	PE before launch	6.43	J	Cleared height	504	mm
Compressed ϕ	170	mm	PE at peak heigh	6.22	J	Time for release	0.168	s
Maximum ϕ	651	mm	% energy loss	3	%	Flight time to peak	0.296	s

Prototype 3b jump2 with main axle removed

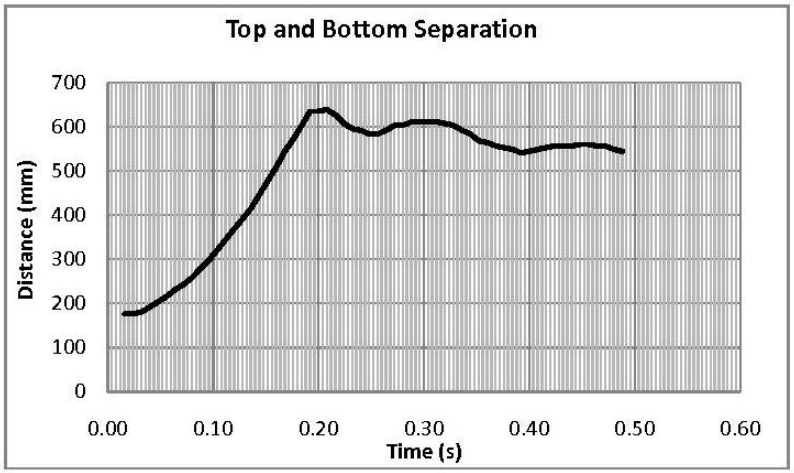

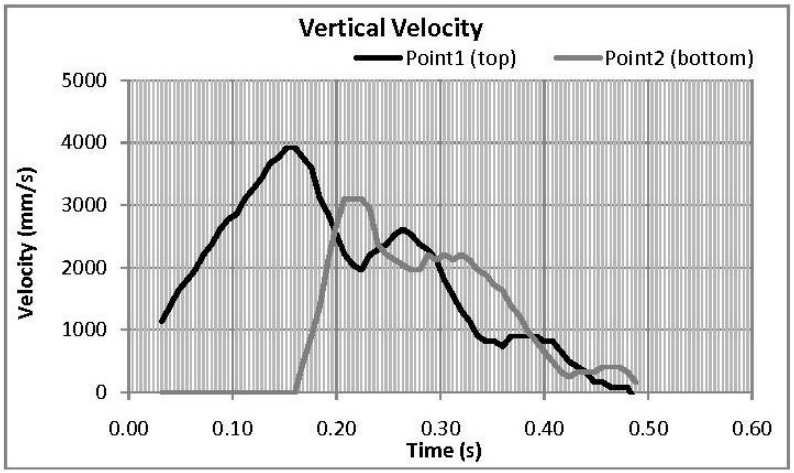

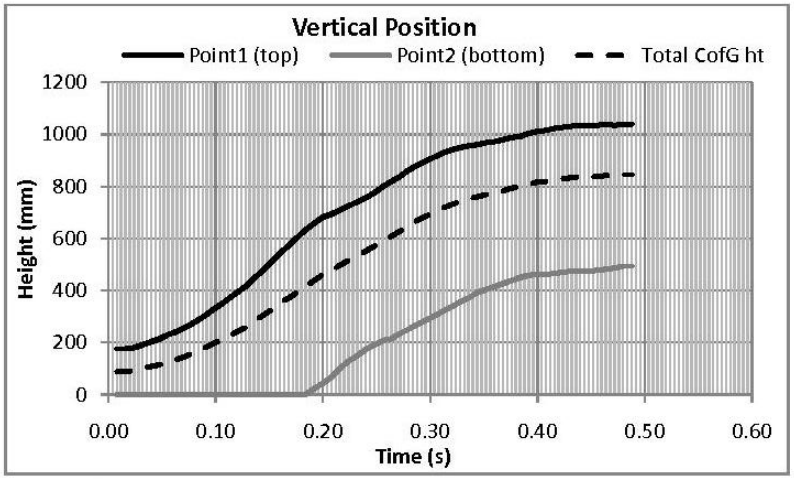

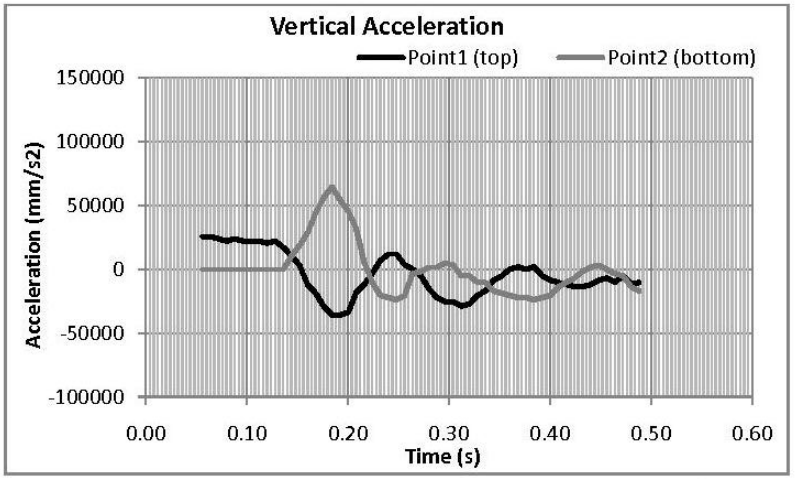

Resting ϕ	570	mm	PE before launch	6.26	J	Cleared height	494	mm
Compressed ϕ	176	mm	PE at peak heigh	5.71	J	Time for release	0.184	s
Maximum ϕ	638	mm	% energy loss	9	%	Flight time to peak	0.296	s

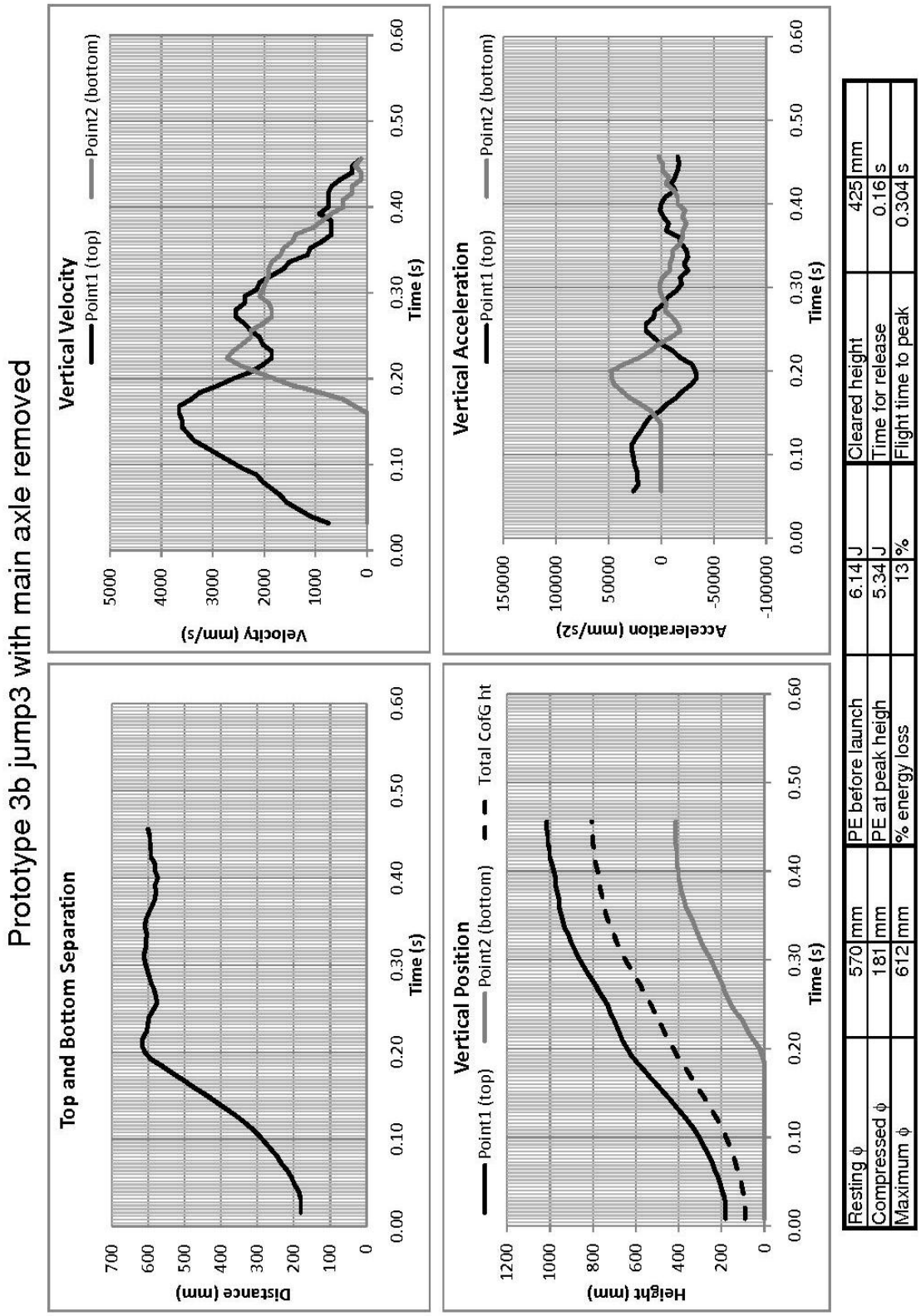
Prototype 3b jump3 with main axle removed
Vertical Velocity
Point1 (top)
Point2 (bottom)
Velocity (mm/s)
Time (s)
Vertical Acceleration
Acceleration (mm/s2)
Top and Bottom Separation
Distance (mm)
Vertical Position
Total CofG ht
Height (mm)
Resting ϕ 570 mm
Compressed ϕ 181 mm
Maximum ϕ 612 mm
PE before launch 6.14 J
PE at peak heigh 5.34 J
% energy loss 13 %
Cleared height 425 mm
Time for release 0.16 s
Flight time to peak 0.304 s

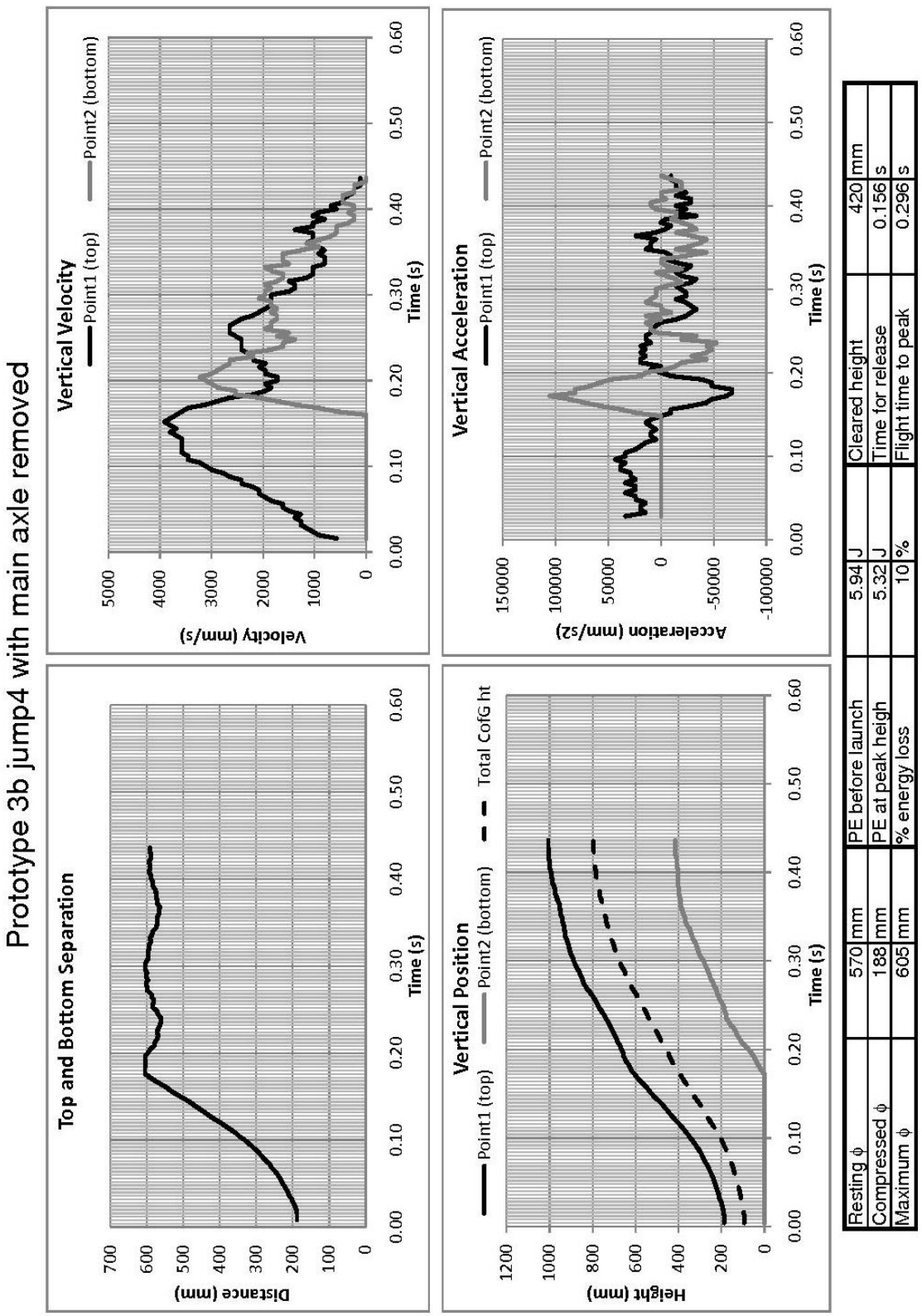

Resting ϕ	570	mm	PE before launch	5.94	J	Cleared height	420 mm
Compressed ϕ	188	mm	PE at peak heigh	5.32	J	Time for release	0.156 s
Maximum ϕ	605	mm	% energy loss	10	%	Flight time to peak	0.296 s

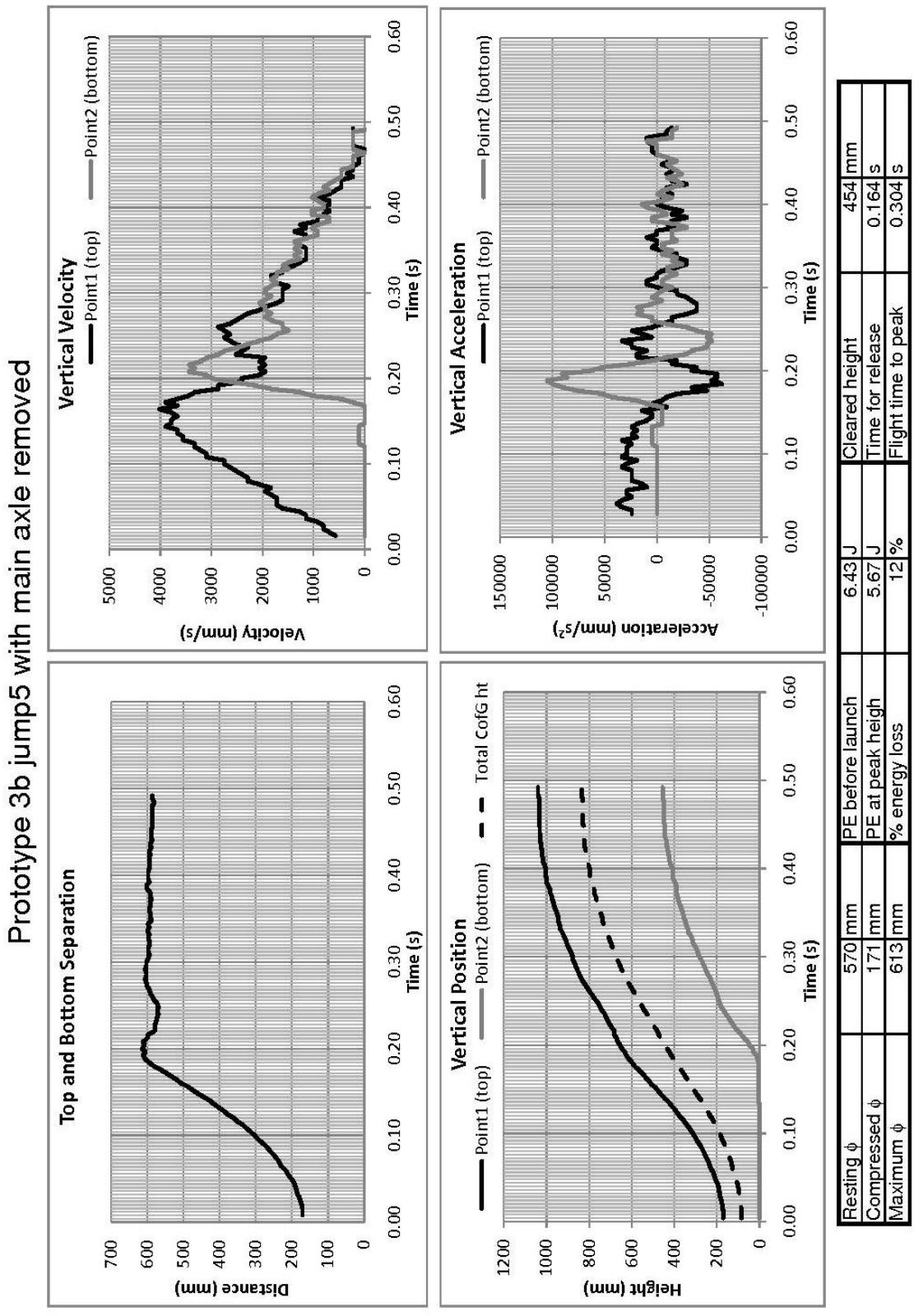

Resting ϕ	570	mm	PE before launch	6.43	J	Cleared height	454 mm
Compressed ϕ	171	mm	PE at peak heigh	5.67	J	Time for release	0.164 s
Maximum ϕ	613	mm	% energy loss	12	%	Flight time to peak	0.304 s